Prifysgol Abertawe
Swansea University

HOUSTON Methodist
LEADING MEDICINE

Tuneable 3D biocompatible scaffolds for biological and biophysical solid-tumour microenvironment studies; applications in Ovarian Cancer

Francesca Paradiso

Submitted to Swansea University in fulfilment

of the requirements for the Degree of Doctor of Philosophy

Swansea University & Houston Methodist Research Institute

2022

Summary

Recently, three-dimensional (3D) tumour models mimicking the tumour microenvironment and reducing the use of experimental animals have been developed generating great interest to appraise tumour response to treatment strategies in cancer therapy. As tumours have distinct mechanics compared to normal tissues, biomaterials have also been utilized in 3D culture to model the mechanical properties of the tumour microenvironment, and to study the effects of extracellular matrix (ECM) mechanics on tumour development and progression. Mechanical cues regulate various cell behaviours through mechanotransduction, including proliferation, migration, and differentiation. In the context of cancer, both stromal cells (cancer associated fibroblasts) and tumour cells remodel the ECM and change its mechanical properties, and the altered mechanical niche in turn is likely to influence tumour progression.

In this study, bovine derived collagen type I and Jellyfish derived marine collagen sources, were tested as biomaterial candidates for cancer studies, moulded to porous scaffolds with tuneable mechanical properties. The resulting interconnected network of collagen fibre constructs, fabricated using lyophilisation provide good control of scaffolding architecture, pore sizes range, high porosity levels, high level of cell viability and low production cost. Importantly these sponge scaffolds were, in the form of 3D models, compatible with a host of cellular and molecular biology assays used to investigate mechanical and biological effects of collagen crosslinking and (hyaluronic acid) HA inclusion on both fibroblasts and ovarian cancer cells.

Stromal cells and cancer cells respond differently to the altered stiffness of their local microenvironment. Fibroblasts, once activated with TGFβ1, converge toward a ‘senescent-like phenotype’, blocking migration and matrix remodelling and promote tumour progression, probably through the secretion of tumour-promoting signals, in stiffer mechanical environments. Cancer cells, of both epithelial and mesenchymal phenotype, respond to increased local matrix stiffness by increasing proliferation while, at the same time, becoming more susceptible to treatment. Mechanically informative scaffolds resemble the physical characteristics of both normal and pathological ovarian tissue mechanics, where ovarian cancer originates. Physical changes observed in the later stage of ovarian cancer disease progression may therefore be fundamental for

the increased cancer proliferation that drives metastatic progression, however opening an interesting window for cancer treatment. Bio-physical inclusive models not only lead the path to unveil complex interactions of biophysical and biological signals in the tumour microenvironment, but they represent a highly informative and effective platform to test novel target therapies with effective costs and high throughput. They can accommodate coculture systems and potentially patients-derived cell cultures, providing a platform to test current and new drugs and to evaluate drug efficacy following a precision medicine approach.

Declaration

This work has not previously been accepted in substance for any degree and is not being concurrently submitted in candidature for any degree.

Signed……  (candidate)

Date ……5/24/22……

STATEMENT 1

This thesis is the result of my own investigations, except where otherwise stated. Where correction services have been used, the extent and nature of the correction is clearly marked in a footnote(s). Other sources are acknowledged by footnotes giving explicit references. A bibliography is appended.

Signed  …… (candidate)

Date ……5/24/22……

STATEMENT 2

I hereby give consent to a no restriction access condition for my thesis. I consent to an immediate deposit of an open access electronic version and print copy available in the Swansea University Library.

Signed  …… (candidate)

Date ……5/24/22……

Table of Contents

Acknowledgments

-*My education was the liberty I had to read indiscriminately and all the time, with my eyes hanging out.*- Dylan Marlais Thomas

Dylan Thomas (27 October 1914 – 9 November 1953) was a Welsh poet and writer, born in Swansea, the place where I started this journey.

The sum of all the moments and all the lives I had the pleasure to enjoy time with during the last years made me the person I am today, a more self-confident woman, a scientist eager to learn and discover, an explorer of the world and a grateful person.

The first person I met was my first mentor, *Lewis Francis*, a wonderful communicator, empathic and laid back who trusted my ideas and skills since the beginning, helping me overcoming many challenges and changes of directions. Your attention for the well-being of the students is not common and your charisma and political skills help me figure out uncommon but fundamental sides of being a leader and mentor. Thank you for challenging me while always asking about how I was feeling/doing in my life.

In this beautiful, green and peaceful landscape of Swansea I met so many people who I profoundly thank for make me laugh, enjoy work and the extra time on many adventures. *Martina* is my sister in travelling and escapes, a compassionate soul always there to listen, cheer me up or bringing to the next adventure (and feeding me, eheh). Your friendship enriches my life and make me feel blessed. *Simone*, a new brother for me, a deep and simple bond that you can't just live without. I enjoy every step that took me to get to know you more and more. I apologize for my phd life complains at the beginning, you showed me how cope the challenges of life with a spirit of playfulness. I cheer every second, travelling, chilling at the park, singing and playing guitar, together. I miss you a lot. *Nav*, always there to support me, always paying attention to my moods and open to listen and give advices. Your words and your friendships feel like warm hugs to me anytime we talk, regardless the distance. In Swansea, my dearest couple *Roberto* and *Claudia* welcomed me in their life for a while and I had so much fun staying with them. *Ludo*, with the little time we add, we created a beautiful, coloured and flowering bond. To all the new friendship that started on the way, I'll bring you with me forever…and to all the people that I had to say goodbye to prematurely, thank you for being part of my life, you mean a lot to me.

The second, unexpected chapter of my PhD life, took place in Houston, Texas where I first met my second mentor, a determined, playful and energetic scientist who guided my way until now, *Francesca Taraballi*.

We've been through many changes and unprecedented challenges during our time together, as results, I feel more self-conscious, organized, focused, motivated and passionate. Thanks to you I learned much more about life in academia, difficulties to face in running lab and creating collaborations, you share with me your daily experiences and I had the chance to see the behind the scene of a professional world that I still want to be part of. Our meetings together taught

me that resolve, focus, willpower, and determination help successful people work hard and stick to their long-term goals. I'm now determined to further pursue my professional goals, while nurturing my work-life balance, too.
In her lab I met such a mixture of expertise, personalities and backgrounds. *Stefania*, the most trustworthy person you could find. I had the pleasure to work with her, to discuss science, hypothesis, results with her but also to enjoy dinners, a jump from a plane and many artistic moment outside work which made my experience here much sweeter. She is a welcoming friend, a beautiful mind and a free spirit. *Stefano*, my wingman in everyday lab sadness and success! We always had a way to joke about a bad experience and I really enjoyed our bike rides after lab, criticizing houses architecture, talking about our life and feelings and playing cards. *Federica* is the most generous soul you can find; she is always there to listen, and I hope I can be there for you too when you'll need me. She is engaged and outgoing, a person who brought positive energy (and the bright energy of the Sicilian sun) to my days. And to the group of *Matte, Gerry and newcomers*…thank you guys for being such an amazing group to have fun with…more to come! *April*, my green lab buddy in the lab, thank you for believing in my little revolution and be part of it, I absolutely love our conversations and your explanations on the American politics, history and much more!
Melissa, my delighting friend, you bring joy and positivity to my life. You welcomed me here and thanks to you I felt like home since the beginning. I would need pages and pages to list our beautiful moments together, I know I can count on you anytime and I feel that pure sense of lightness when I'm with you. *Giuly*, we spent so much time together, cultivating our passions and strengthening our friendship. We are different but oh, so similar. I feel like I own you apologies for not having taken the most of our last time together in Houston, but you are always in my heart and I will make up for it. You are not just a precious friend but also a wonderful person that I want in my life. And *Tamsen*, you need to be here, among the people that made this journey unforgettable, you are the most strong but delicate, thoughtful woman I've met. The combination of your personality traits made you such a unique and charming person. Thank you for welcoming me into your world and home and finally, gifting me with my beloved dog, *Fauci*.

Thank you, *Niman*. Thank you for being my safe harbor in many challenges I found on the way. I'll be immensely grateful to this journey because it led me to you, a lover, a friend, who patiently remind me how important is to cherish and celebrate my life, our life now. My days starts and ends with a smile because of you. I need to mention all your beautiful family, too. How supportive and understanding they are with me, no wonder where such a wonderful man comes from. I love them all.

Alla mia famiglia, custodi del mio passato e testimoni del mio presente. Da qualche anno abbiamo dovuto viverci un po' meno nella quotidianeta', ma ora vi sento vicini come non mai. Stiamo continuando a crescere tutti insieme, ad affrontare nuovi stadi della nostra vita sempre uniti. Le donne di questa famiglia sono i miei Modelli, coloro che mi danno la forza ogni giorno di credere nei miei sogni. *Mamma*, sei il mio faro nella notte, il mio modello di vita e la mia guida in questo mondo, il tuo abbraccio e' l'unico che mi ricorda quanto essere vulnerabili e' una forza, non una debolezza. *Marina*, la mia sorellina lontana, solo scrivendo il tuo nome non riesco a fermare le lacrime. Il tuo supporto costante durante questo percoso, la tua profonda attenzione nei miei confronti e compresione mi hanno dato coraggio in ogni sfida. Le nostre strade convergeranno presto. La mia Zia 'piccolo chimico', scienziata, appassionata e' colei

che mi ha donato questa passione per la scienza e mi ha insegnato a coltivarla in me sin da piccola, a te, devo tutto. Alla mia nonnina, che mi guarda da lassu' che con la forza del suo passato e i consigli d'infanzia mi ha insegnato che bisogna valorizzare e rispettare lo studio e la conoscenza, ed essere grati di avere accesso a queste opportunita' nella vita. Al mio fratellino, forte, sensibile ed indipendente. Mi riempi di gioia con ogni tua storia e mi fa ridere tanto con le tue battute, perdona la mia assenza, sono e saro' sempre al tuo fianco e te lo dimostrero'. Credi in te stesso e fai affidamento su di me, ti aiutero' a valorizzare le tue unicita' ed a capire che puoi realizzare ogni tuo obiettivo. A papa', grazie perche' hai iniziato a chiedermi di raccontarti della mia vita, e stai tentando di addolcire il nostro legame e rafforzarlo. A mio nonno, avrei voluto stringerti per mano e raccontarti di persona il mio progetto e le mie idee, tu saresti stato orgoglioso e mi avresti dato consigli per la mia carriera futura, grazie per essere stato un modello di dedizione ed anche, ogni tanto, sregolatezza. Questo lavoro e' dedicato a te e nonna e alla vostra sete di conoscenza. Alle mie cugine e cugini, zie e zii che mi fanno sentire amata e mi insegnano la vita attraverso le loro esperienze, anche se siamo lontani.

Alle mie amiche di sempre, Federica e Alessia, continueremo a crescere insieme, fianco a fianco come abbiamo sempre fatto. Sapete gia' quanto importanti voi siate per me. E grazie a tutte le amiche/I che hanno coltivato il nostro legame in questi anni lontani, tra qualche messaggio di aggiornamento e chiamate…Ada e Gianluca e molti altri.

Grazie.

There is still a lot to discover, together.

List of Publications

The main results of this PhD work or other collaborative works are currently submitted or accepted to peer-reviewed journals:

1) **F. Paradiso**, M. Quintela, S. Lenna, S. Serpelloni, D. W. James, S. Caserta, R. S. Conlan, L. W. Francis, F. Taraballi. Studying Activated Fibroblast Phenotypes and Fibrosis-Linked Mechanosensing Using 3D Biomimetic Models. *Macromol. Biosci.*, 2022 2100450. https://doi.org/10.1002/mabi.202100450 **(IF 4.9)**
2) **Francesca Paradiso**, Stefania Lenna, S Andrea Gazze, Jezabel Garcia-Parra, Kate Murphy, Lavinia Margaret, Deyarina Gonzalez, Lewis Francis, Francesca Taraballi. Mechano-mimetic 3D scaffolds as a humanized in vitro model for ovarian cancer. *Cells* 2022, 11(5), 824; https://doi.org/10.3390/cells11050824 (**IF 6.6**)
3) **Francesca Paradiso**, Joan C. Fitzgerald, Seydou YAO, Frank Barry, Francesca Taraballi, Deyarina Gonzalez, Robert S. Conlan, Lewis W. Francis. Marine collagen substrates for 2D and 3D ovarian cancer cell systems. *Frontiers in Bioengineering and Biotechnology*, December 2019; doi: 10.3389/fbioe.2019.00343 **(IF 5.2)**
4) **Paradiso Francesca**, Stefano Serpelloni, Lewis W. Francis, and Francesca Taraballi. Accepted Sept 2021. Mechanical Studies of the Third Dimension in Cancer: From 2D to 3D Model, *International Journal of Molecular Sciences* 2021 Sep; 22(18): 10098. doi: 10.3390/ijms221810098 (**IF 4.5**)
5) Parodi, A., Evangelopoulos, M., Arrighetti, N., Cevenini, A., Livingston, M., Khaled, S. Z., Brown, B. S., Yazdi, I. K., **Paradiso, F.**, Campa-Carranza, J. N., De, A., Taraballi, F., Tasciotti, E., Endosomal Escape of Polymer-Coated Silica Nanoparticles in Endothelial Cells. *Small* 2020, 16, 1907693. https://doi.org/10.1002/smll.201907693 (**IF 13.28**)
6) Jeffrey L Van Eps, Joseph S Fernandez-Moure, Fernando J Cabrera, Francesca Taraballi, **Francesca Paradiso**, Silvia Minardi, Xin Wang, Bayan Aghdasi, Ennio Tasciotti, Bradley K Weiner. Improved Posterolateral Lumbar Spinal Fusion Using a Biomimetic, Nanocomposite Scaffold Augmented by Autologous Platelet-Rich Plasma. *Front Bioeng Biotechnol.* 2021; 9: 622099. doi: 10.3389/fbioe.2021.622099 (**IF 5.89**)

7) Bauza-Mayol, G., Quintela, M., Brozovich, A., Hopson, M., Shaikh, S., Cabrera, F., Shi, A., Niclot, F. B., **Paradiso, F.**, Combellack, E., Jovic, T., Rees, P., Tasciotti, E., Francis, L. W., Mcculloch, P., Taraballi, F., Biomimetic Scaffolds Modulate the Posttraumatic Inflammatory Response in Articular Cartilage Contributing to Enhanced Neoformation of Cartilaginous Tissue In Vivo. *Adv. Healthcare Mater*. 2022, 11, 2101127. https://doi.org/10.1002/adhm.202101127 (**IF 9.9**)

List of Tables

List of Figures

Abbreviations

extracellular matrix (ECM)
tumour microenvironment (TME)
glycosaminoglycans (GAGs)
transforming growth factor-beta (TGF-β)
cancer associated fibroblasts (CAFs)
heparan sulphate proteoglycans (HSPGs)
growth factors (GFs)
bone marrow-derived cells (BMDCs)
epithelial ovarian cancer (EOC)
ovarian cancer (OC)
hyaluronic acid (HA)
high molecular mass HA (HW-HA)
low molecular weight HA (LW-HA)
post-translational modifications (PTMs)
lysyl oxidase (LOX)
lysyl oxidase-like (LOXL)
matrix metalloproteases (MMPs)

disintegrin and metalloproteinases (ADAMs)
disintegrin and metalloproteinases with thrombospondin motifs (ADAMTS)
immunohistochemistry (IHC)
nuclear pore complexes (NPCs)
lamin B receptor (LBR)
Yes-associated protein (YAP)
versican (VCAN)
immune checkpoint inhibitors (ICI)
tissue Engineering (TE)
genetically engineered mouse models (GEMMs)
patient-derived xenograft models (PDX)
pharmacokinetic (PK)
basement membrane (rBM)
poly(ethylene glycol) (PEG)
poly(lactide-co-glycolide) (PLG)
BM extract (BME)
nanoparticles (NPs)
(poly(ε-caprolactone) (PCL)
poly(glycolic acid) (PGA)
poly(lactic acid) (PLA)
high-grade serous ovarian carcinoma (HGSOC)
AJCC (American Joint Committee on Cancer)
ovary surface epithelium (OSE)
adipose-derived stem cells (ASCs)
shear wave elastography (SWE)
magnetic resonance elastography (MRE)
atomic force microscopy (AFM)
elastic modulus (E)
1, 4-butanediol diglycidyl (BDDGE)
Dulbecco's Eagle medium (DMEM)
fibroblast associated protein (FAP)
α smooth muscle actin (αSMA)
normal fibroblasts (NFs)
activated fibroblasts (AFs)
double-stranded DNA (dsDNA)
hyaluronidase-1 (*HYAL1*)
tri-calcium phosphate (TCP)

poly-l-lactic acid (PLLA)
poly-dl-lactic-co-glycolic acid (PLGA)
discoidin domain receptors (DDRs)
1-ethyl-3-(3-dimethyl aminopropyl) carbodiimide hydrochloride (EDC)
polyacrylamide (PA)
gelatin-methacryloyl (GelMA)
polydimethylsiloxane (PDMS)
alpha chain of the type 1 (COL1A1)
extracellular vehicles (EVs)
fourier transform infrared spectroscopy (FTIR)
thermo-gravimetric Analysis (TGA)
contact angle (CA)
water contact angle (WCA)
CellTracker™ Green 5-chloromethylfluorescein diacetate (CMFDA)
Principal Component Analysis (PCA)
fibronectin (FN1)
tenascin-C (TNC)
cell secretome (CS)
extracellular vehicles (EVs)
conditioned media (CM)
multiphoton microscopy (MPM)
second harmonic generation (SHG)
pegylated liposomal doxorubicin (PLD)
metastatic scaffold (MS)
normal scaffold (NS)
doxorubicin (DOXO)
doxorubicin-loaded liposomes (DOXO-LIPO)
polydispersity index (PDI)
WW-domain containing transcriptional regulator 1 (TAZ)
tumour–stroma ratio (TSR)
Food and Drug Administration (FDA)
relapse-free period (RFP)
Tumour-Associated Collagen Signature (TACS)
sodium dodecyl sulphate polyacrylamide gel electrophoresis (SDS-PAGE)
quantitative polymerase chain reaction (qPCR)
scanning electron microscopy (SEM)
GPO (Glycine-Proline-Hydroxyproline)

RGD (Arginine-Glycine-Aspartic acid)

membrane type metalloproteases (MT-MMPs)

Adherent Junctions (AJ)

ovarian surface epithelium (OSE)

osteopontin (OPN)

epidermal growth factor–containing fibulin-like extracellular matrix protein 1 (EFEMP1)

mesothelin (MSLN)

PolyHIPE polymer (PHP)

mesenchymal-epithelial transition (MET)

tumour-infiltrating lymphocytes (TILs)

Toll-like receptor 8 (TLR8)

carboplatin (CBP)

American Cancer Society (ACS)

Chapter 1: Introduction

Part of the work presented in this thesis chapter contributed directly to the following peer reviewed journal article.

Paradiso Francesca, Stefano Serpelloni, Lewis W. Francis, and Francesca Taraballi. Accepted Sept 2021. International Journal of Molecular Sciences; *Mechanical Studies of the Third Dimension in Cancer: From 2D to 3D Model* Int J Mol Sci. 2021 Sep; 22(18): 10098. doi: 10.3390/ijms221810098 (**IF 4.5**)

1.1 Matrisome - ECM signature(s) in cancer progression

Often referred to as the ‘matrisome’ and synthesized by cells within a given tissue [2, 3], the extracellular matrix (ECM), is a complex meshwork of proteins and is a fundamental component of multicellular organisms. In a three-dimensional architectural scaffold, the ECM defines tissue boundaries as well as their biochemical and biomechanical properties, linked to regulating development processes such as stem cell niche formations, cellular migration, polarity and axonal projections [4], morphogenesis and maintenance of tissue homeostasis [5]. By binding morphogens and growth factors [6], the ECM also serves as a reservoir for the creation of concentration gradients for haptotactic migration [7] or pattern formation [8, 9]. Acting as an adhesive substrate for cell attachment and migration, ECM proteins also provide biochemical cues interpreted by cell surface receptors such as the integrins [6], and initiate signalling cascades shown to control cell survival, proliferation, differentiation, and stem cell state [7, 8].

The diversity and functional importance of the ECM is highlighted by the occurrence of numerous genetic and acquired connective tissue disorders, where mutations in individual ECM genes are causes of musculoskeletal, cardio-vascular, renal, ocular and skin diseases [10]. Not only aberrant ECM secretion has been shown to interfere with tissue homeostasis, but also the way ECM is dynamically remodelled. Indeed ECM remodelling is essential in physiological processes such as angiogenesis and gland branching morphogenesis, wound healing, as well as being included as a hallmark of cancer invasion and fibrosis [11, 12], where excessive deposition or, conversely, destruction of the ECM is known to occur [13]. Excess ECM breakdown leads to tissue destruction, impairing ECM architectural integrity and homeostasis. On the other hand, excessive ECM manufacturing and deposition, mainly occurring in chronic or severe tissue injuries, can lead to fibrosis if it’s not balanced by ECM degradation [14]. Other diseases include chronic obstructive pulmonary disease, pancreatic ductal adenocarcinoma, spinal cord injury, progression and metastasis of breast cancer, and neurodegenerative conditions in the brain such as Alzheimer's disease [12]. ECM hardening or desmoplasia, alongside aberrant remodelling, has been shown to play a role in disease development.

Desmoplasia (growth of fibrous or connective tissue) may occur around a neoplasm, causing dense fibrosis around the tumour. This ‘scar-tissue’ formation, mainly driven by stromal cells, has been shown to promote tumour progression and dissemination, and has been utilised by pathologists as a marker of poor prognosis - even long before the composition and the complexity of the ECM were uncovered [15, 16]. Directly related to this, the tumour microenvironment (TME) has emerged as a key player in the development of chemoresistance during malignant progression, thereby influencing the development of novel therapies in clinical oncology [17, 18]. As a result, characterizing and modelling the global composition of the normal and diseased tissues matrisome has led to important discoveries [4].

Even if, mostly due to insolubility, the biochemistry of ECM is challenging, the availability of complete genome sequences coupled with extensive literature starting from the 1980s on ECM proteins, now makes it possible to construct a reasonably complete list of ECM proteins [19]. The core matrisome comprises ECM glycoproteins, collagens and proteoglycans (almost 300 proteins, including 43 collagen subunits, three dozen or so proteoglycans, and around 200 glycoproteins) while matrisome-associated proteins include ECM-affiliated proteins, ECM regulators and secreted factors (mucins, secreted C-type lectins, galectins, semaphorins, and plexins, proteases, or enzymes involved in cross-linking, or growth factors and cytokines) [19]. In the following sections, the fundamental nature of the ECM in regulation of normal tissues homeostasis is described alongside the causes and effects of ECM dysregulation during disease onset and progression, especially in the cancer context.

1.1.1 Stromal cells, the biochemical and biophysical modifiers of the ECM

Fibroblasts are a heterogeneous cell population found in connective tissue(s) and are the principal cellular component of the stroma [20, 21]. Genome-wide expression patterns of 50 human fibroblast cultures, isolated from 16 different sites, showed that gene-expression patterns among fibroblast populations from distinct anatomical sites are very divergent, resulting in the specific secretion of extracellular matrix (ECM) constituents, growth factors or differentiation factors [22]. Indeed, stromal fibroblasts are the main contributors to ECM secretion (elastin, collagens,

glycoproteins, glycosamminoglycans), while coordinating the structural organization and thus mechanical properties of tissues and supporting other tissue-resident cell types [23]. Furthermore, they can remodel and degrade matrix secreting enzymes such as the matrix metalloproteinase family [24, 25]. Currently the lack of a reliable and specific fibroblast molecular markers is a limiting factor in studying these fibroblast populations *in vivo* [1]. Some of the well-established indicators of fibroblast phenotype are listed in **Table 1;** as reported - some demonstrate the common genes associated with varying fibroblast populations.

Table 1.1 Fibroblast phenotype markers (adapted from [1]).

Marker	Function	Fibroblast type	Other cell type	Reference
Vimentin	Intermediate-filament-associate protein	Miscellaneous	Endothelial cells, EMT cancer cells and neurons	[26-28]
α-Smooth-muscle-actin	Intermediate-filament-associate protein	Miscellaneous	Vascular smooth muscle cells, pericytes and myoepithelial cells	[29-31]
Desmin	Intermediate-filament-associate protein	Skin fibroblasts	Muscle cells and vascular smooth muscle cells	[32, 33]
Fibroblast-activation protein (FAP)	Serine protease	Activated fibroblasts	Activated melanocytes	[34, 35]
α1β1 integrin	Collagen receptor	Miscellaneous	Monocytes and endothelial cells	[36-38]
Discoidin-domain receptor 2	Collagen receptor	Cardiac fibroblasts	Endothelial cells	[39, 40]

Fibroblasts are central players in both physiological and pathological matrix turnover, orchestrating healthy tissue structure and function while participating in tissue repair. Conversely, fibroblast cells have been shown to assume an aberrant stimulatory role during chronic inflammatory states, including cancer [41, 42]. In pathological conditions such as cancer or chronic wound healing, fibroblasts in the stroma restrain tumour or regenerate the wound. In advanced

stages those fibroblast cells are reprogrammed to support cancer growth or fail to regenerate wound healing [43]. At this stage, fibroblasts are differentiated into myofibroblasts, mainly under transforming growth factor-beta (TGF-β) stimulation and conditions of high tensile stress, increasing both their ability to synthesize ECM components and their contractile capacity. Indeed, this phenotype, characterized by the incorporation of smooth muscle α-actin within the cytoskeletal stress fibres and an increase in the clustering of integrins at focal adhesions, is often associated with fibrotic pathologies or aberrant wound healing. Similar activated phenotypes are induced in fibroblasts during tumour development, in which cancer associated fibroblasts (CAFs), regulate collagen deposition, cross-linking and force-mediated realignment of collagen fibres [1, 44].

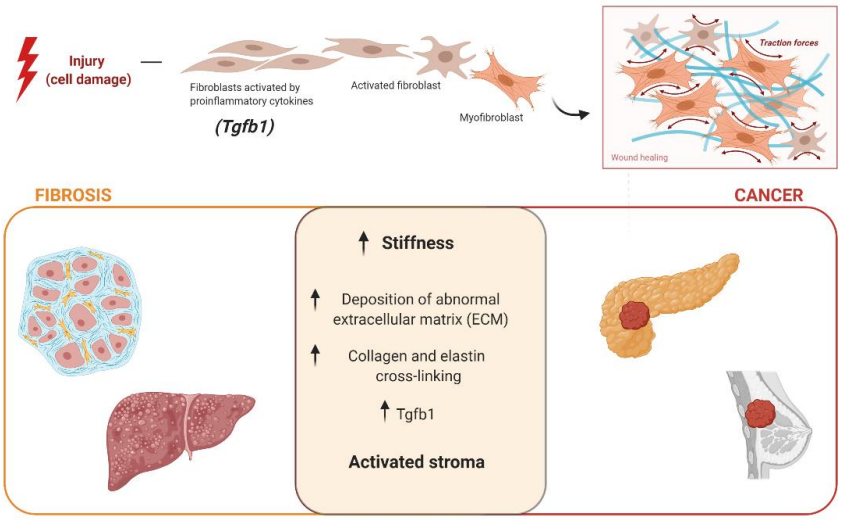

Figure 1.1 Parallelism in the ECM characteristic and stroma between fibrosis and cancer. Image made with Biorender.

The ultimate effect of such stromal reprogramming on the ECM is fibrosis, which is the formation of excess connective tissue causing stromal hardening and scar tissue, also called desmoplasia when specifically referring to the growth of benign fibrous tissue secondary to tissue injury such as cancer or infection [45]. Matrix stiffness, traditionally viewed as an end point of organ fibrosis, is now recognized as a critical regulator of tissue fibrogenesis that hijacks the normal physiologic wound-healing program to promote organ fibrosis [46]; while in tumour a dense fibrotic stroma could raise physical obstacles to immune cell infiltration [47] (**Figure 1.1**). Indeed, therapeutic

strategies that interfere with collagen stabilization reducing ECM content and tumour stiffness showed improved T cell migration and increased efficacy of immunotherapies using immune checkpoint inhibitor anti-PD-1 blockade [48].

1.1.2 ECM types and involvement in tumour progression

ECM is found in 2 different forms which differ in location, function, and composition. First, the basement membrane is a sheetlike, dense network which separates tissues into two distinct compartments, laying underneath epithelial and endothelial cells and surround muscle, fat, and Schwann cells [49]. The basement membrane mainly consists of collagen IV and laminins interconnected through network-bridging proteins such as nidogen and heparan sulphate proteoglycans (HSPGs) [50]. While cells binding to the basement membrane is fundamental for maintaining tissue homeostasis and establishing cellular polarity [51], its remodelling is required by malignant cells to spread into the underlying stroma and become invasive [52]. Also tumours that metastasize at new sites must recruit a basement membrane-containing vascular supply to expand [49].

Secondly, the interstitial matrix is a porous three-dimensional network which guarantees the structural integrity of tissues and organs [53]. The interstitial matrix connects cells in the stroma, modulating cell differentiation and migration, and can also be attached to the basement membrane. Interstitial ECM is composed mainly of collagens I, III, V, hyaluronic acid, fibronectin, elastin. [54]. These components vary among tissues, and the interstitial ECM composition is profoundly modified during normal tissue repair as well as during the progression of various diseases [55]. In cancer, the interstitial ECM remodelling (deposition, modification and degradation) process observed in both biophysical and biochemical changes has shown to influence cell signalling, ECM stiffness, cell migration and tumour progression [56] (**Figure 1.2**).

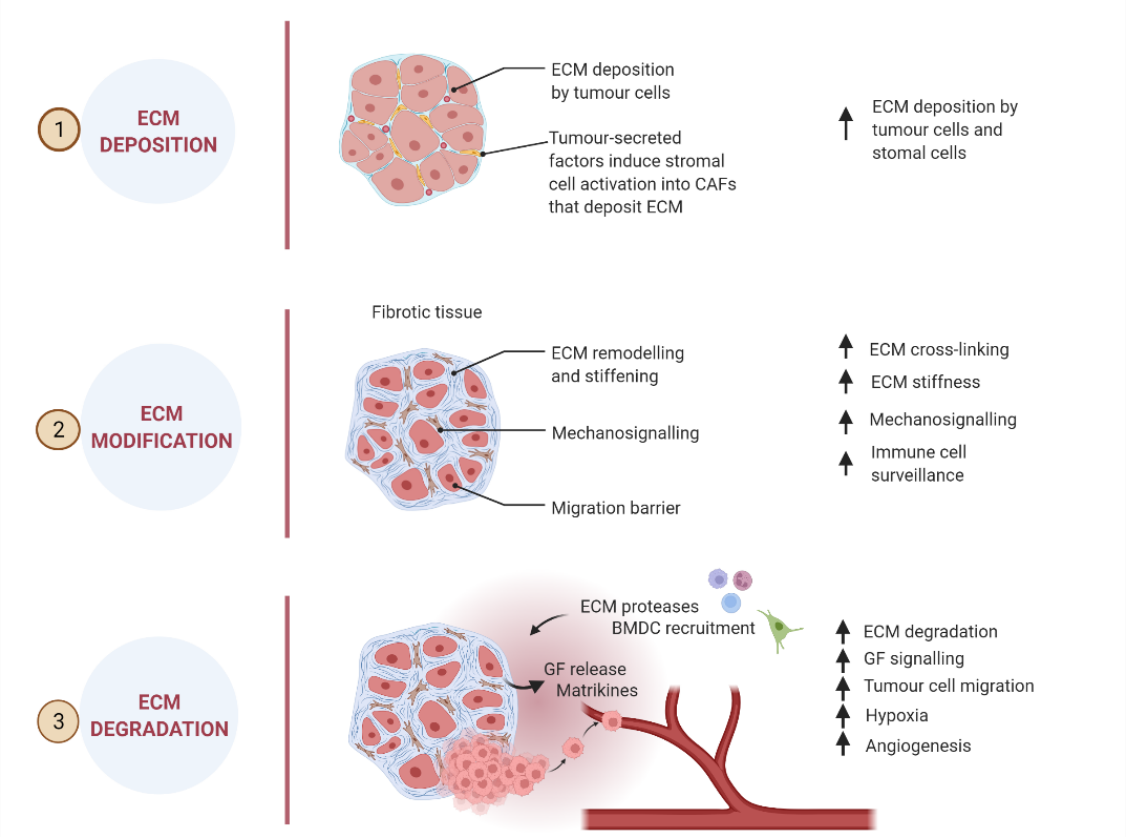

Figure 1.2. ECM remodelling in tumour progression. 1. Tumour-derived factors activate stromal cells which differentiate into cancer-associated fibroblasts (CAFs) leading to the secretion and deposition of large amounts of ECM components along with the cancer cells. 2. ECM-modifying enzymes such as LOX expressed by tumour cells and CAFs cross-link and align collagen fibres, which increases matrix stiffness around the tumour, forming a physical barrier to evade immune surveillance by T-cells. Increased matrix stiffness promotes the interaction between ECM components and cell-surface receptors on tumour cells that trigger mechanosignalling, mediated by integrins. 3. To sustain a tumorigenic microenvironment, tumours cells and resident immune cells secrete cytokines, chemokines and growth factors (GFs), which differentiate and recruit bone marrow-derived cells (BMDCs). BMDCs, CAFs and tumours cells secrete ECM-degrading proteases, including metalloproteins (MMPs). Proteolytic ECM degradation generates bioactive matrikines and releases matrix-bound GFs. These factors induce pro-tumorigenic ECM signalling that promote tumour proliferation, migration, invasion, and angiogenesis. These combined changes to the ECM create a hypoxic environment. Neutrophils secrete potent MMP-9 that degrades ECM and releases matrix-bound Vascular endothelial growth factor (VEGF) that forms a concentration gradient for new angiogenic sprouting. Image made with Biorender.

1.1.3 Changes in ECM composition in cancer.

Complex ECM remodelling processes change overall abundance, concentration, structure and organisation of individual ECM components, thereby affecting the three-dimensional spatial topology as well as biochemical and biophysical properties of the matrix around cells, and consequently the ECM effect on cell fate [3]. The most common tumorigenic alteration of ECM homoeostasis is an increased deposition of fibrillar collagen [57]. Collagen type I, and III, are the most abundant collagens of the interstitial matrix and essential for its structure [58]. Collagen I is a fibrillar collagen with a continuous collagen domain of around 1000 amino acids comprising Gly-X-Y repeats that form a triple helix. For example, in a murine breast cancer model, the increased deposition of collagen I results in progression tumour formation and development of metastasis [59], while compromising drug delivery [60] and has been observed to be linked to cisplatin resistance in epithelial ovarian cancer (EOC) [61, 62]. Not only increased collagen deposition, but also fibronectin, HA and tenascin C released into the interstitial matrix results in a desmoplasia phenotype, similar to the alterations observed during organ fibrosis and in many cancers such as pancreatic [63, 64] and breast [59, 65].

Interestingly, depending on its molecular weight HA functions as a tumour suppressor or a tumour promoter [66]. While the expression of a unique HA with high molecular mass (HW-HA) confers naturally tumour-resistant capabilities to the species of the naked mole rat [67], high level of low molecular weight (LW-HA), in particular small HA oligomers, is associated with poor prognosis in prostate, breast, colorectal and ovarian cancer [68-71]. Signalling through CD44 receptors, LW-HA promotes pro-tumorigenic signalling cascades, migration and increases the resistance to cellular stress [72-74]. Defined ECM protein signatures, like HA LW detection, can help distinguish tumours from normal tissues and are linked to tumour staging and could serve as biomarkers for early cancer detection [75] while their changes could be predictive of clinical outcomes [76, 77].

1.1.4 Changes in ECM modification and organisation in cancer.

After initial synthesis, ECM proteins undergo post-translational modifications (PTMs) which affect matrix interactions with other molecules and cellular receptors, localization within the tissue and ECM degradation [78, 79]. Fundamental for tissue integrity is the covalent crosslinking of collagen fibrils by extracellular enzymes lysyl oxidase (LOX) and lysyl oxidase-like (LOXL), essential for the correct collagen fibre assembly and the increased tensile strength and stiffness [80]. While in normal and soft tissue, they contribute to the creation of curly collagen fibres parallel oriented to the layer of epithelium, LOX expression in tumours leads to increased cross-linking and linearization of collagen fibres and ECM molecules, promoting tumour progression [81]. For example, in breast cancer and in hepatocellular carcinoma (HCC), in proximity to the tumour boundary collagen fibres are linearized, perpendicularly oriented and supportive of invasive tumour growth [57, 82, 83]. Furthermore, other PTMs such as glycosylation are very important for receptor functionality and ECM to cell signalling.

1.1.5 Degradation of the tumorigenic ECM.

Cleavage of ECM components is a central process during ECM remodelling and homeostasis, regulating ECM abundance, composition and structure, while also allowing the release of biologically active molecules (such as growth factors) [13]. The ECM can be cleaved and degraded by families of proteases such as target-specific proteases in the form of matrix metalloproteases (MMPs), disintegrin and metalloproteinases (ADAMs), disintegrin and metalloproteinases with thrombospondin motifs (ADAMTS), and proteases that specifically cleave at serine, cysteine and threonine residues [84, 85]. These proteases are secreted primarily by stromal cells, as well as by cancer cells, indeed immunohistochemistry (IHC) analyses of invasive tumours clearly showed high levels of MMP2, MMP9, MMP13, and MT-1 [86-88].

MMPs are thought to be the most important enzymes involved in ECM degradation. Their activity is low in normal conditions but increased during repair or remodelling processes and in diseased or inflamed tissue. In addition to their proteolytic actions, it is important to mention that they have significant non-proteolytic functions that can alter tumour progression, providing binding and signalling function in invasive cancers [52, 89]. As a consequence of both tumour and stromal-

driven ECM degradation through proteases secretion, a progressive destruction of the normal ECM takes place while it is replaced by tumour-derived ECM. ECM degradation then drives cancer cell motility before ECM-bound soluble signalling molecules, such as growth factors are released, thereby increasing their bioavailability [52]. Finally, the cleavage of long ECM components produces bioactive, shorter fragments (usually referred as bioactive matrikines) with distinct functions that can be pro- or anti-tumourigenic compared to the full-length ECM component (i.e. HA LW pro-tumorigenic increases in tumour tissue) [11].

1.1.6 Mechanotransduction and extracellular matrix homeostasis

Collagen crosslinking, alignment and increased deposition, are the main factors which significantly impact tissue mechanical properties during cancer progression, specifically increasing matrix stiffness around the tumour. As a result of the alterations in the ECM, tumours often are stiffer than normal tissue, a feature applied in clinical diagnosis [90, 91] and known to promote the invasive behaviour of diseases [92] (**Figure 1.3**).

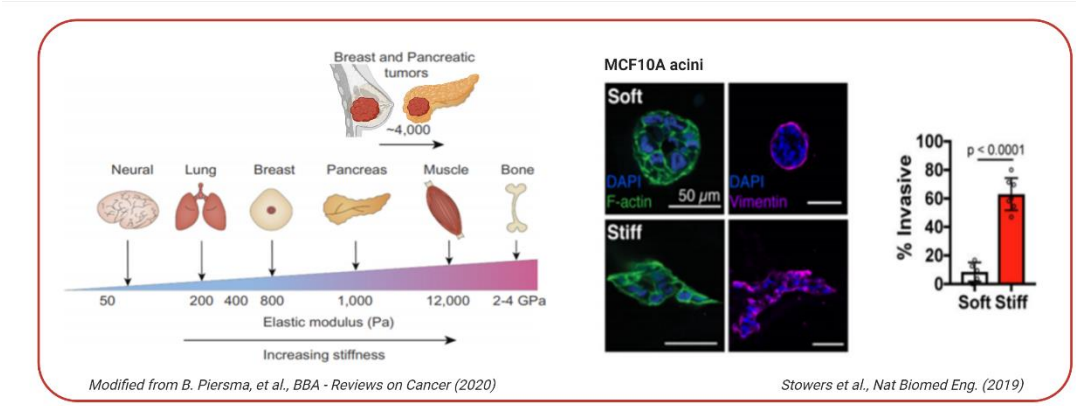

Figure 1.3. Elastic moduli in healthy human tissues and tumours. (left) The ECM in the brain, lung or breast is relatively soft (compliant; <100 Pa), whereas the ECM in tissues that are exposed to high mechanical loading such as skeletal muscle and bone are by comparison stiff (>100 kPa). Tumours are often fibrotic, and the ECM is stiffer than that found in a healthy tissue (~4–10 kPa). [93] (right**)** ECM stiffness induces cytoskeletal tension that perturbs cellular phenotype and invasiveness. Immunofluorescence staining for F-actin, vimentin, DAPI in MCF10A acini after 14

days in soft (top) or stiff (bottom) matrices. Quantification of invasive clusters marks an increase in invasive sites exhibited by tumorigenic phenotype in stiff matrices [92].

Increased matrix stiffness promotes the interaction between ECM components and tumour cell-surface receptors, leading to an altered mechanosignalling environment [94]. These biophysical signals are mostly conveyed by membrane spanning dimers called integrin receptors, which bind to the surrounding ECM and physically bridge them to the cell cytoskeleton, translating mechanical signals into biochemical processes [95, 96]. In this way, focal adhesions and integrin receptors serve as biochemical signalling hubs to initiate mechanoresponsive signalling pathways by concentrating and directing signalling proteins involved in cell polarity, tensile strength response, migration, and invasion [97, 98].

A second set of important players are the signalling components that regulate the assembly of these structures, such as Rho family small GTPases and their downstream effectors such as Rho associated protein kinase (ROCK), myosin light chain kinases, and so on [99]. Mechanical signals transduced from the external microenvironment to the intracellular cytoskeleton can be further transmitted into the nucleus where they can affect nuclear architecture and/or chromatin organization, resulting in both genetic and epigenetic landscape changes [100] (**Figure 1.4**).

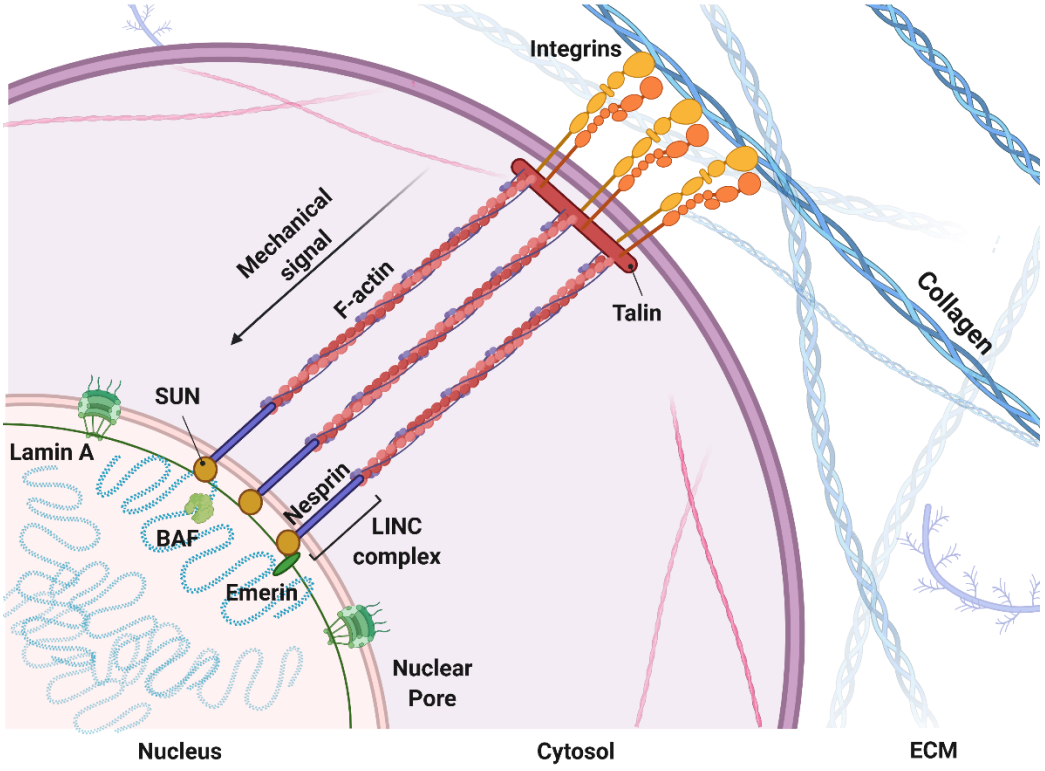

Figure 1.4. Mechanical coupling of the extracellular matrix with the nucleus. Mechanical signals propagation through molecular pathways inside the cytosol and nucleus. Image made with Biorender.

Analogous to focal adhesions, linkers of nucleoskeleton and cytoskeleton protein (LINC) complexes on the nuclear membrane physically connect the cytoskeleton to the nucleoskeleton [101, 102]. This complex comprises of two families, the KASH domain proteins (nesprins) bind to various cytoskeletal constituents, whereas the SUN domain proteins associate with the nuclear lamina (laminins) and nuclear pore complexes (NPCs) [103]. Laminins connect directly and indirectly, through emerin and lamin B receptor (LBR) binding, to regulatory proteins that are involved in chromatin modification, transcriptional regulation, and mRNA processing, while also binding to BAF protein (or BANF1), which binds directly to double-stranded DNA [104]. These anchor complexes that connect the ECM to the nucleus, through the cytoskeleton, can alter the activity of DNA regulatory complexes with consequent changes in chromatin organisation [105], gene transcription [106], RNA splicing, or chromatin modification [104, 107].

Fibroblasts together with smooth muscle and epithelial cells are highly sensitive to mechanical stimuli and the mechanical properties of their matrix [108-110]. Mechanics have been shown to influence migration, regulate cell cycle progression, control gene expression and cell fate [111-114]. In the tumour, cancer cells recognize the increase in ECM stiffness and respond by generating increased traction forces on their surroundings through actomyosin and cytoskeleton contractility [115, 116], inducing oncogenic intracellular signalling to aid tumorigenesis, including activation of FAK, AKT, β-catenin, and PI3K, and inhibition of the tumour suppressor genes PTEN and GSK3α/β [117], which in turn result in altered regulation of proliferation, stemness and chemoresistance [118, 119]. Furthermore, increased tumour stiffness can strongly affect inhabitant stromal cells, activating fibroblasts to a CAF phenotype and ensuring long term maintenance via the mechanosensitive transcription factor Yes-associated protein (YAP) [120, 121].

1.1.6 Translational applications

Remodelling of the tumour ECM impacts every stage of tumorigenesis. In line with this, targeting the ECM component synthesis or post-translational modifications, the enzymes responsible for ECM remodelling and the receptors that transduce their signals, may offer promising therapeutic opportunities for many diseases [4, 122, 123]. In this context, the ECM not only represents a potential therapeutic target but also the characterisation efforts centred on delineating ECM composition could lead to the identification of novel biomarkers of disease. Proteolytic fragments of ECM proteins released in body fluids could be used as readouts for disease progression or treatment efficacy [124-126]. Indeed, as described above, matrix remodelling alters the immune milieu by modulating differentiation, migration, infiltration and polarization of immune cells in the TME [127], therefore identification of specific targets could help disease prognosis or the development of novel immune biomarkers and/or a combination immunotherapy.

For example, detection of versican (VCAN) proteolysis in the TME, detected through neoepitope-specific antibodies [128], may provide a convenient and reliable immune biomarker, as it was proven to be strongly associated with “T-cell inflammation”, helping the selection of patients most likely to respond to immune checkpoint inhibitors (ICI) and other immune-modulating therapies

[129]. ECM components can also be used as therapeutic targets, for example, by using nanobody technology, which can selectively detect these alterations *in vivo* and guide therapeutics to the specific location [130], i.e. conjugating immune checkpoint antibodies or cytokines, to a matrix-binding peptide to potentiate cancer immunotherapy decreasing systemic toxicity and prolonging tissue retention [131-134]. The interest in the use of ECM as a therapeutic tool and its potential is also growing.

Tissue specific ECM-based materials could also represent a promising class of naturally derived biomaterial scaffolds to replace damaged ECM. For example, in porcine models of myocardial infarction researchers found that injecting ECM scaffolds derived from decellularized, normal, porcine myocardial tissue can improve cardiac function [135]. Outside of regenerative therapy, interest in ECM characterization and investigation of cells in their 3D microenvironment milieu have resulted in the development of various 3D platforms that could provide better *in vitro* tools to study the effects of specific matrix perturbations on complex cell–cell and cell–matrix interactions [136]. In this regard, collagen scaffolds and ECM are bridging the divide between Tissue Engineering practices (TE) and cancer biology.

1.2 Preclinical models for stromal matrix and biophysical studies in cancer biology

1.2.1 From 2D to 3D models

Understanding the underlying biology in tumour initiation and progression is the first step to the successful development of new and efficient cancer diagnosis and/or therapies. To achieve this goal, the cellular and structural complexity of the TME needs to be deconstructed into simpler and more predictable systems, to shed light onto the role of key chemical, mechanical and/or physical factors that might drive human pathophysiology, while helping to unveil the intricate interplay of cellular components that orchestrate tumour survival. In order to deliver this, translational models need to provide an environment for cancers to adopt heterogenous cellular states that represent the disease environment, in the presence and absence of therapeutics.

Historically, cancer research has traditionally relied on 2D culture systems [137]. However, many experimental inconsistencies are related to this type of cell culturing, in which cells are grown in a non-physiologically constrained condition. First, cell polarisation is a direct effect of attachment on 2D rigid and flat substrates, with related changes in surfaces receptor orientation and clustering [138]. This can profoundly affect not only ECM production and configuration but also how cells perceive ECM signals with impact on downstream effect like guiding lineage outcomes [139-141]. Furthermore, the wide exchange area of cells to culture media lead to excessive nutrition and oxygenation making it difficult, if impossible, to recreate molecular gradients [142, 143]. Unconstrained migration on 2D substrates can result in cell bioactivities that deviate appreciably from the *in vivo* response, while the immortalization process, through multiple passages, can result in the selection of cancer cells that rapidly proliferate. There is no doubt that immortalized tumour cell lines grown in 2D culture have contributed tremendous amounts of knowledge about the mechanism of cancer, but with a 95% drug failure rate, they have proven a poor drug development model in preclinical studies [144, 145].

Most *in vitro* studies in oncology are performed in 2D and are subsequently validated in *in vivo* animal models. Robust preclinical findings should represent the foundations for efficient drug development in clinical settings, proving efficacy of new therapeutic agents at targeting specific molecules at a concentration achievable for humans. Unfortunately, valid preclinical models are lacking for therapy evaluation, in particular for immunotherapy and antiangiogenic agents [146]. Indeed, both established models in preclinical studies possess numerous limitations; 2D models fail to accurately model the TME while animal models are expensive, time-consuming and can differ considerably from humans [147, 148]. More alarming is that there is evidence of poor reproducibility from preclinical studies with only 11% to 25% of published results could be reproduced [149, 150].

For decades, the most basic and frequently employed mouse models used to assess tumour growth and screen conventional chemotherapy, or candidate drugs, have been simple xenografted or syngeneic mice. Typically, these mouse models involve subcutaneous administration of human (xenograft) and mouse (syngeneic) tumour cells without regard to the organ of tumour origin (heterotopic), or via implantation of tumour tissue or cells into the tissue corresponding to the site

of the tumours origin (orthotopic). Both approaches result in lacking the broad molecular transformation events that occur in human tumours [151]. First, the stromal component of the tumour is not human, so drug response it's not really reflective of the human counterpart, secondly the growth rates of human-derived xenografts are considerably more rapid than primary tumours so they will most likely respond to antiproliferative agents and finally, the immune system of those animals is compromised, hindering the testing of immunomodulatory agents [144]. Other mouse models such as genetically engineered mouse models (GEMMs) circumvent some of these limitations as they are immune competent, but they still suffer from having rodent-derived stroma, mouse dominated immune system and harbouring a 'mouse' tumour [8]. As a result, patient-derived xenograft models (PDX) remain the strongest *in vivo* model for predicting drug response in patients and to study immune-tumour interactions or the effects of immunotherapy agents [152] even if few direct comparisons have been made of PDX and GEMM systems regarding pharmacokinetic and pharmacodynamic (PK) modelling accuracy has demonstrated PDX tumours may be inferior in accurately recapitulating drug PK parameters in some cancer types [153, 154]. Overall, a key drawback of animal models is that they do not represent the primary tumours from which they are derived in terms of tumour heterogeneity and the mechanisms of drug resistance. To fill the gap between 2D traditional tissue culture methods and animals' models, development of new 3D human-based culture systems aims to closely mimic the 3D architecture of primary tumours.

Cancer research has experienced a paradigm shift during the past two decades, as a result, there are a growing number of studies which report differences in phenotype, cellular signalling, cell migration, and drug responses when the same cells are grown under 2D or 3D culture conditions. Indeed, individual cells integrate many external cues — including those that arise from various ECM components, mechanical stimulation, and soluble signals from adjacent and even distant cells to generate a basal phenotype and respond to perturbations in their environment. A particular challenge is the coupling of chemical and mechanical signals [155-157].

1.2.2 Biomaterials for 3D cancer models

Significantly, 90% of cancers have an epithelial origin. A typical epithelial tissue comprises two compartments: a continuous layer of polarized epithelial cells sited on a basement membrane a thin, pliable sheet-like type of extracellular matrix mainly composed of type IV collagen , laminin, heparan sulfate, entactin and fibronectin [158]; and an underlying ECM enriched stroma that contains fibroblasts, immune cells, blood and lymphatic vessels.

The epithelial layer, strongly anchored to the basement membrane, represents a bridge between the external environment of a lumen, duct or cyst and the stroma which interacts with it through physical, biochemical cues and ECM components. The ECM underlying, called interstitial ECM, it's mainly composed by collagens, structural proteins, and proteoglycans and not only controls the bulk and local mechanical microenvironment but act as a reservoir of a series of biomechanical signals like growth factors, cytokines, enzymes, and other diffusible molecules.

In order to recapitulate the 3D organization and ECM of tumours, various natural and synthetic biomaterials have been exploited [159]. In use since antiquity as prosthetics to replace damaged tissues [160], biomaterials characterization and improving in methods of extraction and/or synthesis [161, 162], combined with increasing knowledge of biological process are making them transitioning from merely structural support to sophisticated devices which can impact cells signal transduction through well-defined molecular pathways at various size scales, creating highly defined microenvironments to direct biological responses [163]. Indeed, the same materials can now provide both a basis for *in vitro* mimics of tumours to better screen therapeutic approaches and identify new therapeutic targets, and a means to modulate the microenvironment *in vivo* and direct therapeutic responses against cancerous cells and tumours.

Various natural and synthetic materials have been developed to provide architectural support to interacting cells. Natural ECM-derived biomaterials such as collagen, laminin, HA, and reconstituted basement membrane (rBM or Matrigel) are the most commonly used materials for 3D culture of cancer cells, presenting inherent cytocompatibility, intrinsic cell adhesion properties, and ability to be remodelled by cells but they can hide some drawbacks like batch-to-batch

variability, complex molecular composition, and uncontrolled degradation of these materials [164].

In the 1970-80s, collagen was largely used as a biomaterial in many tissue applications because of its excellent biocompatibility, low antigenicity, high biodegradability and good mechanical, haemostatic, and cell- binding properties [165]. Collagen can be collected from various biological sources including bovine skin, rat tail, porcine skin and human placenta [166-169], however, if used for regenerative medicine purposes, bovine origins involve the risk of infection with diseases such as bovine spongiform encephalopathy while porcine-derived mammalian collagen is increasingly rejected for religious reasons [170]. To solve those issue new sources have been explored like marine organisms [171-175]. Marine wastage accounts up to 85% by weight in the fishing industry so, extraction of collagen from these wastes will contribute to the development of a sustainable pipeline to obtain collagen with a significantly reduced environmental impact [176]. Marine collagens have several advantages such as excellent biocompatibility, lower zoonotic risks, less immunological risk for patients allergic to mammalian products, and less religious restrictions [177]. Among those, type I marine collagen extracted from jellyfish, can provide good availability and easy handling, and it has already been used for different tissue engineering applications such as implants [178] or to support chondrogenically stimulated hMSCs differentiation for cartilage regeneration [170].

Aside from natural materials, synthetic ones such as poly(ethylene glycol) (PEG) and poly(lactide-co-glycolide) (PLG) can provide precise experimental control over biochemical and mechanical properties in modelling the tumour ECM, but they lack natural cell adhesion sites and are not readily remodelled by cells, cell adhesion ligands and biodegradable crosslinkers are often grafted to the polymers. For example, synthetic polymers like PEG or nanofibres scaffolds (RAD16-I) functionalized with adhesive/recognition sites for integrin binding or protease degradation are also useful to study the effect of tumours on ECM [179]. Another class of biomaterials that is increasingly being used in 3D tumour models is naturally-derived polysaccharides such as alginate and chitosan [180-182]. They have great biocompatibility and a broad range of chemical and mechanical properties, but they also lack mammalian cell adhesion sites and often require chemical modification to form gels with desirable physical properties.

1.2.3 Mechano-modelling: inclusion of biophysical signals in 3D cancer systems

Dissecting the effect of biophysical signals on cancer cells during tumour development has become the focus of many *in vitro* studies. The simplicity, low cost, and reproducibility of 2D models made them the mainstay of biological research, but *in vivo* tissue complexity can only be approached using 3D systems. In fact, in three dimensional systems, the mechanical properties can be tuned so that models mimic a wide range of tissue stiffness [183-185], and crucial cellular phenotypes linked to adhesion, spreading, and migration are not constrained to a single layer [186-188]. In 3D systems, sequestration/gradients of soluble biomolecules can be modulated to finely control cells' fate and differentiation [189, 190], and the ECM can be customized to more accurately reproduce the *in vivo* cell experience through varying chemical and mechanical signals [191-193]. Many processes are intrinsically tied to cell-cell and cell-matrix interactions, whether through synthesis, degradation, directed migration, or mechanical cues, and cannot be fully reproduced in conventional 2D cell culture [194-197], e.g., cancer metastasis or cancer-stroma interaction [198-201].

Use of scaffold-based approaches to grow cells in a 3D environment is very common in tissue engineering [202]. The challenges of reproducing microenvironment features in a 3D model has fuelled the scientific community to develop a wide variety of platforms to address different levels of complexity, e.g., cells can be seeded on pre-formed porous scaffolds/fibrous materials (obtained by two-phase emulsion, freeze-drying, or electro-spinning techniques) or encapsulated in biomaterials made of water-soluble polymers, called hydrogels [203-205]. Another promising trend is the use of native ECM obtained by tissue decellularization, employed as scaffold for cell seeding or as an additive component of 3D gels in order to mimic *in vitro* the ECM architecture and chemical/biological properties [206-208]. Furthermore, tissue physiology can be reproduced with the use of adult or pluripotent stem cell-derived organoids, which are self-organized 3D tissue cultures crafted from stem cells to replicate part or much of the complexity of an organ; or cells can be grown in a multi-channel 3D microfluidic cell culture chip that simulates mechanics, activities, and physiological response of specific organs or systems. All these platforms have different levels of complexity and can reproduce certain mechanical features from the native tissue that will be discussed in the following sections (**Figure 1.5**).

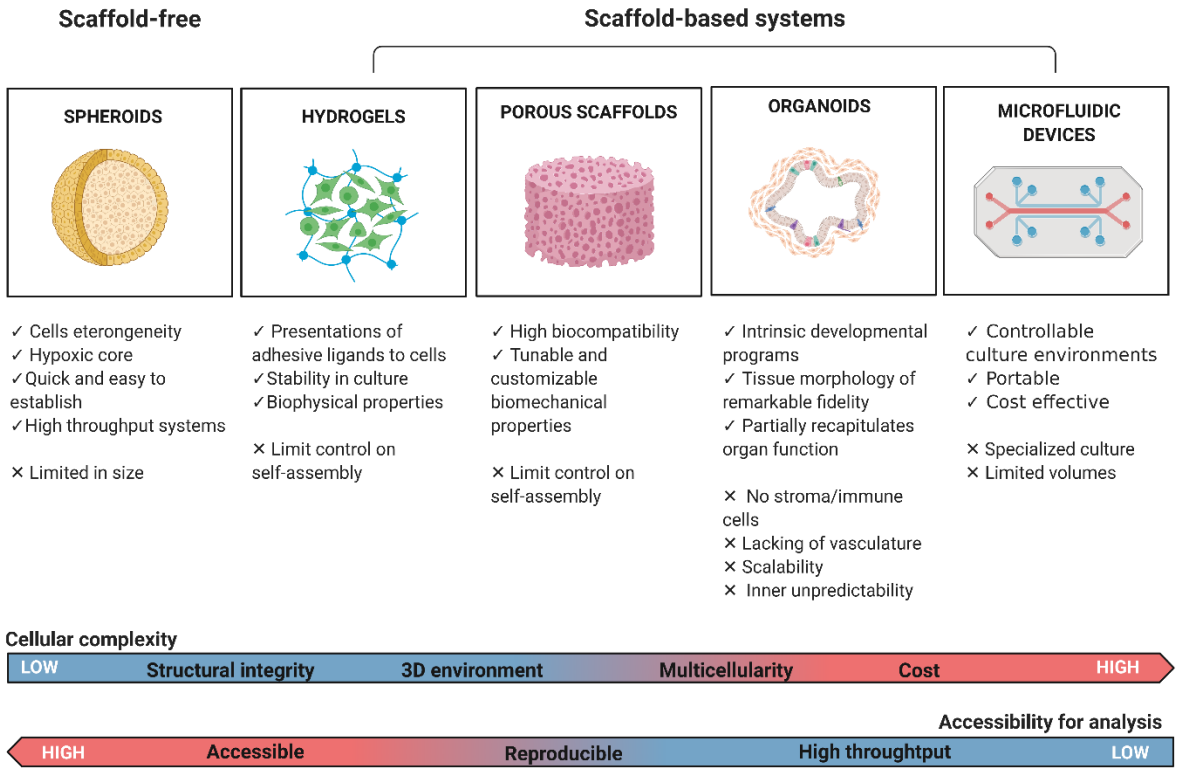

Figure 1.5. Classification of the most common cancer study models with their strengths and limitations. The primary mechanical tests performed on each platform are reported in italics. Biological and technical characteristics of the cancer model are highlighted. On the bottom, 3D *in vitro* systems cellular complexity and accessibility of imaging and analysis. Image made with Biorender.

1.2.5 Scaffold-free 3D models

1.2.5.1 Tumour spheroids

Spheroids are 3D aggregates of a single cell type or heterogeneous cell populations [209]. Cell-cell interactions orchestrate aggregate formation without the support of a scaffolding material while producing their own ECM. Four major techniques are used to induce tumour spheroid

formation *in vitro*: agitation-based techniques, liquid overlay techniques, hanging-drop techniques, and microfluidic reactors [210, 211]. These cultures allow for the recapitulation of important features of TME heterogeneity, such as oxygen gradients and immune infiltration, and they are relatively quick and easy to establish, representing a useful tool for high throughput systems [212]. However, they can be limited in size by the lack of nutrition diffusion to cells inside the cultures depending on the size, and the self-assembling process of cells [213, 214].

Overall, the transport of nutrients to the cells within a tissue in the body is facilitated by either convection of blood in the vascular system and within the interstitial fluid. In avascular tissues, like many of the 3D *in vitro* model developed, nutrient delivery rely on diffusion [215]. Diffusion characteristics present a significant limitation in many engineered tissues, particularly because gas, nutrient, and signalling molecule delivery to cells in cell cultures and tissue constructs is paramount for an optimal development and survival of these tissues [216] and can impact cells viability, differentiation, or function, i.e. lack of oxygen (hypoxia) [217, 218]. But oxygen gradients and hypoxia area can be successfully used to investigate tumour cell adaptations under hypoxia mimicking avascular tumour spaces, since both play key roles in tumour progression and resistance to treatment [219, 220]. For example spheroids exceeding 400 μm in diameter develop a hypoxic core and activate known survival signalling pathways to maintain cell viability [221].

Spheroids can be obtained from immortal cell lines, for example adenocarcinoma tumour cell lines (e.g., SKOV-3) and ovarian cancer metastatic cell lines (e.g., OVCAR-3) [222]. OVCAR-3 cells were recently used to create spheroids by forced floating in ultra-low attachment plates and hanging drop methods to perform drug response analysis with Paclitaxel, a common drug used to treat ovarian cancer. OVCAR-3 spheroids maintained the cell density and higher apoptosis behaviour of ovarian cancer, as well as higher resistance against Paclitaxel treatment when compared with 2D culture, closely mimicking the *in vivo* response [223]. Successful spheroids can also be generated from patient-derived tissue samples, such as 3D spheroid suspension cultures from radical prostatectomy specimens to model organ-confined prostate cancer. Cancerous tissue samples from radical prostatectomy specimens were excised by an uropathologist and preparation of 3D spheroids was done by mechanical disintegration and limited enzymatic digestion followed

by serial filtration. Spheroids formed successfully and stayed viable for up to several months serving as an innovative *in vitro* model of organ-confined prostate cancer [224].

To date, many kinds of spheroids have been developed, including neurospheres, mammospheres, hepatospheres, and embryoid bodies [225-227]. Spheroids can be easily analysed by imaging using light fluorescence, and confocal microscopy and many other techniques are being optimized to gain knowledge on the mechanical features of those systems. The next step forward will be to link mechanical features of the ECM to mechanosensing pathways in the cells, and potentially exploring the genomic, transcriptomic and epigenomic landscape affected by those changes. Furthermore, while the generation of 3D cultures can be more labour-intensive than 2D culture, the routine incorporation of these multi-cellular 3D spheroids into *in vitro* drug efficacy and toxicity testing could effectively bridge the gap between *in vitro* 2D assessment and animal models of disease, fast tracking drug screening and, hopefully, yielding more effective and less toxic drugs as future therapies [69].

1.2.6 Scaffold-based 3D models

1.2.6.1 Hydrogels for spheroids and organoids culture

Polymeric hydrogels are the most represented materials in the regenerative medicine literature and in terms of pharmacological applications, due to their multi-tuneable properties and structural similarity to native ECM [228]. A hydrogel is a 3D network structure composed of cross-linked polymer chains, which has the ability to absorb a large volume of solution. Native ECM is a prototypical hydrogel that promotes cell viability and direct cell adhesion, differentiation, proliferation, and migration through the controlled presentation of mechanical and biochemical cues. Mechanical strength, nutrient transport, topography, and degradation behaviour can be tuned using polymers with different composition, adjusting their crosslinking density and inclusion of bioactive molecules such as cell-adhesion ligands or proteolytic degradation sites [229-232]. General advantages of hydrogel systems include the ability to present adhesive ligands to cells either in native or modified gel, stability of the cultured cells, and the option to modify biophysical properties (e.g., elastic modulus) [233].

Hydrogels for cell culture can be naturally derived, including protein based (collagen, gelatin, silk fibroin, elastin fibrin), polysaccharide based (glycosaminoglycan, alginate, chitosan), a combination of materials like in Matrigel, or decellularized tissue derived [234]. On the other hand, synthetic hydrogel materials comprise polyacrylamide, polyethylene glycol (PEG), polyvinyl alcohol, and poly-2-hydroxyethyl methacrylate, and were first developed in the 1960s [235]. Naturally derived gels are biocompatible and bioactive but are hindered by inherent batch-to-batch variability and difficulties in tuning mechanics and biochemical properties, while synthetic hydrogels are highly reproducible and easy to manufacture, process, or tune for different mechanical studies [236, 237]. They can be degraded by cells and allow for ECM deposition, but as inert materials, they lack some of the native ECM complexity and biological signals, which therefore has to be implemented in those models [238].

3D hydrogel scaffolds can also be designed as platforms for growing complex tissue structures. Mammary-like tissues from primary patient-derived cells were grown on engineered hydrogel scaffolds that incorporated both the protein (collagen, laminins, and fibronectin) and carbohydrate (hyaluronan) components of human breast tissue. Cells rapidly self-organized in the absence of stromal cells and expanded within 2 weeks to form mature tissues containing luminal, basal, and stem cells in the correct topological orientation and also exhibited the complex ductal and lobular morphologies observed in the human breast [239]. A standard, widely used, 3D hydrogel system is Matrigel matrix. This platform is a BM extract (BME) consisting of collagen type IV, laminin, perlecan, etc. [240]. It represents an elective system to grow spheroid structures and as a medium for organoids culture establishments for many tumours, mimicking tissue morphology and unveiling new targets for therapy.

Organoid development was derived from the combination of engineering and biology, resulting in a platform with elaborate conformations of cells interacting in a multi-dimensional system inspired by the self-organizing features of an organ during development *in vivo* [241]. Organoid formation requires embedding and culturing of stem cells or progenitor cells (adult-tissue-resident cells or embryonic progenitors) in a 3D medium. The most used 3D media are Matrigel and Cultrex BME (a laminin-rich ECM secreted by the Engelbreth-Holm-Swarm tumour line) [242]. Once the cells

are encapsulated in the biomaterial, a cocktail of nutrient factors and signals drive the cells to differentiate within the 3D environment, closely resembling the tissue they were derived from [243]. This is considered to be one of the more physiologically relevant 3D culture models because it forms according to intrinsic developmental programs, resulting in remarkable tissue morphology fidelity; it can easily incorporate multiple cell types; and it partially recapitulates organ function [244]. This versatile technology has led to the development of many novel human cancer models, creating the possibility to indefinitely expand organoids starting from the tumour tissue of individuals suffering from a range of carcinomas or using CRISPR-based gene modification to allow the introduction of any combination of cancer gene alterations to normal organoids [245]. Organoids are powerful tools for modelling human organogenesis, homeostasis, injury repair, and disease aetiology, but their lack of vasculature, scalability problems, and inherent unpredictability in their self-organization processes represent some of the obstacles they face. Modelling tissue mechanobiology in those systems is fundamental to fully recapitulate tissue features [246].

To address this feature, nanoparticles (NPs) were adopted to engineer the mechanical microenvironment in organoids [247]. They can be dispersed in the matrix with a controlled distribution (local or global) and affect mechanical forces, but exhibit heterogeneity in magnitude and direction, similar to what occurs *in vivo*. NPs can also impose force at a cellular level after internalization by target cells. Modulation by NPs of the mechanical stresses imposed on tissues or cells through the control of the external activation field (electric, optical, acoustic, or magnetic) is continuous and reversible. For example, a magnetic field can allow for the directed assembly of gel-dispersed magnetic particles into chains, stiffening the mechanical properties of the microenvironment (modulation of storage modulus between ~0.1 and ~80 kPa reversibly), resulting in mesenchymal stem cells' increased proangiogenic potential and initiation of osteogenic signalling during early stages of culture on magnetically stiffened substrates [248].

A recent study reported that matrix stiffness has an impact on organoid growth and stem cell signalling in intestinal organoids. The authors reported employing a synthetic scaffold design, using a PEG backbone with a consistent and chemically defined synthetic hydrogel to allow reversible modulation of mechanics. Higher stiffness was initially required for YAP activation and intestinal stem cell expansion, and subsequently reduced stiffness, thanks to hydrolytically

degradable polymer incorporation, was needed to alleviate the accumulation of compressive forces and permit *in vitro* organogenesis [249].

In another study, intestinal stem cell colonies were encapsulated into allyl-sulphide hydrogels, and their survival was shown to be stiffness dependent, indicating mechanosensitivity. Because YAP/Notch signalling are key players in colony formation and crypt maintenance, they utilized controlled photodegradation to facilitate intestinal organoid differentiation, showing that the size and number of intestinal crypts was dependent on the extent of matrix softening [250]. As discussed, organoids recapitulate many structural and functional aspects of their *in vivo* counterparts. This technology is unique, based on the model's self-organizing properties, highly similarity to — and in some cases, histologically indistinguishable from — actual human organs [251]. Furthermore, if combined with immune cells and fibroblasts, tumour organoids can model the cancer microenvironment, enabling immune-oncology applications. In this exciting and evolving field, organoids can be also used to accurately predict drug responses in a personalized treatment setting [245].

1.2.6.2 Pre-made porous scaffolds

One of the very first approaches employed in tissue engineering was seeding therapeutic cells in pre-made porous scaffolds of biodegradable materials, and over time, researchers developed many different types of biomaterials for multiple applications and different techniques, such as two-phase emulsions and foams, freeze-drying or electro-spinning, and two-photon lithography [252]. In general, there are two different sources for porous scaffold biomaterials, namely natural and synthetic. Natural biomaterials can derive from ECM allografts and xenografts, which can create potential immunogenicity, or they can be made of organic polymers like proteins, polysaccharides, lipids, and polynucleotides. Their high biocompatibility promotes cell adhesion and attachment for excellent cell proliferation and survival. Interestingly, new sources of natural collagen-like materials found in marine sources, including jellyfish *R. pulmo* collagen, are effective for fabrication of 3D devices such as sponges, to mimic tissue architecture complexity for cancer

studies [253]. On the other hand, naturally derived scaffolds' mechanical properties are poor, so they require the addition of synthetic materials and crosslinking for physical stabilization [254].

To this aim, synthetic biomaterials (poly(ε-caprolactone) (PCL), poly(glycolic acid) (PGA), poly(lactic acid) (PLA), and their derivatives) have been developed to overcome some natural scaffolds' limitations, providing tuneable and customizable biomechanical properties, compositions, and geometry to tailor both soft and hard materials [255]. Additional coatings are usually required on those materials to improve their biocompatibility. The scaffold-based cultures provide a physiological context to cancer cells, addressing critical biological and mechanical cues needed to maintain morphological and genotypic tumorigenicity. For example, a 3D micro scaffold was realized by two-photon lithography to explore the role of β-catenin in both mechanotransduction and tumorigenesis. This model showed that 3D microenvironments are *per se* sufficient to activate β-catenin-dependent mechanosensing circuits that can boost breast cancer cell proliferation and invasiveness. They observed that the polymeric 3D cage-like structures initiate nuclear relocation of β-catenin and vimentin expression in epithelial/non-invasive MCF-7 cells [256].

In another study, researchers showed that culturing breast cancer cells in 3D scaffolds that mimic the *in vivo* tumour-like microenvironment enhances their metastatic potential. They used porous PCL scaffolds of approximately modulus 7 kPa, comparable to that of breast tumour tissue, on which MDA-MB-231 cells proliferated and formed tumoroids. Gene expression analysis revealed that cells growing in the scaffolds expressed increased levels of genes implicated in the three major events of metastasis (initiation, progression, and site specific colonization), including cell-cell & cell-matrix interactions and tissue remodelling, cancer inflammation, and the PI3K/Akt, Wnt, NF-κB, and HIF1 signalling pathways, compared to cells grown in conventional 2D tissue culture polystyrene dishes. The cells cultured in scaffolds showed increased invasiveness and sphere formation efficiency *in vitro*, and increased lung metastasis *in vivo* [257].

In line with the previous study, mixtures of rat tail and bovine dermal collagen type I at four different concentrations were used to assess the impact of 3D scaffold inhomogeneities on cancer cell invasiveness properties. Local inhomogeneities are discontinuities in the structure of the

networks. Researchers determined the elastic modulus with AFM in combination with pore size analysis using confocal laser scanning microscopy, which revealed distinct inhomogeneities within collagen matrices. Invasiveness of three breast cancer cell types on those scaffolds varied with different levels of matrix scaffold inhomogeneity, which also influenced the invasion depth that cancer cells achieved. Together, local matrix scaffold inhomogeneity, pore size, and stiffness of the collagen matrices can affect cell migration [258].

On the other hand, cancer cells directly affect the matrix structure. To investigate this, type-I collagen scaffolds have been used as an *in vitro* 3D biomimetic model to study the effects of MDA-MB-231 or MCF-7 breast cancer cells on matrix. MDA-MB-231, which belongs to the aggressive basal-like subtype, increased scaffold stiffness and overexpressed the matrix-modifying enzyme, lysyl oxidase (LOX), whereas luminal A MCF-7 cells did not significantly alter the mechanical characteristics of extracellular collagen. Mechanical testing was performed using a loading device built in-house to apply a state of unconfined uniaxial compression to the collagen scaffolds. When LOX activity was blocked, the ability of MDA-MB-231 to alter scaffold stiffness was impaired. This replicates the behaviour of *in vivo* orthotopic tumours generated by MDA-MB-231 in female immunodeficient mice, which was characterized by a higher collagen content and higher LOX levels than MCF-7 [259].

Overall matrix mechanics affect cell behaviour, but the local mechanical properties of single fibrillar components play a dominant role in regulating cancer cells. By independently controlling fibril diameter and intrafibrillar crosslinking of 3D collagen matrices, researchers showed how fibril bending stiffness instructs cell behaviour of invasive and non-invasive breast cancer cells. They reported that changing the fibril thickness or intrafibrillar crosslinking is sufficient to regulate cell behaviour over a broad parameter range in terms of morphology, clustering, and invasiveness. For example, higher collagen type-I fibril bending stiffness promoted a more elongated cell shape and higher invasiveness in MDA-MB-231 while decreasing clustering but increasing invasiveness in MCF-7 [260].

To conclude, matrix stiffness cues can be easily tuned in porous-scaffold systems, mainly by varying crosslinking type or percentage. Overall mechanics can be analysed by rheology or

tensile/compression testing, while AFM is easily run on the cells surface. These tests need to be further optimized not only for dry but also wet conditions, since the final model system includes both the scaffold's material and cells within liquid media.

1.3 Ovarian cancer

1.3.1 Ovarian Cancer Statistics and survival rates

Ovarian cancer is the seventh most common cancer in women (and the 18th most common cancer overall) worldwide [264]. In Europe among females, breast cancer has the highest proportion of cancer deaths (19.3% in 45–64 and 15.1% in 65+ years), followed by lung (17.9% and 13.7%), colorectal (9.4% and 14.5%), ovary (6.9% and 4.5%), and pancreatic (6.2% and 8.2%) cancers [262]. In USA ovarian cancer is the second most common gynaecologic cancer and causes more deaths than any other cancer of the female reproductive system [263]. Although ovarian cancer may occur at any age, it is more common in patients older than 50 years [265]. The 10-year survival is < 45% and has not improved significantly over the last 30 years [266]. Despite significant efforts, various screening and therapeutic strategies have generally not led to improved overall survival [267, 268].

1.3.2 Origin and disease sub-types

A major challenge to improved diagnostic and therapeutic intervention in ovarian cancer has been a limited understanding of the natural history of the disease [269]. Ovarian carcinoma is a highly heterogeneous group of diseases including different histological subtypes with distinct clinicopathological and molecular genetic features, divided in type I and type II [270]. Type I tumours are divided into three groups: i) endometriosis-related tumours that include endometrioid, clear cell, and seromucinous carcinomas; ii) low-grade serous carcinomas; and iii) mucinous carcinomas and malignant Brenner tumours and develop from benign extraovarian lesions that implant on the ovary, which can subsequently undergo malignant transformation. Type II tumours are composed, for the most part, of high-grade serous carcinomas which can be subdivided into morphologic and molecular subtypes: Immunoreactive, Proliferative, Differentiated, and

Mesenchymal (Mes), of which the Mes subtype – High-Grade Serous Carcinoma (Mes-HGSC) is associated with the worst clinical outcomes [271]. They are thought to originate from intraepithelial carcinomas in the fallopian tube even if some models show a direct evolution from secretory cells precursor cells in the fallopian tube [272] and others seem to primarily involve precursor cells in the ovary [273].

Disseminated from the ovary or fallopian tube, multicellular HGSC spheroids accumulate in the ascites and spread intraperitoneally within the abdominal cavity lining and into visceral tissues, especially the omentum [274, 275]. Metastasis to the omentum results in a transformation of the tissue, primarily composed of adipocytes, to an ECM-rich fibrotic TME, also called desmoplasia, histologically devoid of adipocytes [276] (**Figure 1.6**). Type II tumours present in advanced stage in >75% of cases. They are invariably high grade, develop rapidly, and are highly aggressive. High-grade serous ovarian carcinoma (HGSOC, the major Type II tumour) is the most common histologic subtype of ovarian cancer, accounting for three quarters of ovarian carcinoma [275, 277-279].

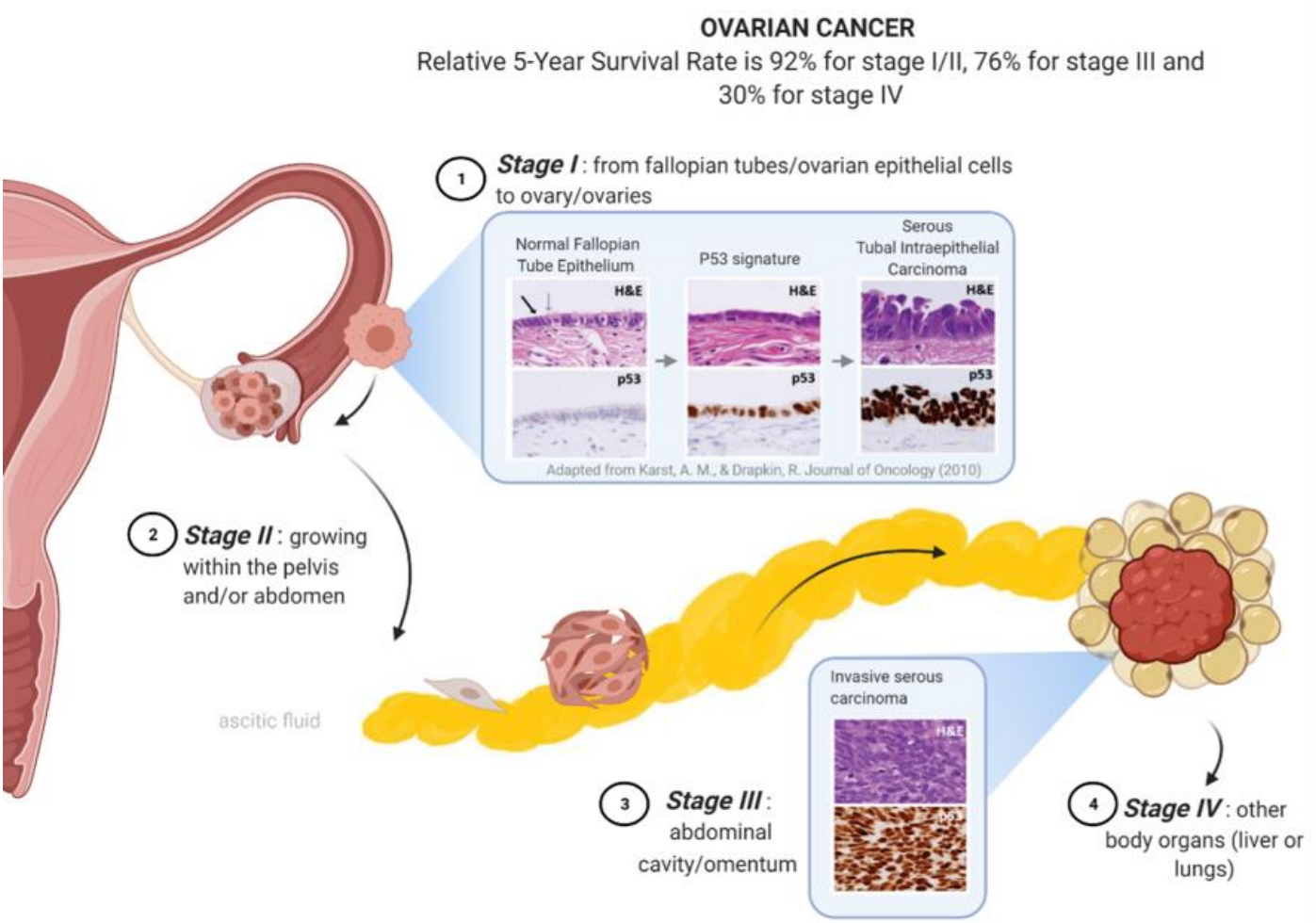

Figure 1.6. Ovarian cancer pathogenesis and progression. Image made with Biorender.

1.3.3 Staging and treatment guidelines

The Gynaecologic Oncology Committee of FIGO in 2014 and AJCC (American Joint Committee on Cancer) TNM staging system revised the staging of ovarian cancer, incorporating ovarian, fallopian tube, and peritoneal cancer into the same system [280]. Both classification systems use three factors to stage ovarian cancer: (i) The extent (size) of the tumour (T) (ii) The spread to nearby lymph nodes (N) (iii) The spread (metastasis) to distant sites (M). In parallel, the surgical staging is determined by examining tissue removed during an operation. Sometimes, if surgery is not possible the cancer will be given a clinical stage instead based on the results of a physical exam, biopsy, and imaging tests done before surgery (American Cancer Society, www/cancer/org). According to the FIGO system by the International Federation of

Gynaecological Oncologists, Stage I is the least advanced stage of ovarian cancer, indicating that cancer is localized only in your ovaries. Stage II cancer hasn't spread to lymph nodes or organs in distant parts of your body, but it has reached organs close to the ovaries. As well as nearby organs like the uterus and bladder, stage III cancer spread into stomach lining, the lymph nodes behind the abdomen, or both. The most advanced stage, stage IV indicates that cancer has spread to some distant organs.

Initial diagnostic tests include transvaginal ultrasonography and serum cancer antigen 125 measurement; however, these tests are not specific for ovarian cancer [265]. The current standard of care is based on surgical cytoreduction and platinum-based chemotherapy, but despite initial good response to the regimen, over 70% of patients develop platinum resistance within 5 years leading to short life expectancy [281].

1.3.4 Understanding the tumour microenvironment

The complex TME which accompanies ovarian cancer progression includes (1) primary tumour with tumour-associated stromal cells (fibroblasts and mesothelial cells) and inflammatory cells (macrophages and leukocytes); (2) non-adherent cells suspended in ascites with inflammatory and mesothelial cells; and (3) metastases to various parts of peritoneal cavity that contact mesothelial cells, adipocytes and fibroblasts at the metastatic site. This heterogeneity of cell types likely impacts tumour histology, growth potential and ability to evade chemotherapy [282, 283]. ECM co-evolves with ovarian cancer cells functions from tumorigenesis to metastases.

In HGSOC, representing the vast majority (75%) of total ovarian cancers, "Fibrosis" or "Mesenchymal" HGSOC molecular subtypes have been identified in all studies and are systematically associated with poor patient survival. This presentation is characterized by high stromal content composed of myofibroblasts and ECM proteins, such as collagen and fibronectin, major causes of tumour stiffness [284]. Indeed, it is known that tumour stiffness is associated with a high content of myofibroblasts and matrix remodelling, consistent with many studies in human HGSOC [285-289]. Interestingly, matrisome signatures were found to correlate with poor overall survival (OS) in patients with HGSOC. For example, a 10-gene signature (*AEBP1, COL11A1,*

COL5A1, COL6A2, LOX, POSTN, SNAI2, THBS2, TIMP3, and VCAN) that encodes ECM proteins involved in collagen remodelling has been identified and validated. Expression of the signature genes is regulated by TGF-β1 signalling and is enriched in metastases in comparison with primary ovarian tumours [290].

Strong association between the density of α-SMA and α-FAP positive cells, two markers commonly associated with activation of cancer associated fibroblasts, and disease score was found in ovarian cancer [291, 292]. Another matrix-associated gene list, the matrix index, significantly correlated with ovarian cancer disease score and tissue modulus, linking cancer malignancy to tissue mechanics. Indeed, significant positive correlations between tissue modulus and disease score in the evolving ovarian cancer TME suggested a close association of tissue stiffness with disease progression and genes associated with cell metabolism, cell communication, wound healing, ECM organization, as well as development, correlated with tissue modulus [292].

1.3.5 Preclinical models for ovarian cancer

One reason for the slow progress made in understanding the biology of ovarian cancer (OC) and translating that knowledge into substantial clinical benefits has been a lack of clinically representative model systems that mimic the progression of the human disease. Indeed, the heterogeneity of 'ovarian cancer' entity, the debate around its origin and the intraabdominal metastasis at the time of diagnosis, pose special challenges to the development of model systems [283]. The two commonly used experimental systems for *in vivo* studies of ovarian cancers are genetically engineered mouse models (GEMMs) and the spontaneous, naturally occurring laying hen model.

All mouse models are genetically induced since experimental mouse strains do not spontaneously develop ovarian carcinomas [293]. Originally, most GEMMs used Cre-lox technology to mutate genes involved in ovarian cancer pathogenesis in the ovary surface epithelium (OSE) but other models have been generated by mutating the secretory cells in the FTE to allow comparison of the effects of genetics and cell of origin on the cancer phenotype [294, 295]. However there is no

spontaneous, genetically similar model of ovarian cancer that parallels the human condition [296], therefore evolution in our understanding of OC initiation, progression and early stages of metastasis is hampered by the need for improved genetic models [297]. The laying hen is the only species besides humans that spontaneously develops ovarian carcinomas at a significant frequency, it is age-related and it is also grossly and histologically similar to that in humans and it metastasizes to similar tissues to women; with an accumulation of ascites fluid, holding promises for ovarian cancer research if additional research tools for the study of this model are developed [298].

Even if most of our knowledge of OC biology to date relies on experiments using cancer cells grown in two dimensions on plastic, studying OC initiation, progression and metastasis in a three-dimensional (3D) system has many advantages. 3D models can incorporate ECM and stromal cells allowing detailed analysis of the contribution of stromal elements to cell adhesion, invasion, and nutrient access; and to assess the influence of the TME on tumour cell survival, proliferation, and differentiation.

Several 3D models have been developed to investigate different stages of the cancer progression. Initial strategies replicated the submesothelial matrix penetration stage, using matrices of collagen or Matrigel mixed with ovarian cancer cell lines [299]. Then spheroids or multicellular aggregates models were developed to mimic the metastatic unit of cancer cells which can be isolated from patient ascites [300]. Another 3D model of OC metastasis, referred to as 3D 'mesothelium-mimetic' or 'omentum-like', include both mesothelial cells and the sub mesothelial ECM interspersed with primary human peritoneal fibroblasts, closely mimicking the superficial layer of the peritoneum ('mesothelium'), replicating OC metastasis steps including adhesion, proliferation and invasion [301]. Using primary human fibroblasts extracted from normal human omentum and cancer cell lines, researchers prove that in the early steps of ovarian cancer metastasis to the human omentum, omental mesothelial cells inhibit, while omental fibroblasts and the ECM enhance, the attachment and invasion of ovarian cancer cells [302]. This model can also be implemented by including other cells type such as adipocytes and macrophages to test treatment effect on the complex tumoral cell microenvironment population [276]. Another interesting model used *ex vivo* human or mouse peritoneal or omental explants to evaluate OC tumour cell interactions with intact peritoneal tissue [303]. Gaining more and more interest, patient-specific cancer organoids are

thought to faithfully recapitulate the biological properties of their tumour of origin. Tumour-derived organoids are derived from resected human tumour biopsy. After processing, adipose-derived mesenchymal stromal or adipose-derived stem cells (ASCs) are retrieved from the biopsy, allowing for the generation of organoids [242].

Ovarian cancer organoids were successfully established in < 3 weeks, capturing the characteristics of histological cancer subtypes and replicated the mutational landscape of the primary tumours [304, 305]. Among many advantages they proved to preserve tumour heterogeneity [306]; using the CRISPR/Cas9 technique, their genome can be manipulated to introduce disease-associated mutations for disease modelling [307, 308]. One of the major limitations of current organoid technology is the lack of microenvironment, a problem which is under investigation in research for a so-called "next-generation organoids", including stromal and immune cells within the organoids or using a microfluidic platform to fully mimic the *in vivo* state [243, 306, 309].

Regardless of the complexity achieved by 3D culture modelling there is still a lack in models that contribute to the understanding of the very earliest events in OC metastasis, the shedding of cells from the primary tumour; but also a meaningful and comprehensive model which will combine biological complexity and mechanical features of disease progression at different stages. Furthermore, another challenge will be adaptation of these 3D and organotypic models to a high-throughput format to facilitate drug screening.

1.4 Motivation and research aims

Biological tissues often experience drastic changes in their microstructure due to their pathophysiological conditions. Such microstructural changes could result in variations in mechanical properties, which can be used in diagnosing or monitoring a wide range of diseases, most notably cancer. Non-invasive techniques, i.e. shear wave elastography (SWE) and magnetic resonance elastography (MRE) [310-312], are currently used in clinic to characterize healthy and diseased tissues *in vivo* but these methods have drawbacks mainly related to the complex structure of the tissues and the location of the organs away from the source of excitation [310, 313].

Assessment of mechanical properties on *ex-vivo* samples, allows more accurate and quantitative evaluation of tissue mechanical abnormalities. While AFM holds the advantage of indentation measurement using a small volume of tissue and high resolution at the single-cell level [314], shear rheometer can be coupled for bulk tissue mechanics, providing promising tools for cancer diagnosis and to assess potential anticancer effectiveness [315-317]. To mimic *in vivo* mechanical changes in a 3D *in vitro* model, sponge scaffolds a technology borrowed from regenerative medicine applications [318] are employed here, and tuned to replicate mechanic features of cancer environment (stiff) and its normal counterpart (soft). These sponge scaffolds were then seeded with fibroblast and/or human ovarian cancer cell lines, to better dissect the function of ECM mechanics on two important compartments implicated in tumour progression, namely the stromal and cancer cells.

Study Hypothesis. The hypothesis for this thesis states that tuneable porous collagen scaffolds are (a) suitable and (b) add significant value to the investigation of the role of the mechanical microenvironment in driving stromal compartment roles and OC tumorigenesis as well as primary cancer metastatic progression and therapeutic resistance. To test this hypothesis, a series of interdisciplinary investigations are conducted combining sponge scaffold fabrication and characterisation with stromal and OC seeding, and downstream analysis, utilising cellular and molecular techniques to decipher important cellular differentiation processes observed in Ovarian Cancer.

Aims and objectives

1. Fabricate a flexible sponge scaffold which enables ECM stiffness and composition to be mimicked. Mechanical and structural characterization of the scaffolds. Adhesion, proliferation, cellular migration, and biocompatibility evaluation.
2. Utilize soft and stiff scaffolds to mimic a fibrotic/desmoplastic tissue and normal counterpart to test normal fibroblasts and activated fibroblasts migration, contractility, whole transcriptome analysis. Analysis of OC SKOV.3 cell line conditioned media effect

on fibroblasts activation on soft scaffolds to establish a model to study the genesis of desmoplastic response.

3. Matching soft and stiff mechanical properties of the scaffolds to corresponding mechanical parameters of normal and ovarian cancer tissue biopsies. Utilise these systems to investigate the molecular signatures of ovarian cancer cell lines with different metastatic potential. Test the effect of scaffold rigidity on migration, proliferation, morphology, and drug response. Evaluate soft scaffold suitability to accommodate coculture of stromal and ovarian cancer cells to recreate TME complexity for drug testing.
4. Compare and contrast traditional mammalian sponges with alternative sustainable sources of collagen (jellyfish, as part of KESS funding) for ovarian cancer 3D model establishment.

Chapter 2: Bioengineering porous scaffolds for 3D cancer research

2.1 Introduction

In cancer research, 2D cellular models have long represented the gold standard *in vitro* methodology, however they fail to represent the complexity of the TME and have more recently been overtaken by more complex 3D culture methods [319-322]. Many of these 3D studies have demonstrated that cancer cells interact extensively with their cellular, biochemical and biophysical microenvironment during proliferation, angiogenesis, metastasis, and chemo- or radiotherapy [323-328].

Centred on biotechnology and tool fabrication, tissue engineering practices provide opportunities to create 3D functional constructs for many applications such as tissue repair or stem cell biology studies, as well as offering great potential for disease model development [329]. Indeed, creating 3D environment(s) that mimic organ(s) or tissue(s), provides meaningful platforms to investigate distinct cancer-microenvironment crosstalk, such as cell-cell populations, cell-ECM and the effect of drug or specific interventions such as gene knockouts that may link gene/protein expression to specific microenvironment functions [330]. These tissue models will never be implanted directly into patients however, they can transform the way we study human tissue physiology and pathophysiology *in vitro*, ultimately providing enhanced disease understanding through patient-tailored therapies that prevent or cure underlying disease.

Established by decades of research, three crucial components (named the TE triad) are needed in order to create an effective 3D construct, a relevant selection of cells, a biomaterial scaffold that provides the structural support for cell attachment and guides tissue development [329], and a network of bio-chemical and biophysical signals that enable crosstalk between cells and scaffolds, to ultimately recreate tissue [331, 332]. Over the last two decades four major scaffolding approaches have evolved for TE, in the form of pre-made porous scaffolds, decellularized extracellular matrix (ECM), cell sheets with self-secreted ECM, and/or cell encapsulation in self-assembled hydrogel matrix [254]. Among these, the most common approach is the use of a pre-

made porous scaffold [332]. This approach harbours a number of advantages, from having the most diversified range of biomaterials available to use, both natural or synthetic [333]; the ability to introduce precise architectural features and microstructures [334]; and the ability to tune scaffold physicochemical characteristics to mimic the physical properties of native tissues [318].

When compared directly to the poor mechanical properties of hydrogels, porous scaffold approaches are well matched to research in tissues that have load-bearing functions or in any tissue where mechanical properties are thought to play a central role in the cellular differentiation processes under investigation [254, 318]. Indeed, easy to reproduce, convenient to handle, and amenable to large-scale use, porous scaffolds now have a wide scope of tissue biology applications [335-338].

In oncology, however, only a few solid tumour microenvironments have been modelled using these approaches. Elements of breast, prostate, and glioblastoma tumours have been investigated using chitosan-alginate or chitosan-hyaluronic acid based-scaffolds for example [323, 339-344]. These scaffolds belong to the category of ‘natural biomaterial, are biologically active and typically promote excellent cell adhesion and growth (26-31). The most representative natural polymer available however, is collagen, which is the most abundant ECM scaffold protein in connective tissues, basement membrane, skin, vascular tissue, brain, spinal cord and many other tissues in the human body [345, 346]. ECM is mainly composed of two classes of biomolecules: fibrous proteins which include collagen, fibronectin, and laminin, and glycosaminoglycans (GAGs), most often covalently linked to protein forming the proteoglycans, such as hyaluronic acid (HA) [347]. Collagens contribute to tissue physical properties and resist tensional forces, while GAGs control hydration by attracting water, due to their polyanionic nature, allowing matrix resistance to compressive forces [348-350].

Finely tuned during homeostasis, changes in ECM composition and remodelling, as well as rate of degradation and deposition, strongly characterize cancer tissues [16]. Increased matrix deposition, matrix remodelling by forces from cancer cells and stromal fibroblasts, matrix crosslinking, increased cellularity, and the build-up of both solid and interstitial pressure, are among the many factors contributing to increased tumours stiffness [351]. As a result, ECM

dysfunctions have been shown to lead to significant differences in stiffness between normal and diseased states of the same tissue type. Benign breast tissue for example has a Young's, or elastic modulus in the low hundreds of pascals (Pa) while average breast tumour stiffness is ~4 kPa; brain tissue is usually in the 10s of range, while brain tumour stiffness has been shown to span up to over 10 kPa; similar trends have been observed in prostate (2 fold increase in prostate cancer tumour stiffness), while the stiffness of mineralized bone in the metastatic niche is ~106 kPa [14, 91, 323, 352-354].

Importantly it is not only ECM composition, but also the architectural organization and degree of crosslinking of components such as collagen and HA, that dictate the mechanical properties of the ECM, controlling how mechanical forces are transmitted to cells [355]. Together with increased collagen crosslinking, increased HA accumulation is a hallmark of almost all diseases in which inflammation and/or fibrosis occur, especially tumour growth and metastasis [356-359]. In pathological settings such as inflammation, local HA production increases substantially [360, 361] and anti-inflammatory, anti-tumorigenic high-molecular weight HA (HA HW, defined as $>5 \times 10^5$ Da) is rapidly catabolized resulting in the presence of fragmented, low-molecular weight HA (HA LW, defined here as <200 kDa) [362-364]. Upon the resolution of inflammation, both the amount and size of HA return to basal levels [365], however, in chronically inflamed tissues such as tumours, shorter HA polymers predominate over a sustained period of time [366].

2.1.1 Mechano-testing: technologies to approach biophysical studies in 3D cancer modelling

The studies of mechanics in 3D systems for cancer research has enabled researchers to develop better technologies and adapt protocols from material science to cancer biology. So far, at a cellular level, mechanics can be measured with methods probing stiffness at the nano-scale and micro-scale, including micropipette aspiration [367-369] and optical stretcher [370] for measuring mechanics of whole cells in suspension, and atomic force microscopy (AFM) for the investigation of single adherent cells [371-374]. For example, many studies used AFM on different types of epithelial cancer cells, showing that cancer cells are generally softer and display lower intrinsic variability in cell stiffness than non-malignant cells [375, 376]. Furthermore, AFM was successfully applied to measure the mechanics of tumour spheroids to promote understanding of

tumour growth in confined environments, showing that tumour spheroids grown in stiff hydrogels were significantly stiffer than those grown in compliant hydrogels [377]. In addition, AFM can reveal the mechanical dynamics of the basement membrane during the invasion process of tumour cells. Morphological imaging by AFM showed that the basement membrane cultured with cancer and stromal cells had higher roughness and more holes during the tumour breaching process but become softer upon cancer cell and fibroblast growth, clearly suggesting basement membrane mechanics are dynamic during cancer invasion and metastasis [378].

Elastic and viscoelastic properties of tissues, cells, and ECM are typically measured using rheology, the study of flow and deformation of matter, to characterize both the elastic (G′, storage modulus) and viscous (G′′, loss modulus) behaviour. Rheology measurements provide an interesting tool to study the interaction between forces and the flow/deformation of materials that exhibit a combination of elastic, viscous, and plastic behaviour, such as normal and tumour tissues [379, 380]. Tissues are composed of colloidal particles, filamentous polymers, and other supra-molecular arrangements, leading to complicated deformations in response to mechanical stress. Rheological measurement probes the mechanical responses of viscoelastic medias but also establishes predictions for mechanical behaviour based on the micro- or nanostructure of the material [381]. Finally, bulk compression or tension analysis is used to measure the elastic modulus (E; Young's modulus), which relates to the architecture of the bulk tissue or the 3D model under investigation [382-384].

Overall mechanical properties of a tissue are meaningful in assessing physical characteristics during processes such as cancer development [385]. Although the TME is of critical importance during initiation and spread of cancer, relatively little is known about its biophysical evolution and how it impacts nuclear processes inside the cells like epigenetic regulation, which have direct consequences on gene expression. Unfortunately, there are few reports addressing the link between tissue mechanics and epigenetics in 3D systems, but we hope that this link will be filled by the growing interest in the field and technological advances. In the following sections, the latest achievements in the field of 3D culturing systems used for dissection of solid tumour TME mechanical changes and reported effects on cancer and stromal cell gene expression, behaviour, and epigenetic machinery.

Utilising a porous scaffold to mimic cancer tissue microenvironment stiffness could help understand the interplay between cells in the TME and the biophysical signals of the ECM, offering new understanding of cell-ECM cross talk and ultimately to molecular targets of disease and novel therapeutic avenues. To replicate native tissues, scaffold constructs must be biocompatible for cellular doping and incorporate mechanical properties/architectural features that enable cells to attach, sense biophysical cues, proliferate, migrate and remodel the matrix, freely and without interference [327, 386, 387]. One cell type shown to be essential in cell-ECM interactions in tissue biology, fibrosis and cancer are activated stromal cells, inclusive of diverse populations dependent on their origins and expression profiles [388] [389]. These stromal cells play an important role in tissues characterised by high matrix stiffness, such as in lung fibrosis [390], but also play an essential role in cancer evolution, as shown in breast cancer [391], pleural mesothelioma [390], lung cancer [392], pancreatic cancer [393] and liver cancer [394].

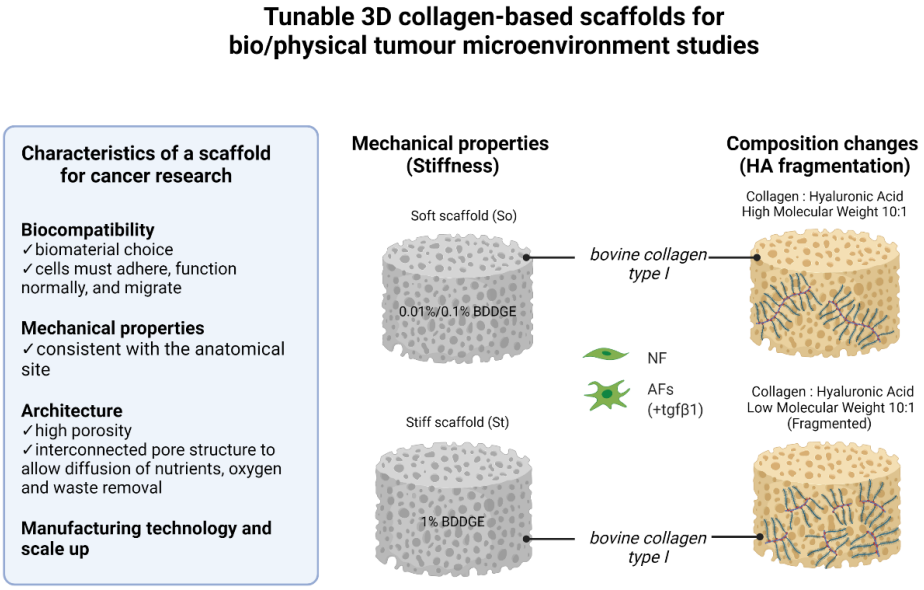

Figure 2.1. Schematic representation of scaffolds properties and fabrications to mimic normal and pathological tissue mechanical and biological characteristics. Image made with Biorender.

In this chapter, two distinct strategies are used to explore collagen scaffold suitability to model the differing ECM stiffness gradients observed between normal and pathological tissues. First, 1, 4-

butanediol diglycidyl (BDDGE) was used to crosslink collagen-type I based scaffolds to reproduce normal and pathological mechanical stiffness features of human tissues. Both stiff and softer scaffolds were tested for fibroblast cell (MRC-5) biocompatibility using normal (NFs) and TGFβ1 activated fibroblasts (AFs) (**Figure 2.1**). In parallel, increasing concentrations of HA LW combined with collagen-type I scaffolds were utilised to obtain a scaffold resembling an ECM with distinct pathological features such as the presence of HA LW and higher stiffness (>kPa). Following optimization, a scaffold that replicated normal tissue characteristics was fabricated using HA HW, to ultimately evaluate both NF and AF behaviour in a diseases-HA LW-stiff vs normal-HA HW-soft microenvironment (**Figure 2.1**). Both the scaffolds fabricated in this chapter combine both biological and mechanical aspects of native tissues (**Fig. 2.1**). Even if 3D cell culture approaches (gel systems and spheroid cultures) have dramatically improved our understanding of the role of 3D culture on tumour cells [395-397], there still exists a need for innovative 3D - models that are capable of recreating distinct tumour mechanical characteristics, that allow for *in vitro* tumour modelling under well-defined and reproducible conditions.

2.3 Results

2.3.1 Strategy 1: Porous collagen scaffold stiffness gradients

2.3.1.1. In vitro scaffold mechanical properties mimic normal and pathological tissues in vivo

Increased tumour and stroma stiffness represents one of the latest updates among the hallmarks of cancer [16]. As evident in the use of palpation for the detection of breast tumours and cancerous lymph nodes in the case of lymphomas, increased stiffness in other tissues such as liver, pancreas, prostate, and lung, has also been linked to disease progression [91, 398, 399]. 1,4-butanediol diglycidyl ether (BDDGE) was employed here to cross-link bovine-derived collagen type I scaffolds. The epoxy groups of this reagent are able to react with both amine and carboxylic acid groups under acidic conditions ($5 < pH < 6.0$) evoking a reaction between epoxide groups and carboxylic acid groups of collagen [400].

Macroscopical imaging of the whole scaffolds showed a porous matrix with interconnected fibres (**Figure 2.2A**). The effect of 1, 0.1%, 0.01 wt% BDDGE concentration effect on scaffold storage and Young's modulus was evaluated using rheology and AFM respectively (**Figure 2.2**). Rheological analysis showed significantly increased storage modulus in the 1%wt (11.27±0.62 kPa) and both the 0.1%wt (3.63±0.46 kPa) and 0.01%wt (1.81±0.24 kPa) BDDGE ($p<0.0001$) counterparts. Similarly, the difference between 0.1%wt and 0.01%wt BDDGE was also statistically significant ($p<0.01$) (**Figure 2.2B**).

These patterns of stiffness gradient dependent on %wt BDDGE were shown at the nanoscale using AFM analysis, reporting a significantly increased Young's Modulus between 1%wt (144.98±10.99 kPa) and both 0.1%wt (15.32±0.32 kPa) and 0.01%wt (4.35±0.577 kPa) ($p<0.0001$). Similar to the bulk property stiffness, 0.1%wt scaffolds were significantly increased compared to the 0.01%wt BDDGE as well ($*p<0.1$) (**Figure 2.2C**). Based on their mechanical properties, at both bulk and nanolength scale, BDDGE collagen scaffolds represent a meaningful and suitable system to model tissue stiffness in pathological conditions, since both storage modulus and young modulus spans within the range of stiffness reported in the literature for normal and pathological tissues [284, 401-403].

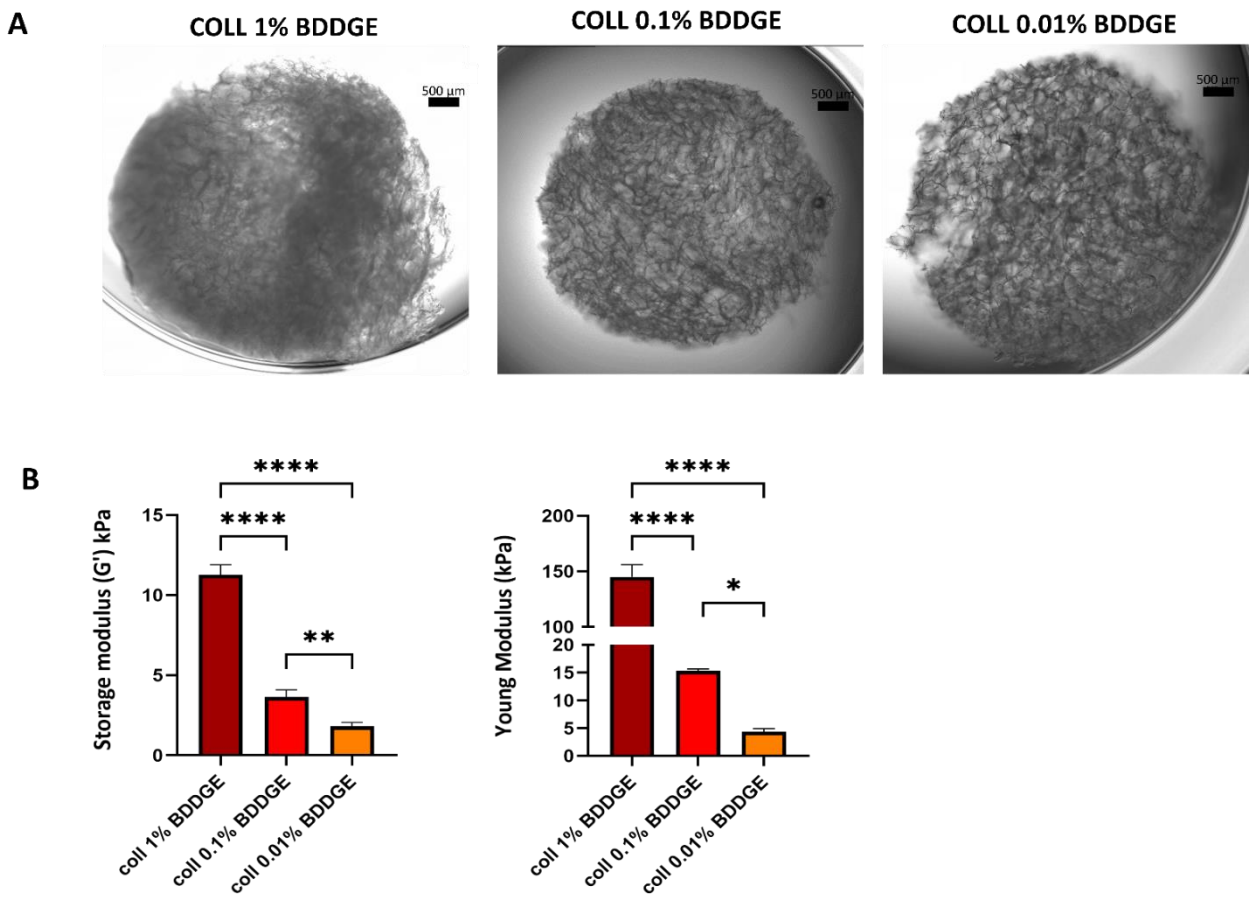

Figure 2.2. Mechanical features of collagen I-scaffolds fabricated using different percentages of crosslinker 1,4-butanediol diglycidyl ether (BDDGE). (A) Brightfield pictures obtained by imaging stitching on digital fluorescence microscope. (B) Storage modulus analysis (kPa) of 1%-0.1%-0.01% BDDGE scaffolds using rheometer (C) Young's modulus (kPa) analysis 1%-0.1%-0.01% BDDGE scaffolds by AFM. Data are mean + standard deviation (n=3). Ordinary one-way ANOVA, ****p<0.0001, **p<0.01, * p<0.1.

2.3.1.2 BDDGE crosslinking doesn't interfere with scaffold porosity organization and chemical/thermostability

Interconnected pores in the scaffold architecture are known to improve mechanical properties, supporting cell growth while enabling nutrient exchange and waste removal [386]. The porous structure of MS and NS after freeze-drying was determined by SEM imaging. At lower magnification, scaffold sample structures are composed of interconnected pores with boundaries

defined by sheet-like structures of fibrillar collagen. At higher magnification, the typical fibrous substructure of collagen sponges can be appreciated (**Figure 2.3A**).

FTIR and TGA were used to characterize how BDDGE crosslinking interfered with collagen composition and determine the material's thermal stability. FTIR spectral analysis showed the characteristic collagen signature with absorption peaks for the amide I (1700–1600 cm^{-1}), amide II (1600–1500 cm^{-1}), and amide III (approximately 1200–1300 cm^{-1}), referring to C=O, N–H and C–N, respectively (**Figure 2.3B**). For TGA analysis, all collagen scaffolds underwent endothermic reaction at around 50°C (evaporation of the water moisture present in the material), while thermal transition and material degradation happened after 100°C of the heating ramp, regardless the percentage of crosslinker used (**Figure 2.3C**).

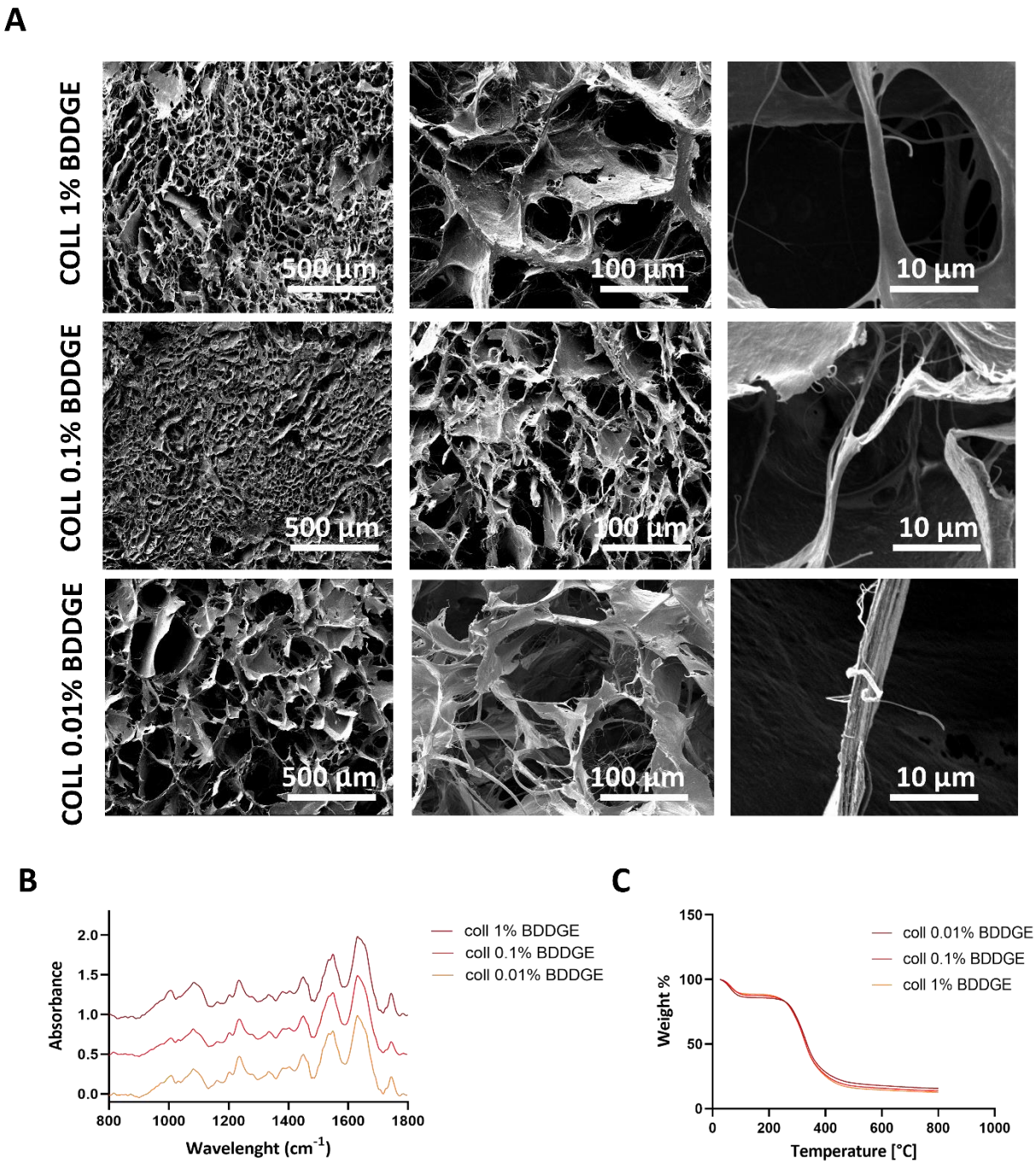

Figure 2.3 SEM imaging of the chemical characterization of collagen I-scaffolds fabricated using different percentages of BDDGE. (A) SEM imaging of scaffolds at different magnifications. (B) FTIR spectra of 1%-0.1%-0.01% BDDGE scaffolds. The spectra highlighted the presence of typical collagen Amide I, Amide II, and Amide III. (C) Thermo gravimetric Analysis (TGA).

2.3.1.3 BDDGE crosslinking doesn't interfere with scaffold biocompatibility

The scaffold biomaterial employed and its structural characteristics can influence cellular viability and adhesion [404, 405]. To assess scaffold biocompatibility, MRC-5 cells were selected, as fibroblast cells have proven to be essential in cell-ECM interactions in tissue biology, fibrosis, and cancer [406]. Cellular viability on the scaffolds was assessed using calcein/EtBr staining and the percentage of live and dead cells assessed using flow cytometry and fluorescence microscopy (**Figure 2.4**). When analysed quantitatively for viability, using calcein/EtBr live-death staining, MRC5 were viable across all the scaffolds and 2D controls, showing 82.5 ± 6.6; 82.9 ± 6.3; 79.7 ± 5.9; 76.4 ± 9.7 for coll 1%-0.1%-0.01% BDDGE and 2D respectively (**Figure 2.4A-C)**.

Fibroblasts were able to attach to, and colonize the scaffolds, as reported by the 3D maximum intensity projection based on 3 layers collected per scaffold, calcein/EtBr live-death staining showed that cells were viable after 7 days of culture (**Figure 2.4D**).

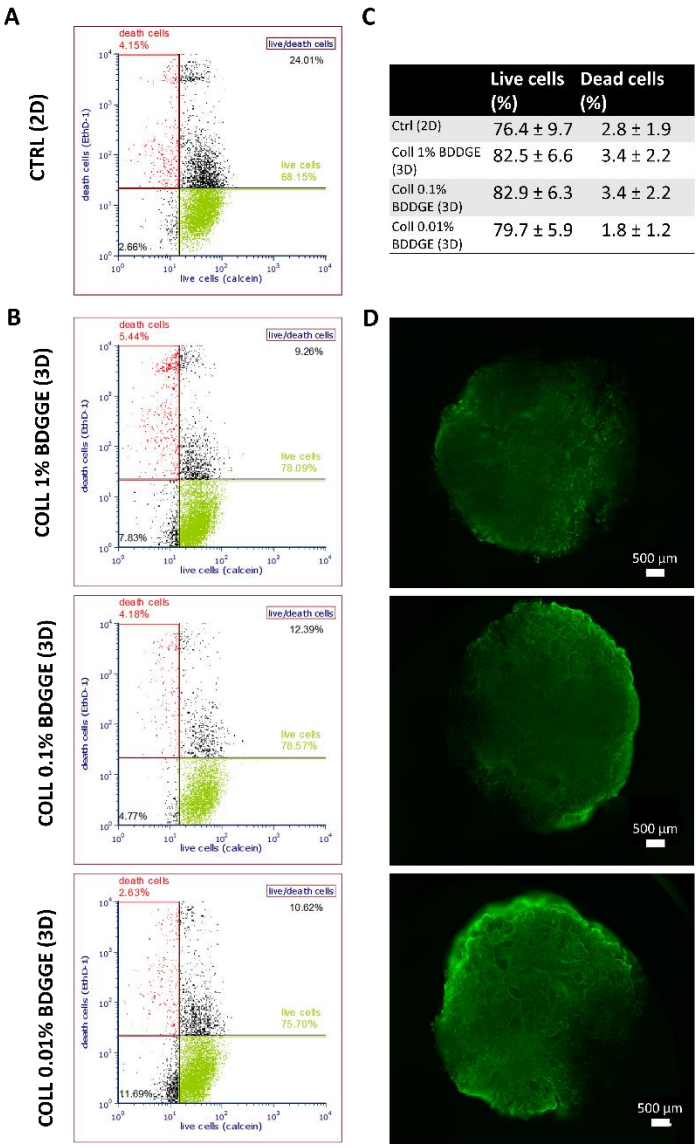

Figure 2.4. Fibroblasts MRC5 were viable and adhere on 1%-0.01%-0.001% BDDGE scaffolds. (A) 2D cell death representative staining analysed with flow cytometry. (B) 3D cell death representative staining analysed with flow cytometry. (C) Quantification of 2D and 3D cell death staining. (D) 3D cell death staining recorded with fluorescence microscopy. Analysis and imaging were performed after 7 days of culture. Scale in images of whole scaffold: 500 µm.

2.3.1.4 Activated Fibroblasts proliferate and soften the stiff (1% BDDGE) sponge scaffolds

In many pathological conditions, such as heart and lung, cancer fibroblasts secrete large amounts of the cytokine transforming growth factor-TGFβ1 which activates fibroblasts, mediating ECM remodelling and fibrosis [407, 408]. In this study, fibroblast activation in AFs was detected by the expression of fibroblast associated protein (FAP) with flow cytometry and activated α smooth muscle actin (αSMA) using Western Blot analysis. FAP is a serine protease that is not expressed in most normal tissues, with the majority of FAP expressed by activated fibroblasts (AFs) responding to the pathologic situations [34, 409]. Another biomarker expressed by all myofibroblasts is α-SMA, which has been found to be upregulated in lung fibrosis and cancer, and evaluated as novel non-invasive serological biomarker for lung disorders by providing a surrogate measure of activated fibroblasts [410].

To test scaffold suitability for stromal studies in pathological and normal mechanical conditions, normal fibroblasts (NFs) were first activated into activated fibroblasts (AFs) using TGFβ1 [409, 411, 412]. TGFβ1 titration was performed using increasing dose of TGFβ1 (0–50 ng/ml) and analysis performed at day 7, evaluating FAP (**Figure 2.5A**) and α-SMA (**Figure 2.5B**) expression. Expression of FAP, followed by flow cytometry, increased under all treatments with 25, 50, 100 ng/ml of TGFβ1. FAP expression seemed to reach a plateau after the lower dose, 25 ng/ml (**Figure 2.5A**). Similar results were obtained for αSMA protein expression, analysed by western blot. No basal expression of αSMA was detected, while an increase in its expression was already induced after 25 ng/ml of TGFβ1 (**Figure 2.5B**). No stats provided. The lower dose, effective in inducing both markers, was selected as elective dose for AF activation in all further experiments.

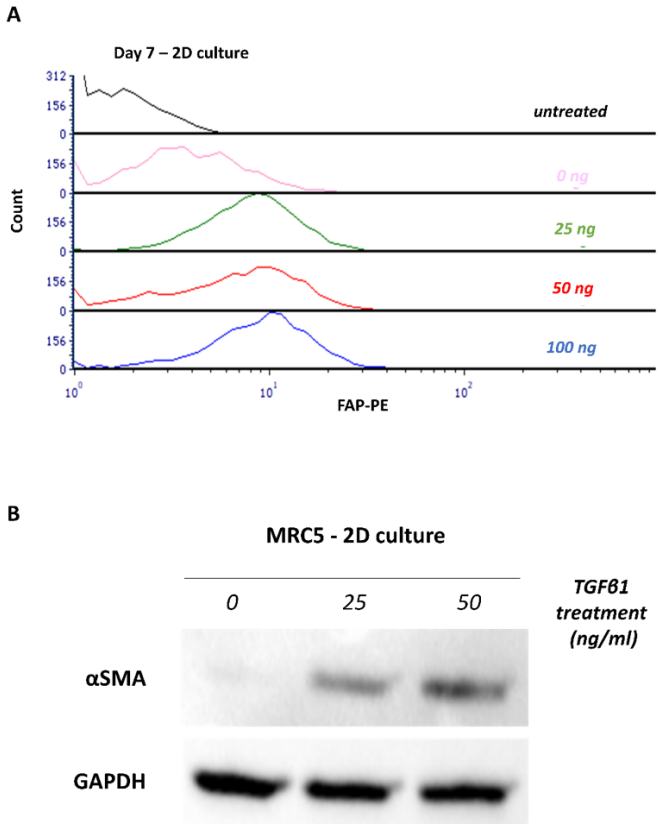

Figure 2.5. TGFβ1 treatment stimulated conversion of NFs into AFs (2D culture). (A) FAP expression after 7 days on 2D culture under TGFβ1 titration 0-25-50-100 ng/ml, assessed by flow cytometry. (B) αSMA protein expression after 7 days on 2D culture under TGFβ1 titration 0-25-50 ng/ml, analysed with western blot. The housekeeping gene GAPDH was used as an internal control. n=1 reported.

The proliferation rate of both NFs and AFs was evaluated on 1%-0.1%-0.01% BDDGE scaffolds, with standard 2D cultures being used as controls. To evaluate cellular proliferation following activation we employed Pico Green assay, an ultra-sensitive fluorescent nucleic acid stain for quantitating double-stranded DNA (dsDNA). The measured amount of dsDNA can then be used as a marker for cell proliferation [413]. 2D cultured cells, showed similar proliferation rates for both NFs and AFs with an increase of 3±0.5 at day3 and 6.8±2.6 at day7 for NFs and 3.2±1.46 at day3 and 5.6±1.23 at day7 for AFs (**Figure 2.6A**). Significant differences were reported between day1 and day7 of both NFs and AFs culturing on 2D (***$p<0.001$, **$p<0.01$).

3D scaffold analysis showed a distinct preference of AFs for 1% BDDGE scaffolds, reporting the highest proliferation rate at day7 compared to day1 (3.2±0.48) ($p<0.0001$); and a lower proliferation on softer matrices, 0.01%BDDGE, at day7 compared to day1 (0.6±0.07) ($p<0.01$), strongly suggesting AFs preference for stiffer matrices. On the other hand, NFs showed a slight preference for 0.1% BDDGE scaffolds with a proliferation rate of 1.8±0.12 compared to day1 ($p<0.0001$) (**Figure 2.6B**). These results support the notion that AFs are present in pathological tissues, usually characterized by fibrosis and linked to increase in stiffness.

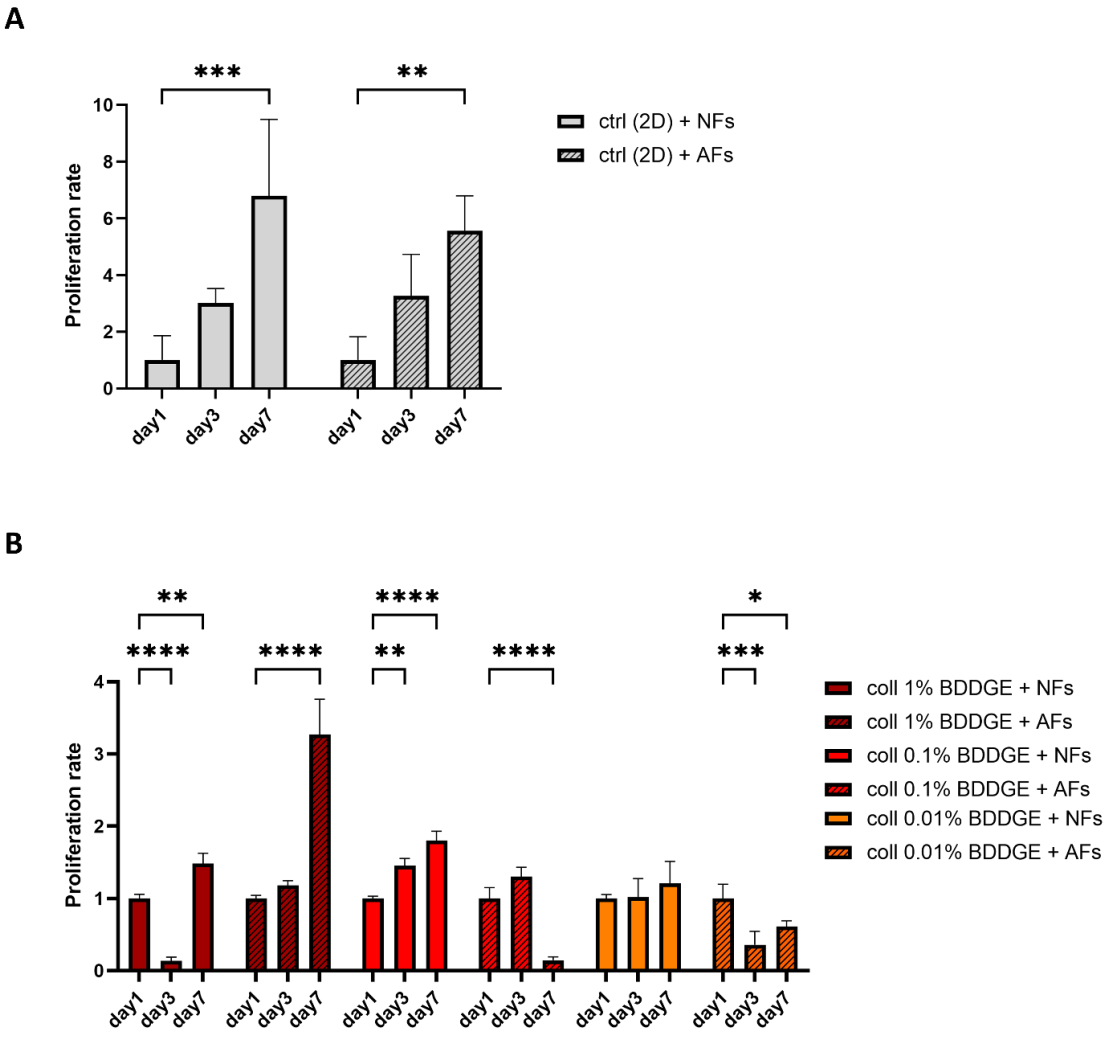

Figure 2.6. AFs fibroblasts proliferate more on 1% BDDGE scaffolds. (A) Proliferation rate of NFs and AFs cultured on 2D assessed by Pico Green assay at day 1, 3, 7. (B) Proliferation rate of NFs and AFs cultured on 3D 1%-0.1%-0.01% BDDGE scaffolds assessed by Pico Green assay at day 1, 3, 7. Data are mean + standard deviation (n=3). Two-way ANOVA, ****$p<0.0001$, ***$p<0.001$, **$p<0.01$, * $p<0.1$.

2.3.1.5 AFs promote soft scaffold shrinking (0.01% and 0.1% BDDGE)

As fibroblasts represent the central cellular effectors of fibrosis [414], a 3D matrix-cell culture system is a useful model to analyse functional and biomechanical features of cell-matrix interactions and pathogenesis, especially fibroblast implications in matrix remodelling [361, 415, 416]. First, the scaffolds were seeded with increasing cellular densities, 25k-100k and 300k of both NFs and AFs and scaffold diameter was analysed in a time span of 7 days, to record macroscopic remodelling of the matrix (**Figure 2.7**). Scaffold diameter analysis was performed using ImageJ with data reported as mean + standard deviation (n=3 scaffolds evaluated for each time point). No significant modification in scaffolds diameter were observed on 1% BDDGE over time for all cell's density utilized (**Fig.2.7A**). On the 0.01% BDDGE scaffold however, the scaffold diameter decreased at day7 compared to day1 for both NFs ($p<0.01$, at 25k cells and p $p<0.001$ for 100 and 300k cells) and AFs ($p<0.0001$) culturing conditions (**Fig.2.7C**). Between 0.1% and 0.01% BDDGE scaffolds, AFs showed the highest capability in promoting scaffold shrinking, especially at cellular densities of 100k and 300k. A cellular density of 100k was picked as standard for the following experiments.

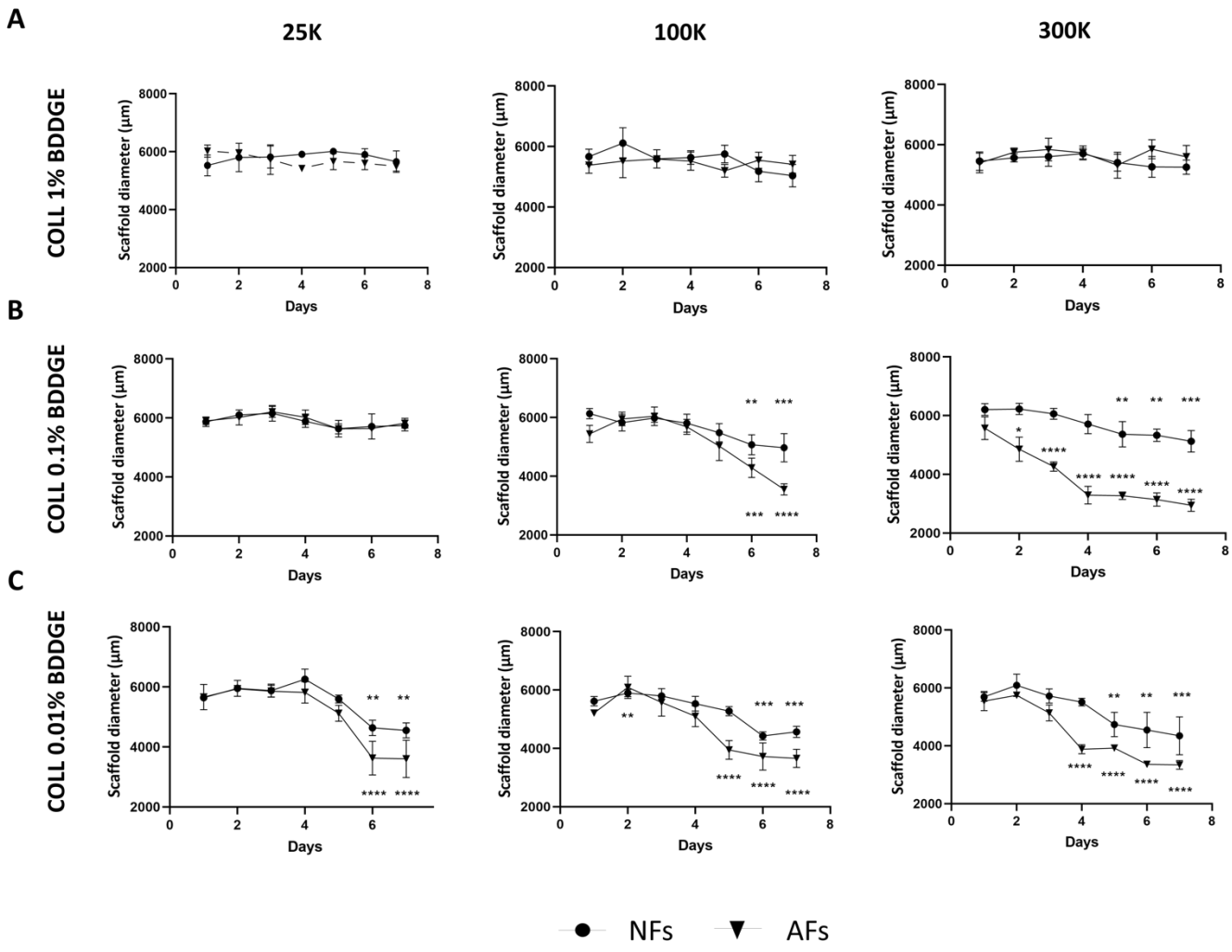

Figure 2.7. AFs culturing promoted higher scaffolds shrinking compared to NFs, except on 1% BDDGE scaffolds. Scaffold diameter analysis over 7 days of culture of NFs and AFs on (A) 1% (B) 0.1% (C) 0.01% BDDGE scaffolds at a cellular density of 25k-100k-300k. Scaffold pictures were recorded with digital microscope and brightfield pictures were analysed with Image J to calculate scaffold diameter. Data are mean + standard deviation (n=3) and statistical analysis performed compared to day1. Two-way ANOVA, ****p<0.0001, ***p<0.001, **p<0.01, * p<0.1.

2.3.2 Strategy 2; Porous collagen porous scaffolds with LW HA OLIGO (403.31 kDa)

2.3.2.1 Inclusion of HA maintains the porous structure of the collagen sponge

In both wound healing (normal) and pathological scenarios such as tumour progression and fibrosis, tissue remodelling processes occur which include changes in HA content and size [417-419]. In tumours, even if HA synthesis increases during remodelling, the increased expression of HA enzymes (hyaluronidases) and macrophage-generated ROS/RNS results in massive HA degradation. Indeed, the accumulation of HA fragments disrupt the homeostatic balance with HA HW altering the integrity of the matrix and resulting in HA HW displacement from cell receptors and changes in HA signalling effects [420].

To mimic the accumulation of HA LW *in vitro* we combined bovine-derived collagen type I with different amounts of HA LW fragments (1:10,1:100 and 1:1000) to create a sponge scaffold. Analysis of SEM images showed a typical 3D sponge scaffold porous structure, shared between the samples tested (**Figure 2.8A**). FTIR and TGA were again used to characterize scaffold composition after HA addition. FTIR spectral analysis showed the characteristic collagen signature with absorption peaks for the amide I (1700–1600 cm^{-1}), amide II (1600–1500 cm^{-1}), and amide III (approximately 1200–1300 cm^{-1}), referring to C=O, N–H and C–N, respectively (**Figure 2.8B**). The absorption bands between 1000-1100 cm^{-1} are typical for carbohydrates and the peak appeared in the col/HA 1:10, showing the presence of HA in the material and the difficulty to detect HA content in 1:100 and 1:1000 coll/HA due to lower amount of HA in the final material composition. For TGA analysis, both materials underwent endothermic reaction at around 50°C (evaporation of the water moisture present in the material), while thermal transition and material degradation happened after 100°C of the heating ramp, for both samples (**Figure 2.8C**).

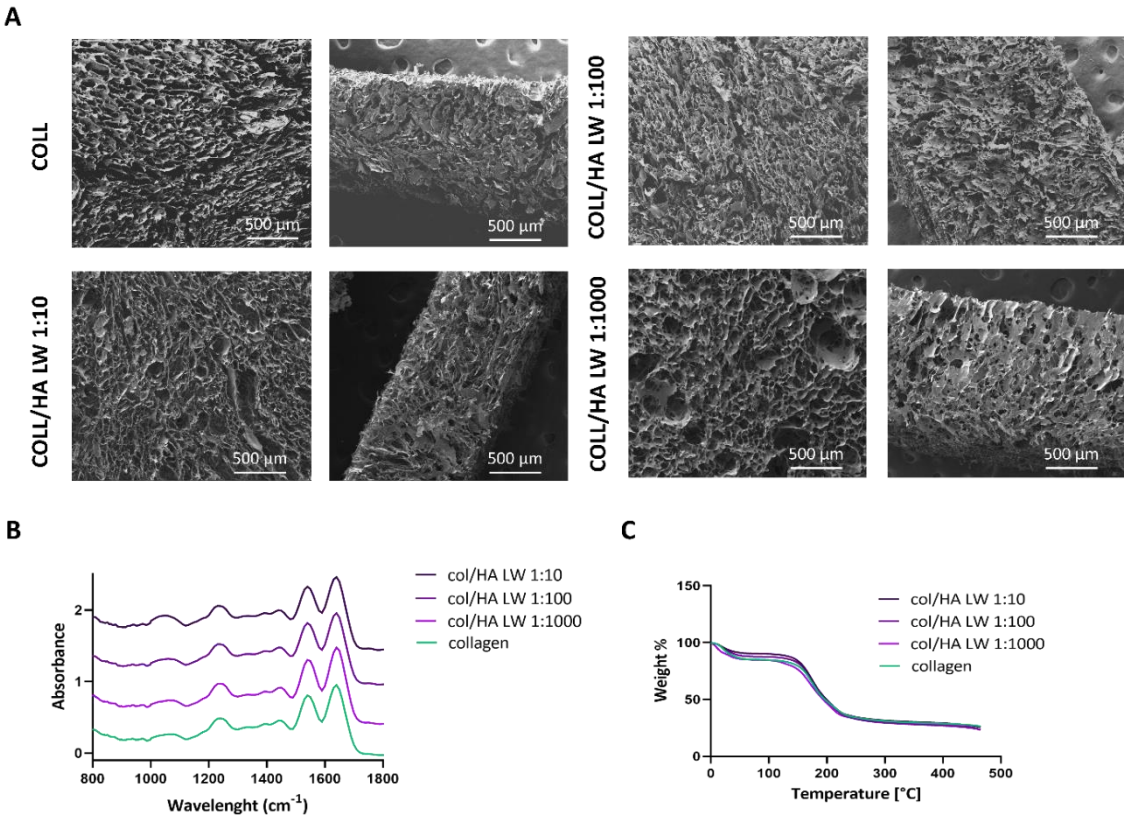

Figure 2.8. Coll/HA LW 1:10-100-1000 showed similar structure, composition and thermostability. (A) SEM magnification of the scaffolds (frontal and transversal). (B) FTIR spectra of scaffolds. The spectra highlighted the presence of typical collagen Amide I, Amide II, Amide III and carbohydrates absorption bands. (D) Thermo gravimetric Analysis (TGA).

2.3.2.2 Coll/HA LW 1:10 mimics pathological tissue stiffness

Since HA is a long polymer chain, forming random coils entangled in solution, and its numerous hydroxyls capture a huge quantity of water by forming hydrogen bonds [421], HA mechanically increases the elastoviscosity in the ECM. For example, during tumour progression both cancer cells and fibroblasts remodel the matrix leading to excessive collagen and HA, contributing to matrix stiffness increases [422]. To evaluate if HA LW content correlated with scaffold model mechanical stiffness, shear rheometry was performed as described previously (**Figure 2.9)**.

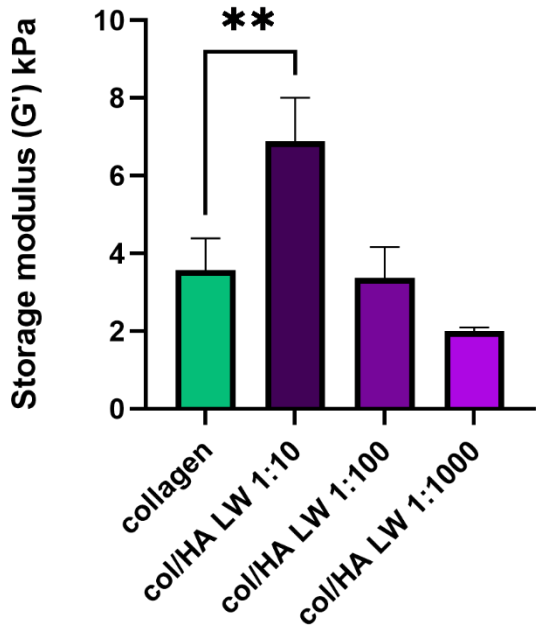

Figure 2.9. Coll/HA LW 1:10 showed increased storage modulus compared to other scaffolds. Rheology analysis of storage modulus (G', kPa) in collagen, coll/HA LW 1:10-100-1000. Data are mean + standard deviation (n=3). Ordinary one-way ANOVA, **p<0.01.

The scaffold storage modulus (G'), at 1 Hz, was significantly increased in coll/HA LW 1:10 (6.88±1.12 kPa) compared to collagen only (3.56 ±0.82 kPa) ($p<0.01$), while no significant difference were reported compared to coll/HA LW 1:100 (3.36±0.80 kPa) and coll/HA LW 1:1000 (1.99±0.10 kPa), suggesting a link between HA content and stiffness.

2.3.2.3 Coll/HA LW 1:10 induces fibroblast proliferation and elongation

Cellular adhesion and biocompatibility are fundamental requirements in the design of a 3D tissue scaffold [423]. These factors are routinely measured using cell viability and proliferations assays for adherent cells such as the MRC-5 fibroblasts used here. First, the Alamar blue assay was used to quantitatively analyse cell viability and proliferation [424]. As reported in **Figure 2.10A**, compared to the scaffold composed of collagen only, the highest rate of cellular proliferation was observed at day7 compared to day3, when grown on coll/HA LW 1:10 ($p<0.001$) while coll/HA

LW 1:1000 showed the lowest cells proliferation rate among all the scaffolds compared to day3 ($p<0.01$).

Fibroblasts, stained for actin and nuclei, adhere and colonize each scaffold as shown by the maximum projection analysis of 3 different z layers collected on the whole scaffolds **Figure 2.10B**, staining patterns on the scaffolds are indicative of cells adhesion and penetration onto the scaffolds, while they could also represents an indication of changes in the underling fibres organization after 7 days of culture. A different cell staining pattern, detected on the coll/HA LW 1:100, suggest a more 'corrugate' organization in that scaffold underneath. This is in line with previous literature showing that fibroblasts cells has the ability to influence ECM organization, specifically, activated fibroblasts (AFs) such as CAFs deform architecture of ECM, influencing cell migration, invasion, and growth, generating tracks that cancer cells follow [425]. As consequent, alignment of matrix fibres have been found in tumours and to be associated with poor patient prognosis [426]. It has been reported that fibroblast cell elongation, related to mechanical stress of the local environment, is a critical factor in normal fibroblasts activation and CAFs genesis [427]. We reported differences in the elongation of fibroblasts across the whole scaffolds between coll/HA LW 1:10 and collagen scaffold (1.78 and 1.58μm respectively, $p<0.0001$) (**Figure 2.10C)** and specifically in the centre portion (**Figure 2.10D)** ($p<0.001$), suggesting a higher cell stretching promoted by collagen/HA LW 1:10 compared to the only collagen scaffold.

Among the scaffolds analysed, only the coll/HA LW 1:10 scaffold succeeded in mimicking both mechanical properties (stiffness) and biological characteristics (HA LW) of pathological tissues. For this reason, the following analysis was carried out using this elective scaffold only.

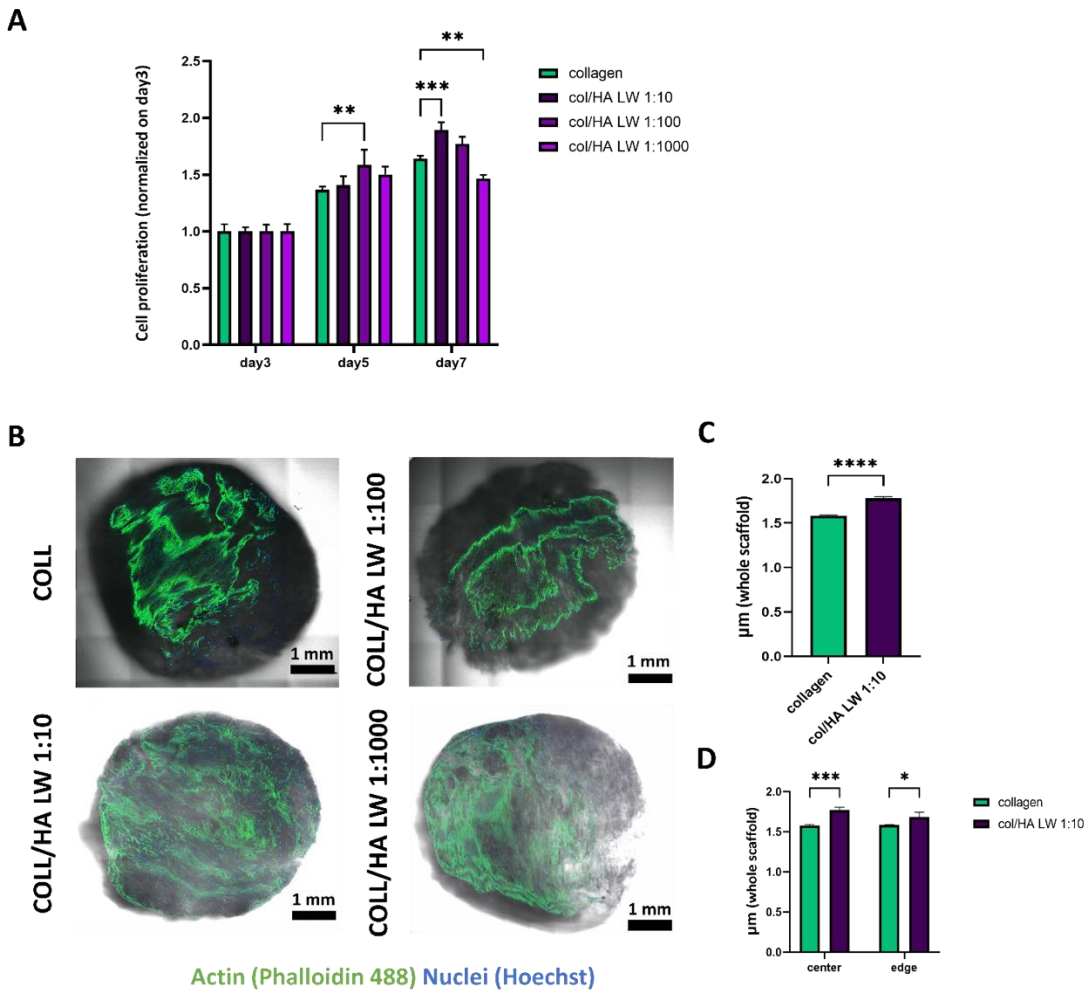

Figure 2.10. Fibroblasts grown on coll/HA LW 1:10 showed increased proliferation and elongation. (A) Alamar Blue cell proliferation analysis performed at day3-5-7 on scaffolds. (B) Phalloidin-488 and DAPI staining on fibroblasts grown on coll, coll/HA 1:10-100-1000 and recorded with fluorescence microscope using stitching feature. (C-D) Analysis of cells elongation on both coll and coll/HA 1:10 scaffolds, evaluating it as whole or dividing centre and edges. Analysis performed with NIS-Elements, Nikon software. Data are mean + standard deviation (n=3). T-test performed, **** $p<0.0001$, ***$p<0.001$, **$p<0.01$, *$p<0.05$.

2.3.3 Strategy 2B: Porous collagen scaffolds using HA LW OLIGO (403.31 kDa) and HA HW (2x106 Da)

2.3.3.1 coll/HA LW and coll/HA HW mimic pathological and normal tissue stiffness

HMW-HA is very abundant in healthy tissues and typically inhibits inflammation [366]. After the ratio of Coll/HA LW 1:10 was established as optimal, for linking pathological trends in biological and mechanical features within a porous scaffold structure, further modification was undertaken using HW HA. The crosslinker EDC/NHS was used, to ensure HA immobilization onto the collagen scaffold through the formation of a stable amide bond [428].

Consistent with chapter results, the scaffold storage modulus (G'), at 1 Hz, was significantly increased in coll/HA LW (14.6±1.21 kPa) compared to coll/HA HW (9.12±0.56 kPa), ($p<0.0001$). Furthermore increasing the collagen/HA LW ratio to 1:1, 1:2.5 and 1:5 lead to significantly lower elastic moduli (3.25±0.09, 4.11±0.08, 4.34±0.15 respectively, $p<0.0001$), proving the 1:10 coll/HA LW ratio the elective for further evaluations (**Figure 2.11)**.

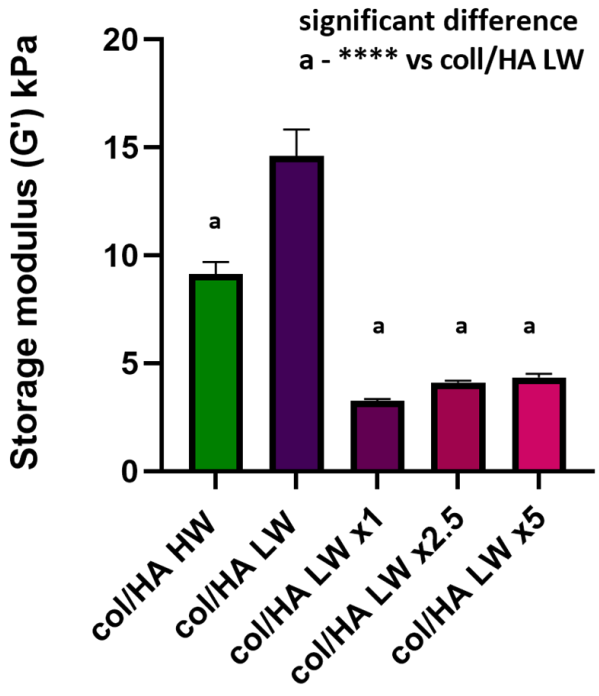

Figure 2.11. Coll/HA LW 1:10 showed increased storage modulus compared to other scaffolds. Rheology analysis of storage modulus (G', kPa) in coll/HA HW 1:10, coll/HA LW 1:10, coll/HA 1:1-1:2.5-1:5. Data are mean + standard deviation (n=3). Ordinary one-way ANOVA, ****$p<0.0001$.

2.3.3.2 HA LW or HW inclusion in collagen scaffolds doesn't impact porous structure and thermostability

SEM image analysis showed a typical porous structure of a 3D sponge scaffold shared between the samples tested (**Figure 2.12A**). FTIR and TGA were used to characterize scaffold composition after HA LW and HW addition. FTIR spectral analysis showed the characteristic collagen signature with absorption peaks for the amide I (1700–1600 cm-1), amide II (1600–1500 cm-1), and amide III (approximately 1200–1300 cm-1), referring to C=O, N–H and C–N, respectively (**Figure 2.12B**). The absorption bands between 1000-1100 cm-1, typical for carbohydrates are present in both coll/HA LW and coll/HA HW, showing HA incorporation in the scaffolds. For TGA analysis, both materials underwent endothermic reaction at around 50°C (evaporation of the water moisture present in the material), while thermal transition and material degradation happened after 100°C of the heating ramp, for all samples tested (**Figure 2.12C**).

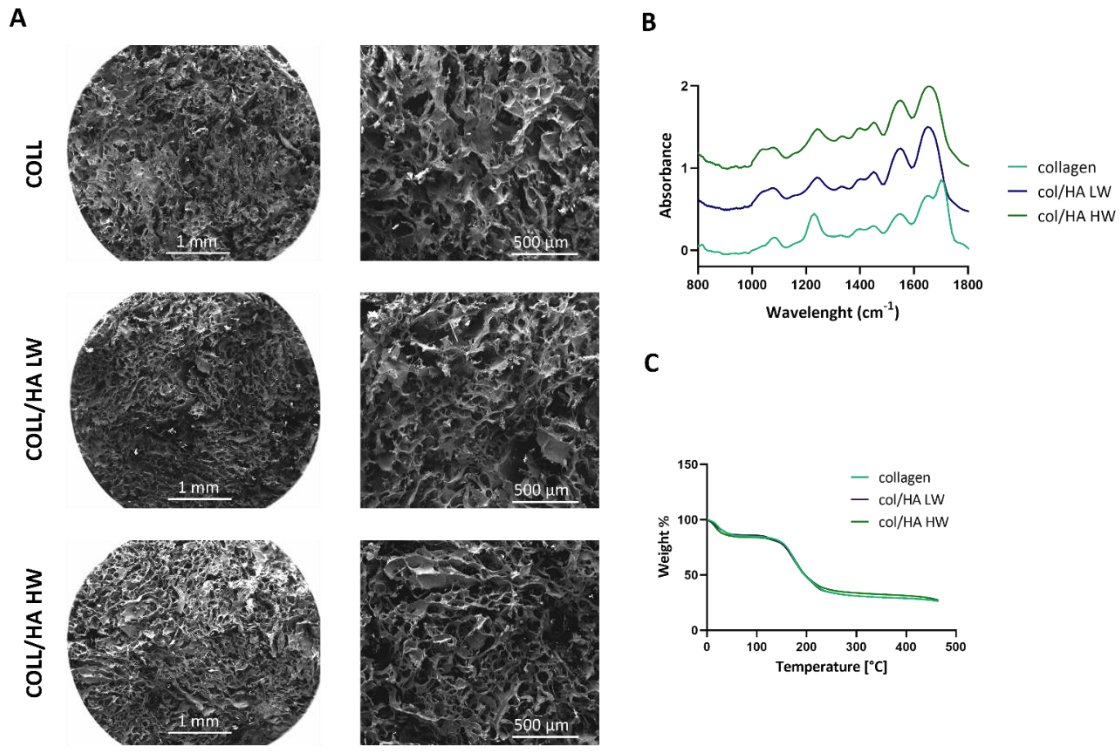

Figure 2.12. coll/HA LW-HW showed similar structure and thermostability of collagen only scaffolds. (A) SEM imaging of scaffolds at different magnifications. (B) FTIR spectra of scaffolds. The spectra highlighted the presence of typical collagen Amide I, Amide II, Amide III and higher carbohydrates absorption bands in coll/HA LW and HW scaffolds. (D) Thermo gravimetric Analysis (TGA).

2.3.3.3 Fibroblasts cells are viable on coll/HA-LW/HW scaffolds

When quantitatively analysed for viability, using calcein/EtBr live-death staining, NFs showed a 76% ± 1.9; 79.2% ± 3.3; 82.3% ± 3.4 calcein-positive cells on collagen scaffold, coll/HA LW and coll/HA HW respectively (**Figure 2.13**).

A

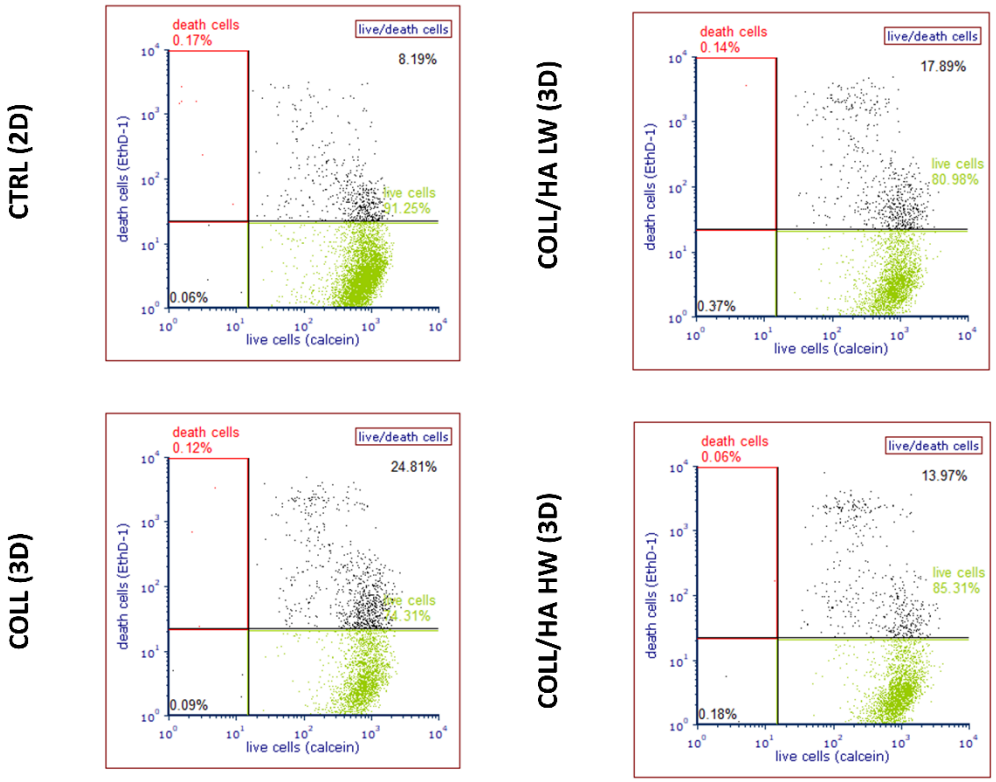

B

	Live cells (%)	Dead cells (%)
Ctrl (2D)	82 ± 12.2	2 ± 2
Coll (3D)	76 ± 1.9	2.7 ± 2.7
Coll/HA LW (3D)	79.2 ± 3.3	3.3 ± 2.8
Coll/HA HW (3D)	82.3 ± 3.4	2.5 ± 2.1

Figure 2.13. Fibroblasts MRC5 were viable and adhere on 1%-0.01%-0.001% BDDGE scaffolds. (A) 2D-3D cell representative death staining analysed with flow cytometry. (B) Quantification of 2D and 3D cell death staining, Data are mean + standard deviation (n=3).

At mRNA level we evaluated a panel of genes related to matrix remodelling, *MMP1*, *MMP2* and *COL1A1*, which code for the pro-α1(I) chain of collagen type I (**Figure 2.14A**). Furthermore, we analysed the expression levels of 2 HA receptors, *HMMR* and *CD44*, together with *HAS2* and Hyaluronidase-1 (*HYAL1*) (**Figure 2.14B**). MMPs are involved in the breakdown of extracellular matrix, specifically, MMP-1 breaks down the interstitial collagens, types I, II, and III. MMP-2, also known as gelatinase A, has a wide range of substrates, which include collagen, elastin, endothelin, fibroblast growth factor, MMP-9, MMP-13, plasminogen, and TGF-β [429, 430]. CD44 is the major cell-surface HA-binding transmembrane glycoprotein which, after binding with HA HW is thought to translate anti-inflammatories cues from the ECM [363, 431]. *HYAL1* encodes for a lysosomal hyaluronidase responsible for the hydrolysis of intracellular hyaluronan of all sizes into fragments and it is usually found overexpressed in many tumours [432-434]. Our analysis revealed an overexpression of MMP1 in all 3D models compared to 2D, with the highest expression fold change in fibroblasts cultured on coll/HA HW (3.64±0.31, $p<0.0001$). Overexpression of *COL1A1* follow a similar pattern with the highest expression fold change in fibroblasts cultured on coll/HA HW (2.62±0.30, $p<0.01$). Among the HA-related genes only the receptor CD44 expression was increased on coll/HA HW scaffolds with a fold change of 2.22±0.15 compared to the 2D control ($p<0.05$), suggesting its involvement in HA HW recognition in this model, as previously reported [420].

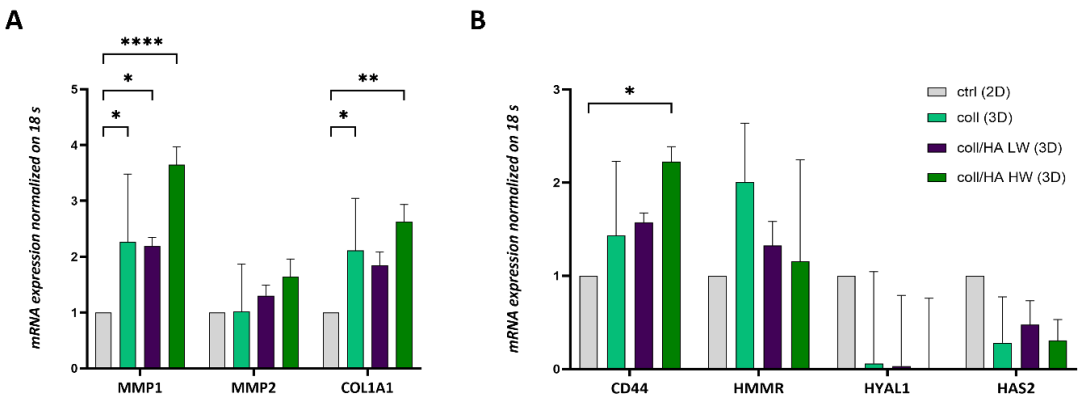

Figure 2.14. mRNA level analysis of ECM-remodelling related genes and HA-related genes. (A) Metalloproteinases genes (MMP1-MMP2) and COL1A1 mRNA expression in fibroblasts at day 7 of culturing on 2D, 3D collagen and 3D coll/HA LW-HW. (B) HA receptor (CD44, HMMR), synthase (HAS2) and hyaluronidase (HAS2) mRNA expression in fibroblasts at day 7 of culturing on 2D, 3D collagen and 3D coll/HA LW-HW. Data normalized to ctrl (2D), standard deviation of control not reported. Data are mean + standard deviation (n=3). Two-way ANOVA, ****p<0.0001, ** p<0.01, *p<0.05 .

2.3.3.4 Scaffold mechanics are impacted by cell proliferation and do not induce an activated phenotype in fibroblasts

To evaluate changes in scaffolds mechanics after cells seeding, we analysed the elastic component of the scaffolds, called storage modulus, at day3 and day7 after seeding with NFs (**Figure 2.15A**). To further confirm results in Figure 7 on this chapter, overall, cells culturing on scaffolds decrease their overall stiffness (compared to the empty scaffolds shown in Fig.5); specifically coll/ha HW showed a decrease in storage modulus at day7compared to day3 (3.95±0.13 and 1.98±0.06 kPa respectively, p<0.0001), suggesting a potential higher proliferation of fibroblasts when cultured on coll/HA HW, proved before in this chapter (Figure 5 and 7). To further test this hypothesis, we asked how much the cellular component in the scaffold analysed at day 7, influences the overall mechanic. We decellularized the scaffolds incubating it with 0.5% SDS and we verified cellular content using PicoGreen assay (**Figure 2.15B**). Rheological analysis after decellularization at day7

showed that cellular part collaborates in the softening of the bulk scaffold stiffness, indeed both coll/HA LW and coll/HA HW reported significant increase in storage modulus after undergoing decellularization (7.7±0.44 and 2.94±0.22 kPa respectively) compared to the corresponding cellularized scaffolds (4.4±0.31 and 1.98±0.06 kPa respectively, $p<0.0001$ and $p<0.01$) (**Figure 2.15C**).

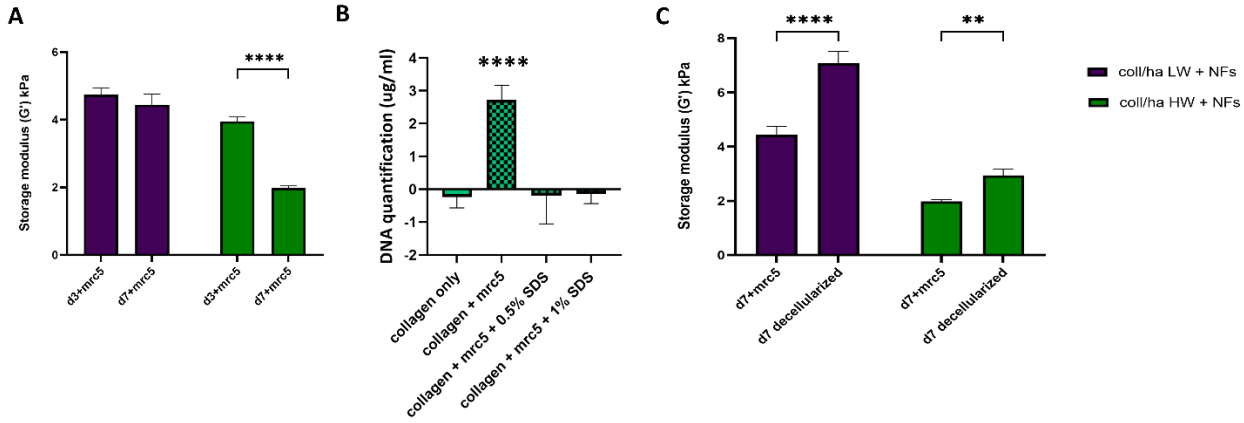

Figure 2.15. NFs culturing on coll/HA HW promote decrease in its stiffness. (A) Rheology analysis of coll/HA LW and HW storage modulus (G', kPa) at day3 and day7 of NFs culturing. (B) DNA quantification after decellularization protocols on collagen scaffolds. (C) Rheology analysis of coll/HA LW and HW storage modulus (G', kPa) at day7 before and after decellularization. Data are mean + standard deviation (n=3). Two-way ANOVA, **** $p<0.0001$, ** $p<0.01$.

Finally, as both stiffness and biological modification are included among the cancer cell hallmarks [16], scaffold influence on fibroblasts activation was evaluated. The expression of FAP was again analysed using flow cytometry (**Figure 2.16**). While FAP expression is promoted by TGFβ1 treatment in both 2D and 3D culturing conditions, coll/HA HW doesn't have any effect on FAP expression while coll and coll/HA LW resulted in small, non-significant increase.

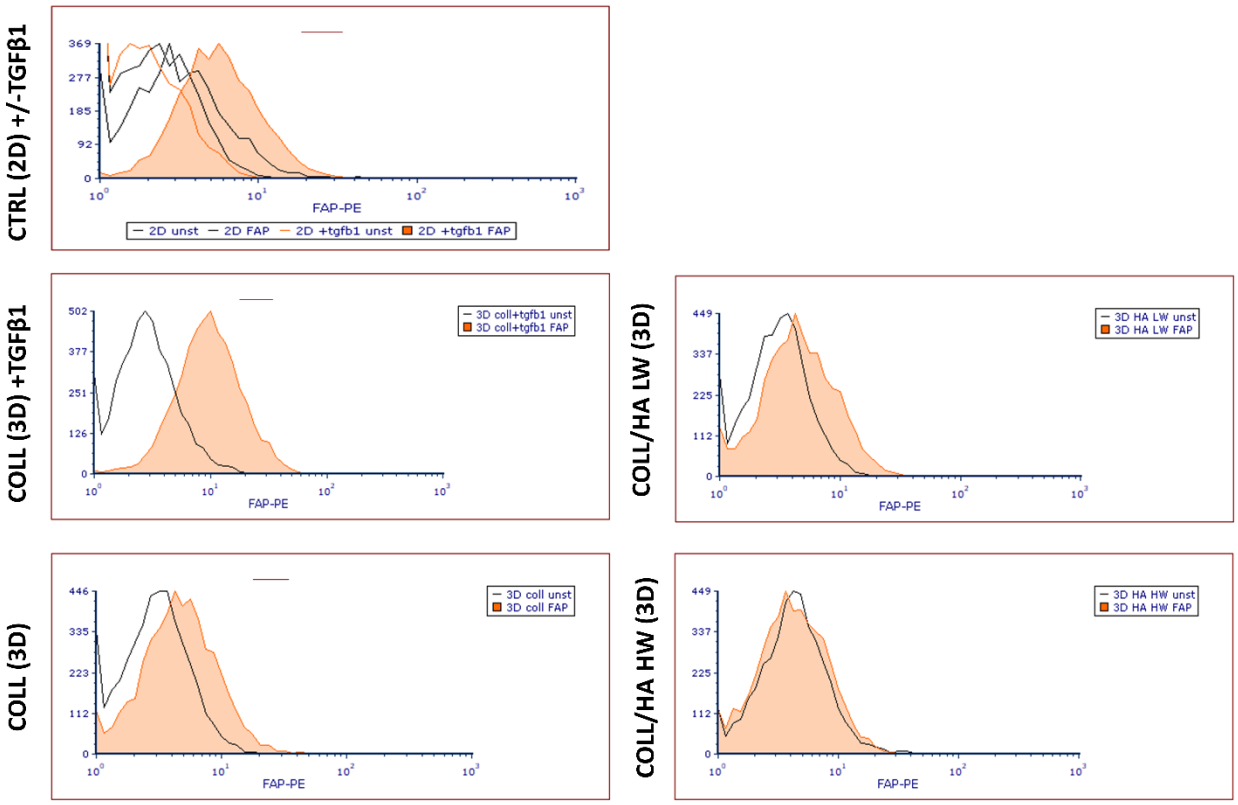

Figure 2.16. TGFβ1 treatment but not HA LW inclusion in the scaffold fabrication promote FAP expression. FAP expression after 7 days on 2D ctrl, 3D collagen and 3D coll/A LW-HW was assessed by flow cytometry. FAP expression after 7 days on 2D and 3D collagen under TGFβ1 25 ng/ml treatment was used as positive control of NFs activation into AFs.

2.4 Discussion

Although there are increasing examples of established 3D cell culture approaches in the form of gel systems and spheroid cultures, that have dramatically improved our understanding of the role of 3D culture on tumour cells [395-397], few have employed the porous scaffold matrices that have made significant improvements in the TE and RM space. There is a need for innovative 3D tumour models that are capable of recreating distinct tumour mechanical characteristics, that allow for *in vitro* tumour modelling under well-defined and reproducible conditions, and the results presented here explore the opportunities and suitability for collagen sponge scaffolds in this space. Using a cross discipline material, biochemical and cell/molecular analysis approach, the data

presented show and defend the suitability of sponge scaffolds as tools to model distinct mechanical cancer microenvironment cues *in vitro*.

Typically, in tissue engineering, three individual groups of biomaterials are used in the fabrication of scaffolds: ceramics, synthetic polymers and natural polymers [435]. Ceramic scaffolds, such as hydroxyapatite and tri-calcium phosphate (TCP), are used for bone regeneration applications since they are characterized by high mechanical stiffness (Young's modulus), very low elasticity, and a hard brittle surface, mimicking the mineral phase of native bone, enhancing osteoblast differentiation and proliferation [436], but they have failed in sustaining the mechanical loading needed for remodelling in clinical applications [437]. Synthetic polymers including polystyrene, poly-l-lactic acid (PLLA), polyglycolic acid (PGA) and poly-dl-lactic-co-glycolic acid (PLGA) [438-440], have shown much success as they can be fabricated with a tailored architecture but a major drawback is in the degradation process of PLLA and PGA as they degrade by hydrolysis, producing carbon dioxide and therefore lowering the local pH which can result in cell and tissue necrosis [441]. Finally, natural biomaterials are bioactive, biodegradable and allow host cells to produce their own extracellular matrix and remodel the scaffold. However, depending on the scaffold employed they generally have poor mechanical properties, which limits their use in, for example, load bearing orthopaedic applications.

Collagen was selected as a scaffold material in this research, primarily due to its high biocompatibility and bioactivity as a natural polymer. Collagen is the most abundant structural protein in the connective tissues, representing one-third of the total protein content in the body [442] in humans and its homology across species provides low antigenicity and high biocompatibility [443, 444]. Generally referred as "collagen sponge", collagen is employed here to create a highly porous structure, fabricated following thermally induced phase separation, where collagen molecules are separated from the water-based solvent is due to freezing cycles before a vacuum drying process leading to the sublimation of ice crystals [445], resulting in easy control of the architecture and mechanical properties of the resulting structure [446-448].

These mechanical features can be altered further by modulating collagen concentration, phase separation temperature, by mixing collagen solutions with other natural polymers such as GAGs

[446] or by employing crosslinking strategies [400]. As result, the interconnected pore networks and surfaces or fibres of the scaffold structure provide support for cell adhesion, while also presenting a niche growth environment with stiff and tuneable mechanical properties, unlike other 3D models such as hydrogels, which have good biocompatibility but most often low mechanical properties, risk of poor distribution of cells and nutrients in an architecture which is more difficult to control, therefore, has less reproducibility of the exact architectures desired and high degradation rates [449]. Both the 3D scaffolds fabricated in this chapter proved very easy handling and optimal oxygen and nutrient exchange, thanks to their porous nature. They also permitted the removal of detached cell, cell debris, as well as cell retrieval for further analysis, alongside a unique opportunity to study soluble factors present in culture media, which can freely diffuse in the hollow channels between the cell clusters and then be collected for analysis.

Since collagen, as is the case in all-natural polymers, has relatively poor mechanical properties, differential strategies were explored to introduce or tune this important microenvironment factor into the culture systems chosen. Mechanical forces within the cancer TME regulate cancer progression in many solid tumours leading to an increase in stiffness from the normal to the pathological condition with a value varying based on the tumour under evaluation [450, 451]. For example colon carcinoma has a stiffness ranging from 1 to 4 kPa [452]; the stiffness of normal breast tissues is around 4 kPa, while for cancerous breast tissues is approximately 12 kPa [119, 453] . In comparison, tissue-culture plastic has a stiffness of up to 100,000 kPa [454].

To successfully reproduce specific mechanical gradients, two different strategies were implemented; BDDGE cross linking and modification of collagen composition with EDC-NHS crosslinking and HA, a natural tumour component shown to be modified in both disease and distinct disease stages [455-457]. Using the freeze drying and vacuum-based fabrication process described, both were incorporated and tested for their effect on sponge scaffold mechanics, cellular compatibility, adhesion, proliferation and differentiation. Many cross-linkers used for collagen stabilization and mechanical properties enhancement react at amine and carboxylic acid sites, which are amino acids commonly part of integrin ligands, i.e. Arg-Gly-Asp (RGD) and Gly-Phe-Hyp-Gly-Glu-Arg (GFOGER). Those binding sites are crucial for collagen interaction with a variety of cell trans-membrane receptors including integrins and discoidin domain receptors

(DDRs) [458]. The cross-linking type and amount can therefore influence both scaffold mechanics and cell adhesion, by limiting the number of integrin ligands available for binding [459, 460]. This is further amplified as a challenge, as collagen is a protein which only reveals an RGD binding site sequence following denaturation to gelatin [461]. Instead, interactions with native collagen fibres, made via fibrillogenesis and crosslinking, operates via GFOGER binding, which is dependent on collagen's helical structure [462]. Minor alterations of this sequence also act as ligands, but GFOGER has the highest binding affinity, leading to the greatest attachment [463, 464]. The removal of these vital groups can alter cellular differentiation, adhesion and migration [465, 466].

A widely used crosslinker, glutaraldehyde (GA), which incorporates into the scaffolds has proven to be a very effective scaffold stabilizing approach, however it is associated with a high levels of cytotoxicity [467]. Other strategies, such as incorporating epoxy-based cross-linkers into collagen, have been shown to enhance its mechanical properties [468, 469]. BDDGE, as a bi-functional epoxy-based chemical cross-linker, is water soluble and has been found to produce materials with high tensile strength and improved elasticity [470, 471]. Cross-linking of bi-functional BDDGE is pH dependent and occurs through secondary amine bond formation via epoxide ring opening by amine groups of collagens under slightly basic pH conditions, and occurs mainly via the amine groups of (hydroxy)lysine, with an observed decrease in histidine while the amounts of carboxylic acid groups unchanged [471]. As a result, there is a low competition of the crosslinker with cells' adhesion receptors binding to either RGD and GFOGER motifs indeed cells adhesion and viability on this scaffold is optimal.

1-ethyl-3-(3-dimethyl aminopropyl) carbodiimide hydrochloride (EDC), is another water soluble, carbodiimide, cross linker. EDC does not incorporate in the final structure and also catalyses a reaction between carboxylic acids and amine groups, lowering potential cytotoxic effects due to the cross-linker itself [472] as well as competition for cells' binding sites. For those reasons we employed and optimize this strategy to fabricate coll HA scaffolds, allowing recording of cells' response depending only on HA LW or HA HW incorporation and its resulting mechanical properties. Comparing the resulting scaffolds mechanics, the closest range to cancer tissues is represented by the scaffolds fabricated using the crosslinking method with BDDGE which resulted in a stiffness range of 11.27±0.62 kPa for 1%wt, 3.63±0.46 kPa for 0.1%wt and 1.81±0.24 kPa for

0.01% BDDGE; while the HA final constructs spanned in a smaller stiffness range difference between the pathological, 14.6±1.21 kPa for coll/HA LW, and normal 9.12±0.56 kPa for coll/HA HW scaffold. As previously reported in literature, stiffness range comparable to either cancer tissue or its normal counterpart [473], as demonstrated for breast, brain and prostate cancers [14, 91, 323, 352-354], were achieved with BDDGE crosslinking which will be the elective model for mechanobiology studies later on in the thesis.

Although materials such as Matrigel® offer a nutrient rich TME, their low stiffness lies within the native stiffness range of a limited amount of human tissues, including brain tumour models, 180 Pa. For collagen-based hydrogels, instead, the most common way to modulate stiffness is to increase collagen density achieving 330 Pa (low density, 2mg/ml) and 1.6 kPa collagen (higher density 4.0 mg/ml) [352, 474, 475]. Also spheroids and hanging drop formations will have limited collagen density other than what the cells produce, with a corresponding low stiffness, measurable through AFM, in the range of 100–500 Pa [476]. Microfluidic devices will also not have any collagen unless injected, mainly hydrogels. Hydrogels have a collagen concentration of 0.2% or less, whilst Matrigel® is available at 0.2–0.4%. Usually hydrogels have a collagen concentration of 0.2%, while in native tissues, like tendons, the collagen density is 12% and accounts for 1–10% of skeletal muscle dry weight [477]. This collagen density directly impacts the stiffness of the ECM the 3D model provides, even if stiffness is not only dependent on collagen itself, but rather a combination of all ECM components as a whole [478], the purpose of including HA in the scaffold fabrication.

The stiffness of hydrogels can be tuned through various methods, depending on the compositions and crosslinking mechanisms of the hydrogels [479]. For example, synthetic hydrogels using polyacrylamide (PA) be adjusted by tuning the concentrations of the monomer and crosslinker achieving a tuneable elasticity of 0.5–50 kPa [480, 481], or hydrogel stiffness can be dynamically increased through diffusing additional photoinitiator and reactive polymers to allow for a secondary photo crosslinking. However, PA gels are synthetic, so they do not contain any of the components of *in vivo* extracellular matrix and even if functionalized with ECM derived proteins and fibres, the adhesion sites will be limited to one surface of the cell, causing the cells to take on a 2D morphology similar to that of cells on glass or a petri dish [482].

Among all the hydrogels, gelatin-based hydrogels are increasingly used to mimic TME, because of their inherent bioactivity and protease degradability, they can be crosslinked via chain-polymerization, or chemically modified via gelatin-methacryloyl (GelMA) reaching a maximum of 13 kPa, or via orthogonal click chemistry, such as the thiol-norbornene photo click reaction and tetrazine-norbornene click chemistry [483-486]. Also, chemically modified-HA based hydrogel uses photopolymerization as secondary crosslinking to control stiffness once a primary network is form, achieving a reported range of 0.5-1.5kPa [487, 488].

A little more tricky is to tune natural-derived materials stiffness in hydrogels, for example wedge-shaped collagen fibroblast-seeded construct were fabricated, then the construct was compressed into a thin gel sheet, thus creating a stiffness gradient across the construct reporting a very high range of 1 to 2 MPa, which they claim being similar to the native tissue range (e.g. skin, tendon) [489]. Unfortunately, the process of compressing the wedges alters the density of fibres within the matrix, too which could impact on the experimental result, since cell invasion is highly affected by the size of 3D gel pore sizes [490, 491]. Another study used deposited Matrigel on a wavy polydimethylsiloxane (PDMS) mould, resulting in an environment of continuously changing stiffness while keeping constant the fibre density, protein concentration, and other factors, which allowed the cells seeded on the Matrigel surface to sense the differential stiffness across the surface [492]. Compared to the listed hydrogel techniques, porous scaffold employed to replicate *in vivo* mechanic, uses a natural derived material with no modification in its sequence or folding structure, keep a constant fibre density, optimal porosity, and finely tuned crosslinking to allow cells adhesion and invasion. Furthermore, the process of fabrication has been optimized to be quick, tuneable, and scalable.

As another advantage, scaffold-based culture system can maintain higher cell densities than conventional two-dimensional (2D) cell culture [493]. Interestingly, 3D porous scaffold models also allowed us to assess matrix changes over time during cell culturing and consequently mechanical changes, reporting an impairment of AFs contractile abilities on stiff matrices such as the 1% scaffolds. This didn't impact cellular proliferation rate which resulted to be high on stiffer materials, i.e. 1% BBDGE and coll/HA LW scaffolds. When this proliferation increase was

observed, it correlated with mechanical effect, determining a storage modulus variation under cell culture. An increase in cells proliferation was linked to a softening of the matrix, suggesting the suitability of rheological analysis to detect mechanical variation over time derived from biological changes. The effect of stiffness as promoter of cellular proliferation is well known in many cells types such as smooth muscle cells [494], fibroblasts [489, 495] , bone marrow mesenchymal stem cells (BMMSC) [496], which then contribute to further disease progression [497-499]. On the other side the effect on matrix softening on cellular phenotypes will be further explored in the next chapters.

Mechanical forces have been demonstrated to alter the gene expression and regulation of cell signalling, providing appropriate substrate stiffness vital to living cell functions. Matrix rigidity is increasingly appreciated as an important mediator of cell behaviour. It regulates cell signalling broadly, with effects on growth, survival, and motility [498]. Indeed, we evaluated mRNA expression in response to HA inclusion, since changes in HA-mediated cellular signalling occur when a small percent of the fragmented pool passes a threshold that is enough to tip the balance and change the outcome of cellular function. In the TME, HA LW has the potential to influence stromal cells, infiltrating inflammatory cells and cancer cells, facilitating tumour cell adhesion and migration [500-504]. We first evaluated both metalloproteinases MMP1 and MMP2, since it is known that fragments HA, which are typically produced at sites of inflammation or in a tumour site, can activate dendritic cells or promote cancer cells upregulation of matrix metalloproteases (MMPs) [505, 506].

Furthermore, we evaluated the expression of α-chain of the type 1, indicative of collagen deposition. In parallel we evaluated fibroblasts ability to detect HA changes in the environment analysing receptors CD44, HMMR expression and fibroblasts ability to affect HA content through HYAL1 hyaluronidase and HAS2 synthase expression. Indeed, although HA fragments can originate from hyaluronidases breakdown of high molecular HA, HAS isoenzymes might also be regulated to synthesize specifically smaller HA molecules [507]. CD44 is a membrane receptor for hyaluronic acid; previous studies have shown that CD44 is highly expressed in cancer cells and may be proteolytically cleaved at the ectodomain by MMP1 (induced by HA LW); this process of

inducing CD44 cleavage plays a critical role in cancer cell migration [508, 509]. Surprisingly, NFs expression of MMP1 and CD44 was higher on coll/HA HW scaffolds, indicating a responsive behaviour of NFs to long, anti-inflammatory HA instead of the well-known HA LW. Those results will need further investigation to better understand the signal exerted by HA HW on NFs through CD44 receptor in a non-pathological setting, and to clarify if MMP1 is in charge to cleave CD44 in this context, too.

Comparing the two strategies employed in this chapter, it is evident the strong potential of both in cancer research investigations. More in line with the subsequent research hypothesis in this thesis, the closest range to cancer tissues is represented by the scaffolds fabricated using the crosslinking method with BDDGE, while the HA final constructs spanned in a higher stiffness range. To conclude, employing BDDGE crosslinking strategy to study mechanical constrains in cancer microenvironment represents the most scalable, reproducible, and meaningful strategy in line with this thesis aim. Our characterization and evaluation of sponge scaffolds biocompatibility provide an accurate starting point to understand the cellular and molecular mechanisms involved in cancer-microenvironment interactions. Above all, these models contribute to overcome the use of conventional 2D culture systems and to acquire overall awareness towards the implementation of 3D culture systems in our daily *in vitro* experiments and screenings.

Chapter 3: Studying Activated Fibroblast Phenotypes and Fibrosis-Linked Mechanosensing Using 3D Biomimetic Models

The work presented in this thesis chapter contributed directly to the following peer reviewed journal article:

F. Paradiso, M. Quintela, S. Lenna, S. Serpelloni, D. W. James, S. Caserta, R. S. Conlan, L. W. Francis, F. Taraballi. Studying Activated Fibroblast Phenotypes and Fibrosis-Linked Mechanosensing Using 3D Biomimetic Models. *Macromolecular Biosciences 2022* https://doi.org/10.1002/mabi.202100450 **(IF 4.9)**

3.1 Introduction

Pathological conditions such as chronic or repeated injuries and irritation can lead to failure to heal and subsequent tissue fibrosis [510], as a dysregulated outcome of the tissue repair response following injury [336]. Indeed the relationship between cellular and ECM components of tissues, titled Dynamic reciprocity, has been shown to be a crucial factor in orchestrating both normal physiological function(s), and disease development [511].

The ECM of fibrotic tissue is characterized by increased collagen and fibronectin synthesis [512], while local tissue fibroblasts become activated and increase their contractility and secretion of inflammatory mediators [513]. In a physiological setting, these changes initiate a wound healing like response. When damage is minor or non-repetitive, a transient increase in the deposition of ECM components supports efficient wound healing and restoration of functional tissue homeostasis. However, when the injury is repetitive or severe, ECM components accumulate excessively, with consequent tissue architecture disruption, organ dysfunction, and ultimately organ failure [514, 515]. The resulting increase in matrix stiffness, traditionally viewed as an end point of organ fibrosis, is now recognized as a critical regulator of tissue fibrogenesis, that promotes organ fibrosis, while hijacking the normal physiologic wound-healing program [516].

The subsequent ECM-cell interactions result in tensional, compressive, and shear forces that are translated into biochemical signalling through a process known as mechano-transduction [99]. Through this signalling process, matrix stiffness has been shown to control a range of cellular activities, including migration, adhesion, phenotypic modulation, and survival linked to oncology [517], alongside activation of a ‘myofibroblast program’ in fibroblastic cells [518, 519]. Indeed, matrix remodelling in fibrotic tissues is thought to be similar, to that in the formation of premetastatic niches [520].

In many solid tumours, the formation of fibrotic tissue is referred as a desmoplastic response [521, 522]. Desmoplasia is a fibrotic state, with matrix dysregulation characterized by increased deposition, altered organization, and enhanced post-translational modifications of ECM proteins,

often seen in chronic inflammation 15]. At the cellular level, desmoplasia involves fibroblast cell expansion and activation, alongside elevated angiogenesis, therefore resembling many of the facets of chronic tissue fibrosis [523]. This process occurs in many advanced carcinomas, including breast cancer, and is responsible for the clinical presentation of a tumour as a 'lump' [524-526]. Investigating how matrix remodelling that occurs in tumour settings, and the resulting tumour-associated tissue fibrosis, may help to create an environment for primary and secondary tumour colonization of the tissue is one area of intense activity [527]. Indeed, in some of the most well-studied tumour types such as breast, pancreas, lung, and colon, tumour growth is usually associated with a dense fibrotic stroma and their aggressiveness is often associated with higher collagen levels alongside extensive dense, linearized, and cross-linked tissue ECM [398, 452, 528, 529]. As a result, malignant tissue are typically stiffer than their normal counterpart, with studies showing that normal breast tissue is up to 20 times softer than its neoplastic counterpart [530]. Breast and pancreatic tumour stiffness has been exploited to detect cancer mass either by physical palpation or using imaging modalities such as magnetic resonance imaging, computerized tomography, or elastography [531, 532].

At a cellular level, pathological fibrosis is driven by a feedback loop in which the fibrotic ECM is both a cause and consequence of fibroblast activation, known as myofibroblasts or herein referred to as activated fibroblasts (AFs). The origin of myofibroblasts has been shown to be tissue dependent [533] and they can be activated by many stimuli such as reactive oxygen species, pathogen-released activators, and many other soluble molecules secreted by infiltrating cells [534, 535]. Specifically, transforming growth factor-beta (TGFβ1) is a potent fibroblast activator, enhancing fibroblast contractile capacity, inducing the incorporation of smooth muscle α-actin (α-SMA) within cytoskeletal stress fibres and increasing focal adhesion clustering, all of which represent a typical phenotype in fibrotic pathologies or aberrant wound healing [536-538]. In parallel, as a result of structural ECM changes, biomechanical signals are also thought to initiate and sustain tissue fibrosis [99, 539].

TGF-β1 is also thought to promote tumour initiation and progression [540, 541]. In many solid tumours, reciprocal TGFβ1 signalling between cancer cells and the TME promotes cancer progression by activating fibroblasts into cancer-associated fibroblasts (CAFs) [542, 543]. CAFs

usually exert a pro-tumorigenic effect, enhancing tumour phenotype and promoting tumour growth, cancer cell proliferation, angiogenesis, invasion, and metastasis [1, 544, 545]. Indeed, fibroblasts adjacent to the tumour express genes mainly related to stress and inflammation [546], and as observed in breast cancer, macrophage dysfunction can enhance the process of inflammation, contributing to metastasis [547]. Resulting from CAF activation and consequent production of a dense connective tissue, altered biomechanical properties often induce tumour metastasis, angiogenesis, and hypoxia [93, 94].

In line with this, cultivating tumour stromal cells in 3D systems can allow more in-depth investigations by fully recapitulating the cell-matrix interactions observed in tumour tissue. Precise 3D scaffold fabrication enables the production of tissue-like materials, closely mimicking native tissues for various applications, from regenerative medicine to cancer research [548-554]. Exploiting porous scaffold collagen-based material, we investigate stiffness effects on both normal fibroblasts' (NFs) and activated fibroblasts' (AFs) cellular migration, morphology, functionality, and gene expression profiles **(Figure 3.1)**.

Among the fabricated scaffolds explored in the previous chapter, here two scaffolds were selected to fully replicate both soft/physiological (So, 0.01% BDDGE) and stiff/fibrotic-like (St, 1% BDDGE) tissue matrix environments. The work presented in this chapter, further establishes the advantages of 3D modelling and the tuning properties of porous scaffolds while establishing a foundation for further exploration of the role of the stroma in fibrotic/desmoplastic tissue responses. As such, these scaffold-cell models represent a meaningful and reliable platform to combine biological and biophysical cues in a 3D system, envisioning a stroma-ECM model for fundamental research of pathologies characterized by the dysregulation of ECM homeostasis, drug discovery and personalized medicine.

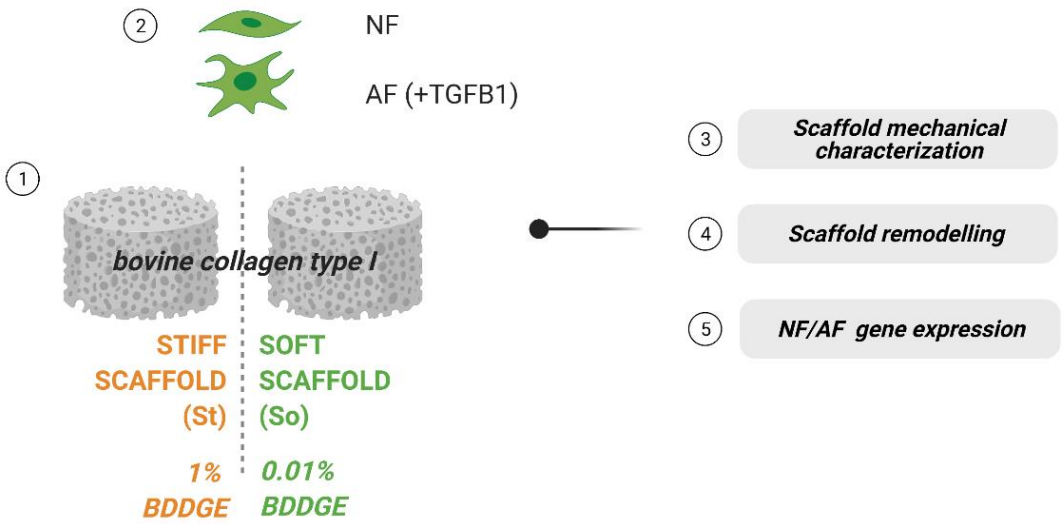

Figure 3.1. Schematic representation of scaffolds employed to mimic normal and pathological tissue mechanic. Image made with Biorender.

As activated fibroblasts play a fundamental role in cancer, where they are called cancer associated fibroblasts (, we tested ovarian cancer cell line SKOV.3 conditioned media (CM, also referred as secretome) ability to promote fibroblast activation, reproducing fibroblast activated phenotype promoted by TGFβ1 using ovarian cancer cell derived secretome (**Figure 3.2**). As extensively described in literature, tumours are surrounded by complex microenvironment made of cellular components (fibroblasts, endothelial cells, adipocytes, immune cells, and neuroendocrine (NE) cells), and acellular ones (extracellular matrix (ECM), extracellular vehicles (EVs), and cytokines) [555]. Among the acellular components of the complex TME, the cell secretome refers to the collection of secreted proteins including numerous enzymes, growth factors, cytokines and hormones or other soluble mediators [555]. The secretome encompasses both proteins, which contain a signal peptide and are processed via the endoplasmic reticulum and Golgi apparatus through the classical secretion pathways, as well as proteins shed from the cell surface and intracellular proteins released through non-classical secretion pathway or exosomes [556]. In the tumour setting, factors secreted by stromal fibroblasts or CAFs, transduce signals to cancer cells as well as to themselves establishing reciprocal reinforcement of growth and progression signals in various types of cancer [282, 557, 558]. Among those factors, as demonstrated in early chapters,

TGFβ1 is a ubiquitously-expressed cytokine that mediates a wide spectrum of biological processes, including the promotion of fibroblasts activation [559]. TGFβ1 can be produced by the tumour cell itself or other cells in the tumour microenvironment including stromal cells, macrophages and platelets [560].

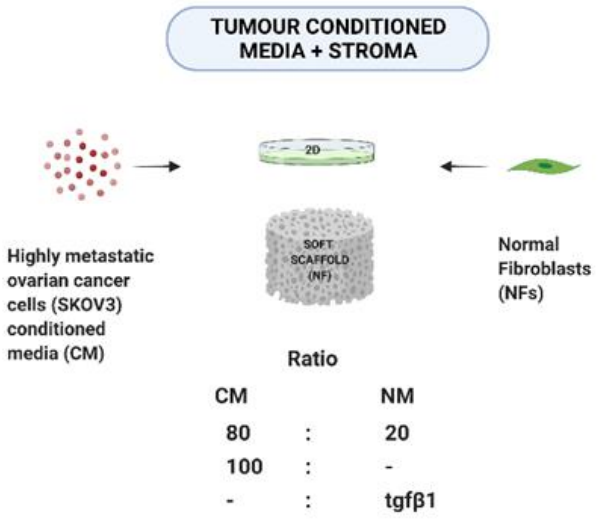

Figure 3.2. Schematic representation of experimental plan used to investigate SKOV.3 derived CM influence on fibroblast activation.

3.3 Results

3.3.1 So (0.01% BDDGE) and St (1% BDDGE) collagen scaffolds mimic normal and fibrotic tissue

As one of the main components of interstitial matrix, collagen type I is an elective biomaterial used in *in vitro* scaffold model development [569]. As collagen crosslinking can influence tissue strength and elasticity, we exploited two different percentages of the cross linker BDDGE to specifically reproduce the mechanical features of both native and dense fibrotic tissue [93, 570].

The optimized conditions of 1% BDDGE was chosen to mimic tumour-fibrotic/stiff tissue (St) and 0.01% to mimic normal/benign/soft tissue (So), as described in chapter 2. Scaffold mechanics were analysed at the nanoscale using AFM, showing a 36-fold increase in stiffness between St (144.58 ± 0.010 kPa) and So (4.35 ± 0.005 kPa) ($p<0.0001$); **Figure 3.3A**). Representative force curves recorded during the analysis were reported in **Figure 3.3B**.

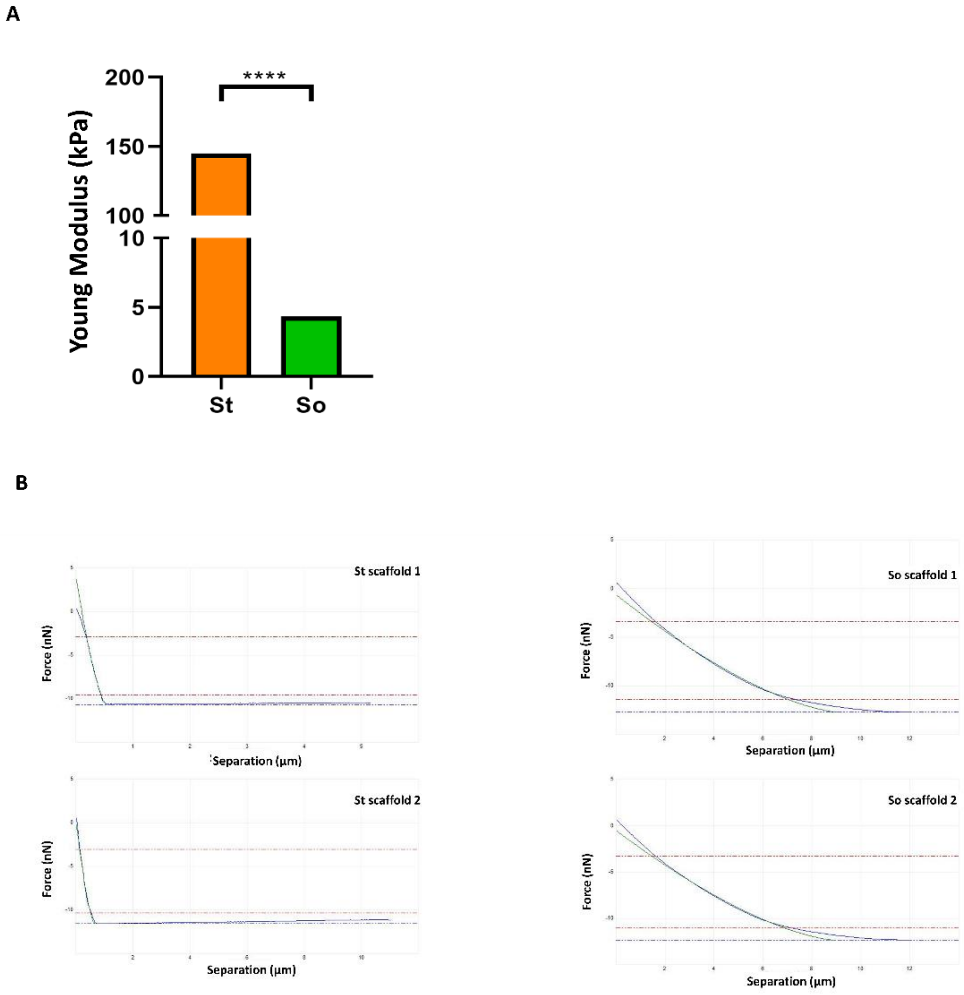

Figure 3.3. Mechanical features of native normal/cancer tissue are mimicked in a 3D collagen-based in vitro system, using different percentage of crosslinker 1,4-butanediol diglycidyl ether (BDDGE). (A) Atomic Force Microscopy analysis of Young modulus (kPa) in St and So scaffolds. (B) Representative plots of force/separation curve for mechanical characterization using AFM. Two extended ramp force for St and So scaffolds are reported since they were used for Young's modulus calculations.

Shear rheometry was used to calculate the mechanical parameters of the bulk scaffolds [385], in order to characterize the elastic, elastoplastic, and viscous flow behaviour of both St and So at the

tissue scale. St storage modulus and loss modulus at 1Hz (11.271 ± 0.619 kPa and 0.67 ± 0.187 kPa, respectively) were significantly increased compared to those of So (1.816 ± 0.24 kPa and 0.259 ± 0.043 kPa, respectively) ($p<0.0001$, $p<0.05$) (**Figure 3.4A**), indicating greater viscoelasticity of St compared to So scaffolds. Representative curves indicating samples frequency sweeps run at fixed 0.1% applied strain are reported in **Figure 3.4B**. Furthermore, the scaffold tan δ was analysed as G"/G', and both scaffolds showed values less than 1, confirming their solid-like behaviour. St scaffolds showed lower tan δ (0.06 ± 0.003) compared to So (0.14 ± 0.008), indicating a greater ability of the So material to absorb energy and relieve stress when compared to the St material (**Figure 3.4C**).

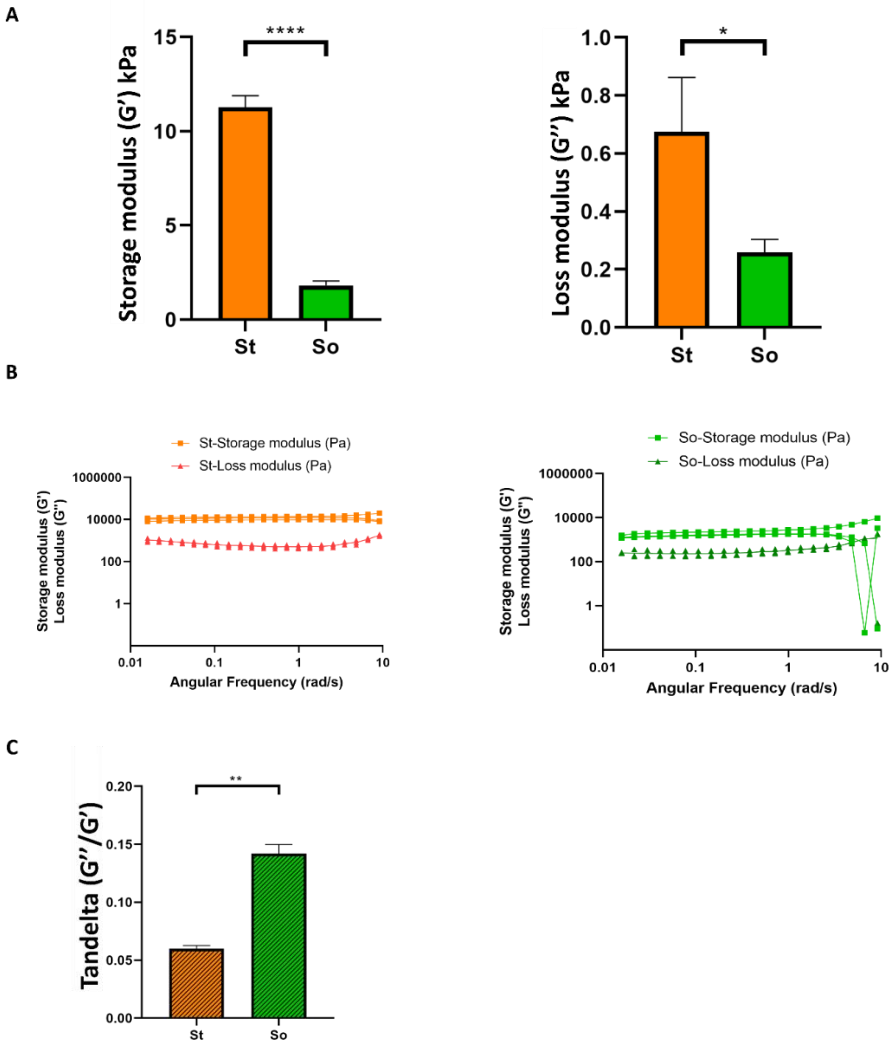

Figure 3.4. Rheology analysis confirming solid-like behaviour of St/So scaffolds with higher elastic modulus in St scaffolds. (A) Rheology analysis of storage modulus (G', kPa) and loss modulus (G", kPa) in St and So scaffolds. Data are mean + standard deviation (n=3). T test with Welch's correction, ****p<0.0001, *p<0.05. (B) Frequency sweeps were run at fixed 0.1% applied strain. During the frequency sweep, the frequency is varied while the amplitude of the deformation (shear stress) was kept constant at 0.1%. (C) tanδ (G"/G') analysis of St and So. Data are mean + standard deviation (n=3). T test with Welch's correction, **p<0.01.

Analysis of SEM images of both So and St showed the typical porous structure of a 3D sponge scaffold (**Figure 3.5A**). Porosity measurements showed that St scaffolds exhibited an average pore size of 5000 ± 400 μm^2, corresponding to an average diameter of 80 µm, compared to an average So pore size of 2564 ± 698 μm^2 and an average diameter of 57 µm (Figure 2B; p<0.01), with comparable pore circularity (**Figure 3.5B**). Fourier transform infrared spectroscopy (FTIR) and thermo-gravimetric Analysis (TGA) were used to characterize scaffold composition after crosslinking. FTIR spectral analysis for both St and So showed that the amide I (1700–1600 cm^{-1}), amide II (1600–1500 cm^{-1}), and amide III (approximately 1200–1300 cm^{-1}) peaks, which constitute the characteristic signature of collagen material, were reported in both St and So sample profiles, with no significant differences observed (**Figure 3.5C**). Similarly, no significant difference was observed between St and So samples using TGA analysis. Both materials underwent endothermic reaction at around 100°C (evaporation of the water moisture present in the material), while thermal transition and material degradation happened after 200°C of the heating ramp, for both samples (**Figure 3.5D**). Finally, to validate scaffold suitability for cell seeding, contact angle (CA) measurements were used, showing both scaffolds had hydrophilic properties (CA < 90°), with no significant differences observed between the two materials (**Figure 3.5E**).

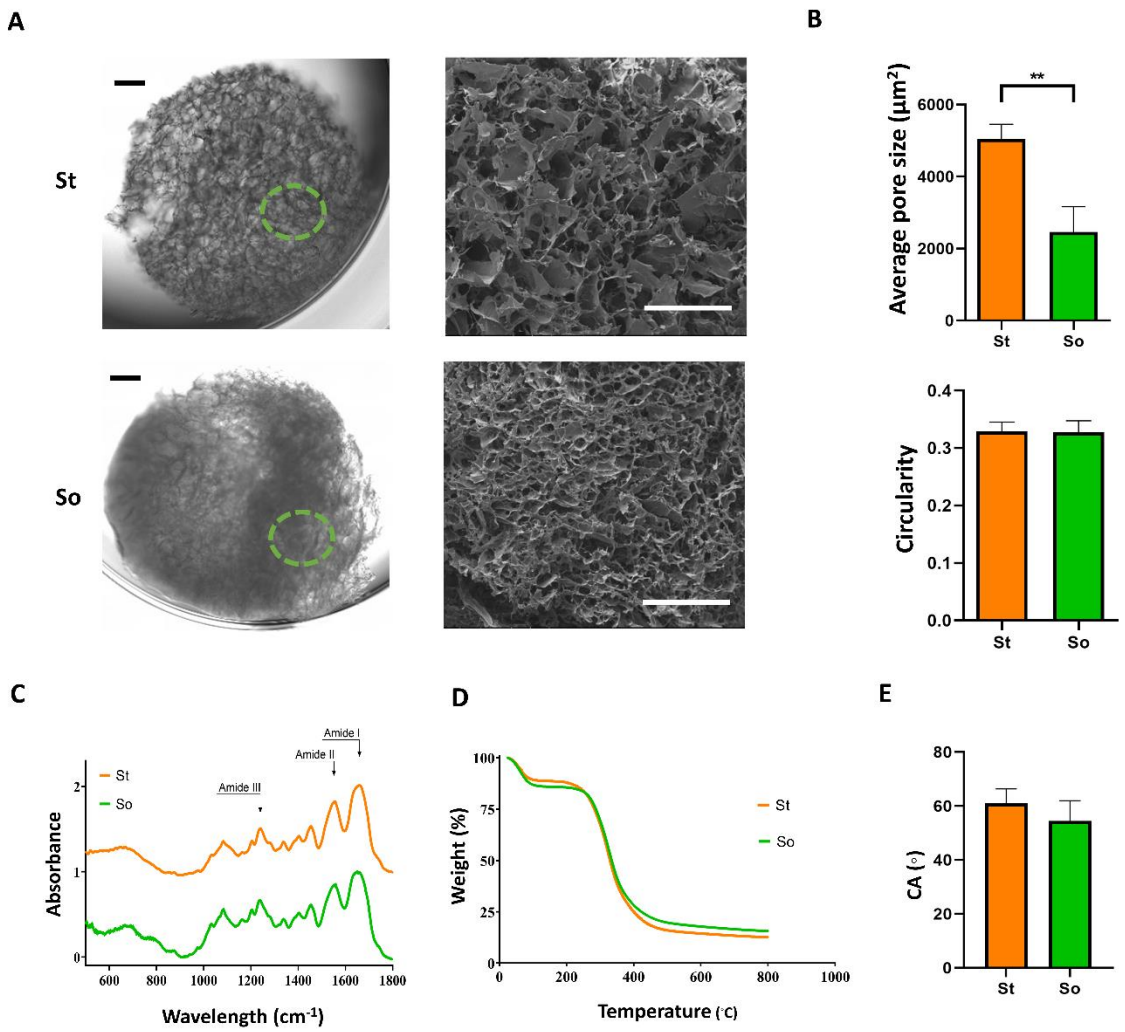

Figure 3.5 St scaffolds showed higher average pore sizes, but same composition and hydrophilic properties compared to So. (A) Bright-field images of whole scaffolds (left), SEM magnification of the scaffolds (right). (B) SEM analysis of average pore size (µm^2) and circularity. Data are mean + standard deviation (n=3). T test with Welch's correction, **p<0.01 (C) FTIR spectra of St and So scaffolds. The spectra highlighted the presence of typical collagen Amide I, Amide II, Amide III. (D) Thermo gravimetric Analysis (TGA). (E) Water contact angle (WCA) measurements.

3.3.2 Scaffolds support fibroblasts colonisation and activation with TGFβ1.

In order to develop a model to study NF and AF response to stiffness within a 3D environment and assess the suitability of the 3D collagen scaffolds for stromal studies, MRC5 cells were used and were activated (AFs) at D3 after seeding on scaffolds using a dose range of TGFβ1. As demonstrated in chapter 2, TGFβ1 treatment stimulated conversion of NFs into AFs on 2D culture. First, we tested if cells seeding in a 3D environment could interfere with fibroblasts activation under TGFβ1 treatment. To do so, we compared 2D culture with 3D collagen scaffold (we used the normal/soft scaffold for testing), evaluating gene expression of AFs markers FAP and αSMA.

Fibroblasts were treated with TGFβ1 at day3 and day6 after seeding on 3D scaffolds. Compared to 2D culture, 3D scaffold culture showed an increase in gene expression of both FAP and ACTA2 (α-SMA) after TGFβ1 treatment, highlighting the substrate dimensionality effect on fibroblast activation (**Figure 3.6A**). To determine the elective dosage to induce fibroblasts activation in a 3D environment, we analysed AFs markers expression compared to the untreated scaffolds (NFs culture), reporting a significant increase in ACTA2 (α-SMA) (3.8-fold) and FAP (4.6-fold) expression following treatment with 25 ng/ml of TGFβ1 on soft scaffolds ($p<0.001$ and $p<0.0001$). Similarly, increased expression of ACTA2 (α-SMA) (2.7-fold) and FAP (2.5-fold) were observed when treated with 50 ng/ml of TGFβ1 ($p<0.01$ and $p<0.05$) (**Figure 3.6B**).

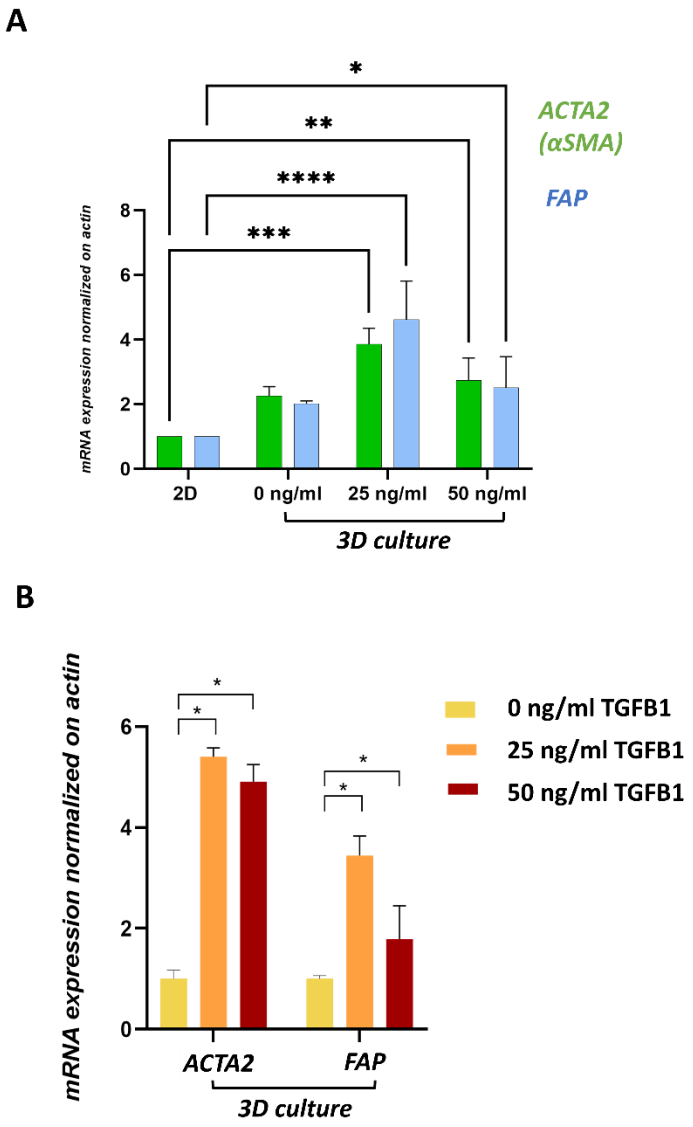

Figure 3.6. TGFβ1 treatment stimulates conversion of NFs into AFs (3D culture). (A) ACTA2 (αSMA) and FAP mRNA expression under 0-25-50 ng/ml TGFβ1 treatment. Data normalized on 2D control. Data are mean + standard deviation (n=3) (B) ACTA2 (αSMA) and FAP mRNA expression under 0-25-50 ng/ml TGFβ1 treatment. Data normalized to untreated 3D So scaffold control. Data are mean + standard deviation (n=3). T test with Welch's correction, *p<0.05.

Fibroblast activation was confirmed under 25 ng/ml TGFβ1 following FAP expression using flow cytometry on both 2D and 3D So and St scaffolds (**Figure 3.7**). As result, the optimal TGFβ1 dose to induce NFs conversion to AFs was confirmed to be 25 ng/ml TGFβ1.

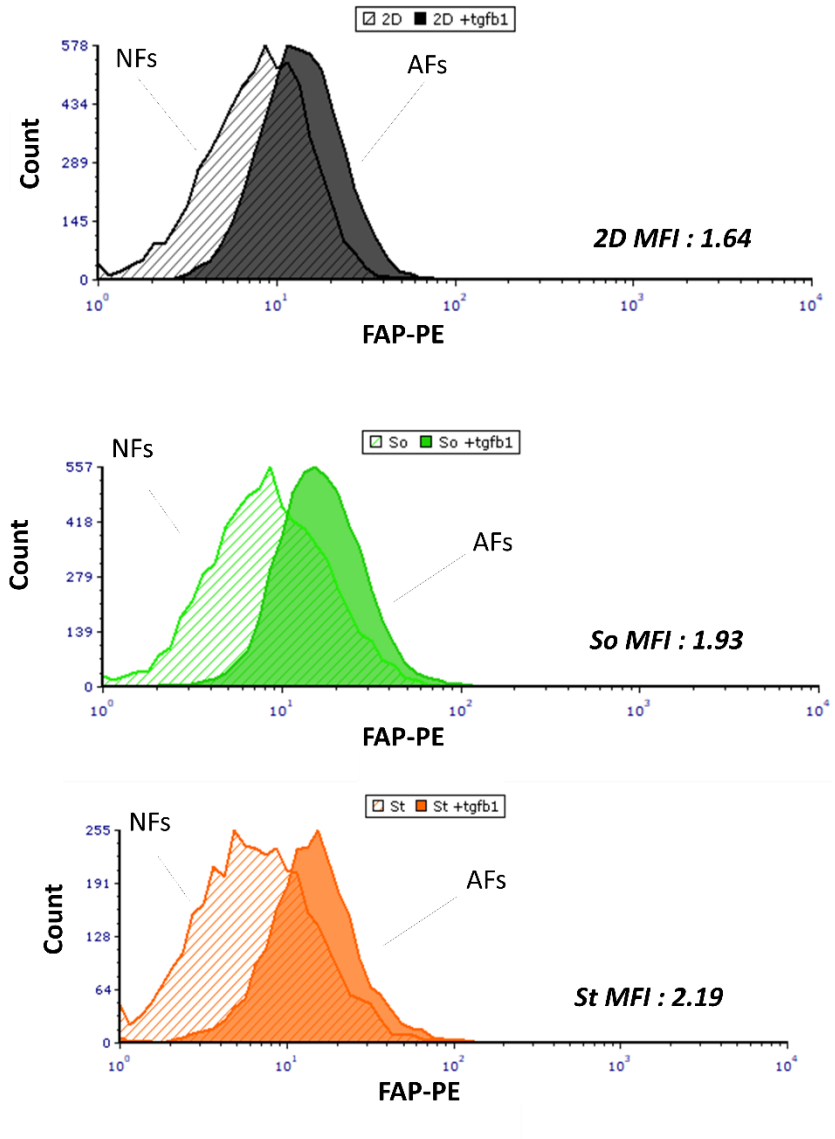

Figure 3.7. TGFβ1 treatment stimulates conversion of NFs into AFs (3D cultures). FAP expression assessed with flow cytometry on 2D, So, and St scaffolds after 25 ng/ml TGFβ1 treatment. MFI = minimum fluorescence intensity.

After establishing the protocol to activate fibroblasts, their ability to attach, grow, and colonize the differential mechanical scaffolds was determined. Cell death was monitored after 7 days of seeding in 2D and 3D (St and So), using calcein/ethidium bromide staining, and assessed by flow cytometry and epifluorescence microscopy. When analysed quantitatively for viability, NFs and AFs were both viable, exhibiting calcein-positive staining on both St (NFs: 84%±7.2, AFs: 87.3%±6.1) and So (NFs: 81%±6.4, AFs: 84.3%±6.9) (**Figure 3.8**). Fluorescence images of the

whole scaffolds were collected setting an automatic focus on the green channel (live cells/calcein) for all the scaffold areas collected (only one plane) , and then performing a final stitch to obtain the whole scaffold rendering. From those pictures, NFs and AFs showed a homogeneous distribution at day7 on all the scaffold surface with no differences or specific distribution patterns (**Figure 3.9).**

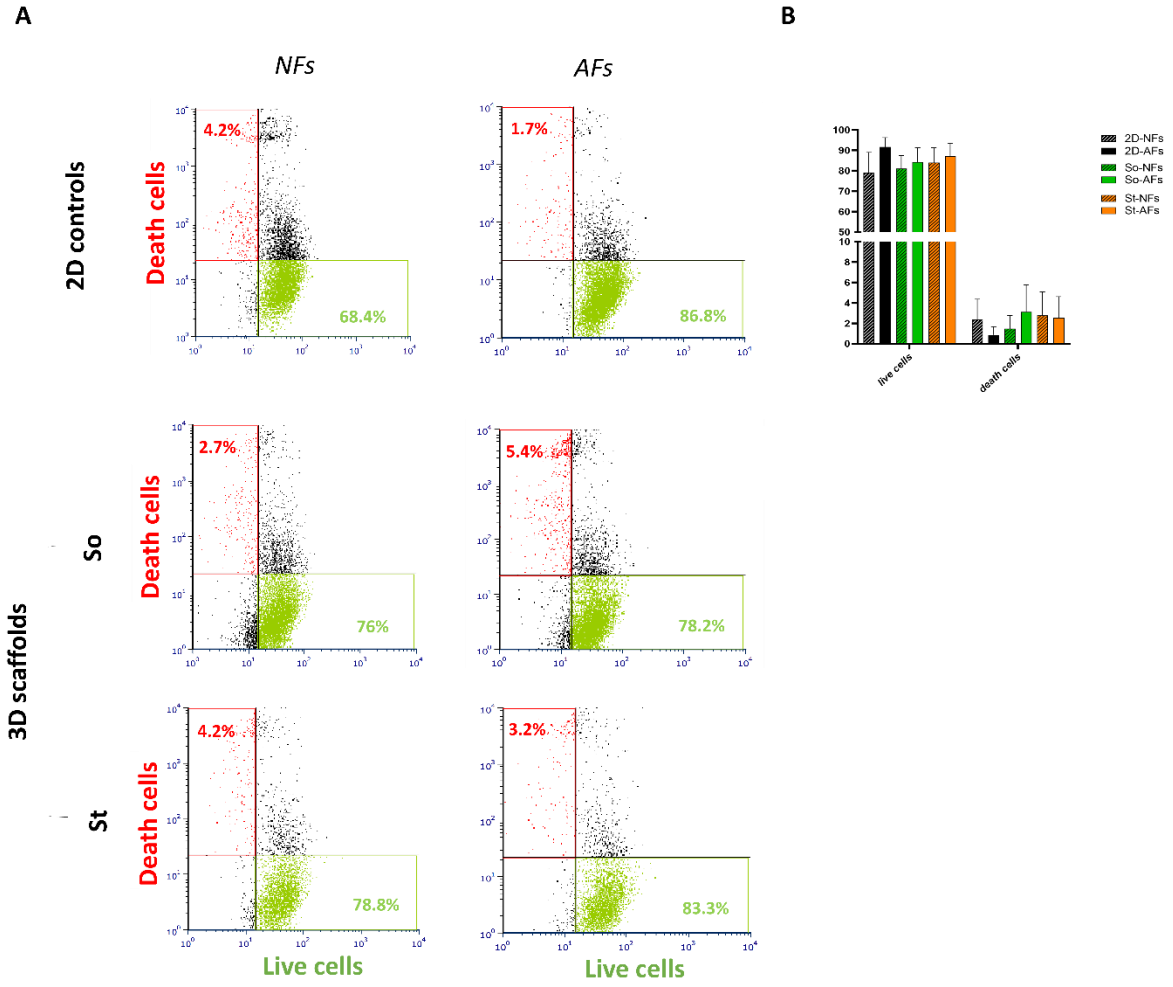

Figure 3.8. NFs/AFs were viable and proliferated on both St and So scaffolds. (A) Representative plots of cell live/death staining analysed with flow cytometry and (B) statistical analysis.

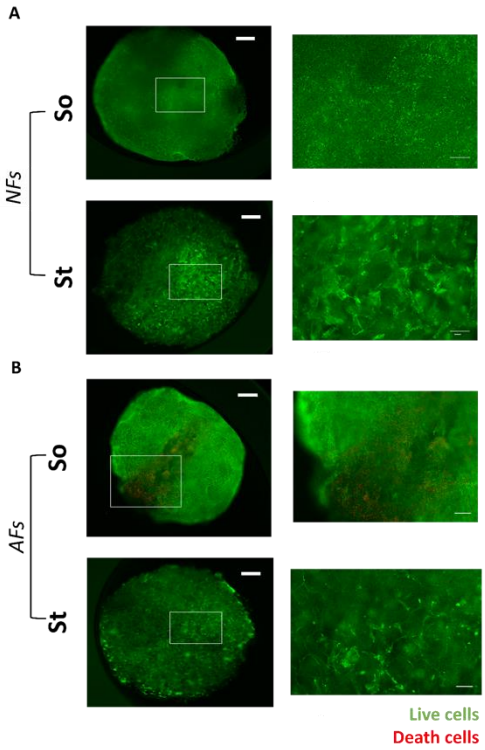

Figure 3.9. NFs/AFs were viable and colonized both St and So scaffolds. Cell live/death staining analysed with fluorescence microscopy. Analysis and imaging were performed after 7 days of culture. Scale in images of whole scaffold: 500 µm, scale in magnified images: 100 µm. Data are mean + standard deviation (n=3).

3.3.3 Fibroblast migration and morphology is altered in stiffer mechanical environment

Durotaxis is a type of directed cell migration in which cells respond to a gradient of extracellular stiffness [571]. For example migration of fibroblasts toward areas of established fibrosis, characterized by high stiffness, amplifies the fibrotic response [403, 572]. Rigidity sensing and durotaxis are thought to be important elements in wound healing, tissue formation, and cancer [573]. To study this phenomenon in 3D sponge system we evaluated fibroblast migration pattern and length on 3D scaffolds, using live cell confocal imaging analysis of NFs and AFs cultured in 3D, stained for calcein (live cells) and DAPI (nuclei) (**Figure 3.10**). A step size of 10 µm and a total of 800 µm size range was recorded for each scaffold, within 2hrs cycle interval over 24 hrs between day3 and day4 of culturing under normal media condition or under TGFβ1 addition. Analysis was performed using the Cell Sens software object tracking input on each image collected in the z interval before the stitching to obtain the whole scaffold rendering. Analysis was performed on DAPI (nuclei) channel for track length and displacement while cells circularity was determined using the calcein channel. Rendered movement tracking showed that AF directionality in So

scaffolds followed a specific pattern, converging towards the centre of the scaffold, while NFs had more random motility, with no specific direction (**Figure 3.10A**, top). Conversely, NFs and AFs grown on St scaffolds showed very few and short movements (**Figure 3.10A**, bottom). Overall, the migration path of both NFs and AFs grown in St scaffolds was significantly decreased in both track length and displacement compared to So (**Figure 3.10B-C**; $p<0.05$), suggesting an impairment of cell migration on the stiff material. Cellular morphology was also impacted by substrate stiffness, with both NF and AFs showing statistically higher cell circularity when cultured on St materials (**Figure 3.10D,** $p<0.01$ and $p<0.05$), in part explaining the limited motility.

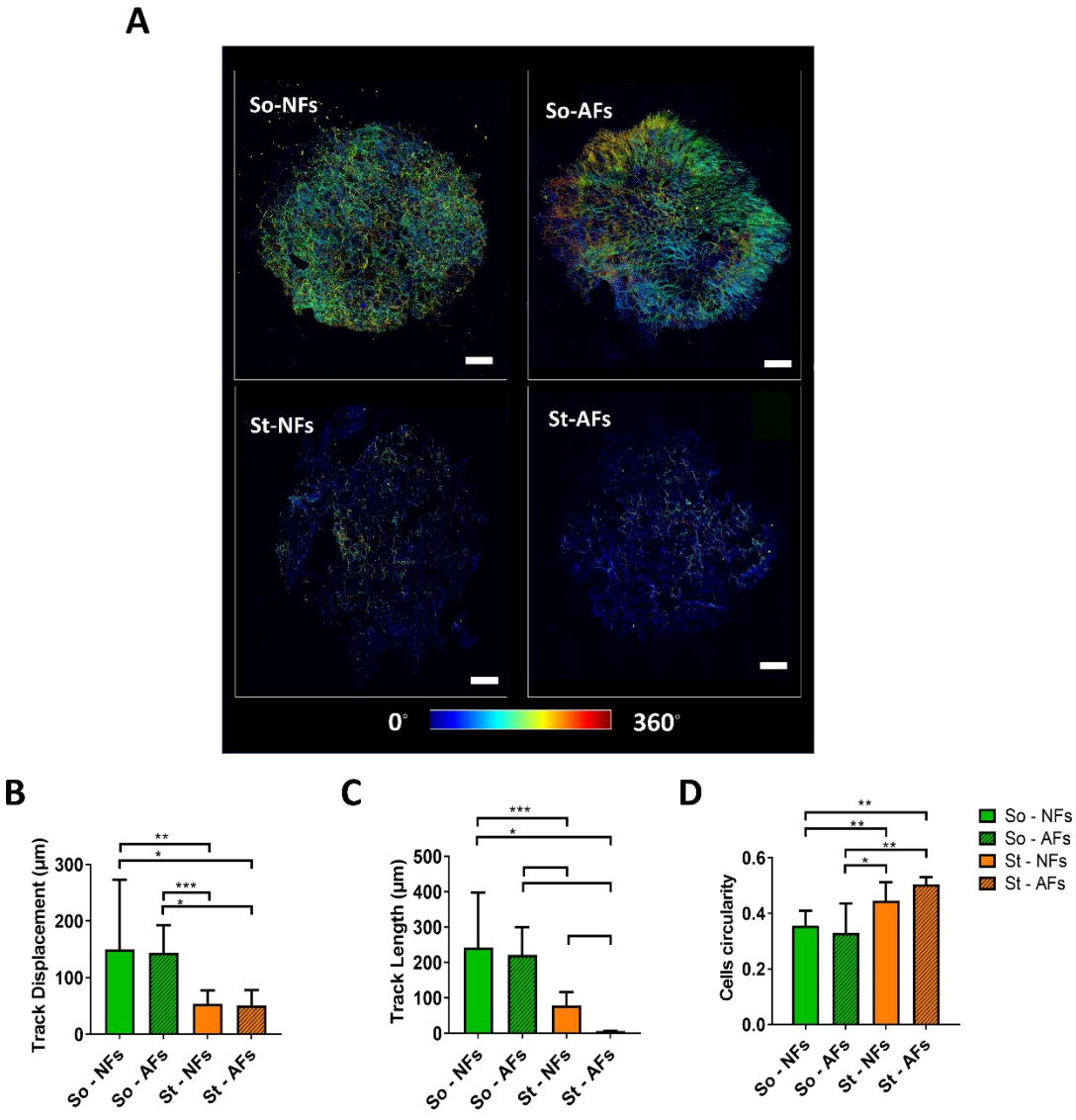

Figure 3.10. NFs and AFs grown on St scaffolds showed shorter migration distance across scaffold and higher cell circularity compared to those on So. (A) Live imaging rendering of the whole 3D scaffold (800-µm height) of NFs and AFs grown on St and So scaffolds from day 3 to day 4. Migratory tracks are shown using a rainbow scale. Scale bar: 600 µm. (B) Track length (in µm), (C) track displacement (µm), and (D) cell circularity were analysed using cellSens software. Data are mean + standard deviation of 30 areas, *p<0.05, **p<0.01,***p<0.001, ****p<0.0001.

3.3.4 Collagen fibre alignment is prevented on St scaffolds

The orientation of collagen fibres appears to play a critical role in tumour progression and fibrosis [574-576]. Specifically tumour-associated collagen signatures (TACS) are classified as markers of tumour progression [577]. When remodelling of the stroma progresses to the final stage, collagen fibres become bundled and aligned perpendicular to the tumour boundary, termed TACS-3, creating highways on which tumour cells are observed to migrate *in vivo*, and correlates with increased invasion and metastasis in mouse models [528], and it represents an independent prognostic signature that correlates strongly with poor patient survival [82]. The main players in this are fibroblasts which are capable of using Rho and Rho kinase (ROCK)-mediated actin-myosin contractility to orient collagen fibres [578-580]. Additionally, fibroblasts can deposit matrices containing aligned fibronectin or collagen in vitro [581]. While it is known that enhanced collagen deposition leads to a significantly stiffer ECM, and collagen matrices can be stiffened via cross-linking without altering the network architecture, it is unclear how aligning collagen matrices affects other architectural and mechanical features [582].

To investigate if fibroblasts activation and scaffolds plasticity will result in a modified collagen fibre alignment, we computationally analysed collagen orientation from different areas of the scaffold using a Fluo View^{TM} 3000 confocal microscope after 7 days of culture. The predominant orientation, for both NF and AFs, was around 0 degrees among all the So samples, whereas the orientation was more dispersed, shifting to mostly -45 and 45 degrees in both cell types on the St materials. Interestingly, AFs on St scaffolds showed a hybrid pattern with a prevalent distribution between -45 and 45 degrees and no predominant direction (**Figure 3.11A**). 6 images for each

scaffold were obtain from the maximum projection of a 200 µm z stack and analysed with Fiji plugin OrientationJ. Representative images of a collagen fibre and scaffold areas (utilized for analysis) are shown in **Figure 3.11B-C**. This data, alongside the rounded phenotype and reduced track length and displacement, support the inactivity of AFs on this stiffer scaffold.

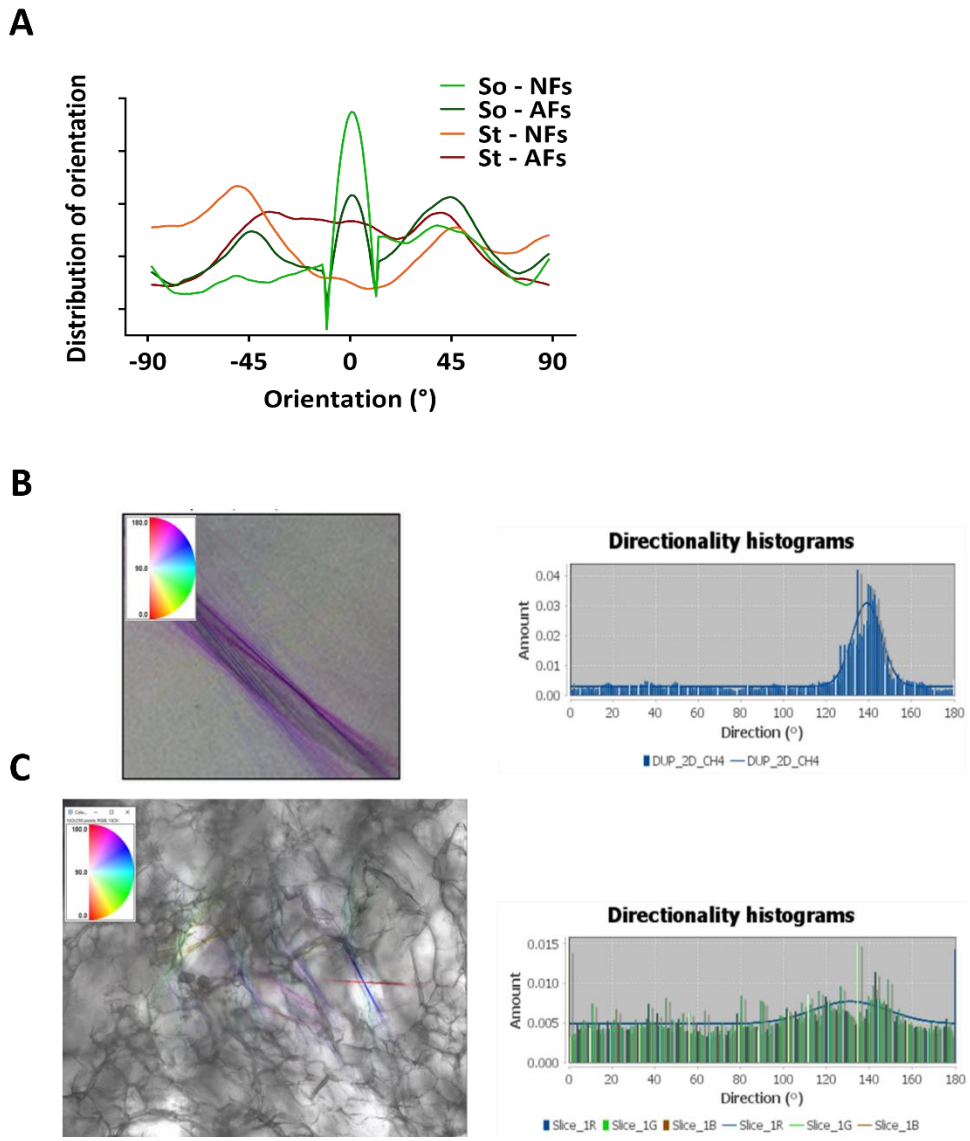

Figure 3.11. Representative images and directionality histograms of a single collagen fibre and a scaffold image. (A) Collagen orientation analysis at 7 days of culture. (B) Representative brightfield pics of a single fibre and a (C) scaffold image collected and analysed with Fiji plugin OrientationJ.

3.3.5 Scaffold remodelling and stiff substrate-promoted mechanotransduction

To test fibroblasts' contraction activity and ability to remodel collagen scaffold microenvironment, we recorded diameter changes over 7 days in culture. The shrinking effect on both So and St scaffolds was recorded from day 3 with live cell imaging, demonstrating that both NFs and AFs actively contract the So matrix between days 3 and 4 of culture (Videos from 1-4). Starting at 4 days to 7 days of culture, scaffold shrinkage was higher in So scaffolds culture with AFs compared to NFs (NFs/AFs : day4 5512.4µm ±130.5/3884.3µm ±158.9; day5 4739.6µm ±420.5/3921.6 µm ±17.9;day6 4546.5µm±612.4/3363.9µm±72.1; day7 4345.4µm ±655.1/3341 µm ±151.4, $p<0.05$) demonstrating the susceptibility of So materials to remodelling as well as higher contractility function of AFs compared to NFs in So scaffolds. No significant change in St scaffolds shrinkage was recorded for either NF or AF cells after 7 days (**Figure 3.12**). Neither NFs or AFs showed an ability to promote St collagen scaffold contraction between days 3 and 4 (Videos, calcein-only staining and multiview).

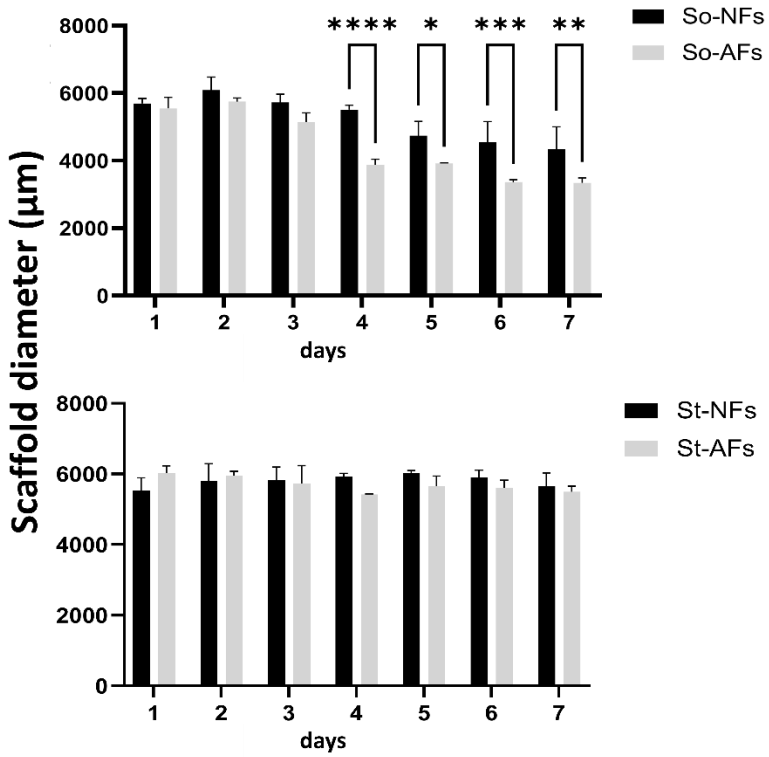

Figure 3.12. So scaffolds' diameter decreases more under AFs culturing than NFs, while St scaffolds diameters doesn't change. Scaffold diameter analysis over 7 days of culture of NFs and AFs on So scaffolds (top) and St scaffolds (bottom). Data are mean + standard deviation (n=3). Data are mean + standard deviation (n=3).

H&E staining suggested that So scaffold shrinking resulted in a dense matrix (eosin, extracellular matrix) after 7 days, with cells more in contact with each other (haematoxylin stain, purplish blue) whereas St scaffolds don't vary its structure (**Figure 3.13**).

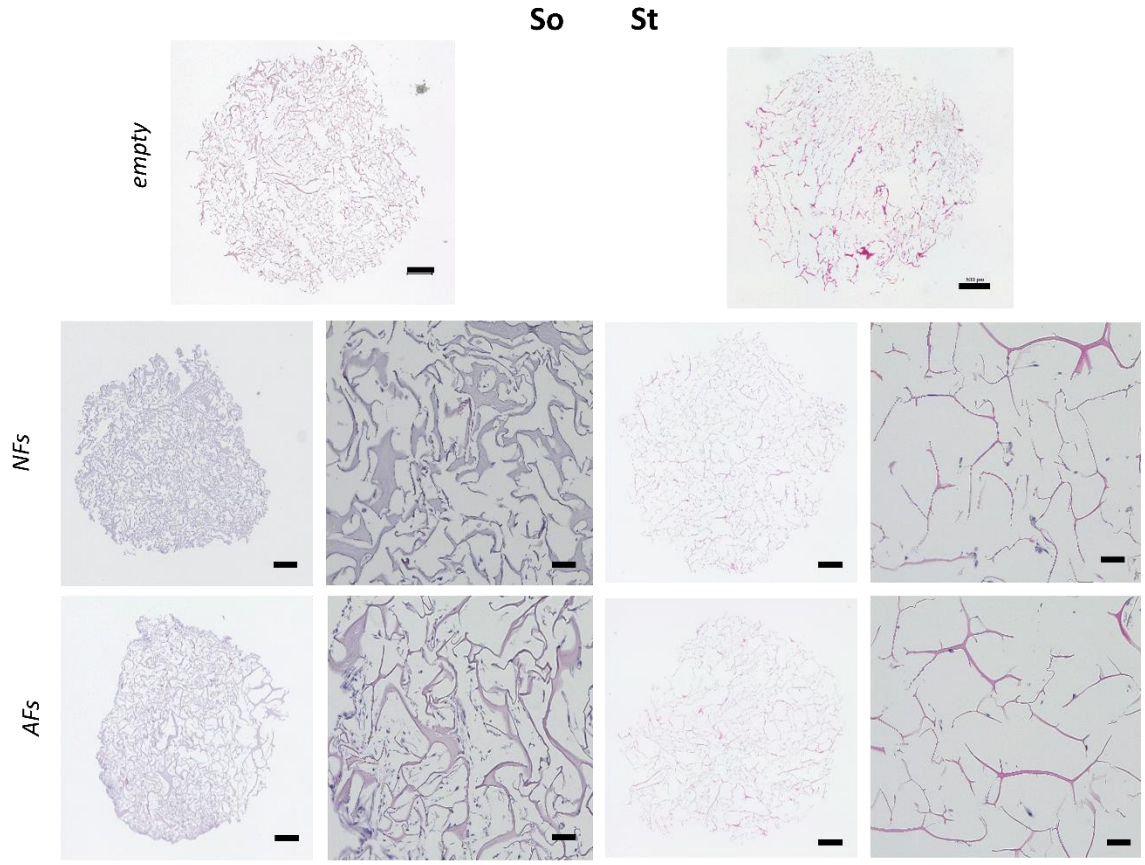

Figure 3.13. Scaffolds histology shows a denser matrix on So scaffolds after culturing AFs and NFs. H&E staining of empty and cellularized scaffolds with NFs and AFs at day 7. Scale in images of whole scaffold: 500 µm, scale in magnified images: 100 µm.

3.3.6 Fibroblast inactivity promoted by St scaffolds doesn't impact cell cycle transitions or proliferation

It is classically believed that resident fibroblasts in any tissue become activated during wound healing and revert to their inactive state upon resolution, however, in cancer, this activation often becomes irreversible, leading to formation of CAFs [1]. Also during fibrosis regression, fibroblasts are not fully eliminated but become inactivated, reverting to a quiescent, antiproliferative state [583].

To investigate if migration and remodelling blockage promoted by St scaffolds on NFs and AFs is linked to an induction of fibroblasts 'resting' or 'quiescence' state, cell cycle and proliferation was evaluated using propidium iodide to quantify DNA content (**Figure 3.14**) and CellTracker™ Green 5-chloromethylfluorescein diacetate (CMFDA) staining (**Figure 3.15**). Cell cycle analysis by quantitation of DNA content was one of the earliest applications of flow cytometry [584]. In this application, cells that are in S phase will have more DNA than cells in G1. They will take up proportionally more dye and will fluoresce more brightly until they have doubled their DNA content. The cells in G2 will be approximately twice as bright as cells in G1 [585].

Representative histograms of PI cell cycle analysis are reported in **Figure 3.14A**. Using quantitative analysis to assess the cell cycle state of the cell from DNA content showed a higher number of cells in the G1 and S phases was observed in 2D compared to 3D ($p<0.05$), with no significant differences observed between NFs and AFs grown on So and St scaffolds (**Figure 3.14B**). To assess if the recorded number of cells in G1 will transition to S phase for synthesis of DNA, resulting in cell division and subsequent mitosis [586], we assessed proliferation using CMFDA (**Figure 3.15**). Representative histograms used for analysis are reported in **Figure 3.15A**. Overall, fibroblasts in 2D presented a slightly higher number of cell generations (up to generation 8) compared to 3D but no significant difference in number of generations was reported with this analysis (**Figure 3.15B**). We concluded that St scaffolds impairs fibroblasts functionality but not proliferations and generations formations.

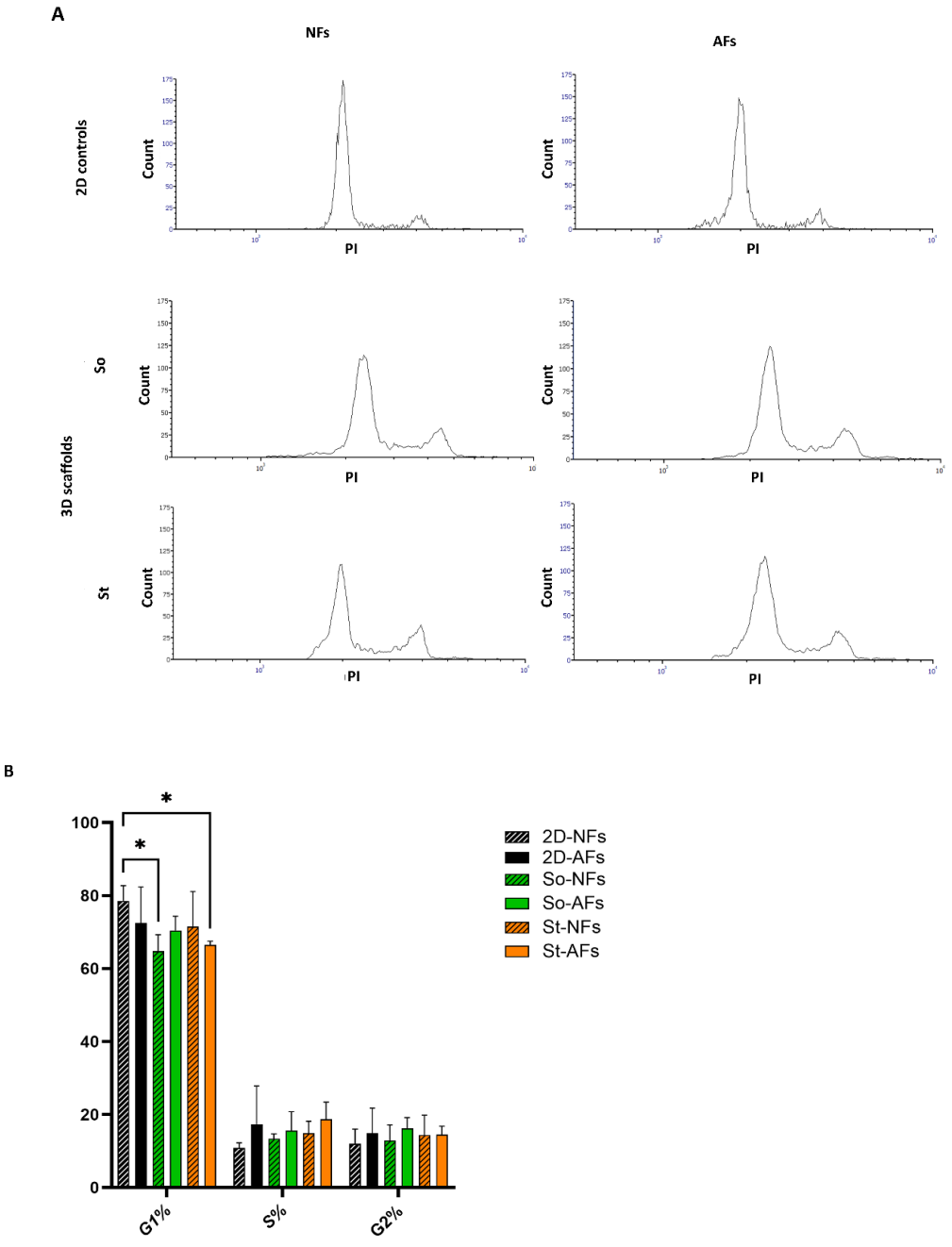

Figure 3.14. St materials culturing doesn't affect cell cycle. (A) Propidium Iodide (PI) raw data cell cycle analysis using flow cytometry and (B) analysis. Analyses were performed after 7 days of culture.

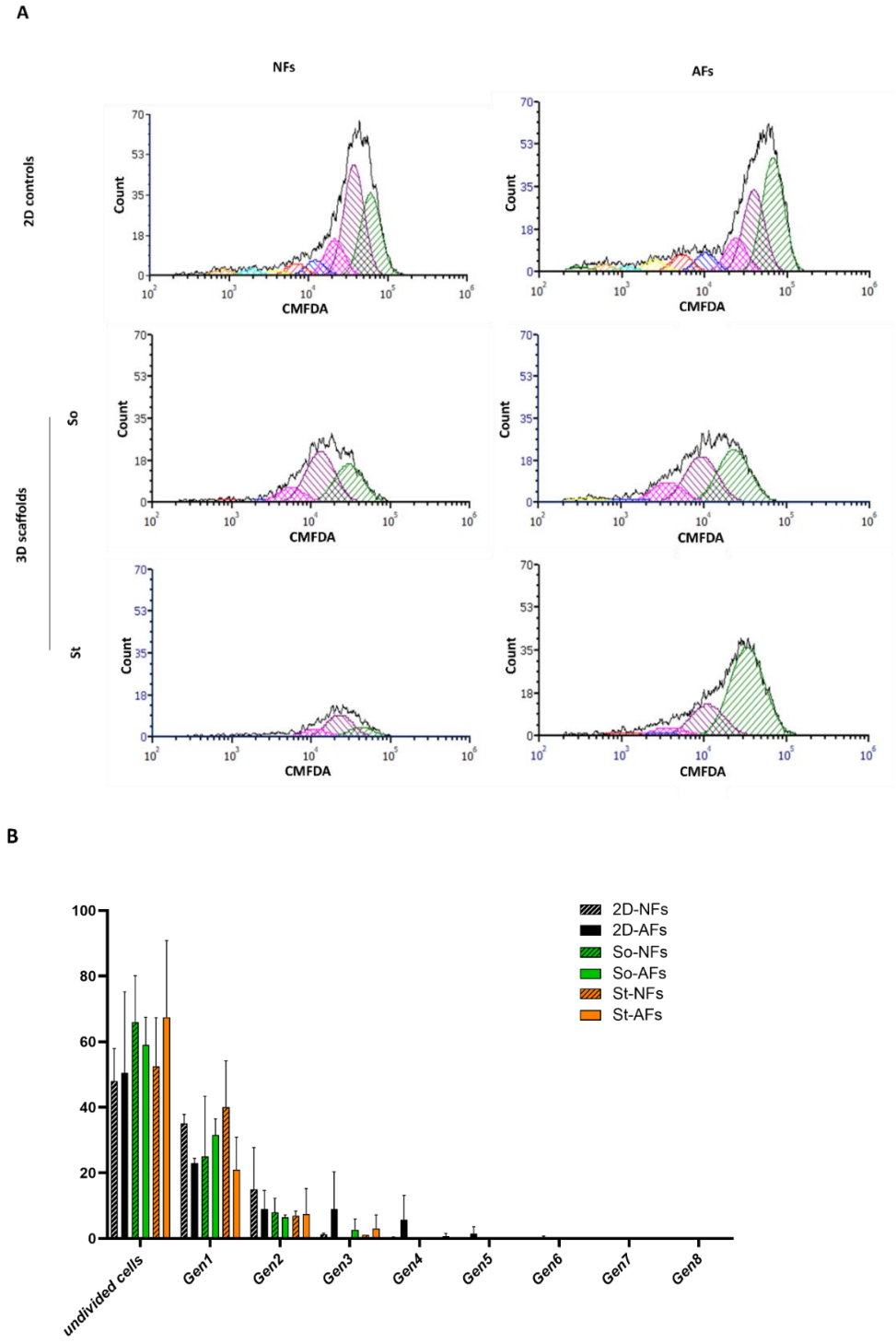

Figure 3.15. St materials culturing doesn't affect proliferation. (A) CellTracker™ Green 5-chloromethylfluorescein diacetate (CMFDA) generation analysis flow cytometry raw data and (B) analysis. Analyses were performed after 7 days of culture.

3.3.7 St scaffold mechanics don't change under NFs/AFs culturing condition, while inducing YAP overexpression.

Utilising rheology, we evaluated whether the recorded macroscopic changes in scaffold diameter resulted in physical properties changes after 7 days of culture. A significant decrease in the So material storage modulus was observed at day 7 when cultured with NFs or AFs, compared to both empty scaffold (So D0, $p<0.01$) and So scaffold on day 1 (So-NFs/AFs vs D0; $p<0.01$ and $p<0.05$). No changes were observed in St elastic properties (**Figure 3.16**). No significant variation was observed in scaffold material loss modulus for either So or St scaffolds (**Figure 3.16, right**), further highlighting the plasticity of the softer So material to remodelling and the suitability of rheology analysis to test bulk tissue mechanic of fresh biological samples.

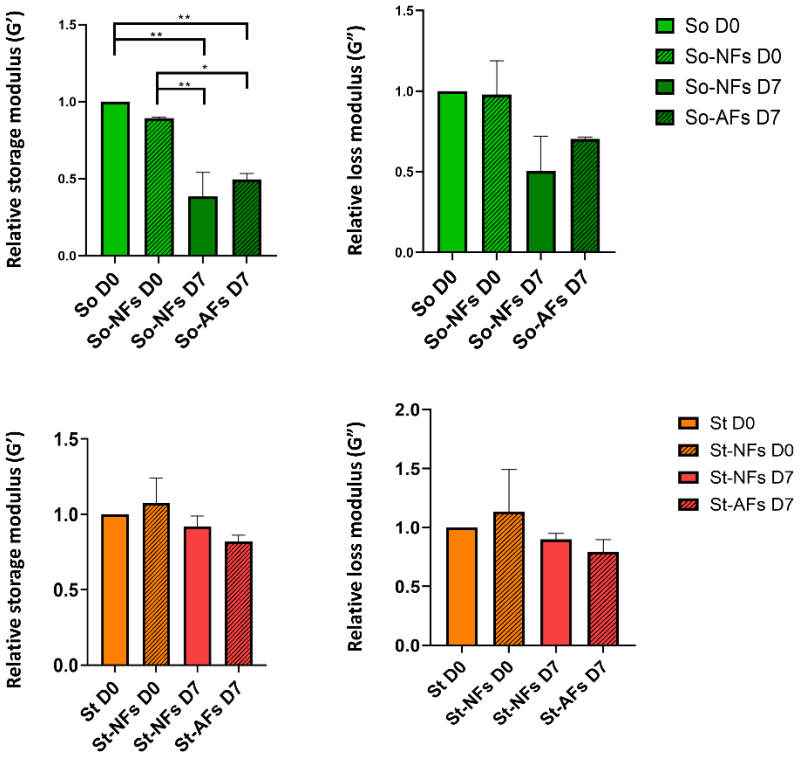

Figure 3.16. So, scaffolds remodelling result in So scaffolds softening. Rheology analysis of storage modulus (G', left) and loss modulus (G", right) in St and So scaffolds. Data normalized to D0 controls. Data are mean + standard deviation (n=3). T test with Welch's correction, **p<0.01, *p<0.05.

Mechanical changes in the microenvironment can strongly affect cells at the transcriptomic level through a process called mechanosensing [587]. We evaluated the expression of two master mechanosensors and transcriptional activators, *Yap1* and *Taz*, which are known mechanosensors and oncogenes, triggering cancer initiation and growth of most solid tumours [588]. Specific overexpression of the oncogene and mechanosensor YAP was observed on St scaffolds (**Figure 3.17**). Interestingly, many evidences indicates that YAP activation and overexpression is implicated in resistance to targeted therapies, chemotherapy (like DNA damaging agents), radiation, and immunotherapies [589] and also its chronic expression upregulated indices of fibrosis and inflammation in the absence of additional stress [590].

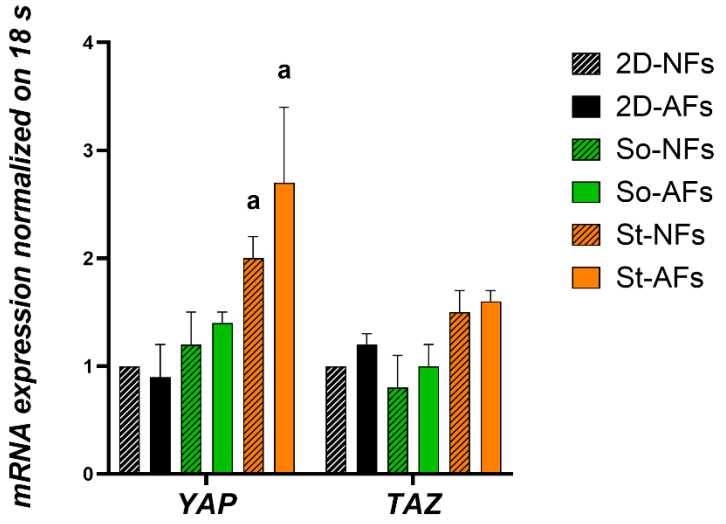

Figure 3.17. YAP is induced by St scaffolds on both AFs and NFs. Mechanosensing-related genes (*YAP*, *TAZ*) mRNA expression in NFs and AFs at day 7 of culturing on 2D, So scaffolds, and St scaffolds. Data normalized to 2D control-NFs. Data are mean + standard deviation (n=3).

3.3.8 NF/AFs gene expression is impacted by scaffolds stiffness

Different AF cell behaviour between So and St substrates is observed, with the So material stimulating AF migration and matrix reorganization resulting in scaffold shrinkage, while the St scaffold promoted AF mechanosensing seemingly resulting in impaired AF migratory properties

and contractile functionality. To investigate these distinct AF phenotypes and understand mechanistic differentiation in terms of gene expression profiling, transcriptome-wide RNA-seq was conducted on AFs grown in 3D on So and St scaffolds after 7 days, using 2D culture of both NF and AF populations as relative controls.

Upon receipt of the raw files, FastQC analyses was performed to monitor the quality of the data. Phred scores are a measure of the accuracy of base calling from the sequencer. A Phred score of 40 indicates that there is a 99.99% chance that the base was called correctly, and a score of 30 indicates a 99.9% chance that the base was called correctly. An average Phred score of greater than 30 is usually considered sufficient. All samples met this criterion (**Table 3.1**). Statistics relating to mapping of reads to the genome are shown in **Table 3.2**. For all samples, >80% of reads are uniquely mapped confirming the validity of the data.

Table 3.1. FASTQ quality scores for each sequencing run.

File Name	Q1%	Q10%	Q25%	Q50%	Q75%	Q100%	Mean
A_2D NFs	29	35	36	36	36	37	35.82262
A_2D NFs	27	34	36	36	36	37	35.49504
A_2D CAFs	29	35	36	36	36	37	35.8442
A_2D CAFs	27	35	36	36	36	37	35.57637
A_So NFs	29	35	36	36	36	37	35.80783
A_So NFs	27	35	36	36	36	37	35.57458
A_So CAFs	28	35	36	36	36	37	35.82692
A_So CAFs	27	35	36	36	36	37	35.63125
A_St NFs	28	35	36	36	36	37	35.79867
A_St NFs	27	35	36	36	36	37	35.56892
A_St CAFs	28	35	36	36	36	37	35.83452
A_St CAFs	27	35	36	36	36	37	35.69236
B_2D NFs	28	35	36	36	36	37	35.84201
B_2D NFs	27	35	36	36	36	37	35.57498

B_2D CAFs	29	35	36	36	36	37	35.84985
B_2D CAFs	27	35	36	36	36	37	35.53889
B_So NFs	28	35	36	36	36	37	35.82767
B_So NFs	27	35	36	36	36	37	35.57949
B_So CAFs	28	35	36	36	36	37	35.82712
B_So CAFs	27	35	36	36	36	37	35.62871
B_St NFs	28	35	36	36	36	37	35.80843
B_St NFs	27	35	36	36	36	37	35.56776
B_St CAFs	29	35	36	36	36	37	35.85974
B_St CAFs	28	35	36	36	36	37	35.73892
C_2D NFs	28	35	36	36	36	37	35.77635
C_2D NFs	27	35	36	36	36	37	35.54497
C_2D CAFs	29	35	36	36	36	37	35.87072
C_2D CAFs	27	35	36	36	36	37	35.54733
C_So NFs	28	35	36	36	36	37	35.822
C_So NFs	26	34	36	36	36	37	35.42615
C_So CAFs	28	35	36	36	36	37	35.80585
C_So CAFs	27	35	36	36	36	37	35.69676
C_St NFs	28	35	36	36	36	37	35.80708
C_St NFs	27	35	36	36	36	37	35.68599
C_St CAFs	29	35	36	36	36	37	35.85304
C_St CAFs	28	35	36	36	36	37	35.70025

Table 3.2. Sequence alignment and quality mapping.

Treatment	Read Length	No. of Reads	% Uniquely Mapped	% Mapped to too many loci	% Unmapped	Coverage
A_2D NFs	300	85980329	94.27%	2.90%	2.83%	14.74

A_2D CAFs	300	90748849	94.28%	2.89%	2.83%	15.56
A_So NFs	300	96532086	93.70%	2.85%	3.44%	16.45
A_So CAFs	300	84577932	94.46%	2.79%	2.76%	14.53
A_St NFs	300	82408329	94.75%	2.84%	2.41%	14.2
A_St CAFs	300	82771004	94.52%	2.86%	2.62%	14.22
B_2D NFs	300	90243975	94.16%	3.17%	2.67%	15.45
B_2D CAFs	300	96044153	93.90%	3.13%	2.97%	16.4
B_So NFs	300	92364058	93.99%	3.25%	2.76%	15.78
B_So CAFs	300	85642219	93.31%	3.70%	2.98%	14.53
B_St NFs	300	77974162	93.80%	3.19%	3%	13.3
B_St CAFs	300	90681533	93.72%	3.00%	3.29%	15.45
C_2D NFs	300	78264746	92.61%	3.65%	3.74%	13.18
C_2D CAFs	300	81839143	94.05%	2.84%	3.11%	13.99
C_So NFs	300	103174928	93.88%	3.27%	2.85%	17.61
C_So CAFs	300	95692330	93.91%	3.04%	3.06%	16.34
C_St NFs	300	80649950	94.09%	3.27%	2.64%	13.8
C_St CAFs	300	91041532	93.87%	2.89%	3.24%	15.54

3.3.8.1 Sample comparisons

Principal Component Analysis (PCA) provides information on the overall structure of the analysed dataset. PCA clearly showed the generation of distinct clusters, suggesting that both substrate stiffness and TGFβ1 activation led to distinct AF phenotype differentiation at the transcriptome level (**Figure 3.18**). Good reproducibility was observed between biological replicates and the most significant separation between data sets was between the activated and not activated state of fibroblasts promoted by TGFβ1 treatment.

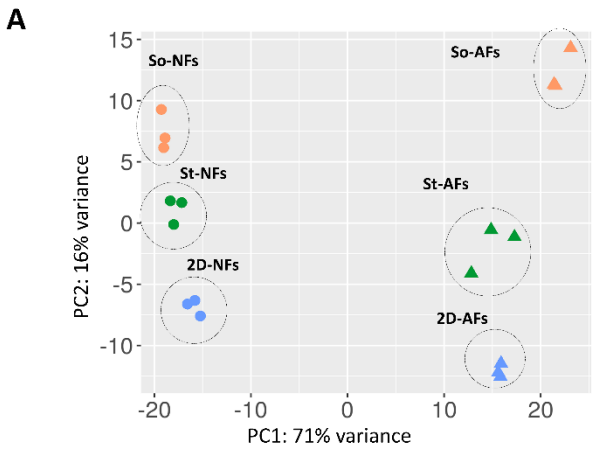

Figure 3.18. Datasets separation derived mostly from fibroblasts activation state. (A) Principal Component Analysis (PCA) of each biological replicate/condition.

To confirm fibroblast activation under TGFβ1 treatment, regardless of the substrate, the TGFβ1 'core' transcriptomic profile was analysed, reporting all the genes in common between AFs grown among both 2D and 3D substrates (217 genes), confirming the expression of AF biomarkers including *FAP* and *ACTA2* (α-SMA) that are representative of TGFβ1-driven fibroblast activation (**Figure 3.19)**.

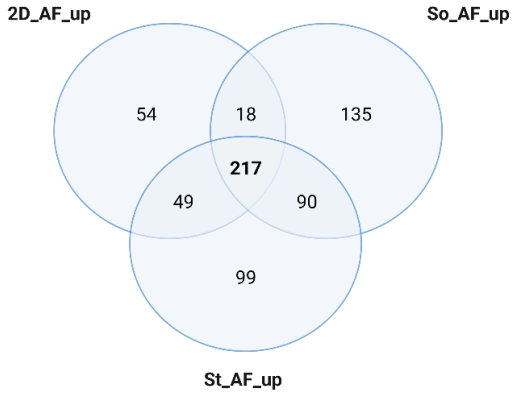

Tgfβ1 core transcriptomic (n = 217)

ACTC1	ADAM12	BHLHE40	ACTA2	APCDD1L	ABC7-42404400C24.1	APCDD1L-AS1	CACNA1H	BPGM	ADAMTS6	AGPS
AMIGO2	ADAM19	CH507-42P11.8	BCL11A	BGN	CACNA2D3	ATP10A	CLTCL1	CNN1	AKAP5	BMF
COL10A1	ANKRD1	COL11A1	COL7A1	COL4A1	CARMN	CASC15	CTPS1	CNNM2	ARHGAP31	C9orf3
DACT1	CDH2	CTD-3035K23.7	FAP	COL5A1	CDH6	CDKN2B	EXTL1	COL4A2	ATXN1	DCBLD1
EGR2	ESM1	DNM3OS	FN1	DSP	EDN1	CHN1	GADD45B	CSRNP1	C1orf198	DENND1B
ELN	HMCN1	FBLN5	FZD8	FBN1	FAM196B	CHRNA1	GLI2	DGKI	CALD1	ETV6
FOXS1	KIF26B	HHAT	HIVEP3	HOXA3	GATA6	EDIL3	HS3ST3B1	FAM101B	CDH11	FBXO32
HTR1D	KRT81	HHIP	LTBP2	INHBE	GLI1	EPHB3	INHBA	IGF1R	COL16A1	FERMT2
IGFBP3	MSC	ITGA11	MYOCD	ITGB3	LIMS1	FAM46A	ITGB5	IL11	COL1A1	FRMD6
LINC01614	MURC	LINC00862	NALCN	KCNG1	LMCD1	FOXN3	MICAL2	KCTD15	FOXP4	GREM2
MDFI	NUAK1	LINC01583	NCAM2	KSR1	MSC-AS1	GALNT10	MMP1	KISS1	ITGA1	IGFBP7
MEOX1	PCDH1	PCED1B	NRP2	MFAP2	PPME1	HHIP-AS1	PAWR	NEDD9	LDB3	JPH2
MYCT1	PCDH10	SCG5	PMEPA1	MMP2	PRRX1	ITGBL1	PCDH9	SAMD11	MBOAT2	PDGFC
NOX4	PRR5L	SEL1L3	SGK1	NFATC2	RNF150	KIAA1549L	PELI1	SLC6A6	MFAP4	PDLIM5
PIK3AP1	RP11-121P12.1	SERPINE2	SMAD7	NREP	SKIL	LRRC17	PGM2L1	SULF1	MIR193BHG	PODNL1
POSTN	SYTL5	SLC1A3	SPDL1	PLXDC2	SLC19A2	NTM	PTPRN	TENM3	OSBPL10	SLC1A4
RP11-84D1.1	TGFBI	SLC46A3	THBS1	SNAI1	SPSB1	P4HA3	SEMA3C	TMEM2	SERPINE1	SPECC1
SPOCK1	WNT7B	STK38L	THBS2	SPHK1	TNS1	PLEK2	SGCD	TSC22D3	TENM4	
TNFAIP6	XIRP1	TCF4	TPM1	SYT16	VCAN	PPP1R13L	SOX4	ZNF281	TIMP3	
ZPLD1	XYLT1	TGFB2	UCN2	UNC5B	VDR	PRDM1	SYNE1	ZNF365	TSPAN13	

Figure 3.19. 3D core transcriptomic analysis of AFs grown on all the substrates. The Venn diagram reports the number of the upregulated genes upon TGFβ1 treatment on all substrates. In gene list detail (n = 217), biomarkers used in the previous figures of the manuscript are highlighted.

To evaluate gene expression variations in response to changes in the microenvironment stiffness, in both AFs and NFs variations between cell types in So and St environments was assessed. Referring to the whole dataset of gene expressed in 3D conditions, AFs showed a higher number of genes uniquely identifying St culturing conditions (1133, 6.3% of the total) compared to So (872, 4.9% of the total); while the highest number of uniquely identifying genes for NFs was found under So condition compared to St (1386, 7.5% and 899, 4.9% respectively) (**Figure 3.20**). The core 3D transcriptome of both NFs and AFs cultured on St/So showed distinct and significant

differences compared to their 2D cultured counterparts (**Figure 19**). Remarkably, the number of upregulated genes in AFs cultured within the 3D scaffolds compared to the 2D substrate where higher than that observed in NFs (228 vs 110 upregulated genes), as shown in **Figure 3.21A-B**. When these gene lists were analysed via pathway analysis for the key upregulated pathways, a number of AF-related pathways related to matrix remodelling and the acquisition of an active/contractile phenotype were identified, including degradation of the ECM and collagen formation; ECM structural constituents conferring tensile strength and response to mechanical stimuli; and pathways related to pathological situations like fibrosis and the inflammatory response (**Figure 3.21A**). On the other hand, upregulated pathways of NFs grown on 3D vs 2D showed an increase in ECM-receptor interaction, focal adhesion, collagen binding involved in cell-matrix adhesion and extracellular matrix components (**Figure 3.21B**). Both pathways analysis proved an active interaction and sensing of both AFs and NFs with 3D scaffolds and a peculiar response of AFs on 3D scaffolds regarding their mechanical nature, related to response to mechanical stimuli and fibrosis-related signature.

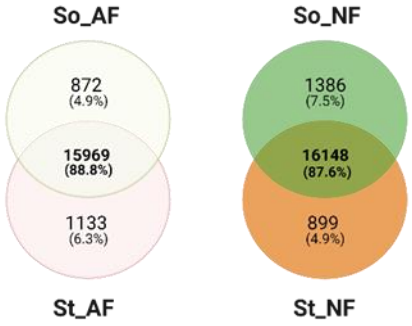

Figure 3.20. AF gene expression is impacted by St culturing, activating many DNA-related pathways. (B) Venn diagram of genes unique and in common between AFs and NFs grown in So and St scaffolds. (C) Volcano plot of NFs grown on St vs So.

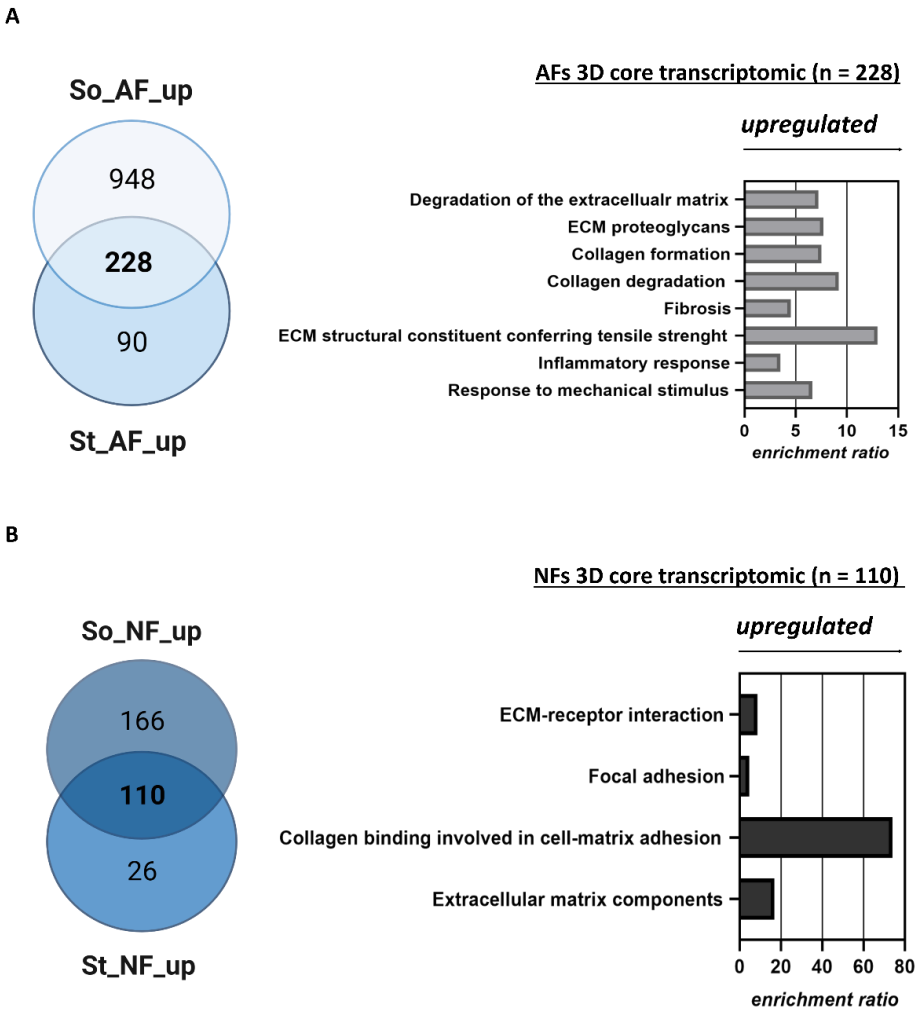

Figure 3.21. 3D core transcriptomic analysis of AFs and NFs compared to 2D. (A) (left) Venn diagram reporting the number of AF upregulated genes cultured on So and St scaffolds compared to 2D. (right) Pathway analysis of the genes upregulated in 3D AFs vs 2D AFs (n = 228). (B) (left) Venn diagram reporting the number of NF upregulated genes cultured on So and St scaffolds compared to 2D. (right) Pathway analysis of the genes upregulated in 3D AFs vs 2D NFs (n = 110).

To investigate the unique signature promoted by substrate stiffness, differential analysis was performed to highlight gene pathways expression variations among NFs and AFs cultured on St versus So. Our analysis reported few significantly upregulated and down regulated genes for NFs between St versus So culture (76 upregulated and 90 downregulated; $p<0.05$; **Figure 3.22A**), but many more differentially expressed genes in AFs, showing 557 upregulated and 606 downregulated genes on St compared to So ($p<0.05$; **Figure 3.22B**). Among them, both NFs and

AFs grown on St showed an upregulation of pathways such as regulation of chromosome organization and segregation, microtubules, cell cycle, signalling by Rho GTPases, and central regulators of actin reorganization, and consequently, function in cellular processes such as cell migration, wound healing, cell adhesion, cell polarity, membrane trafficking, and cytokinesis [591, 592]. On the other side, both showed a downregulation of ECM constituents and organization (**Figure 3.23A-B**).

Of note is the characteristic response of AFs on St materials compared to So. The changes among the upregulated genes are more pronounced and involve DNA replication, DNA damage responses like double-strand break repair, and mitosis-related pathways like cytokinesis, M phase, and cell cycle enrichment. Interestingly, upregulation of genes related to gastric cancer and retinoblastoma were only found in AFs under St culturing, with a loss of ECM-related functions and downregulation of locomotory behaviour, tissue remodelling, and extracellular constituent gene-related pathways (**Figure 3.23B**). In line with those observations, we further compared AF and NF profiles under different culturing conditions, trying to shed light on the underlying characteristic patterns that sensitize AFs to St substrates compared to NFs.

A

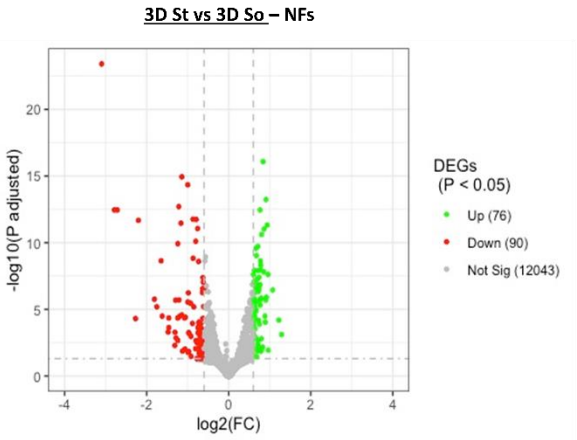

B

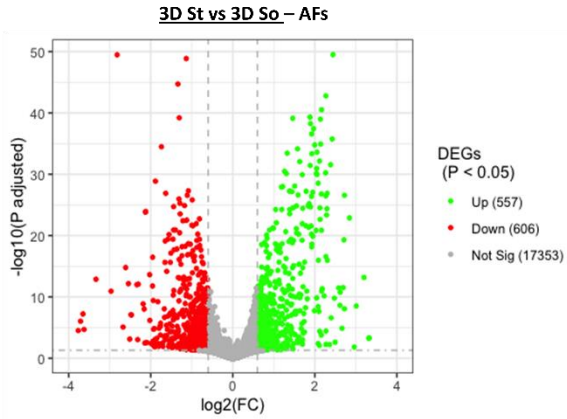

Figure 3.22. NF/AFs gene expression is impacted by scaffolds stiffness. (A) Volcano plot of NFs grown on St vs So. (B) Volcano plot of AFs grown on St vs So.

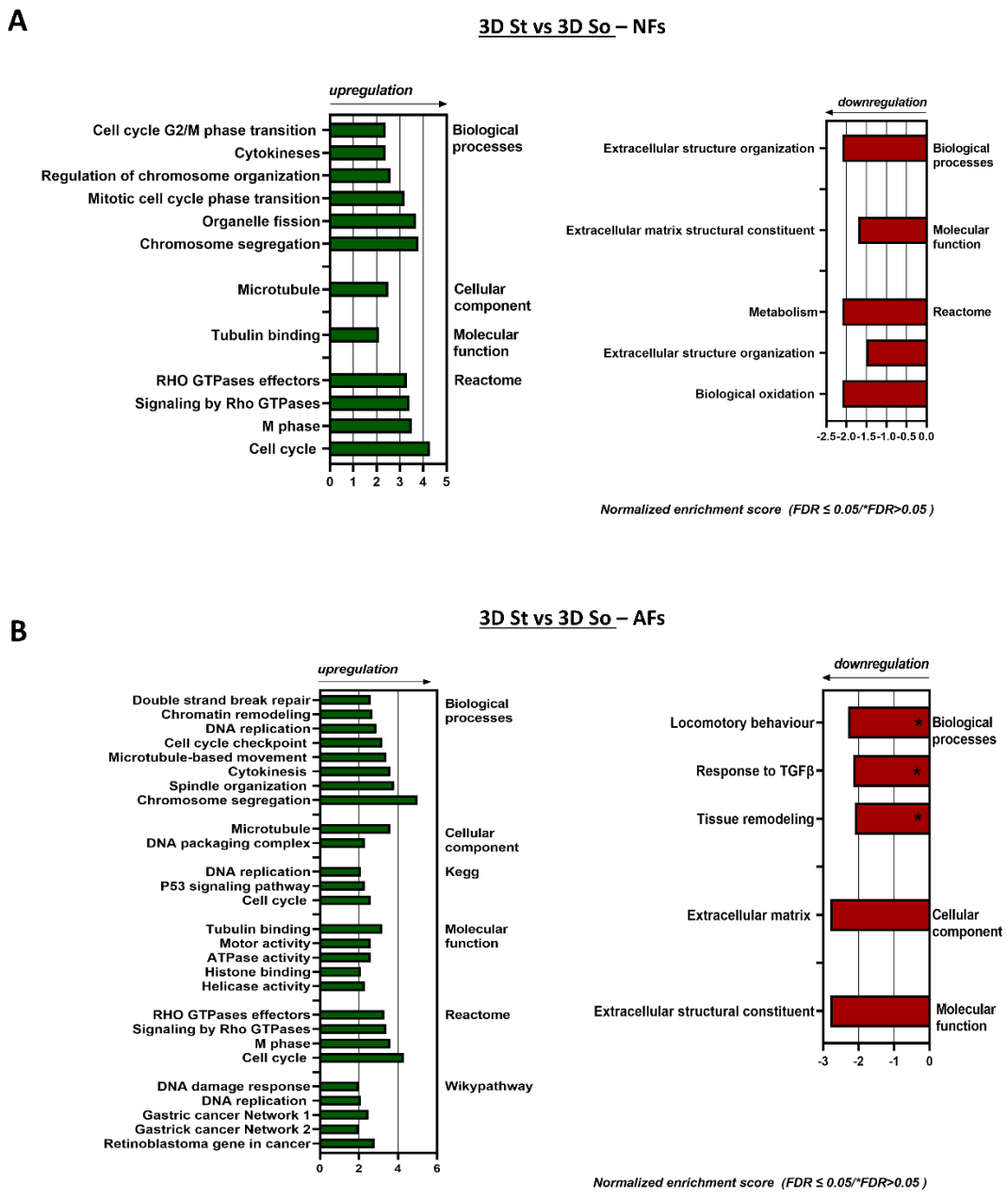

Figure 3.23. AF/NFs gene expression is impacted by St culturing, activating many DNA-related pathways. (A) Differential analysis of gene expression pathways upregulated (left) and downregulated (right) in NFs grown on St vs So. (FDR<0.05) (B) Differential analysis of gene expression pathways upregulated (left) and downregulated (right) in AFs grown on St vs So. (FDR<0.05).

We investigated the effect of fibroblast activation at the gene expression level on each substrate. In the whole gene dataset, we recorded a higher number of unique genes expressed by NFs on both

2D and So materials compared to AFs (2D:1363, 7.5% of total; So:1454, 7.9% of total); a more even distribution of those genes was found on St materials for both NFs (1064, 5.9% of total) and AFs (1119, 6.2% of total) (**Figure 3.24**), suggesting two distinct traits, but equivalent in number of genes, acquired by NFs and AFs on St scaffolds.

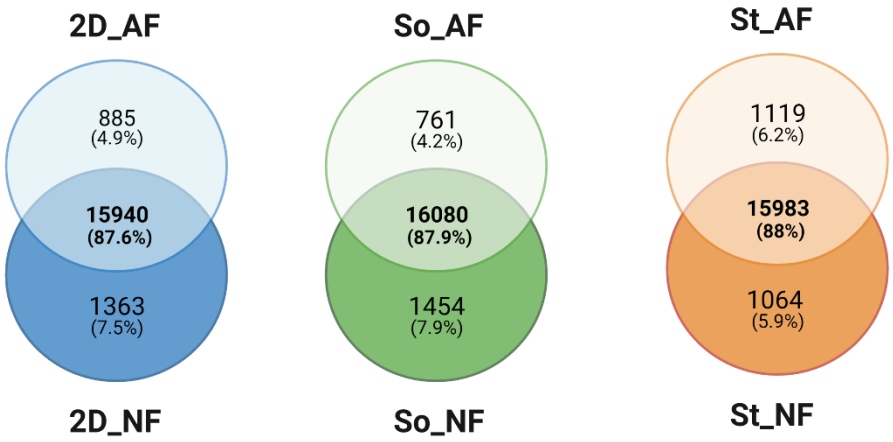

Figure 3.24. AF and NF share common gene signature among culturing conditions. (A) Venn diagram of genes counts unique and in common between 2D-grown AFs and NFs, So-grown AFs and NFs, and St-grown AFs and NFs.

A deeper analysis comparing AF versus NF gene expression profiles on each substrate was performed to unveil how the cytokine activation effect could be amplified or weakened by the mechanical nature of the substrate. 2D cultured AFs acquired a typical functional state related to upregulation of ECM structural constituents as the top upregulated gene pathways in our analysis, conferring elasticity and tensile strength (**Figure 3.25A)**. As expected, AFs grown on 3D So scaffolds showed an upregulation of genes related to ECM component degradation and synthesis, ECM remodelling, but also elastic fibre formation and matrix metalloproteases, suggesting an active contractile phenotype acquisition and enzyme-dependent ECM degradation (**Figure 3.25B)**. Similar to what was observed on So scaffolds, AFs grown on St showed an upregulation of syndecan interactions pathways, a co-receptor recognized to promote liver and cardiac fibrosis [593] and an upregulation of ECM-related pathways mainly related to collagen remodelling, i.e., collagen binding/degradation/formation but also biosynthesis and modification. Interestingly, AFs grown on St scaffolds showed specific upregulation of gene expression pathways related to

pathological diseases, spanning from fibrosis and collagen diseases to prostate and colorectal cancer (**Figure 3.25C**).

The whole-transcriptome RNA analysis clearly confirmed that the surrounding matrix stiffness can promote differential gene expression landscapes, especially in AFs. AFs on the So scaffold seemingly acquired a pro-remodelling phenotype, with higher z-score values of collagen (COL1A1) and fibronectin (FN1), coupled with higher integrin expression, TGFβ1 amplification (TGFB1), and MMP2 expression; while St scaffold culturing inhibits or reduce the expression of those markers, while specifically promoting TNC and MMP1 increase expression (**Figure 3.26**). Tenascin-C (TNC) is an extracellular matrix protein that is expressed at low levels in normal adult tissue but is highly expressed around many tumours including ovarian tumours, although serum TNC levels have been found to be elevated in epithelial OC patients, it has no predictive or prognostic roles on survival [594], another study on colon cancer cells showed that myofibroblast-derived TNC is required to enhance cancer cells pro-invasive activity [595], furthermore, TGFβ and PDGFβ were found to trigger the expression of TNC by fibroblasts [596]. Finally, TNC protein has been shown to exhibit significant elasticity [597] which may suggest that it may still be involved in maintaining the fibrotic process by playing a regulatory role.

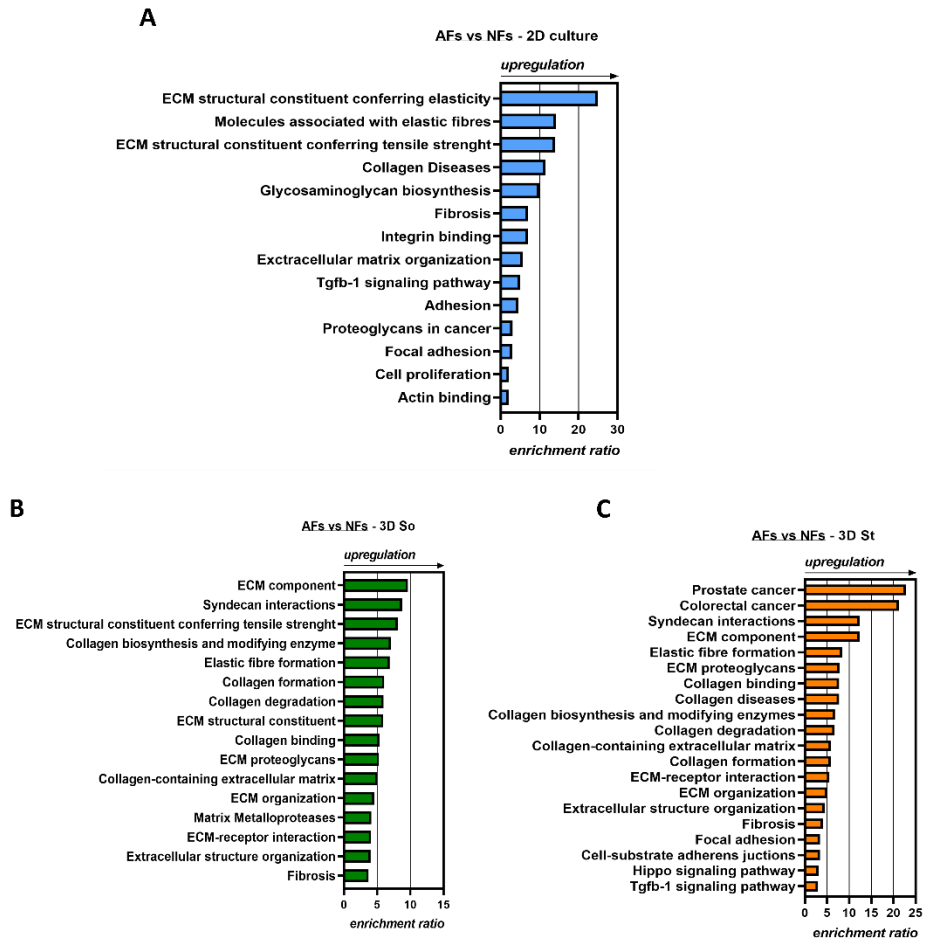

Figure 3.25. Stiffer substrate impacts AF remodeling functions and promotes DNA replication and DNA repair and replication-related pathways. (A) Differential analysis of gene expression pathways upregulated in AFs vs NFs on 2D. (B) Differential analysis of gene expression pathways upregulated in AFs vs NFs on 2D. (C) Differential analysis of gene expression pathways upregulated in AFs vs NFs on 2D.

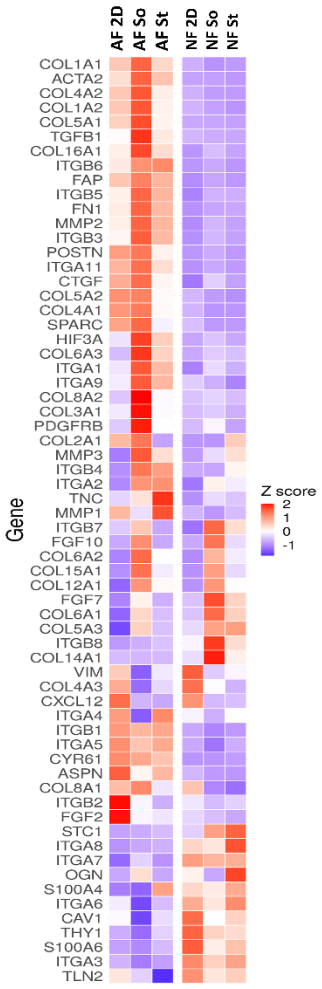

Figure 3.26. Heat map of significant genes expressed in AFs and NFs cultured on 2D, St, and So scaffolds.

3.3.9 SKOV3 condition media activate fibroblasts into activated fibroblasts

The tumour-stroma crosstalk is mainly mediated by soluble paracrine factors, cell–cell contacts and extracellular vehicles (EVs) trafficking [598]. Cell communication via soluble factors and extracellular vesicles, the so-called cell secretome (CS) is also referred as conditioned media (CM). It is usually used as standard approach to test cells-specific secretome involvement in proliferation, migration, and invasion of other cells type, i.e. cancer and stromal cells crosstalk [599-601].

Specifically, SKOV3 was chosen as representative of highly invasive human ovarian adenocarcinoma cell line as its secretome was shown to efficiently activate fibroblasts into a CAFs-like state [602] . After previous testing at different time point (24hr, data not shown) and as

suggested form the literature [603, 604], SKOV3 conditioned media (CM) was collected after 48hours of culturing (cells confluence of 80%) and incubated normal fibroblasts MRC5 with different concentrations of SKOV3 CM for 48 hours to evaluate NFs activated biomarkers expression and viability. To evaluate fibroblasts activation status under CM incubation, FAP expression was evaluated in 2D and 3D culture with a concentration of CM 80-20 (80% CM and 20% normal media, NM) and CM (100%), following indications provided in literature to evaluate the best concentration dose of CM to be effective in inducing CAFs [605].

As previously discussed in chapter 3, Fibroblast Activation Protein (FAP) is a well-defined marker, expressed at high levels on the cell surface of CAFs, promoting malignant and invasive behaviour of epithelial cancers. High stromal expression levels of FAP are detected both at sites of tissue remodelling in non-diseases adult tissue but, if highly express in tumour stroma correlate with poor prognosis [606]. As demonstrated in the previous chapter, treatment with TGFβ1 strongly induce FAP expression in normal fibroblasts indeed we used it as positive control to test CM capability to induce the same phenotype. On 2D both CM 80-20 and CM 100 induced FAP expression as in the positive control with (**Figure 3.27A**), suggesting that both concentrated and diluted CM are suitable for CAFs induction. As controls, the two media alone without SKOV3 secretome failed in inducing FAP expression. On 3D culture, CM 100% was selected as elective treatment, reporting a strong FAP induction on normal fibroblasts grown on normal/soft porous scaffolds comparable to the effect induced by TGFβ1 control, too (**Figure 3.27B**).

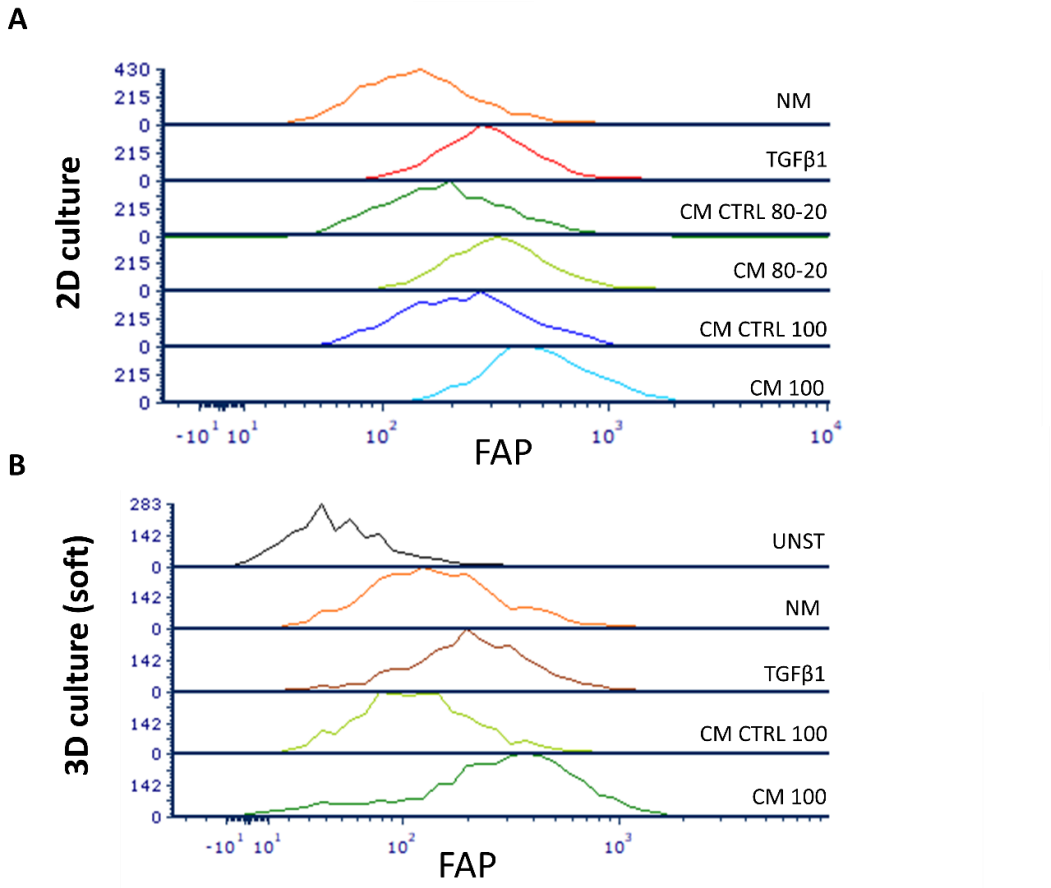

Figure 3.27. CM and TGFβ1 treatment stimulate conversion of NFs into AFs in both 2D and 3D culture. (A) FAP expression assessed with flow cytometry on 2D, (B) FAP expression assessed with flow cytometry on 3D soft scaffold.

Since conditioned media from SKOV.3 is made up of McCoy's 5A basal media (which contains the reducing agent glutathione, bacto-peptone, and a high level of glucose) combined with the secretome of SKOV3 while MRC5 are usually grown on DMEM/F-12 (a formulation combining DMEM's high concentrations of glucose, amino acids, and vitamins with F-12's wide variety of components); to verify MRC5 fibroblasts viability under new culturing conditions, i.e. 100% SKOV3 CM, fibroblasts were analysed quantitatively for viability, using calcein/EtBr cell-death staining on 2D and 3D NS substrates under normal media (NM), normal media + TGFβ1, 100% SKOV3 media (CM ctrl) and 100% SKOV3 conditioned media (CM).

2D culture viable cells reported a percentage of 88.2%±6.8, 93.7%±1.8, 87.2%±5.4, 94.1%±1.6 for NM, NM + TGFβ1, CM ctrl and CM respectively (**Figure 3.28A**); while on 3D soft scaffold 83%±4.6, 85.55%±5.4, 85.9%±5.6, 88.3%±5.2 for NM, NM + TGFβ1, CM ctrl and CM respectively (**Figure 3.28B**). Representative dot plots of the live-death analysis are reported in **Figure 3.28.** Incubation with 100% CM from SKOV3 doesn't affect MRC5 cells viability on 2D and 3D substrates.

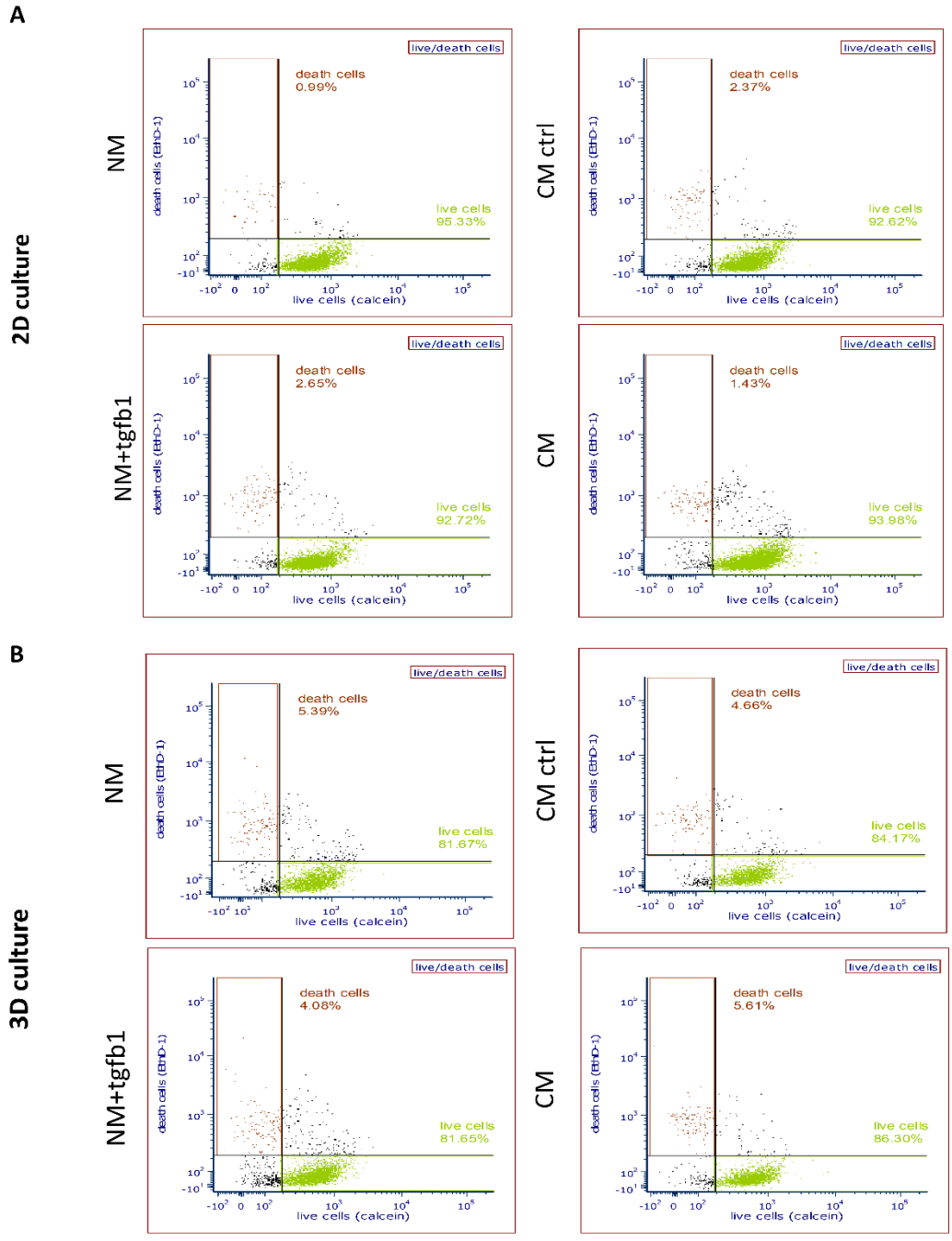

Figure 3.28. MRC5 fibroblasts were viable under CM culturing on both 2D and 3D substrate. Cell death staining analysed with flow cytometry of MRC5 fibroblasts on (A) 2D (C) 3D soft scaffold.

At mRNA level we evaluated a panel of genes related to matrix remodelling, *MMP1*, *MMP2* and *COL1A1*, which code for the pro-α1(I) chain of collagen type I (**Figure 3.29**). MMPs are involved in the breakdown of extracellular matrix, specifically, MMP-1 breaks down the interstitial collagens, types I, II, and III while MMP-2, also known as gelatinase A, has a wide range of substrates, which include collagen, elastin, endothelin, fibroblast growth factor, MMP-9, MMP-13, plasminogen, and TGF-β [429, 430]. It was shown that stimuli like TGF-β1, TNF-α, or epidermal growth factor augmented the secretion of MMP-2 from fibroblasts [607] and, therefore facilitate cancer cell migration in the tissue or inflammatory cells into the injured tissue [25].

Among the gene tested, the only one upregulated gene in response to both CM and TGFβ1 in 2D and 3D culturing conditions was *MMP2* (**Figure 3.29**, ****$p<0.0001$), further supporting CM effect in inducing fibroblasts activation.

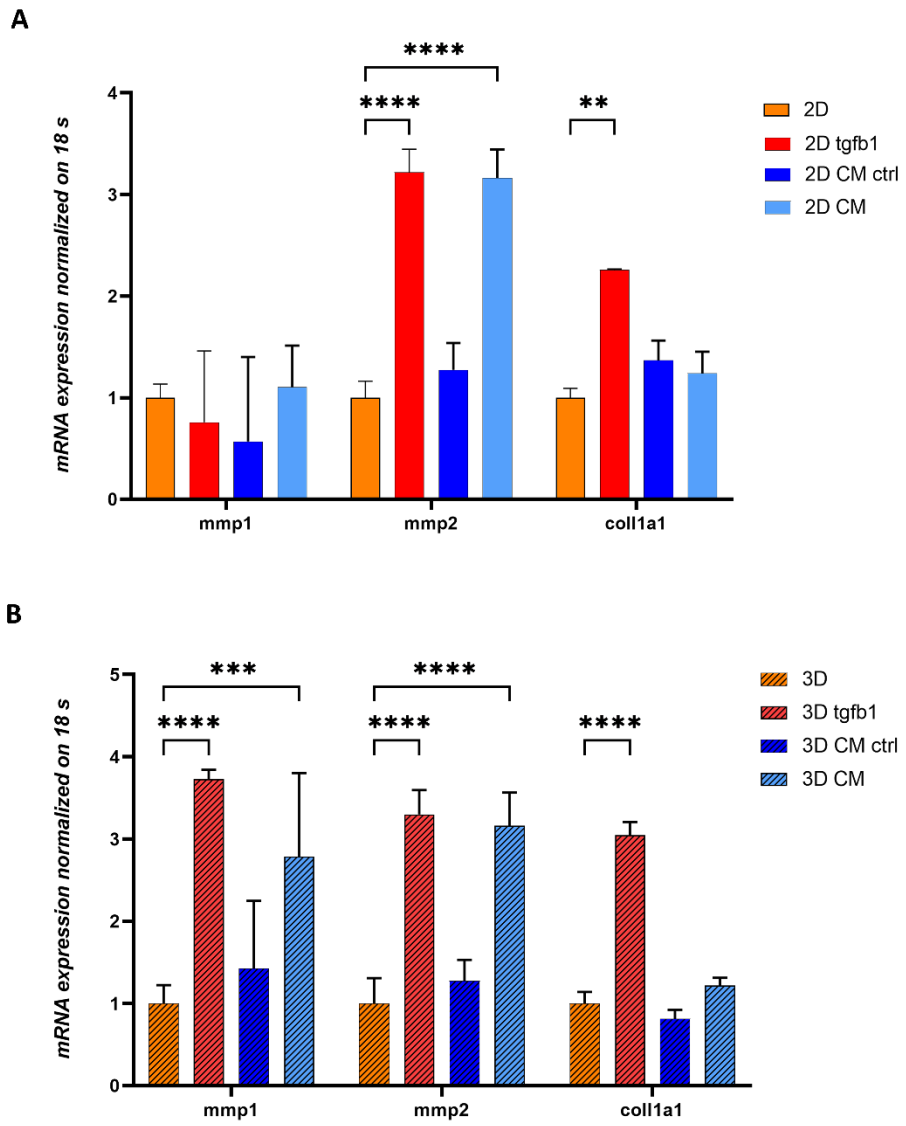

Figure 3.29. mRNA level analysis of ECM-remodelling related genes and HA-related genes. Metalloproteinases genes (MMP1-MMP2) and COL1A1 mRNA expression in fibroblasts at day 7 of culturing on 2D (A), 3D soft NS (B). Data are mean + standard deviation (n=3). Two-way ANOVA, ****p<0.0001, ***p<0.001, ** p<0.01.

To verify if incubation of fibroblasts with CM will induce mechanical macroscopic changes in scaffold physical properties after 7 days of culture rheology was performed. A significant decrease in the 3D/NS scaffold storage modulus was observed at day 7 when cultured with NFs under CM (** p<0.01) and TGFβ1 (* p<0.05) compared to NFs grown on NS scaffolds (**Figure 3.30A**). No significant variation was observed in scaffold material loss modulus for every condition (**Figure 3.30B**).

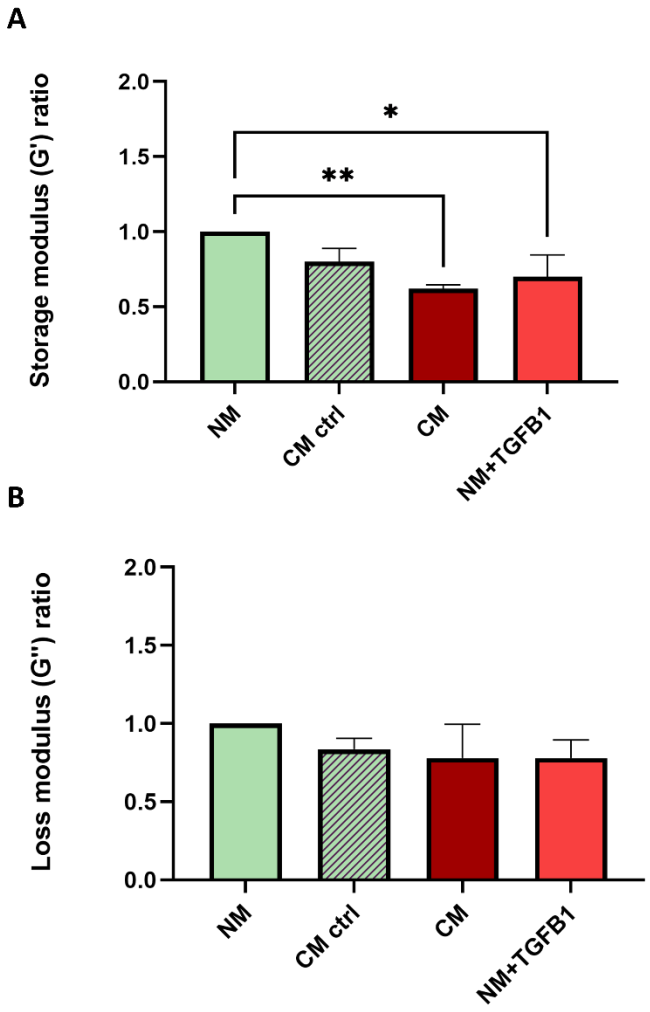

Figure 3.30. NS scaffolds remodelling result in softening under CM and TGFβ1 treatment. Rheology analysis of storage modulus (G') in NS scaffolds; (B) Rheology analysis of loss modulus (G"). Data normalized to normal media sample (NM). Data are mean + standard deviation (n=3). Ordinary one-way ANOVA, **p<0.01, *p<0.05.

3.4 Discussion

The close relationship between fibrosis and the progression of solid tumours is well documented. Tumours, in particular carcinomas, activate, exaggerate, and prolong the latent wound-healing program of the host tissue [608-610], resulting in a tumour niche that resembles a site of chronic wound healing [611]. The mutual presence of myofibroblast cells, referred to here as activated fibroblasts with smooth-muscle (SM)-like features, have emerged as a particularly common hallmark of this close relationship [13, 612]. AFs play a role in the synthesis of ECM and in force generation, resulting in ECM reorganization, wound contraction, and, importantly, altered tissue mechanics driven by altered fibrin, fibronectin, and collagen crosslinking and rearrangement [613]. Collagen crosslinking has been shown to accompany tissue fibrosis that increases the risk of malignancy [614-616].

In the present study, the mechanical and tensional features of normal and pathological tissue were mimicked to explore how ECM stiffness may affect NF and AF phenotype behaviour, and gene expression profiles. Already an elective platform in tissue engineering, we utilize highly porous permeable scaffolds in the broader spectrum of cancer research. As discussed extensively in chapter 2, such scaffold structures provide appropriate void spaces for mass transport and neovascularization while acting as a template for de novo tissue formation with tuneable mechanical features [617]. For the fabrication we utilised a freeze-drying technique while employing BDDGE as crosslinking strategy to produce bovine collagen type I-based interconnected porous structures with controlled and reproducible porosity and fibre organization, resulting in a tuneable system for 3D mechanical studies [554, 618, 619].

In a native tissue context, cells are exposed to a variety of mechanical stimuli including hydrostatic pressure, shear, compression, and tensile force [620]. For this reason, soft biological tissues can be described as viscoelastic materials. Viscoelastic fluids (such as biological materials, known also as Bio-Soft-Matter) exhibit the characteristics of both a viscous fluid and an elastic solid [91]. To fully characterize the mechanical components of our model, we coupled micrometre-scale Young's Modulus analysis using AFM with a bulk assessment of scaffold viscous/elastic

properties using shear rheometry. Overall, St scaffolds showed significantly higher Young's and shear modulus values compared to So, replicating the in vivo mechanical stiffness reported for many tumours such as breast and colon [385]. As a result, we were able to recreate the mechanical differences in the collagen matrix reported between diseased tissue (St; 1% BDDGE) and corresponding native tissue (St, 0.01% BDDGE), mimicking tissue fibrosis and desmoplastic areas [401, 621-624]. Scaffold pore size and interconnectivity, as well as mechanical rigidity, have been shown to affect cell attachment [625]. In our So and St scaffolds, even if the pore sizes are significantly different, they span a range of optimal cell adhesion [626, 627]. Furthermore, we can exclude that cell migration could be affected by the recorded pore sizes since they do not fall within a size range that would limit cell migration by physical arrest, based on previous studies [628].

We selected MRC5 cells as the fibroblast cell line and activated them with a cytokine pro-fibrotic factor TGFβ1, to promote AF activation as confirmed by the expression of two known biomarkers: FAP [629] and α-SMA [630]. MRC5 cells were previously used for both fibrosis studies (e.g., lung fibrosis [631, 632]) and stroma/desmoplastic response studies (e.g., ovarian cancer [633], liver cancer [634], pancreatic cancer [393], hepatocellular carcinoma [635]); while TGFβ1 is routinely used as a master regulator of fibrosis [636, 637] and as pro-inflammatory tumour microenvironment signal to promote CAF activation [633, 638]. Among the activation biomarkers used, FAP is a type II cell surface serine protease expressed by fibroblastic cells in areas of active tissue remodelling such as tumour stroma and healing wounds [35, 639]. Furthermore, fibroblasts isolated from chronic fibrotic tissues are known to typically express higher α-SMA levels, leading to an increased contractility and cellular morphological change [640]. Noteworthy is that α-SMA+ fibroblast infiltration was significantly increased in the tumour stroma compared with that in benign breast tissue expression and correlated significantly with larger tumour size [641].

In addition, employing 3D platform analysis enabled many features of the AF phenotype recorded *in vivo* to be studied *in vitro*. Using 2D substrates limits studies of cellular behaviour such as migration and active contractility. Specifically, cell movement and differentiation occurs in response to environmental stimuli with the aim of achieving appropriate physiological outcomes; i.e., when stimuli are mechanical, cells can sense substrate stiffness through probing and contraction of actin fibres [1]. In human fibrotic organs, fibroblasts show increased ability to obtain

a migratory phenotype [642]. Within tumours, peritumoral CAF migration and accumulation is often associated with increased deposition of ECM components in desmoplastic areas [643]. It has been suggested that CAFs in those areas are capable of executing a migratory program, characterized by accelerated motility and collective motility configuration, promoting cancer migration [426, 644, 645]. In this model, the softer So material was the only environment where both NF and AF cell migration was promoted, unveiling different migratory patterns for AFs and NFs. The directions of AF tracks converged to the centre of the So scaffold whereas NFs did not show specific directionality.

Migration and ECM remodelling can also depend on contractile forces exerted by fibroblasts themselves [646]. In tumour settings for example, CAFs most proximal to the cancer cells usually exhibit a myofibroblasts phenotype and are highly contractile [537, 647]. Indeed, NFs and AFs cultured on So showed significant reduction in scaffold diameter size during 7 days of culture, with a more pronounced shrinking effect of AFs, indicating a higher contractility phenotype for AFs than NFs on So materials. Tissue contraction mediated by AFs is considered the most important cause of increased interstitial pressure, which strongly delays drug delivery to cancer tissues [648]. Such increased contraction forces resulted in a decreased storage modulus after 7 days of AF culture on So, suggesting that in the early stages of both fibrotic and desmoplastic responses, AF activation does not result in higher stiffness. At the cellular level, cells sense and respond to the altered mechanical forces, for example through YAP mechanosensing, as shown in our stiffer St models, in turn driving the expression of a wide range of genes associated with AFs [120, 649]. Within the softer So scaffold, however, we speculated that the observed cellular response may reproduce an early nesting or niche environment where cancer cells could migrate, grow, and proliferate rapidly. Alternatively, So scaffolds may mimic an early stage of the healing process, i.e., the granulation phase, where myofibroblasts (activated collagen secreting, α-SMA+ fibroblasts) are responsible for facilitating wound closure both by tractional forces and contraction [650, 651].

The whole-transcriptome RNA analysis clearly confirmed that the surrounding matrix stiffness can promote differential gene expression landscapes, especially in AFs. AFs on the So scaffold seemingly acquired a pro-remodelling phenotype, with higher z-score values of collagen and

fibronectin, coupled with higher integrin expression, TGFβ1 amplification, and MMP expression. The stiffer (12-kPa) scaffold, St, resulted in an arrest in contractility, remodelling, and active AF phenotype alongside an enrichment of pathways related to DNA replication, chromatin remodelling, and cell cycle control. Also noteworthy was the upregulation of gene expression pathways related to pathological diseases in AFs compared with NFs, spanning from fibrosis and collagen-related conditions to prostate and colorectal cancer. Such AF phenotypes, promoted only on a stiff 3D microenvironment, seemingly support the suitability of the St scaffold model to mimic disease states and reinforce the notion of common ground between activated stroma in both fibrosis and the cancer microenvironment.

The wide-ranging matrix-, cellular-, and molecular-resolution findings of this study reinforce the importance of studying both NF and AF phenotypes in 3D, biologically relevant environments. To link the AFs phenotype induced by TGFβ1 with a CAFs-cancer related phenotype, we utilized an indirect co-culture experiments, specifically incubating NFs with conditioned media from the highly invasive ovarian cancer cell line SKOV3. Previous studies reported the ability of cancer cells to activate fibroblasts, via secretome; for example condition media from colon cancer cells, but not adenoma cells, was able to activate fibroblasts by inducing FAP expression [601], or conditioned medium of gastric cancer mouse model tumour cells induced VEGFA expression promoting angiogenesis, both in embryonic and gastric fibroblasts [652].

As demonstrated for TGFβ1 treatment, also SKOV3 derived CM induced both FAP expression and, at mRNA level, MMP2 in both 2D and 3D and MMP1 only on 3D, further supporting CM effect in inducing fibroblasts activation. RNAseq analysis of fibroblasts primed with SKOV3 CM on 3D scaffolds, soft and stiff, will be the next step to perform, comparing the final gene signature with the data we collected so far. Since it is known that TGF-β1 can be produced by the tumour cell itself [653, 654], secreted at higher level by SKOV3 after 2 days of culture more than other ovarian cancer cell lines like OVCAR-3 and Caov-3 [557] and contributing to induced trans differentiation of normal ovarian fibroblast to a myofibroblast phenotype characterized by elevated reactive stroma marker α-smooth muscle actin (α-SMA) [655], we aspect that SKOV3 CM will induce similar effect to the one recorded in this study but at the same time we could delineate a

specific ovarian cancer-related response of fibroblasts normal and activated in a soft and stiff microenvironment mimicking normal and desmoplastic stage of the disease.

As a platform for drug testing and basic TME research, such porous collagen scaffolds lend themselves to scalable, affordable expansion. As we demonstrated, AFs are strongly affected by substrate rigidity, shifting their gene expression profile to promote DNA replication and DNA repair-related pathways, an interesting phenotype not yet fully described and investigated in such reproducible *in vitro* 3D model systems. Further investigations may address important questions such as whether it is possible to tune myofibroblast fate, reprogramming stromal tissue inhabitant cells in favour of a 'healing' tissue rather than a pathological one. Furthermore, could this be achieved through manipulating ECM parameters such as mechanical stiffness or identifying molecular pathways that promote ECM re-organization, altering the niche environment, thereby sensitizing stromal cells to re-programming? If employed in certain niche environments, the introduction of highly controlled, 3D culture systems may begin to overcome clinical challenges in both fibrosis and cancer tumorigenesis/metastasis.

As a therapeutic strategy, targeting the effectors of myofibroblast activation, deactivation, and fate programs is one option [656-659]. We could also inhibit myofibroblast intracellular (contraction) or extracellular (stiffness and strain) stress as another promising approach to suppress myofibroblast activation or to drive myofibroblasts into controlled suicide [660, 661]. Furthermore, ECM remodelling and crosslinking factors, such as matrix metalloproteases and lysyl oxidases, could be targeted to change ECM mechanics [55, 662-664]. As previously shown, reprogramming cell-specific lineages is possible with the addition of soluble induction factors, but, as shown here, cells can change their expression profile and acquire a specific lineage due to the stiffness and elasticity of their local, matrix environment. For example, soft matrices that mimic brain are neurogenic, stiffer matrices that mimic muscle are myogenic, and comparatively rigid matrices that mimic collagenous bone prove osteogenic [114]. In our model, AFs grown on 3D So materials can provide an effective and meaningful tool to explore tissue biological and biophysical changes and related ECM modifications occurring in first stages of fibrosis and tumour desmoplastic responses, whereas St materials could represent a snapshot of a late-stage fibrotic tissue, where stromal cells enter a 'twilight' zone [665-667]. Testing therapeutics on this platform

could be helpful to highlight potential antifibrotic drugs and/or to study AFs plasticity in response to microenvironment mechanical reprogramming.

3.5 Conclusion

Cells respond to alterations in the mechanical properties of their external surroundings by adjusting their intracellular tension through the cytoskeletal network, while signalling external changes to the nuclei, in turn affecting gene expression profiles. At the same time, intracellular tension changes result in alterations in ECM reorganization, thereby changing the mechanical properties of the matrix [668]. We employed a natural polymer collagen type I biomaterial scaffold to investigate mechanical alterations and track their effect on stromal cells in a 3D model that mimicked microenvironment mechanical dysfunctions observed in pathological conditions such as fibrosis and cancer. Using sponge scaffolds, we controlled the porosity and organization of the material and tested its stiffness and viscoelastic properties, reporting how changes in collagen crosslinking strongly impact the phenotype of AFs in a 3D setting, providing a meaningful platform to investigate both pre-fibrotic and late stages of fibrosis and tumour dysplasia mechanical characteristics.

Chapter 4: Mechano-mimetic 3D scaffolds as a humanized *in vitro* model for ovarian cancer

The work presented in this thesis chapter contributed directly to the following peer reviewed journal article.

Francesca Paradiso, Stefania Lenna, S Andrea Gazze, Jezabel Garcia-Parra, Kate Murphy, Lavinia Margaret, Deyarina Gonzalez, Lewis Francis, Francesca Taraballi. Mechano-mimetic 3D scaffolds as a humanized in vitro model for ovarian cancer. Accepted Feb 2022. *Cells; Mechano-mimetic 3D scaffolds as a humanized in vitro model for ovarian cancer* (IF 6.6)

4.1 Introduction

The field of cancer biomechanics aims to better understand not only how cancer cell behaviour is affected by mechanical changes in the microenvironment, but also how tissue mechanical features can be exploited to detect specific disease stages, while enabling the discovery of potential new diagnostic tools and/or therapies [669]. The role of mechanical constrains in tumorigenesis has been well-studied in breast cancer for example, where stiffening and remodelling of the ECM accompany the promotion of breast carcinoma cell proliferation, local tumour cell invasion and progression [670, 671]. Indeed, increased density and reorganization of collagen fibrils around malignant breast tumours appears to facilitate local tumour cell invasion [11, 672]. As a result nonlinear optical imaging methods such as multiphoton microscopy (MPM) and second harmonic generation (SHG) imaging have been used to visualize local changes in collagen fibril density around invasive breast tumours [59].

Similar to breast cancer, OC evaluation with MPM and SHG imaging has revealed altered collagen fibril density and topology, linked to increase stiffness and fibrosis, and associated with both primary and disseminated OC [673-675]. Some evidence suggests that OC tissue mechanical changes may also result from inflammation in the form of endometriosis [676, 677].
The origin of the epithelial ovarian cancer (EOC), most common type of OC is still under debate but it is postulated to develops in the epithelial tissue, from any of three potential sites, (a) the surfaces of the ovary, (b) the fallopian tube, or (c) the mesothelium-lined peritoneal cavity [678, 679]. Independent of origin, to invade the surrounding tissue and metastasize, ovarian carcinoma cells undergo an epithelial-to-mesenchymal transition and then, carried by the peritoneal fluid (ascites), they form multicellular aggregates (metastatic units), termed spheroids [680], overcome anoikis and attach preferentially on the abdominal peritoneum or omentum, which is the principal physiologic target for EOC dissemination [681, 682].

The most common form of ovarian carcinoma is high-grade serous (HGS), usually diagnosed in an advanced stage (stage III, 70% of cases [282]) and is an inherently aggressive malignancy, thus accounting for the majority of ovarian cancer deaths [683, 684]. At this late disease stage,

chemotherapy resistance occurs, for reasons yet unknown [685]. Carboplatin with paclitaxel represents the standard first-line chemotherapy regimen for ovarian cancer patients however, only 40%–60% of patients will achieve complete remission, with a high risk of neurotoxicity, which can persist more than a year after the treatment [686, 687]. Consequently, other more efficacious or tolerable options were evaluated, i.e. pegylated liposomal doxorubicin (PLD). PLD is an anthracycline encapsulated within a sterically stabilized liposome which increases the agent's circulating half-life in the body and limits its toxicity profile, significantly lowering cardiac toxicity and myelosuppression compared to conventional doxorubicin [688]. Now a widely used agent for the treatment of patients with recurrent or refractory ovarian cancer, there are however limited indications supporting PLD as a monotherapy regimen [689-691].

Increased matrix stiffness is closely linked to tumour progression [692, 693], however malignancy of metastatic ovarian cancer has been shown to be increased on soft matrices. Indeed, ovarian cancer cells on soft matrices are more proliferative and more resistant to standard chemotherapeutic drugs [31]. Since ovarian cancer mechanics and biophysics studies have resulted in contradictory findings, the exploration of mechanotransduction within ovarian cancer, is still understudied [25]. Furthermore, many of the mechanical studies in OC have been performed on spheroids and 2D polyacrylamide gels [694, 695], when the inclusion of mechanical constraints while designing an *in vitro* model, to fully mimic native tumour tissue biology, requires the use of 3D culture platforms [587]. Rapid advances in 3D cell culture systems such as those developed in this PhD, enable the recapitulation of tumour specific cell differentiation and tissue organization, opening new possibilities for studying the underlying biochemical and biomechanical signals between cancer cells and the TME [163, 696].

Using those sponge scaffold 3D culture systems, this chapter investigates the role of substrate stiffness in affecting OC cell behaviour and chemoresistance *in vitro*. Following the assessment of fresh OC tissue to define the stiffness parameters of both peritoneum/cancer and normal ovarian mechanical features, we mimic the stiff (MS, metastatic scaffold) and soft (NS, normal scaffold) tissue properties using 3D porous matrices; testing their utility and suitability for reproducing *in vivo* tissue mechanics while serving as platform for drug testing. Three human OC cell lines OVCAR-3, high-grade serous ovarian adenocarcinoma cell line**,** Caov-3, derived from human

papillary ovarian adenocarcinoma cell line and SKOV3, human ovarian adenocarcinoma cell line, were seeded and cultured in 3D and monitored for their ability to sense, colonize, proliferate, and remodel the collagen rich scaffold environment under different stiffness stimuli. Following successful culture, OC cell-matrix models were tested for their sensitivity to doxorubicin and liposomal-doxorubicin formulations [697] (**Figure 4.1**). The results obtained, show that proliferation and mechanosensing response(s) to microenvironment stiffness, are OC-cell line specific, while higher sensitivity to chemotherapy is a common effect promoted by stiff matrices across all cell lines used. An effective model to investigate cancer genesis and progression and test treatment options should be inclusive of players from different tumoral compartments [698-700]. Currently, many *in vitro* models are composed of one type of cells, lacking the complex cellular interactions within the tumour microenvironment required to be physiologically relevant [701]. 3D systems now, more than ever, must allow for the combination of multiple cell types, creating multicellular structures, enabling TME relevant factors to be included during therapeutic testing [698, 702].

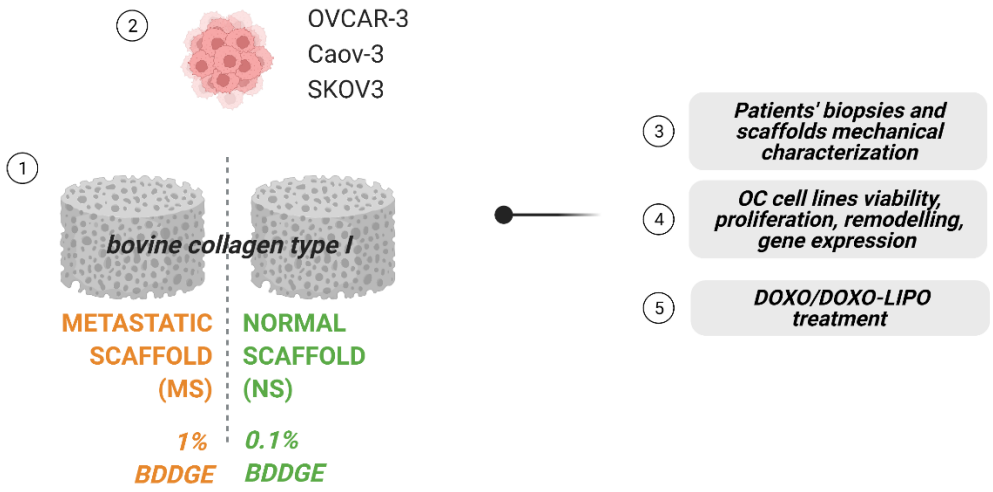

Figure 4.1. Schematic representation of scaffolds employed to mimic normal (NS) and metastatic (MS) tissue mechanics. Image made with Biorender.

To increase the complexity of the model under evaluation, we established a coculture system combining stromal cells with SKOV3 ovarian cancer cell line. As reported in the previous chapter SKOV3 secretome has the potential to activate normal fibroblasts, suggesting that this model could be explored to study stromal activation processes and, consequently ECM dysfunctions progression, promoted by tumour cells in 3D. At the same time, the combination of normal/soft scaffolds with SKOV3 and MRC5 in different tumour/stroma ratio(s) could provide a snapshot of normal (poor stroma), pre/malignant (ratio 1:1), malignant (high stroma) ovarian cancer tissue stages (**Figure 4.2**). Further optimization of this model is ongoing and aim to recreate a more representative model of tumoral/stroma interaction to test therapeutics venues.

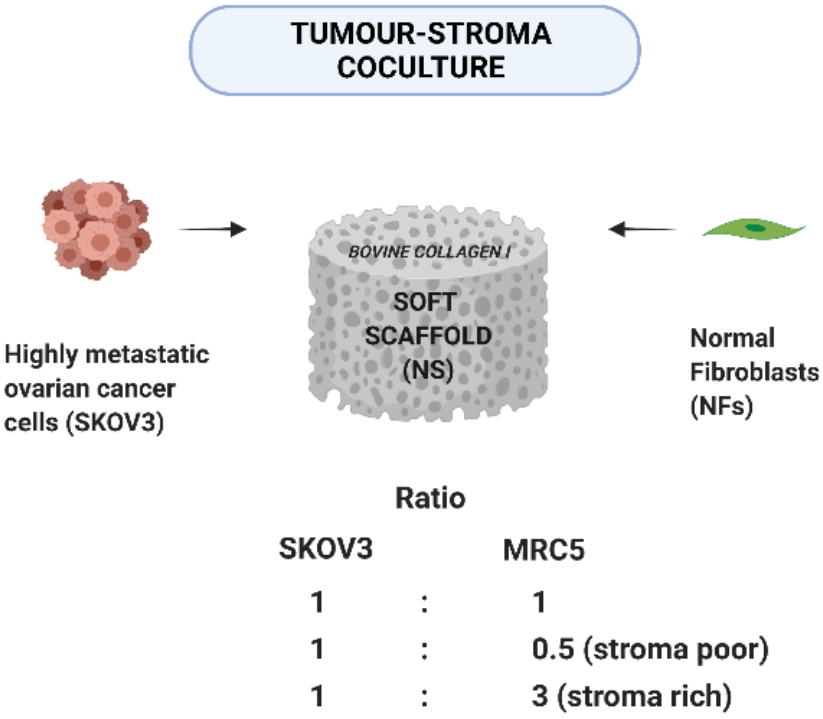

Figure 4.2. Schematic representation of experimental plan employed to study tumour-stroma interaction on NS soft scaffolds. Image made with Biorender.

4.3 Results

4.3.1 HGSC cancer tissues showed higher stiffness and ECM content compared to normal ovaries samples

The mechanics of cells and tissues can be measured by many methods including, among others, magnetic twisting cytometry, optical tweezers, and atomic force microscopy (AFM) [517]. Of these methods, however, AFM is the most widely used tool for this purpose [517, 703, 704]. AFM is an extremely high-resolution tool, which can be used to observe the morphology of a sample, and quantitatively measure its mechanical properties at atomic resolution. It is a widely applied tool for biomechanical studies of pathologically altered samples [705-707]. Specifically, in the tumour context, AFM investigation of changes in ultrastructure and mechanical properties within tumour tissues and cells made it possible to differentiate between healthy and cancer biopsies taken from patients suffering from glioblastoma [708], breast [709, 710], cervical [711], prostate [712] and liver [713]cancers, providing a tool which could be used as a basis for clinical adjuvant diagnosis [714].

One of the main AFM advantages is the need of small samples amount, which leads to a significant reduction of the patient's discomfort a small and the capability of measurements in liquid conditions mimicking natural ones [705, 715]. In AFM, mechanical properties of cells or tissues are quantified through the relative Young's (elastic) modulus which measures the resistance of a material to elastic (recoverable) deformation under load here, indentation with AFM probe, identifying the stiffness of the material [716]. This parameter is a relative value that is dependent on various factors like experimental conditions, AFM probe geometry, and/or form of biological sample (cells, section, or biopsy). Thus, as the first steps of elasticity measurements, an optimization of experiment conditions, and protocols for sample preparation, has to be performed.

As previously reported in literature, tissue fixation can affect mechanical properties of the tissue or device under investigation, i.e. it results in an increase of Young's modulus [372, 717]. Fixation is common practice to preserve tissue integrity so, in order to obtain a more reliable mechanical description of OC biopsies tissue we tested and optimized different protocols for sample

preparation while evaluating different AFM settings to sample them. First, the effect of ethanol fixation on tissue's Young's Modulus were evaluated comparing a fresh or fixed with 70% EtOH tissues.

Indeed, when a material is applied by a load, if that material is stretched beyond the limit of elasticity, that will not recover its original form and will reach to the breaking point [718]. To avoid sample disruption and misleading data, we also performed AFM under a low and high trig threshold (2nN-6nN). Trig threshold limits forces on the sample and tip. It is set to the tip deflection magnitude which causes the piezoelectric actuator to begin retracting if a trigger is in use (Bruker, Force Volume Glossary). Analysis performed at AFM with a sample of a benign cystadenofibroma tissue, demonstrated that fixation protocol strongly increases tissue young modulus while both trig thresholds used gave similar results, so they are both suitable to be used in our analysis (**Figure 4.3**). We decided to use fresh samples as more representative of *in vivo* tissue mechanics and to indent them with a trig threshold of 6nN.

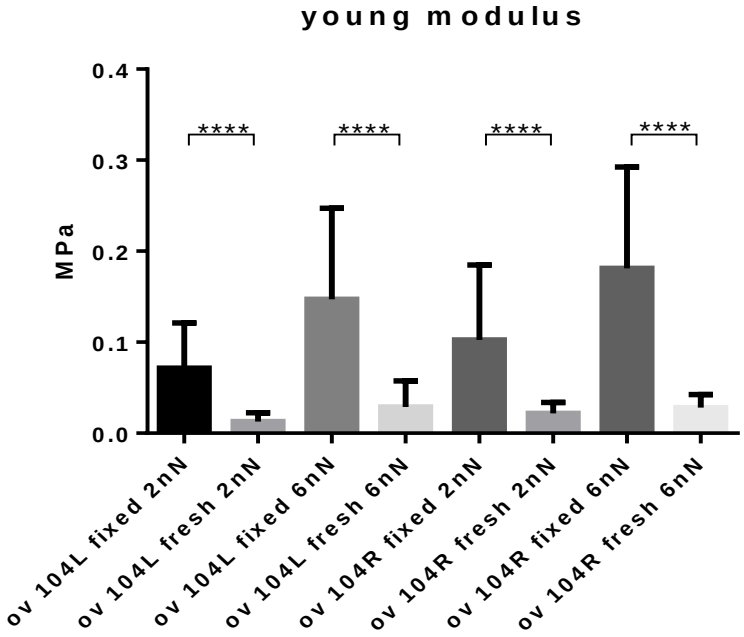

Figure 4.3. Fixation with EtOH 70% strongly affects tissue mechanical properties. Trig threshold: 2nN,6nN; Tip radius : spherical 5μm boro; Section thickness : 10μm thick; Sample tested: benign cystadenofibroma (left and right biopsy)

Changes in mechano-cellular phenotype, are associated with cancer progression, and AFM can provide quantitative mechano-markers that may have translational significance for the clinical diagnosis of cancer [378]. A detailed analysis of patient biopsy mechanics, derived from both high-grade serous carcinoma (HGSC) stage III and normal ovary tissues, were performed at the nanoscale using AFM. After pooling 3 samples for each category, the final analysis showed a 5.5-fold increase in stiffness between HGSC IIIa (0.11±0.034 MPa) and normal ovary (0.02±0.016 MPa) ($p<0.01$; **Figure 4.4A**). Individual patient samples were reported in **Figure 4.4B** to highlight inter-patients' variability, however confirming previous literature, described above, reporting a higher stiffness in HGSC cancer tissue compared to normal ovary. Indeed normal ovary control (ctrl1) is much softer and more elastic compared to other forms of benign tumours it confirmed how those tumours, even if they represents a non-cancerous growth that does not spread (metastasize) to other parts of the body and is not usually life-threatening [719] (**Figure 4.4C**). While fibromas are benign tumours that are composed of fibrous or connective tissue; cystadenoma have a smooth outer surface and contain one or more thin-walled cysts filled with clear, watery fluid [720], which could explain a lower stiffness.

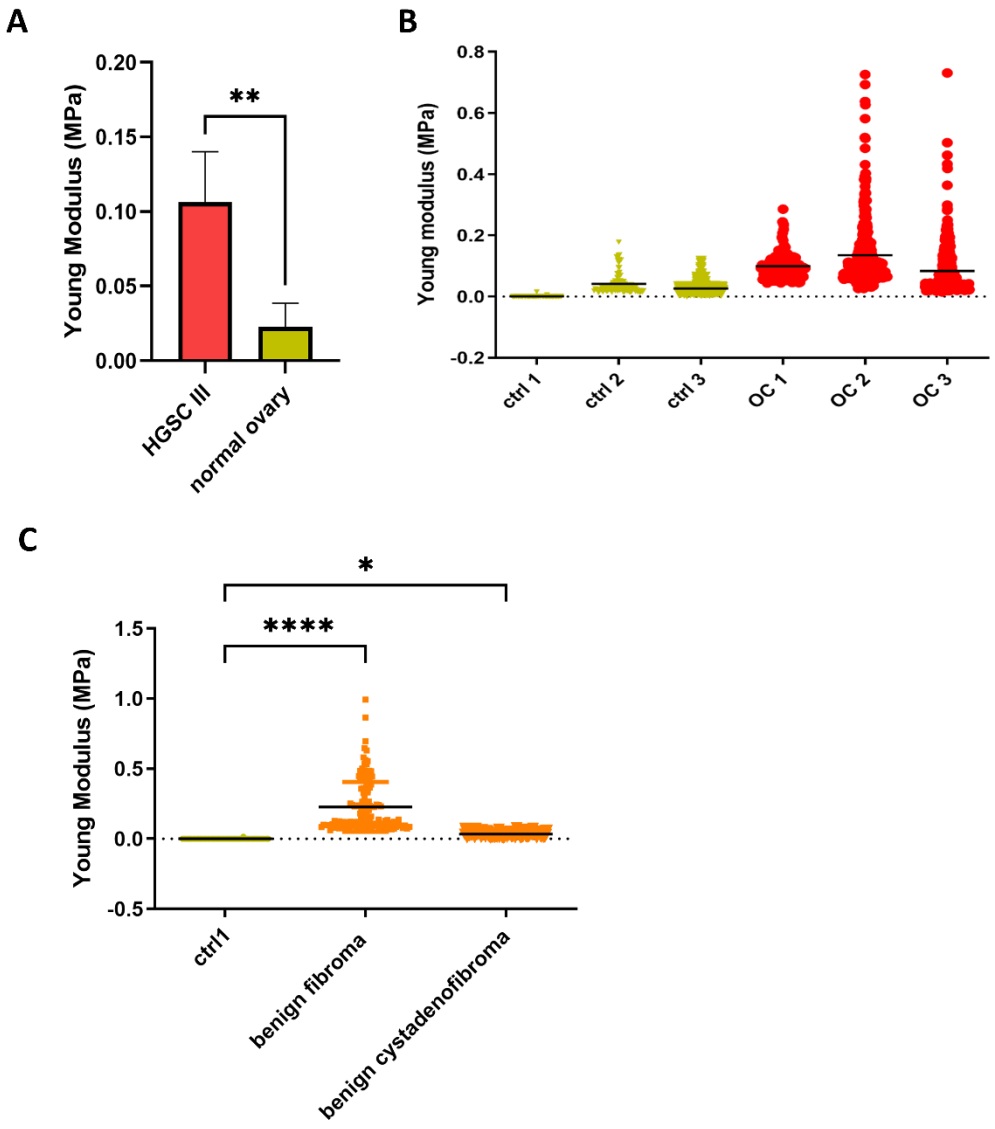

Figure 4.4. Mechanical features of normal and cancer tissues are mimicked in a 3D collagen-based *in vitro* system by using different percentages of crosslinker 1,4-butanediol diglycidyl ether (BDDGE). (A) Young's modulus (MPa) analysis of HGCS III and normal patient-derived biopsies by AFM. (B) Young's modulus (MPa) analysis of 3 HGCS III (OC1-2-3) and 3 normal patient-derived biopsies (ctrl 1-2-3) by AFM. (C) **Fig.** AFM analysis of normal ovary compared to other benign forms of ovarian cancer. Data are mean + standard deviation (n=3). T test with Welch's correction or Two-way ANOVA, ****p<0.0001, **p<0.01.

Tumour initiation and progression are accompanied by complex structural changes in the extracellular matrix (ECM) and cellular architecture, which led to differentiable mechanical characteristics and signalling [91]. The resulting tissue mechanic is a sum of a diverse range of

objects belonging to tissues [721]. The cellular parts include different cells such as epithelial cells and fibroblasts; the non-cellular parts include both fibrous (mostly collagenous) and non-fibrous zones, in which the latter includes a wide range of tissues such as endometrial and sebaceous glands, adipose tissue, vessel walls, mucinous layer, and keratin layer depending on the disease [99]. Such variety of objects define a wide range of elastic moduli which are altered during pathological conditions, especially in the non-cellular part [722, 723].

To investigate the tissue features underlying the alteration of nanomechanical properties during ovarian cancer progression, we performed a H&E staining of patients' biopsies samples (**Figure 4.5**), confirming a higher presence of ECM/fibrotic tissue in the HGSC IIIc derived samples (**Figure 4.5B**) compared to normal ovary controls (**Figure 4.5A**). While lower magnification of the control tissues showed normal tissue histology, with some oocytes, follicles mainly in the cortex (outermost layer of the ovary) and the medulla composed of stroma and blood vessels [724]. Significant nuclear atypia and some nuclear pleomorphism (> 3x variation in size) with large, bizarre and multinucleated forms; stroma accumulation with a higher ECM content (eosin, pink staining) evident in the HGSC IIIc samples.

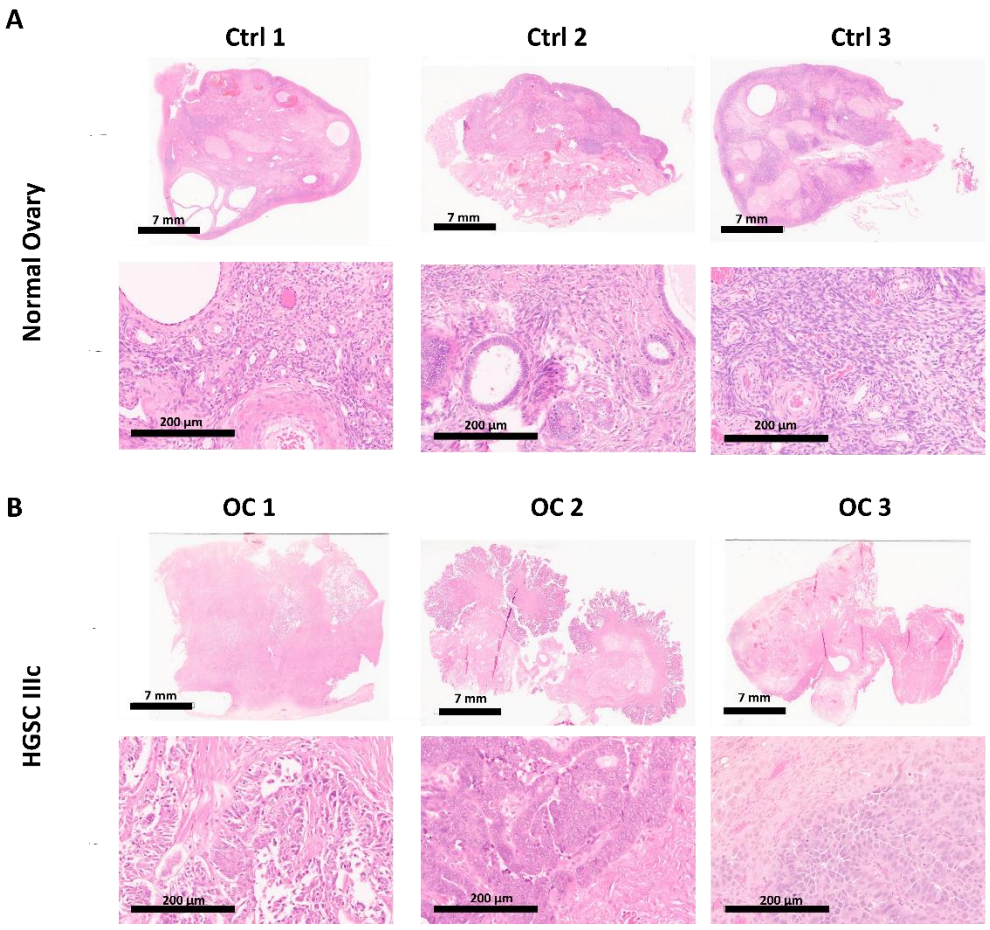

Figure 4.5. H&E characterization of patients' samples. (A) H&E staining of 3 normal ovary biopsies samples. (B) H&E staining of 3 HGSC IIIc biopsies samples. Images were acquired with 4x and 20x objective.

4.3.2 Mechanical features of normal and cancer tissues are mimicked in a 3D collagen-based in vitro system BDDGE crosslinker

AFM data from native tissues were successfully mimicked in a 3D collagen type I-based scaffold model. To match the *in vivo* mechanical features with a meaningful *in vitro* system we selected 1% and 0.1% w/v BDDGE crosslinked scaffolds. Consistently with the characterization performed in chapter 2, they showed a Young Modulus value of 0.144±0.010 MPa for metastatic scaffolds and 0.015±0.0003 MPa for the normal scaffolds ($p<0.0001$; **Figure 4.6A)**. Subsequent compressive tests were carried out to evaluate the compressive strength and stiffness of the

scaffolds. The results, summarized in **Figure 4.6B**, showed that higher force was required to compress MS (0.54±0.028 N) compared to NS (0.16±0.025 N) ($p<0.0001$), further confirming MS higher stiffness properties.

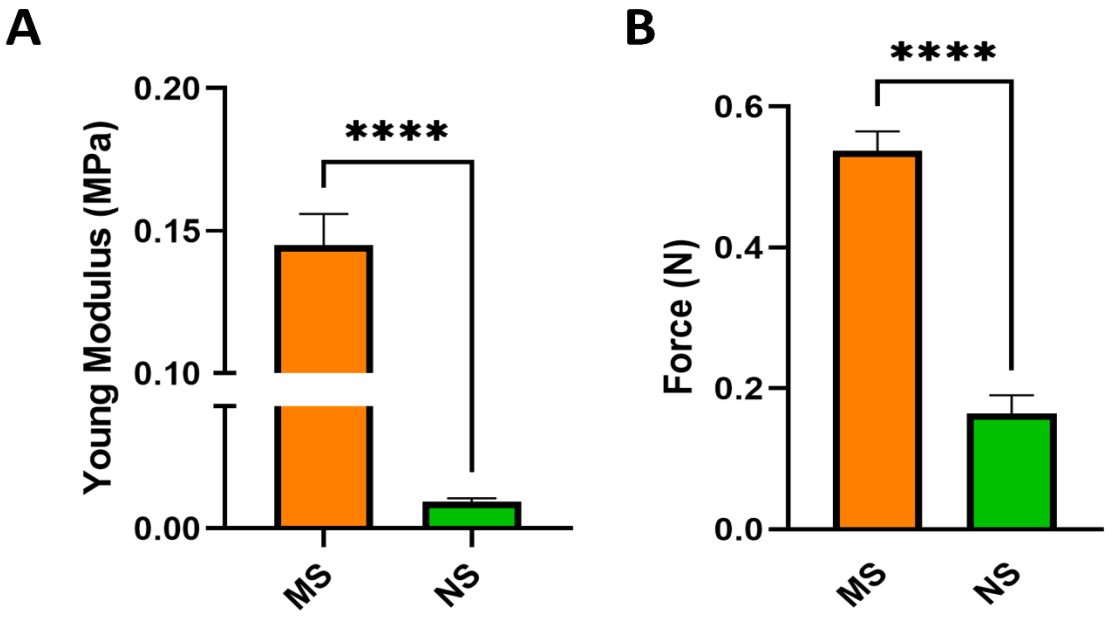

Figure 4.6. Mechanical features of normal and cancer tissues are mimicked in a 3D collagen-based *in vitro* system by using different percentages of crosslinker 1,4-butanediol diglycidyl ether (BDDGE). (A) Young modulus (MPa) analysis of MS and NS scaffolds by AFM. (B) Compression test analysis of MS and NS scaffolds. Data are mean + standard deviation (n=3). T test with Welch's correction, ****$p<0.0001$, **$p<0.01$.

The porous structure of MS and NS after freeze-drying was determined by SEM imaging (**Figure 4.7A**). At lower magnification, samples' structures are composed of interconnected pores with boundaries defined by sheet-like structures of fibrillar collagen. At higher magnification, the typical fibrous substructure of collagen sponges can be appreciated. Porosity measurements showed that MS and NS exhibited a comparable average pore size around 2,500 μm^2, corresponding to an average diameter of 56.4 µm, with comparable area % of 30 μm^2 covered by pore structures and pore circularity around 0.37 (**Figure 4.7B**). FTIR was used to characterize scaffold composition after crosslinking. FTIR spectra, reported in **Figure 4.7C**, showed the characteristic collagen vibration peaks like Amide I (1,700–1,600 cm^{-1}) and Amide II (1,600–

1,500 cm^{-1}), related to the stretching vibration of C=O bonds and to C–N stretching and N–H bending vibration, respectively, for both scaffolds.

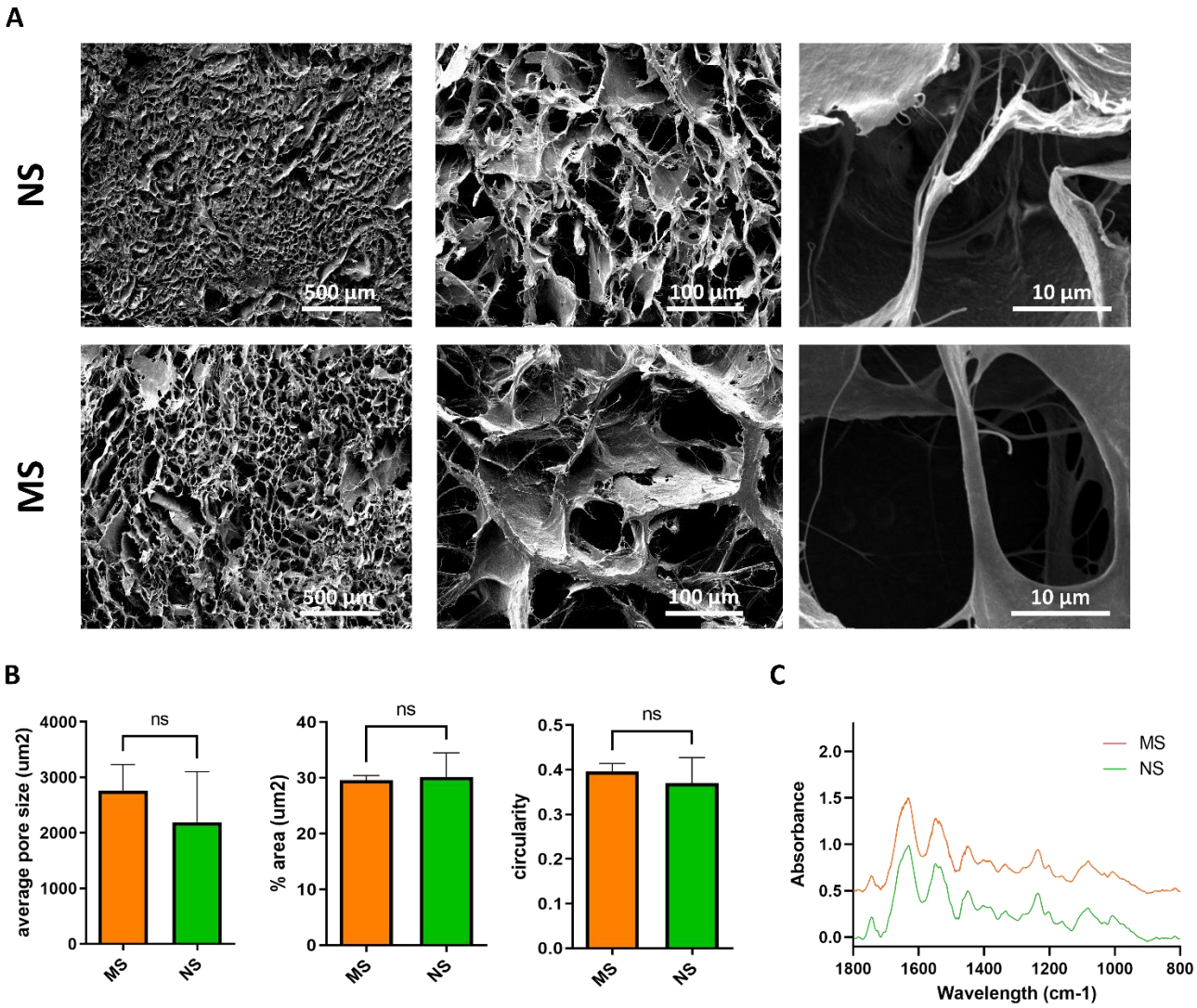

Figure 4.7. NS and MS scaffolds showed common pore sizes, pore coverage, and composition. (A) SEM imaging of NS and MS scaffolds at different magnifications. (B) SEM analysis of average pore size (μm^2), % area covered by pore structures, and circularity. T test with Welch's correction performed. (C) FTIR spectra of MS and NS scaffolds. The spectra highlighted the presence of typical collagen Amide I, Amide II, and Amide III.

4.3.3 Ovarian cancer cell line on 3D scaffolds are viable and colonize the scaffolds

Three cell lines, derived from ovary (OVCAR-3, Caov-3) or peritoneal ascites (SKOV3) of OC [725] were employed, to test their morphology and behavioural phenotype, in response to microenvironment stiffness. First, cell death was monitored after 7 days of culture on NS or MS, using calcein/ethidium bromide staining, assessed by epifluorescence microscopy, and quantified by flow cytometry (**Figure 4.8**). All three cell lines were able to attach to, and colonize the scaffolds, as reported by the 3D maximum intensity projection based on 3 layers collected per scaffold (**Figure 4.8 A,C,E**). When analysed quantitatively for viability, calcein-positive OVCAR-3, Caov-3, and SKOV3 percentage was 84.29%±6.5 (**Figure 4.8A**), 88.75%±10.4 (**Figure 4.8C**), and 80.83%±5.8 (**Figure 4.8E**), respectively, on MS and 91.39%±7.04, 93.01%±5.3, and 87.95%±4.3 on NS, with no statistical differences in cells viability between the two scaffolds. No morphological changes were detected after 7 days of culture of cancer cells lines on scaffolds, as shown by F-actin immunofluorescence staining. All those cells morphologies have been described in 2D as epithelial (ATCC) instead on 3D scaffolds, OVCAR-3 maintained their cuboidal/epithelial shape (**Figure 4.8B**), Caov-3 acquired a spindle-shaped morphology (**Figure 4.8D**), and SKOV3 an elongated spindle-shaped morphology (**Figure 4.8F**).

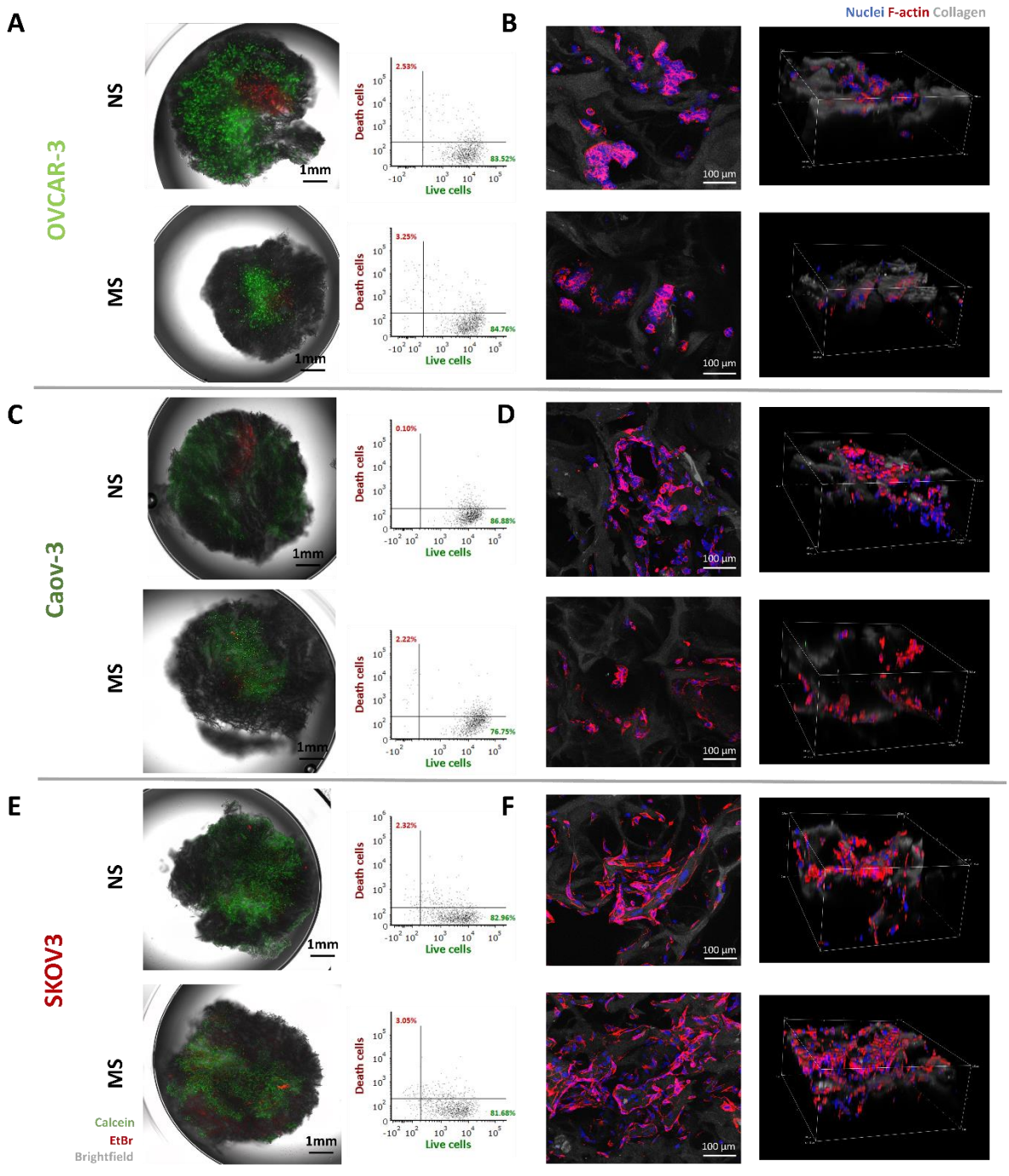

Figure 4.8. Ovarian cancer cell lines were viable and did not change their morphology when cultured on both MS and NS scaffolds. Cell death staining analysed with fluorescence microscopy and flow cytometry of (A) OVCAR-3, (C) Caov-3, and (E) SKOV3 cells. Immunofluorescence staining of F-actin and DAPI in (B) OVCAR-3, (D) Caov-3, and (F) SKOV3 cells. Analysis and imaging were performed after 7 days of culture. In lateral projection pictures, Z-size: 200 µm, Step size: 10 µm.

4.3.4 SKOV3 and Caov-3 cells proliferate more rapidly on MS scaffolds

Cancer cell proliferation rate was assessed by CellTiter-Glo®. OVCAR-3 proliferation rates showed no differences between MS and NS until day 10 of culturing, at which point, OVCAR-3 proliferation was observed to be significantly higher on NS scaffolds when compared to their MS counterparts (8.6±0.19 and 7.7±0.5, respectively $p<0.05$) (**Figure 4.9A**). Caov-3 showed a 1.3-, 1.2-, and 1.2-fold increase in proliferation at days 4, 7, and 10 respectively, when culture within the MS compared to NS (**Figure 4.9B** $p<0.05$). SKOV3 showed higher proliferation rates on MS scaffolds from day 7, reporting a 1.08-fold increase in proliferation at day 7 and 1.05-fold increase at day 10 on MS compared to NS (**Figure 4.9C** $p<0.05$). Among the ovarian cancer cells tested, different responses were recorded in term of proliferation rate promoted by microenvironmental stiffness, resulting in higher proliferation rate of Caov-3 and SKOV3 on MS compared to NS.

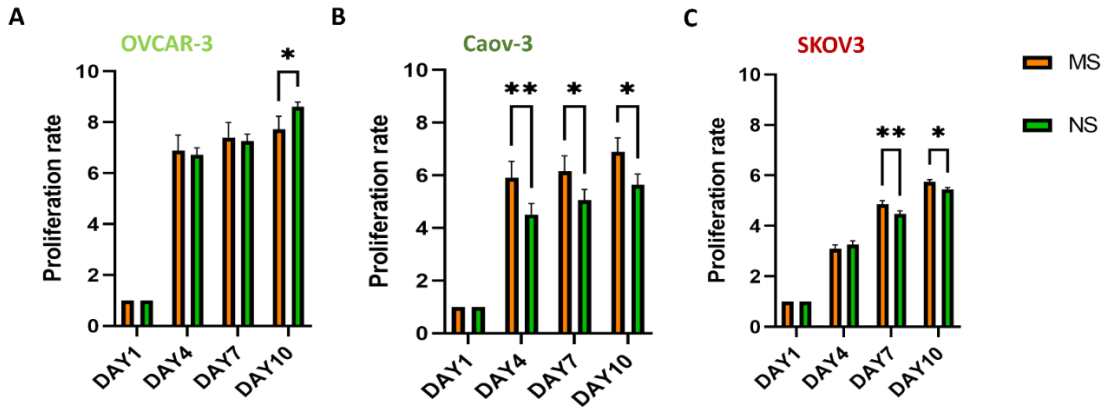

Figure 4.9. SKOV3 and Caov-3 cells proliferate more on MS scaffolds while OVCAR-3 proliferate more on NS scaffolds. CellTiter-Glo® analysis of ovarian cancer cell proliferation rate from day 1 to day 10 on MS and NS scaffolds of (A) OVCAR-3, (B) Caov-3, and (C) SKOV3 cells. Data are mean + standard deviation (n=3). Statistical analysis performed with Two-way ANOVA. **p<0.01, *p<0.05.

4.3.5 OVCAR-3 and SKOV3 culture leads to MS scaffolds softening

Tissue mechanics is thought to be a combination of both cellular and matrix stiffness [620, 726]. Cancer cells have both the ability to remodel the surrounding environment and, at the same time, appear to be softer than their healthy counterparts [727]. It is difficult, within the 3D scaffold structures to measure cellular stiffness, therefore, to understand how 3D scaffold culturing may influence overall scaffold tissue mechanics, we evaluated bulk mechanics, using rheometry, at day 1 and day 7 of culture (**Figure 4.10A-F**), to assess cells influence to tissue mechanic early after seeding on scaffolds and later on after a week of proliferation.

After 1 day of culturing, MS and NS scaffolds still harboured significant differences in their storage moduli ($p<0.01$ and $p<0.05$) under culturing of all OC cell lines: OVCAR-3-culture scaffolds were 0.093±0.041 MPa for MS and 0.012±0.002 MPa for NS; for Caov-3 were 0.032±0.005 MPa for MS and 0.012±0.004 MPa for NS; and for SKOV3 were 0.039±0.011 MPa for MS and 0.012±0.0004 MPa for NS (**Figure 4.10A-C-E**). After 7 days of culture a decrement in MS storage modulus was observed for OVCAR-3 culture, MS 0.030±0.006 MPa, NS 0.005±0.004 MPa (**Figure 4.10A**), suggesting a softening of the scaffold mechanic; the same effect was recorded in the loss modulus (**Figure 4.10B**); Instead no differences in storage modulus at day7 were observed for Caov-3, MS 0.029±0.007 MPa, NS 0.012±0.0004 MPa ($p<0.01$) compared to day1 (**Figure 4.10C**). Loss modulus followed the same pattern as storage modulus (**Figure 4.10D**). As for OVCAR-3, also SKOV3 cell culture reported a significant decrease in both MS and NS at day7 of culture (MS 0.021±0.002 MPa, NS 0.007± 0.001 MPa (**Figure 4.10E**); No significant differences were recorded for loss modulus at day7 between the scaffolds (**Figure 4.10F**).

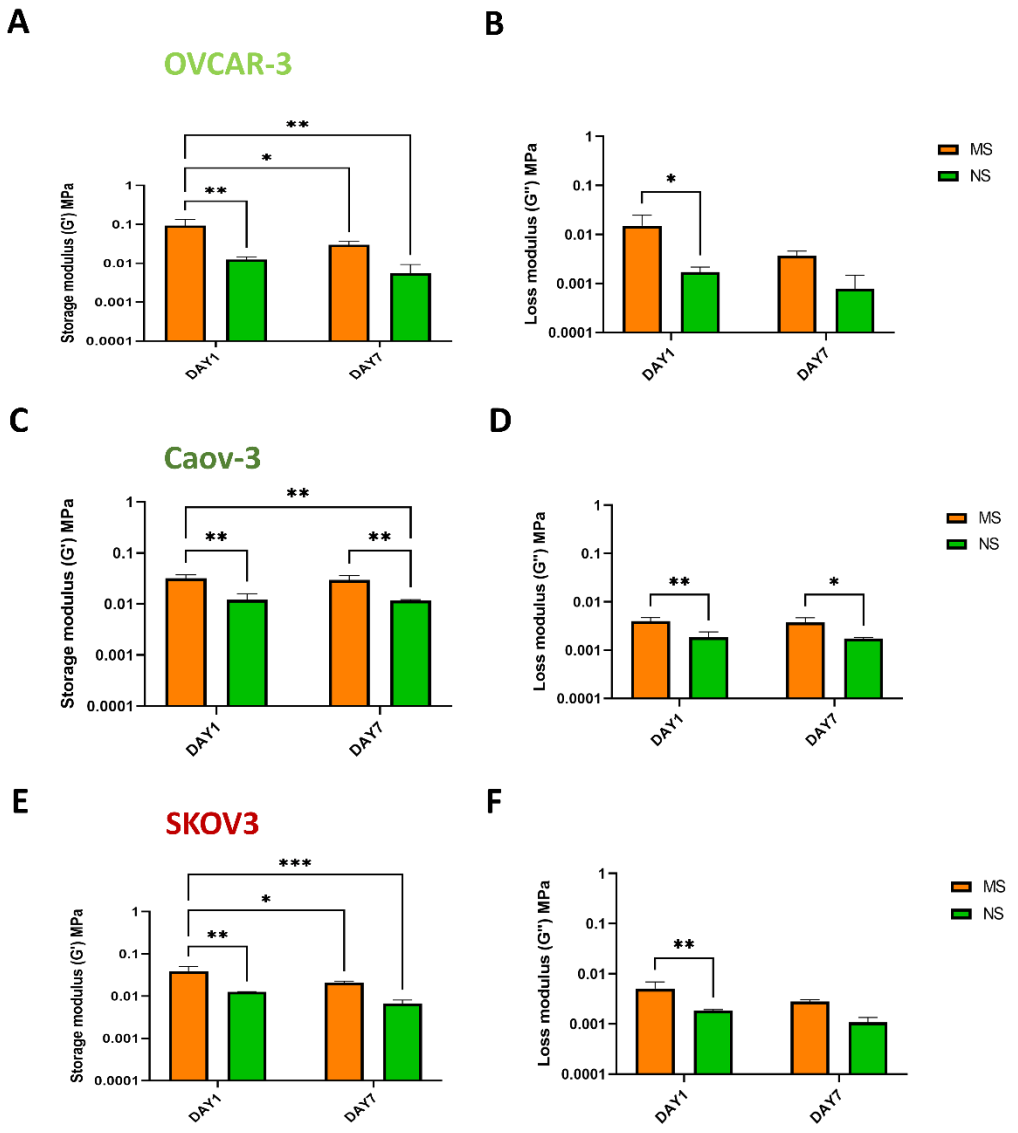

Figure 4.10. Bulk mechanical properties are slightly changed by OVCAR-3 and SKOV3. Rheology analysis of storage modulus (G') in MS and NS scaffolds at days 1 and 7 of OVCAR-3 (A), Caov-3 (C), and SKOV3 (E) culture. Rheology analysis of loss modulus (G", right) in MS and NS scaffolds at days 1 and 7 of OVCAR-3 (B), Caov-3 (D), and SKOV3 (F) culture. Data are mean + standard deviation (n=3). Statistical analysis performed with two-way ANOVA. ****p<0.0001, ***p<0.001, **p<0.01, *p<0.05.

4.3.6 Hippo pathway effectors activation is specific to the SKOV3 cell line

Mechanical changes in the microenvironment can strongly affect cells at the transcriptomic level through a process called mechanosensing [587, 728, 729]. Yes-associated protein (YAP)

overexpression has been reported for several human tumour entities, including prostate, ovarian, colon, liver, lung and pancreatic cancer [730] and it was shown to be a powerful prognostic marker of poor survival in ovarian cancer and being able to induce ovarian tumours when expressed in the Drosophila ovary [731]. Since YAP is also a well-known master mechanosensor, together with WW-domain containing transcriptional regulator 1 (TAZ) [588], we evaluated their expression in relation to 3D scaffold systems in all three OC cell lines (**Figure 4.11**). Among the ovarian cancer cell lines tested, only SKOV3 reported a 2.2-fold increase in *YAP1* expression and a 2.7-fold increase in *TAZ* expression on MS compared to NS, supporting mechanosensing-related pathway activation promoted by increased substrate rigidity (**Figure 4.11C** $p<0.0001$); suggesting differential and specific oncogenic role of YAP [732] and its potential use as predictor factor [733] for high proliferating and metastatic SKOV3 cell lines. At transcriptional level both *YAP1* and *TAZ* showed a downregulation on MS scaffold at day 7 compare to NS in OVCAR-3 and Caov-3 ($p<0.01$ and $p<0.05$; **Figure 4.11A-B**). Interestingly, many evidences indicates that YAP/TAZ activation and overexpression is also implicated in resistance to targeted therapies, chemotherapy (like DNA damaging agents), radiation, and immunotherapies [589].

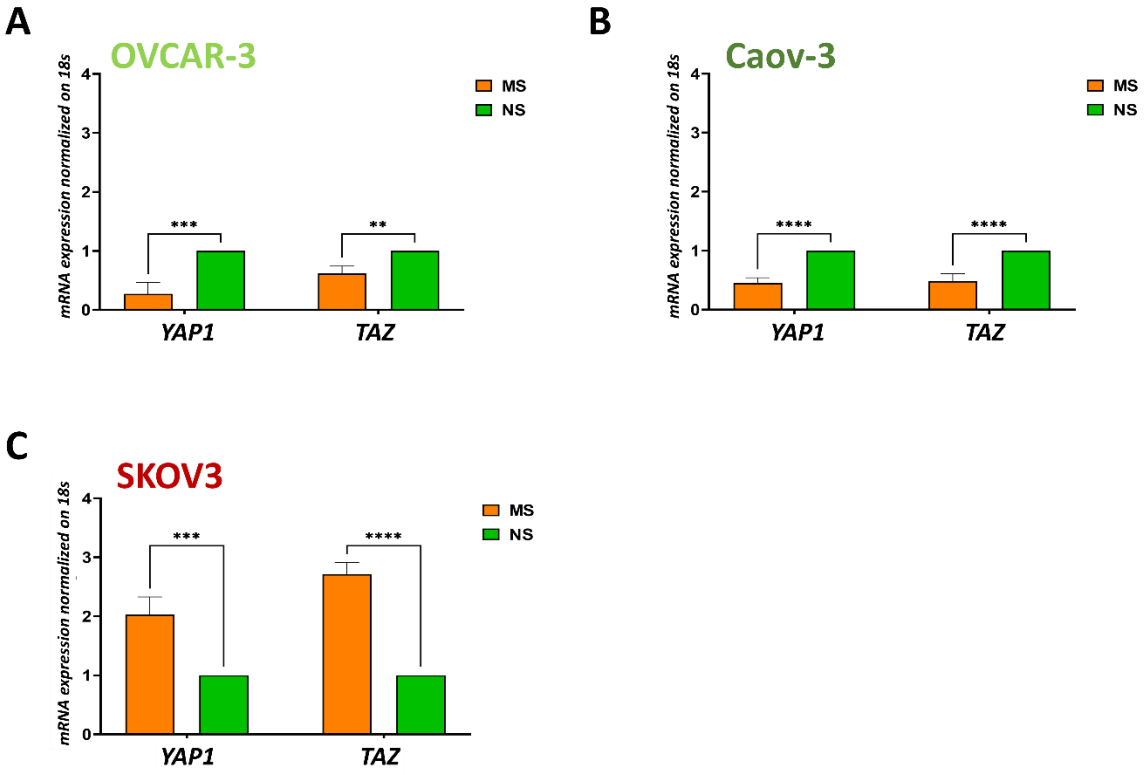

Figure 4.11. Hippo pathway activation is specific to the SKOV3 cell line. mRNA expression of mechanosensing-related genes (*YAP* and *TAZ*) in OVCAR-3 (A), Caov-3 (B), and SKOV3 (C) cultured scaffolds at day 7. Data normalized to NS scaffolds. Data are mean + standard deviation (n=3). Statistical analysis performed with two-way ANOVA. ****p<0.0001, ***p<0.001, **p<0.01, *p<0.05.

4.3.6 MS scaffold culture sensitises OC cells to DOXO and DOXO-LIPO treatment

To evaluate the link between stiffness of the substrate, mechanosensing and resistance to chemotherapy we employed the 3D model platforms to test ovarian cancer cell sensitivity to mainline chemotherapeutic treatments, doxorubicin (DOXO) and doxorubicin-loaded liposome (DOXO-LIPO). Similar formulations of doxorubicin have been reported effective and with tolerable side-effects in either combination therapy with carboplatin or as mono-therapy for recurrent or platinum-resistant ovarian cancer [734].

A liposome is a spherical vesicle having at least one lipid bilayer which can be modified and act as a drug delivery vehicle for administration of nutrients and pharmaceutical drugs, such as lipid nanoparticles in mRNA vaccines, and DNA vaccines [735]. Liposomal technology is being used in increasing amounts in the therapy of a variety of cancers, including ovarian cancers [736]. Liposomes were fabricated in house, using 20 mg of total lipids including DPPC, DSPC, DOPX, and cholesterol (molar ratio 5:1:3:1) dissolved in methanol:chloroform solution (1:3 v/v), employing the extrusion where the liposome suspension is passed through a membrane filter of defined pore size [737].

The physicochemical features of conventional liposomes [738, 739] were retained when loaded with DOXO. Indeed, DOXO encapsulation did not significantly affect the size and polydispersity of DOXO-LIPO. Indeed, compared to empty liposomes (hydrodynamic size = 184±2.0 nm; PDI = 0.15±0.151), DOXO encapsulation did not alter nanovesicles' diameter (hydrodynamic size = 183.5±2.8 nm), and only slightly decreased size distribution (PDI = 0.08±0.015) to values that are still below 0.2, thus indicating a very high size homogeneity [740]. Surface charge was very similar between empty liposomes (Z potential = -8.4±0.6) and DOXO-LIPO (Z potential = -8.42±0.94)

(Figure 4.12A). DOXO loading efficiency into liposomes was 93.9%±3.63 (**Figure 4.12B**) with a release kinetics of DOXO from liposomes of 16.5% after 8 hours and a 56% DOXO release after 72 hours (**Figure 4.12C**).

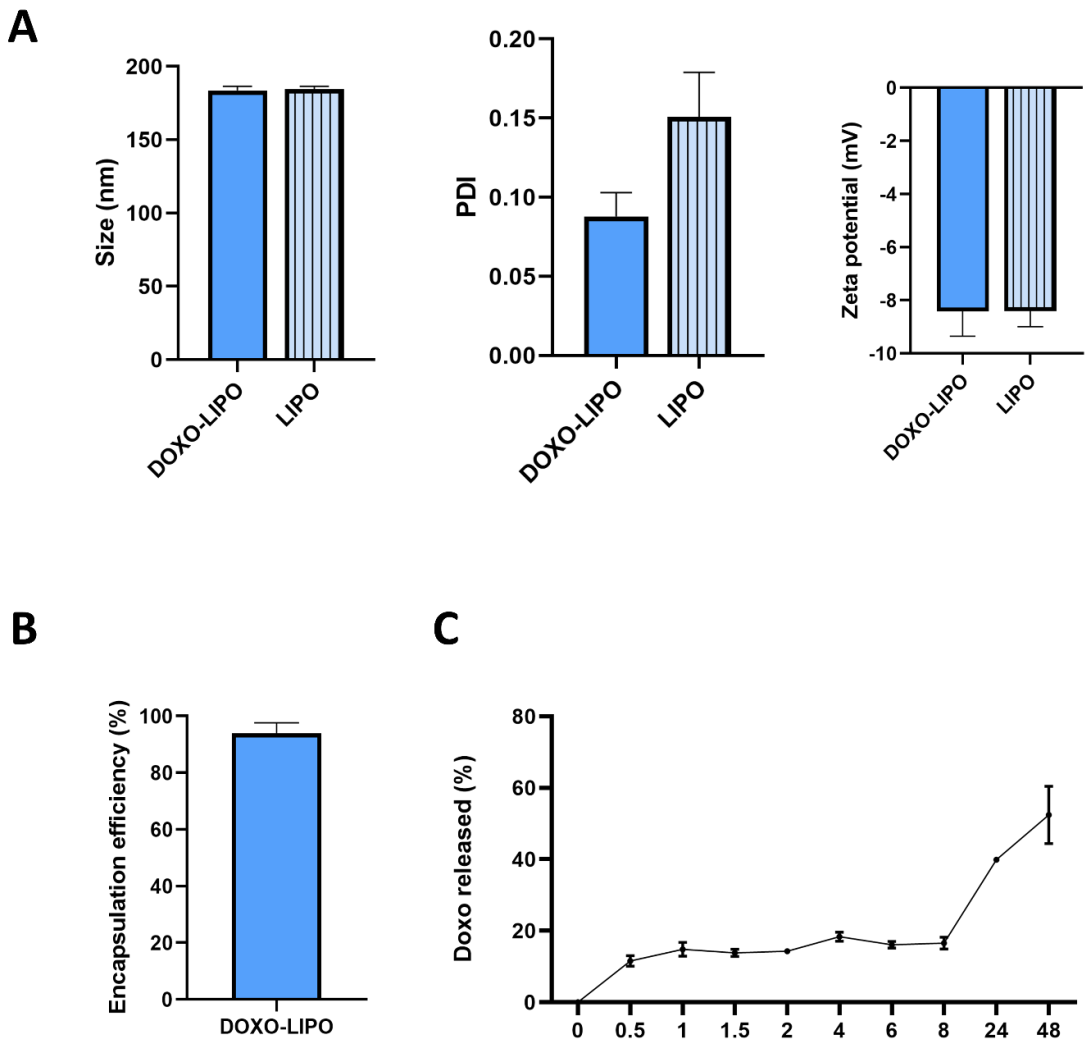

Figure 4.12. Physical and pharmaceutical characterization of empty (LIPO) and doxorubicin-loaded liposomes (DOXO-LIPO). (A) Dynamic light scattering and zeta potential measurements comparing empty LIPO and DOXO-LIPO. (B) Encapsulation efficiency and (C) release profiles of DOXO-LIPO in PBS +10% FBS (50:50) at 37 °C obtained following doxorubicin fluorescence. Data are mean + standard deviation (n=3).

The *in vitro* cytotoxicity of free DOXO, DOXO-LIPO, and empty liposomes was tested against OVCAR-3, Caov-3, and SKOV3 cell lines grown in 2D culture, on NS, and on MS. In 2D culture,

MTT assay was used to evaluate cell viability and proliferation (**Figure 4.13)**, and in 3D culture growth inhibition was assessed using CellTiter-Glo® **(Figure 4.14)**. After normalization against untreated cells, we observed a similar effect of free DOXO and DOXO-LIPO in reducing all ovarian cancer cells' viability in 2D, while the control of empty liposomes did not affect cells' viability after either 48 or 72 hours of treatment. Interestingly, OVCAR-3 in 2D were the most resistant to treatment after 48 and 72 hours in the lower dose range, showing a reduction of cell viability at 72 hours of 64, 43, and 35.8% for DOXO and 75, 46, and 42.6% for DOXO-LIPO at concentrations of 0.0625, 0.125, and 0.25 µM, respectively (**Figure 4.13A**).; while at the same concentrations, Caov-3 showed reductions of cell viability of 30, 21, and 11% for DOXO and 45, 35, and 21% for DOXO-LIPO (**Figure 4.13B**) and SKOV3 showed reductions of 21, 10, and 8% for DOXO and 30, 10, and 8% for DOXO-LIPO (**Figure 4.13C**).

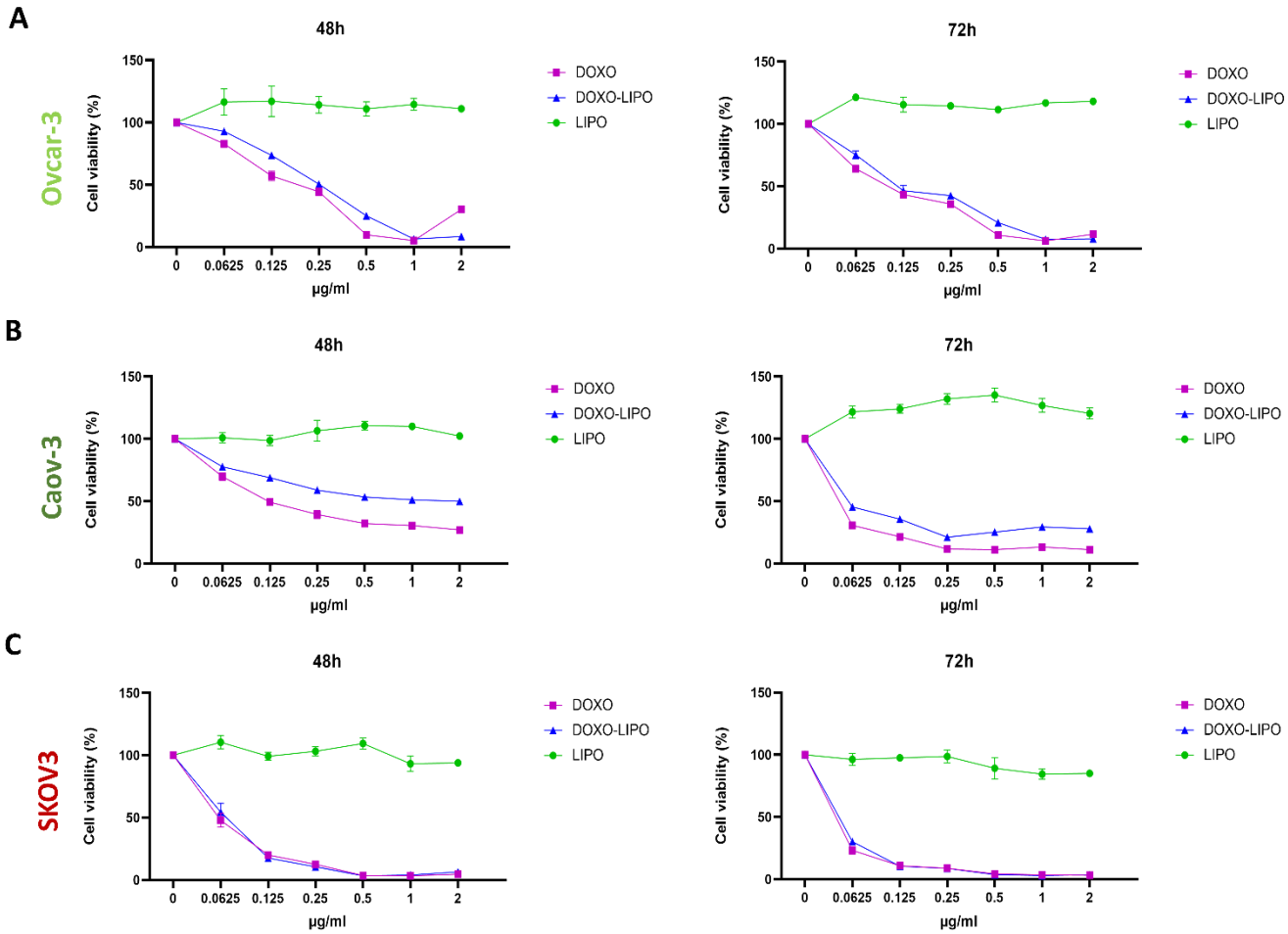

Figure 4.13. DOXO free and DOXO LIPO cytotoxic effect on ovarian cancer cell lines in 2D after 48h and 72h of treatment. MTT analysis after 48h and 72h of DOXO free and DOXO-LIPO treatment for OVCAR-3 (A), Caov-3 (B), SKOV3 (C) ovarian cancer cell lines. Data are mean + standard deviation (n=3).

On 3D *in vitro* scaffolds, cells were initially treated with a dose range from 0.25 to 5 μg/ml DOXO and DOXO-LIPO and their availability checked after 72h (**Figure 4.14).** Empty liposomes had minimal effect on the proliferation of all cancer cell lines. OVCAR.3 cells showed more sensitivity to DOXO treatment than DOXO-LIPO on both NS and MS scaffolds; the IC50 for NS scaffolds corresponded to 0.25 and 0.50 μg/ml on NS scaffolds and 0.25 μg/ml on MS scaffolds, for DOXO treatment; DOXO-LIPO IC50 was around 5 for NS scaffolds and 1 for MS, suggesting an higher sensitivity to the drug on MS (**Figure 4.14A**). Caov-3 cells reported a similar IC50 for both DOXO and DOXO-LIPO of around 0.50 μg/ml; similar effect was recorded on MS scaffolds (**Figure 4.14B**), showing no treatment sensitivity effect promoted by substrate stiffness. Finally, SKOV3 cells reported a IC50 of around 0.50 and 1 μg/ml when cultured on NS scaffolds; while MS scaffolds showed an IC50 of 0.25 μg/ml, showing increased sensitivity to DOXO and DOXO-LIPO treatment of SKOV3 cell when cultured on MS scaffolds (**Figure 4.14C**).

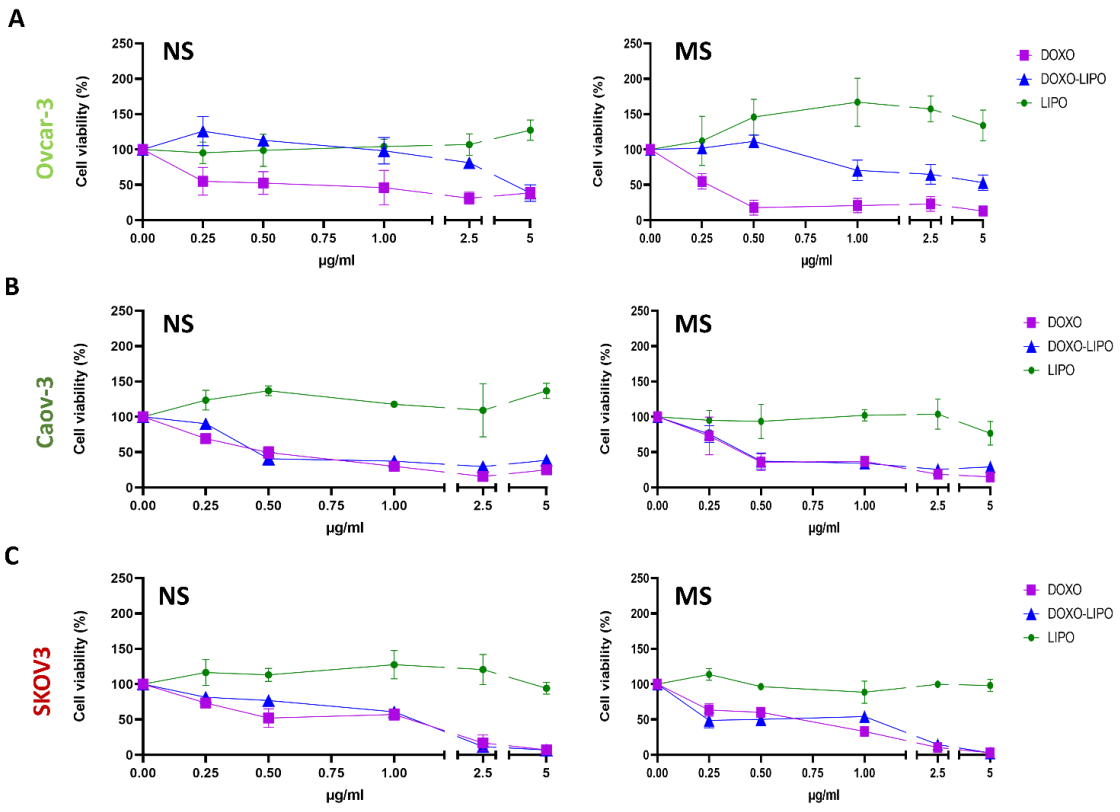

Figure 4.14. DOXO free and DOXO LIPO cytotoxic effect on ovarian cancer cell lines in 3D MS and NS after 72h of treatment. Cell TiterGlo analysis on cell viability under DOXO free, DOXO-LIPO and LIPO treatment for OVCAR-3 (A), Caov-3 (B), SKOV3 (C) ovarian cancer cell lines. Data are mean + standard deviation (n=3/5).

Focusing our attention on low and high dose close to the IC_{50} value (0.25 and 1 µg/ml), we summarized cells' sensitivity findings on NS and MS scaffolds in **Figure 4.15**. Overall, both 0.25 and 1 µg/ml of DOXO and DOXO-LIPO had a higher cytotoxic effect on 2D cultures rather than 3D MS and NS. DOXO-LIPO and DOXO show comparable effects among all cell lines tested, with the only exception of OVCAR-3 cells in 3D culture in which free DOXO had a greater cytotoxic effect compared to DOXO-LIPO (DOXO and DOXO-LIPO, 1 µg/ml, MS : 20% and 70% cell viability; NS: 46% and 98% cell viability). **(Figure 4.15A-B)**. Interestingly, Caov-3 was more sensitive than the other two cell lines to both DOXO and DOXO-LIPO at 1 µg/ml, reporting a cytotoxic effect comparable to the one obtained in 2D (DOXO: 13%, 36%, and 30% and DOXO-LIPO: 29%, 34%, and 37% for 2D, MS, and NS, respectively) (**Figure 4.15C-D**). Finally, SKOV3

showed a DOXO and DOXO-LIPO, 1 µg/ml, MS : 33% and 50% cell viability; NS: 57% and 63% cell viability, respectively (**Figure 14.15E,F**).

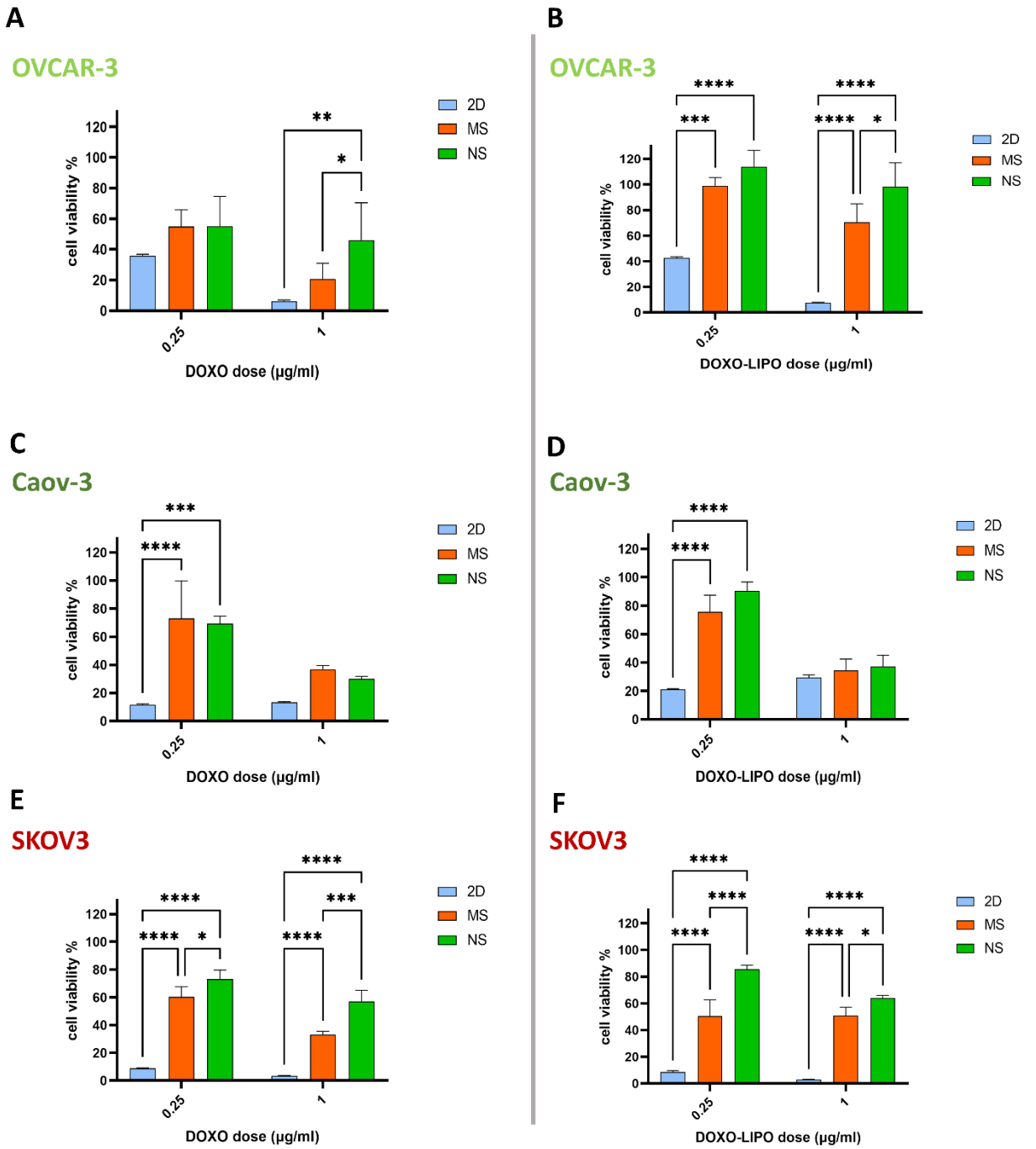

Figure 4.15. DOXO and DOXO-LIPO cytotoxic effects on ovarian cancer cell lines grown in 2D culture and 3D MS and NS. MTT and CellTiter-Glo® analysis of cell viability under 0.25 and 1 µg/ml DOXO and DOXO-LIPO

treatment for OVCAR-3 (A-B), Caov-3 (C-D), and SKOV3 (E-F) ovarian cancer cell lines at 72h. Data are mean + standard deviation (n=3/5). Statistical analysis performed with two-way ANOVA. **** $p<0.0001$, *** $p<0.001$, **$p<0.01$, *$p<0.05$.

4.3.7 Scaffold compatible co-culture system to mimic low to high stroma tumour environments

Tumour–stroma ratio (TSR) is defined as the proportion of tumour cells relative to surrounding stroma, and it has been recognised as a potential prognostic factor for various solid tumours [741]. As demonstrated for gastric cancer, colon cancer, oesophageal cancer, epithelial ovarian cancer, TSR, might help identifying high-risk cancer patients [742-746]. According to the literature, stromal reaction in tumours such as advanced breast carcinoma corresponds to the diffuse pattern of CAF's localization within the tumour [698]. To replicate this within a scaffolded 3D environment is a difficult challenge.

Using MRC-5 cells consistent with chapter 3, a co-culture model to investigate OC-TME stromal, cancer cell interactions was developed, with preliminary data showing the suitability of the porous scaffold strictures for this application. The soft, normal scaffold was utilised as a preliminary pilot experiments to start establishing the model since it was the only one analysed so far to promote remodelling. In the previous chapter it was proven to be the most suitable material to induce both fibroblasts remodelling and migration but while also supporting OC migration and promoting chemoresistance. Differential TSR was replicated in the 3D setting, by seeding a total of 100k cells, comprised of differential cancer cell to stromal, SKOV3/MRC-5 cell ratios. These are representative of normal/stroma poor tissues (1:0.5); normal/pre-malignant tissues (1:1), pathological/malignant stroma rich tissues (1:3).

First, we tested a simultaneous seeding protocol of MRC-5 fibroblasts and SKOV3 [698]. In order to visualise the cell types and their interactions within the 3D environment. MRC5 cell line membranes were stained in red (PKH26 Red Fluorescent Cell Linker Kit) before seeding while phalloidin and Hoechst staining were performed at day7 on the whole cellular population, to evaluate cell specific distribution on the soft scaffolds at day7 (**Figure 4.16**). The red staining,

representative of fibroblasts cell membrane, showed an homogeneous, interspersed presence of fibroblasts cells within the scaffold with cancer cells, a feature reported in some OC tumours [747].

The 1:3 SKOV3/MRC5 ratio seems to result in smaller scaffolds diameter (**Figure 4.16E-F**) and, with the addition of TGFβ1 treatment on the 1:1 and 1:3 coculture the cellular density seems higher compared to the other scaffolds (**Figure 4.16D-F**). Quantitative analysis is undergoing.

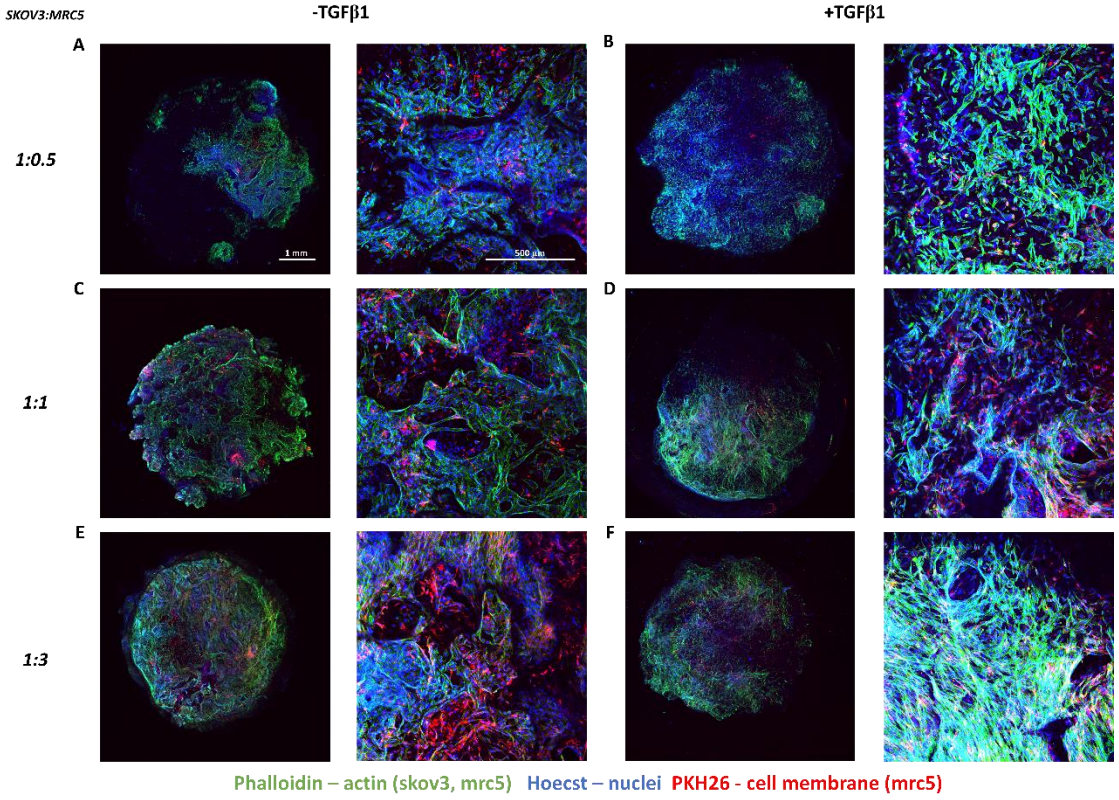

Figure 4.16. SKOV3/MRC5 coculture on NS scaffolds. Phalloidin (actin), Hoechst (nuclei), PKH26 (cell membrane mrc5) staining analyzed with confocal fluorescence microscopy (A) SKOV3/MRC5 1:0.5 (B) SKOV3/MRC5 1:0.5 + TGFβ1; (C) SKOV3/MRC5 1:1 (D) SKOV3/MRC5 1:1 + TGFβ1 (E) SKOV3/MRC5 1:3 (F) SKOV3/MRC5 1:3 + TGFβ1. Analysis and imaging were performed after 7 days of culture. Maximum Projection was reported. Low magn. 2x objective, Z-size: 773 µm, Step size: 10 µm; High magn. 1x objective, Z-size: 247 µm, Step size: 2 µm. n=1

When cancer develops, the stroma undergoes vast changes to become fibrotic and activated. The ECM becomes denser and more rigid, because of its compositional changes (alternative forms of connective fibres, such as tenascin and fibronectin), which cancer cells can invade through [748].

To test if MRC5/SKOV3 cells coculture will be able to induce changes in scaffold physical properties after 7 days of culture, rheology was performed. A significant decrease in the 3D/NS scaffold storage modulus was observed at day 7 for all coculture conditions tested ($p<0.05$) and as reported in chapter 3, in the MRC5 only control (**Figure 4.17A**). A similar significant decrease in loss modulus was recorded at day7 for 1:05 and mrc6 only culture (**Figure 4.17B**). As expected, TGFβ1 treatment promoted a further softening of the scaffolds at day7 in the 1:3 coculture, probably related to a higher presence of fibroblasts in culture or an increase proliferation of the cells type in that condition (**Figure 4.17C**). Overall, those results are indicative of a cellular proliferation induction of the cells utilized in the coculture system, soft phenotype of cancer cells was probably contributing to it and not enough fibrosis or new abnormal matrix deposition occurred. This is in line with results from chapter 2, too, where fibroblasts proliferation and contraction on NS didn't contribute to higher stiffness. As results, TGFβ1 treatment is confirmed to be a central player in promoting scaffold remodelling also in a coculture system but to better replicate mechanical endpoint of fibrosis/desmoplasia events occurring in tumour microenvironment we will need further testing using this model.

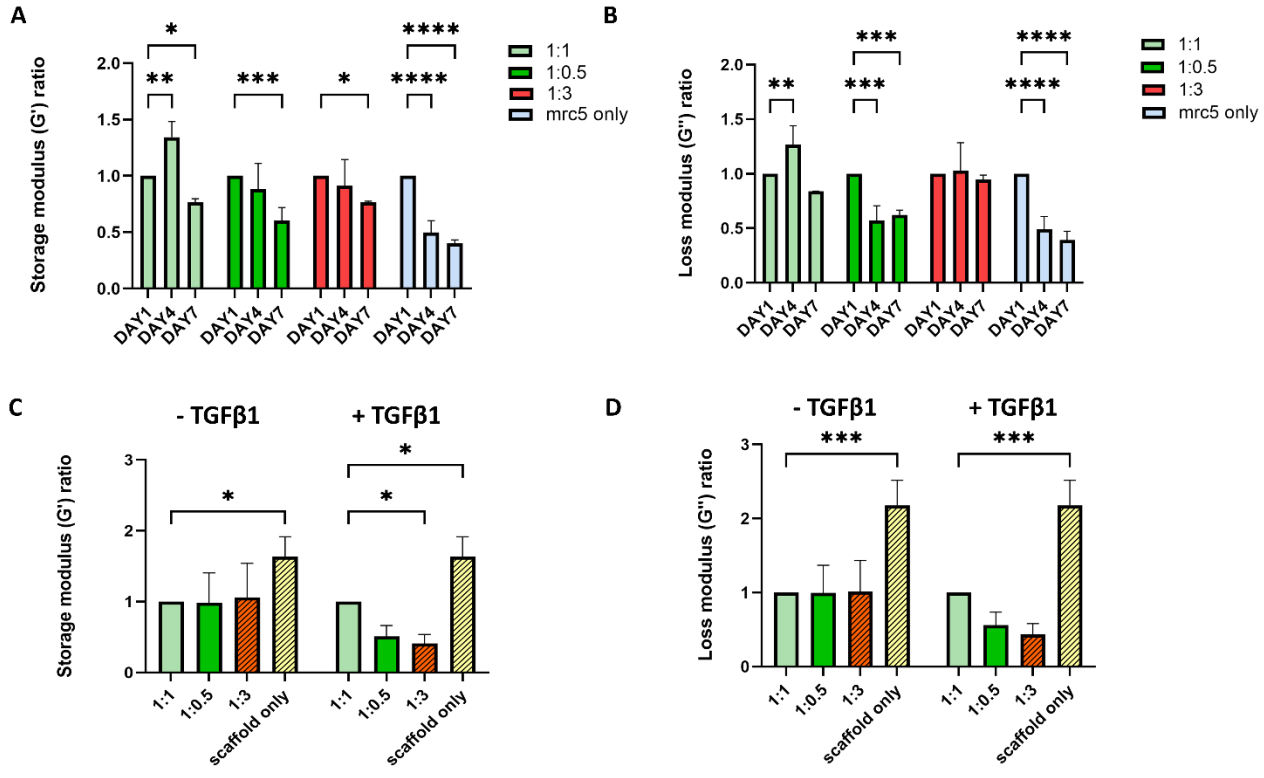

Figure 4.17. NS scaffolds coculture results in scaffold softening after 7 days. Rheology analysis of storage modulus (G') in NS scaffolds; (B) Rheology analysis of loss modulus (G"). Data normalized to normal media sample (NM). Data are mean + standard deviation (n=3). Ordinary one-way ANOVA, **p<0.01, *p<0.05.

4.4 Discussion

In the tumour setting, biomechanical and biochemical elements, alongside stromal cells, work together and are crucial for the maintenance of ECM homeostasis, shown to control cancer cell fate during progression. Indeed, loss of mechanical homeostasis in the TME accompanies tumorigenesis and also contributes to invasion and metastasis [749], since, at the cellular level, cancer cells actively respond to externally applied forces and then couple to intracellular signalling pathways and effectors [750].

From a biophysical standpoint, solid tumour cancers have been shown to share physical characteristics; however, those are affected by specific mechanical cues linked to the tissue of origin [751-754]. For example, brain tumours are soft, whereas pancreatic tumours are rigid [755, 756]. In such tissues, the inputs conveyed from the surrounding microenvironment are transmitted through surface receptors to cellular compartments and ultimately its nucleus, where they can influence gene expression and promote disease development and differentiation [104, 757]. Tuneable collagen sponge models allow cancer cell proliferation, morphology, migration, and drug response to be monitored in differential mechanical and biophysical contexts. In line with this, the use of 3D matrices to build physically meaningful platforms for drug testing is essential, since cells grown in 2D dish cultures experience a different force pattern, which could impact drug treatments outcome evaluation.

NS and MS 3D *in vitro* model mimic the differences in stiffness between normal ovarian tissue and pathological HGSC stage III derived tissue, respectively as proven by AFM analysis (MS (0.144±0.010 MPa) and NS (0.015±0.0003 MPa)). A systematic mechanical characterization of tumour tissue mechanic of patients biopsies or having diagnostic tools able to detect changes in patients' tissue mechanic, could provide guidelines for clinical mechanopathology evaluation [385], ultimately helping doctors during diagnosis or deciding which tumours are most likely to

develop chemoresistance, improving prognosis. Our results are in line with previous research which analysed tumour stiffness *in vivo*. For example, researchers employed Supersonic shear wave elastography in a Patient-Derived Xenografts (PDX) mouse models engrafted with HGSOC tumours isolated from patients, recording a significantly increase in tumour stiffness (120 to 140 kPa) over time in Mesenchymal HGSOC, while it remained low (not higher than 60 kPa) in Non-Mesenchymal tumours.

"Fibrosis" or "Mesenchymal" HGSOC molecular subtypes have been identified in all HGSOC studies and is systematically associated with poor patient survival. Characterized by high stromal content composed of myofibroblasts and ECM proteins, such as collagen and fibronectin, major causes of tumour stiffness [102]. In the same study, in few cases, they observed a new tumour nodule emerging from a stiff mesenchymal tumour, interestingly, the new nodule of little size was softer than the established initial tumour, suggesting tumour proliferation could originate with an initial soft state. The data presented here, is also in line with observations made in other cancer types. In breast cancer, malignant tissue is typically stiffer than its normal counterpart with studies showing that normal breast tissue is 20 times softer than its neoplastic counterpart [103]; elastic moduli of healthy thyroid tissue (9.0–11.4 kPa) can increase by a full order of magnitude to 44–110 kPa in patients with papillary adenocarcinoma [104]. Furthermore, storage modulus of MS and NS scaffolds spans in range of stiffness reported in the literature referring tissues/organs stiffness ranging from 0.2-64 kPa [105-107].

To test the mechano-responsive potential of ovarian cancer malignancy, we selected three adenocarcinoma ovarian cancer cell lines: OVCAR-3 and Caov-3 derived from ovary and SKOV3 derived from ascitic fluid from post-chemotherapy patients. OVCAR-3 and Caov-3 possess TP53 mutations and substantial copy-number changes, key characteristics of HGS while SKOV3, based on its genetic profile, is categorized as non-serous [758, 759]. Although these cell lines can be divided into different categories by their mutation profiles, their behaviours *in vitro* do not necessarily segregate the same way and, most interestingly, the cell lines do not all behave as expected based on their putative identity. Indeed, cell lines derived from non-serous carcinomas (e.g., SKOV3) were shown to migrate more quickly and were more likely to invade into Matrigel and collagen I substrates than cell lines derived from high-grade serous carcinomas (e.g., OVCAR-

3) [760]. Furthermore, other researchers found that SKOV3 had high tumorigenicity when injected intraperitoneally, whereas OVCAR-3 had low tumorigenicity when inoculated in nude mice over 6 weeks [761].

For this reason, we selected relevant HGSC and non-serous tumour derived ovarian cancer cell lines to investigate mechanosensing behaviour in response to different 3D biomechanics scaffolds. All cell lines employed colonized and were viable on both MS and NS with no changes in morphology. However, looking at the migration depth in the scaffolds recorded by immunofluorescence staining, SKOV3 and Caov-3 showed higher invasiveness compared to OVCAR-3. Indeed, previous findings suggest that changes in stiffness of the cancer cell niche, as would be encountered by disseminated or metastatic OCCs, represents mechanism to further promote EMT [15]. A significant difference was recorded in the proliferation rate, showing higher proliferation of OVCAR-3 on NS while both Caov-3 and SKOV3 had higher proliferation rates on MS, suggesting higher responsiveness to rigid substrates. The higher rate of proliferation of OVCAR-3 and SKOV3 compared to Caov-3 resulted in a lower storage modulus after 7 days of culturing for MS, suggesting a link between cells proliferation and softening of the scaffolds recorded with rheometry. This phenomenon could be linked to two phenomena reported in literature. First, cancer cells are physically softer than normal cells [112, 113] and metastatic cancer cells are more mechanically compliant than their non-metastatic counterparts [114, 115], contributing to the overall softening of the tissue. Second, previous findings suggest that a reduction in the stiffness of the cancer cell niche, as would be encountered by disseminated or metastatic OCCs, is a mechanism to promote EMT [116], suggesting that the progressive softening of the matrix is a crucial step to promote metastasis.

YAP and TAZ are transcriptional coactivators pervasively activated in human malignancies. Their activation in cancer cells impacts the behaviour of cancer cells themselves by regulating the capacity to proliferate and adjust their metabolism to the altered cellular context, promoting the acquisition of stem-like properties, drug resistance, and migratory capacity that allow tissue invasion and metastatic dissemination. Interestingly for the present study, YAP/TAZ are sensors of the structural and mechanical features of the cell microenvironment including changes in mechanotransduction, inflammation, oncogenic signalling, and inhibition of the Hippo pathway

[762, 763]. Many correlations between high YAP and TAZ expression with poor patient outcome were reported for breast, colorectal, liver, and pancreatic cancers [588]; specifically, TAZ is thought to play an important role in breast cancer progression with both mRNA and protein expression reported to be preferentially higher in triple-negative breast cancer than in the other subclasses [764-767]. Previous research reported that SKOV3 cells express a low amount of endogenous YAP (and lowest activity) compared to Caov3 and OVCAR3, which instead showed a higher level of both YAP expression and its activity [768]. Interestingly, we observed that while OVCAR-3 and Caov-3 downregulated YAP/TAZ expression on MS, SKOV3 cells increased the expression of both markers on MS compared to NS, suggesting a specific YAP/TAZ upregulation linked to high stiffness microenvironment.

Aside from intrinsic molecular mechanisms [769], tumour chemoresistance is also affected by the biochemical and physical properties of the tumour microenvironment [770-772]. Specifically, the chemotherapeutic response of ovarian cancer cells *in vitro* is markedly affected by substrate stiffness; for example, during an evaluation of ovarian cancer tumour response to standard chemotherapeutic drugs (cisplatin and paclitaxel), antiproliferation effects were directly proportional to the stiffness of the substrate, so ovarian cancer cell lines grown on softer substrates with a lower elastic modulus were less sensitive to chemotherapeutic agents [773].

First-line management for ovarian cancer consists of surgery plus platinum-based combination chemotherapy, typically cisplatin or carboplatin, with the addition of a taxane, either paclitaxel or docetaxel [774]. Nevertheless, more than 70% of patients experience relapse after first-line therapy [775]. For patients who experience partially platinum-sensitive relapse (progression within 6 to 12 months after the last platinum-based chemotherapy treatment), the treatment has not yet been standardized [776-780]. Approved by the US Food and Drug Administration (FDA) in 1995, Doxil (doxorubicin HCl liposome injection, Tibotec Therapeutics, Division of Ortho Biotech Products, L.P.) was the first nano-drug marketed in the United States for the treatment of ovarian cancer in women whose disease has progressed or recurred after platinum-based chemotherapy [781]. Many clinical trials showed response rates, progression-free survival, and overall survival similar to other platinum-based combinations but with a more favourable toxicity profile and convenient dosing schedule when Doxil was tested [782, 783].

In line with those results, the cytotoxic effects of free DOXO and DOXO-LIPO was tested on cis-platinum resistant SKOV3 [784], OVCAR-3 [785], and Caov-3 [786] grown in 2D and on 3D MS and NS. A higher resistance to treatment in 3D vs 2D culturing conditions was observed, further stressing the importance of adopting 3D models to perform more reliable *in vitro* drug screening and dosing; furthermore, among the different ovarian cancer cell lines, Caov-3 was more sensitive to both DOXO and DOXO-LIPO treatment, pointing out the necessity to include many different cell lines when performing cancer studies or primary cells when evaluating potential patient-treatment responses. Finally, both OVCAR-3 and SKOV3 showed a higher resistance to treatment when grown on NS and a more sensitive phenotype when grown on stiffer MS thus confirming previous study reporting cell growth inhibition by doxorubicin in response to ECM rigidity [787].

These results can be linked to the effect observed, where OC cancer cells proliferate more on stiff matrix. Indeed, OVCAR-3 showed higher proliferation rate since day4 on both NS and MS compared to the other cell lines and it showed an increase on NS compared to MS only at day10; for both Caov-3 and SKOV3 higher proliferation rates on MS were recorded since day4 and day7 respectively. Since doxorubicin mechanism of action is to stop the growth of cancer cells, intercalating into DNA and disrupting of topoisomerase-II-mediated DNA repair to generate free radicals [788], it was hypothesised that increased stiffness in the microenvironment may increase cancer cell proliferation and, consequently, make them more susceptible to treatments that block cells growth.

Finally, to fully address tumour complexity a normal scaffold, soft material prone to remodelling by fibroblasts as demonstrated in the previous chapters, was combined with a coculture of SKOV3 and MRC5 cells, in different ratios to mimic the TSR of normal/premalignant and malignant tissues. TSR represents the proportion of tumour cells relative to surrounding stroma, and it correlates with patients' outcomes [741-746]. It can serve as prognostic factor, as shown for breast cancer where patients with more than 50% intra-tumour stroma were quantified as stroma rich and patients with less than 50% as stroma poor. Stroma-rich tumours had a had a 2.92 times higher risk of relapse and lower five years relapse-free period (RFP) compared to stroma-poor tumours [789].

As preliminary results, the co-culture models showed an intersperse, homogeneous spatial organization of MRC5 and SKOV3 cells when seeded simultaneously, which resulted in smaller scaffolds diameter in stroma rich scaffolds and higher cellular density when high stroma was combined with TGFβ1 treatment. According to the literature, stromal reaction in tumours such as advanced breast carcinoma corresponds to the diffuse pattern of CAF's localisation within the tumour, similar to that recorded in this model system [698]. Further optimisation on seeding protocols and staining is required to better reflecting the clinical situation, however.

First, the incorporation of NF and CAF in this 3D culture system could help in the characterisation of the ECM components derived from the resulting coculture system. It will help delineate similarities of the matrisome signature resulting from *in vitro* models and their *in vivo* counterpart, to provide a possibility to study fibrosis progression. Similarly, this process is under evaluation in other spheroids based models for breast cancer [698], aimed at optimising antifibrotic therapies in cancer treatment. Secondly, reproducing the TSR obtained from histological analysis of the specific tumour under investigation [742, 746, 790, 791], will enable optimal investigation of fibrotic reactions. Indeed, for example, the mesenchymal molecular subtype represents 50% of the HGSOC cases diagnosed, presenting with a strong desmoplastic reaction and accumulation of both ECM proteins and CAFs [284]. Indeed mesenchymal HGSOC display stiffness heterogeneity, between the core (stiff) and the periphery (soft); reproducing those feature in a 3D model with the inclusion of the right ratio of cancer cells and fibroblasts could help understand what determines those differences in tissue mechanics and how to manipulate or restore normal homeostasis. Finally, assessment of both soluble and insoluble secreted factors and of direct contact factors in the fibroblast–epithelial interactions that influence epithelial ovarian cancer cell growth can be facilitated in this model system, leading to infinite new disease understanding as a basis for novel diagnostic and therapeutic strategies.

To summarize, the inclusion of physical parameters in 3D *in vitro* model design will help configure a microenvironment closer to native tissue, which could sustain meaningful cell culture conditions, i.e. cancer-stroma coculture, addition of immune cells to for cancer research and drug testing. Envisioning a clinical application, the use of patient-derived primary cells in combination with a

3D biomechanical scaffold could be used to assess the likelihood of a favourable outcome to a tumour treatment and eventually suggest possible alternative patient-tailored options.

Chapter 5: Alternative, marine sourced sustainable collagen substrates for ovarian cancer cell systems

The work presented in this thesis chapter is sponsored by Jellagen, a life science company in South Wales under the banner of CALIN funding (ERDF). Significant results contributed directly to the following peer reviewed journal article.

Francesca Paradiso, Joan C. Fitzgerald, Seydou YAO, Frank Barry, Francesca Taraballi, Deyarina Gonzalez, Robert S. Conlan, Lewis W. Francis. Marine collagen substrates for 2D and 3D ovarian cancer cell systems. Frontiers in Bioengineering and Biotechnology, December 2019; doi: 10.3389/fbioe.2019.00343 **(IF 5.2)**

5.1 Introduction

Collagens represent 30% of total protein mass in mammals, providing a fundamental structural component of extracellular matrix (ECM) in all connective and interstitial tissue [792]. Since the discovery of collagen II by Miller and Matukas (1969) [793], 26 new collagen types have been discovered, which have been classified into subfamilies based on their supramolecular assembly, namely fibril-forming collagens, fibril-associated collagens, network-forming collagens, anchoring fibrils, transmembrane collagens, basement membrane collagens and others with unique functions [792, 794].

Fibril forming collagens share a common structural feature, the triple helix, which can make up 96% of their structure (collagen I) to less than 10% (collage XII) [795]. The triple helix is composed of three polypeptides, α chains, composed of the peptide triplet repeat Gly-X-Y (X = proline, Y = hydroxyproline), conserved structural features which are crucial in mediating the spectrum of collagen functions [792]. Biological sources of collagen type I include vertebrates' skin, porcine/bovine/ovine tendon tissue and rat tail, while bovine, porcine and chicken cartilage tissues provide a good source for collagen type II. The ability of these collagen sources to be fabricated into varying scaffold forms such as hydrogels, sponges, fibres, films, and hollow spheres provide tools for mimicking complex biological and mechanical features of native tissue [796-798]. Furthermore, by tuning scaffold porosity, shape and topography, clinicians can have access to a powerful array of controlled structures for tissue grafting, that can promote cell growth/differentiation, additionally, bioinspired collagen-based *in vitro* culture methods provide a base for ECM substitutes in pathologic models for drug screening [799].

Mammalian collagen devices are used in many biomedical applications due to their excellent biocompatibility, high biodegradability and good mechanical, haemostatic, and cell-binding properties [165]. Conversely, complex collagen extraction methods, together with limited and expensive collagen sources, and the risk of infection with transmissible diseases such as spongiform encephalopathy, transmissible spongiform encephalopathy and foot and mouth

disease, have led to the exploration of alternative functional collagen sources with low immunogenicity and reduced risk of causing transmissible disease [800].

Many non-mammalian species, both vertebrate and invertebrate, have been evaluated as new and alternative collagen sources. Such collagen sources have predominantly been used in different applications including bone tissue engineering and related diseases, and cosmetic and/or skin care [801, 802]. To date, marine-derived collagens have largely been used in the food, pharmaceutical and cosmetics industries, and to a much lesser degree for biomedical research and clinical applications [803]. Marine species include invertebrates such as cuttlefish, sea anemone, prawn, star fish, sponges, sea urchin, octopus, squid or vertebrate like fish and marine mammals have been evaluated [800]. Extraction of collagen from jellyfish species, has been limited to *Somolophus meleagris* [177, 804], *Rhizostomous* jellyfish [804], *Chrysaora* sp. jellyfish [805], and *Rhopilema esculentum* [806]. Of these, collagen derived from *Rhizostoma Pulmo* has been shown to have a high degree of similarity to mammalian type I collagen: closest melting temperatures when crosslinked with EDC, similar structure (existence of two different α chains, two 1α chains and one 2α chain), high biocompatibility when tested with fibroblasts, epithelial, osteoblastic and fibrosarcoma cells, confirmed by the assembly of focal adhesions [807] (**Table 5.1**).

R.Pulmo collagen	Mammalian collagen
2α1 chains, 1α2 chain	2α1 chains, 1α2 chain
Tm = 28.9 °C	Tm = 33 °C
high biocompatibility	high biocompatibility
Focal adhesion development	Focal adhesion development
High bio sustainability	Low bio sustainability
Less hydroxyproline content	Normal hydroxyproline content

Table 5.1. Content adapted from: Addad, S. et al, *Marine Drugs 2011*

Fibril forming collagen type I is the major component of tissue ECM, exerting both mechanical and biological functions. It contributes to tissue architecture and strength while interacting with

cells through several receptors, promoting cells growth, differentiation, and migration [795]. In a tumour setting collagen remodelling (degradation and redeposition) strongly affects tumour infiltration, angiogenesis, invasion and migration [57, 808].

As described throughout this thesis, dysregulation in collagen deposition or its degradation is implicated in many stages of ovarian cancer (OC) progressions. Normal ovarian tissue has a specific collagen signature characterized by thin, long wavy fibrils, parallel to the epithelial boundary, while, during cancer progression collagen organization facilitates cancer cell migration by creating a net of thick and short fibrils, usually perpendicular to the epithelial/cancer growing boundary, known as Tumor-Associated Collagen Signature (TACS-3) [809, 810]. Collagen remodelling and physical reorganization not only exert a pro-migratory function but are also associated with chemoresistance [811]. It is important therefore that any sustainable or alternative source of collagen for human OC models and investigation interacts with cellular components and enables collagen remodelling processes which can then be interrogated with a spectrum of cellular and molecular techniques.

In line with the KESS funded, industrial objectives of the funded PhD scheme, this chapter undertakes a comprehensive evaluation of *R. pulmo* collagen to determine its utility in supporting OC cell growth, proliferation and migration. All of this work was conducted in collaboration with Jellagen (Cardiff, UK). *R. Pulmo* collagen structure and aminoacidic composition was characterised, prior to its use as a coating or scaffold, to validate its suitability as a support substrate for both 2D and 3D cell culture systems [299, 694, 812] (**Figure 5.1**). As a sustainable alternative to mammalian/vertebrate sources, which serves to deliver advances in the communities' desire to reduce its reliance and impact on the use of mammalian species and their derived products, *R. pulmo* derived collagen offers a reliable substrate for *in vitro* studies, recapitulating physiologically cancer cell environments.

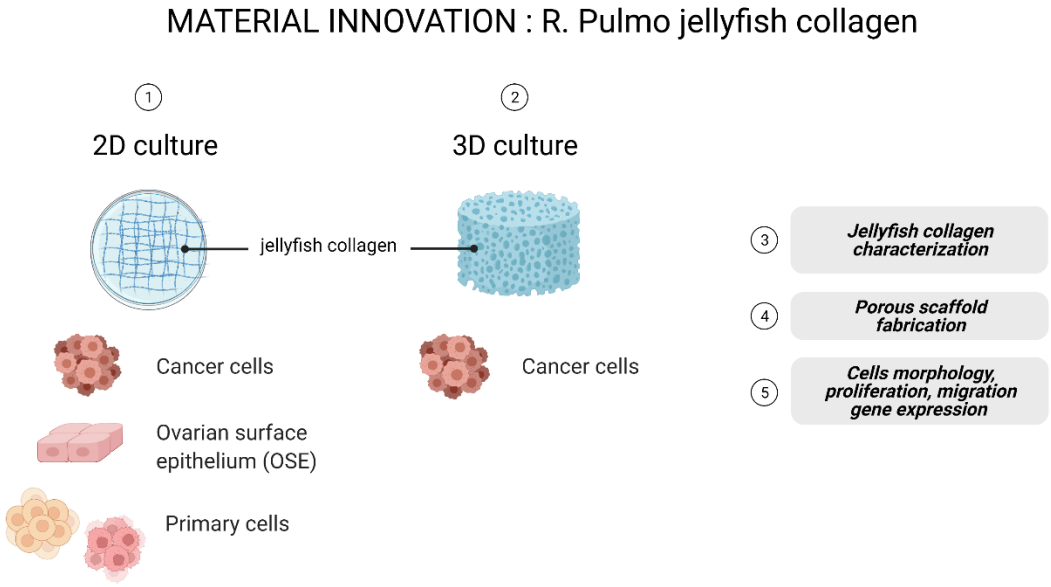

Figure 5.1 Schematic representation of experimental flow, cell, models use in this chapter. Image made with Biorender.

5.3 Results

5.3.1 R. pulmo jellyfish collagen structural features and amino acid composition.

Collagen is a building material for most tissues and organs, important as structural protein and promoting protein for cell growth and differentiation, both functions strongly depending on the specific structure of collagen fibres [813]. The basic structure of collagen type I is composed of three polypeptide α-chains (two α1 chains and one α2 chain), termed the coil, which are wound around each other [814]. SDS PAGE was used to characterise *R. pulmo* peptide chain composition compared to mammalian collagens.

Under reducing conditions, *R. pulmo* collagen chain number and size were found to be present in the expected 2:1 ratio of α 1to α 2monomeric), with β (dimeric) and γ (trimeric) forms also being

observed, and closely matched the SDS-PAGE profile of high-purity rat tail and bovine type I collagen samples, thus demonstrating very similar chain composition between type I mammalian and *R. pulmo* collagen (**Figure 5.2A**).

Collagen has a long conserved evolutionary history, and it clearly contributed to the development of early multicellular organisms [815]. Mammalian integrin collagen receptor motifs found in collagens, such as GPO (Glycine-Proline-Hydroxyproline) [816] and RGD (Arginine-Glycine-Aspartic acid), have been suggested as a mechanism by which mammalian cells anchor to collagens in mammals and other vertebrates [817]. Collagen amino acid composition is crucial to support cell attachment and for stability and triple helix thermal behaviours. Whilst mammalian and *R. pulmo* exhibited very similar collagen chain composition, differences in amino acid content were observed. Consistent with previous reports [177], *R. pulmo* collagen contained less hydroxyproline and proline, 1.52% and 3.43% respectively, compared to rat and bovine type I collagen (**Figure 5.2B**). Whilst these amino acids are known to be important in the formation and stability of the tertiary structure (triple helix) and thermal stability properties of collagen type I, the reduced content of these amino acids did not appear to affect the structure of *R. pulmo* collagen [798]. Also, Glycine, Alanine, Glutamic Acid were less represented in *R. Pulmo* with 11.87%, 3.30%, 4.19% respectively.

A

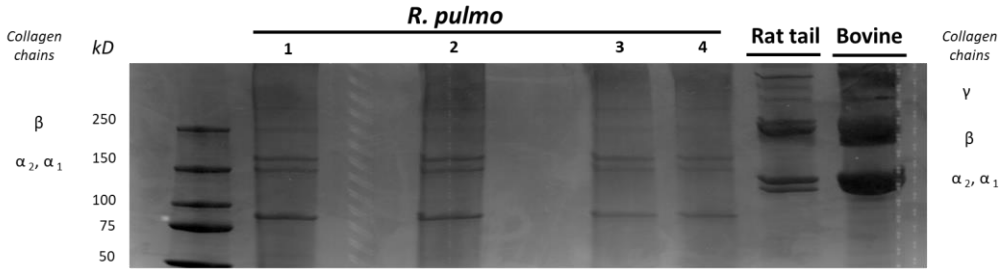

B

	Rat Tail	Bovine	*R. Pulmo*
Aspartic Acid	3.92%	4.27%	3.80%
Hydroxy-L-proline	7.64%	9.97%	1.52%
Threonine	1.93%	1.75%	2.02%
Serine	3.20%	3.04%	2.11%
Glutamic Acid	6.11%	6.79%	4.19%
Proline	9.61%	12.40%	3.43%
Glycine	24.71%	28.69%	11.87%
Alanine	8.33%	10.26%	3.30%
Valine	1.92%	1.89%	1.55%
Cystine	0.06%	0.06%	0.08%
Isoleucine	1.11%	1.23%	1.35%
Leucine	2.79%	2.77%	2.61%
Tyrosine	0.54%	0.27%	0.46%
Phenylalanine	1.14%	1.08%	0.63%
Hydroxylysine	0.68%	0.89%	1.37%
Lysine	2.24%	2.39%	1.38%
Histidine	0.42%	0.39%	0.20%
Arginine	3.90%	4.51%	2.24%

Figure 5.2. R. pulmo jellyfish electrophoretic banding and amino acid composition. (A) SDS-PAGE analysis of *R. Pulmo*, rat tail and bovine collagens. *R. Pulmo* collagen was loaded by volume: lane 1: 12ul, lane 2: 10ul; lane 3: 6ul & lane 4: 3ul. 30 ug of rat tail and bovine collagen were used as controls. (B) Samples of acid solubilized *R. Pulmo*-rat tail-bovine collagen were compared for their amino acid composition.

FTIR generates a spectral fingerprint that can provide structural insights into collagen structure based on the presence and intensity of distinct peaks that correspond to amide A/B and amide I, II and II bonds crucial to the formation of the triple helix. The main absorption bands in *R. pulmo*

collagen were amide A (3283 cm^{-1}), amide B (2934 cm^{-1}), amide I (1647 cm^{-1}), amide II (1550 cm^{-1}) and amide III (1238 cm^{-1}), typical bands for collagen type I (**Figure 5.3**).

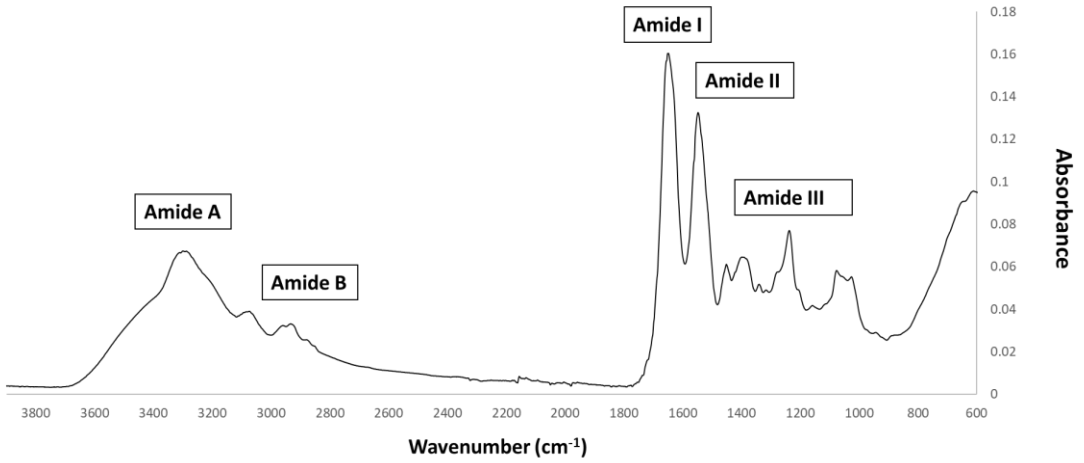

Figure 5.3. FTIR spectrum of collagen from *R. Pulmo* jellyfish. Attenuated total reflection (ATR)–Fourier–transform infrared spectroscopy (FTIR) spectra reveal the collagen bands in *R. Pulmo* collagen, with collagen I specific Amide pattern.

The amide band spectral patterns of *R. pulmo* derived collagen was comparable to mammalian collagens sources (**Table 5.2**). Amide I, II, III peak frequencies were like collagen I extracted from mammalian sources. Amide I was 1647 cm^{-1} in *R. Pulmo*, close to 1659 cm^{-1} of collagen from human placenta and 1532 cm^{-1} from rat tail tendon collagen. Amide II peak was 1550 cm^{-1}, very similar to the one from human placenta 1555 cm^{-1} and rat tail tendon 1546 cm^{-1}. Finally, Amide III showed a peak frequency of 1238 cm^{-1} in *R. Pulmo*, compared to 1240 cm^{-1} from human placenta and 1243 cm^{-1} from rat tail tendon. The absorption intensity of 1550 cm^{-1} (amide II) indicated that hydrogen bonding is present [818, 819]*;* while absorption intensity of 1238 cm-1 (amide III) confirmed that triple helical structure is intact [818]. FTIR confirmed the triple helix structure, high extent of intermolecular structure, and similar secondary structure of the proteins between different sources of collagen [818].

	Peak frequencies (cm^{-1})				
Region	R. Pulmo jellyfish	Human placenta (a)	Rat tail tendon (b)	Normal range in proteins	Assignment
Amide A	3283	Ns	3282	3400-3440	N-H stretch coupled with hydrogen bond
Amide B	2934	Ns	Ns	3100	CH_2 asymmetrical stretch
Amide I	1647	1659	1632	1600-1700	C=O stretch/hydrogen bond coupled with COO^-
Amide II	1550	1555	1546	1510-1580	NH bend coupled with CN stretch, CH_2 bend, COO^- symmetrical stretch, CH_2 wag
Amide III	1238	1240	1243	1200-1300	NH bend coupled with CN stretch, C-O stretch

Ns = not shown

(a) Belbachir, Karima, et al. "Collagen Types Analysis and Differentiation by Ftir Spectroscopy." *Analytical and bioanalytical chemistry* (2009)

(b) Benedicto de Campos Vidal et al. "Collagen type I amide I band infrared spectroscopy ". *Micron* (2011)

Table 5.2. FTIR spectrum peaks assignment of collagen from *R. pulmo* jellyfish and comparison with mammalian type I collagen extracted from human placenta and rat tail tendon.

5.3.2 Ovarian cancer cells grow and proliferate on 2D jellyfish collagen substrates.

Collagen controls tissue architecture and strength while interacting with cells affecting their growth, differentiation, and migration [799]. During cancer progression collagen structure undergoes rearrangement becoming aligned perpendicular to the invading boundary (TACS-3), thus exerting a promigratory environment facilitating cancer migration [809, 810] and is implicated in OC progression [809]. Commonly use cell lines SKOV.3 and OVCAR.3 were isolated from ascites of patients with HGSC. In vivo and in vitro studies reported different invasive behaviour between SKOV.3 and OVCAR.3 , showing high and low invasive potential in Matrigel, respectively [820]; high and low tumorigenicity when injected intraperitoneally, respectively [761]; portraying both tumorigenic and less tumorigenic advanced stage disease [760, 821].

To evaluate biocompatibility, SKOV.3 and OVCAR.3 were cultured on *R. pulmo* collagen coated culture plates and monitored for viability (collagen cytotoxicity), proliferation and morphological changes over 5 days of culture. SKOV.3 and OVCAR3 cell morphology was not-affected by the nature of the cell culture substrate (**Figure 5.4A**), SKOV.3 retained their mesenchymal-like phenotype and OVCAR.3 showed *in vitro* epithelium morphology with a characteristic grape-like clusters pattern [822]. Growth rate over 5 days, normalized on day 1 cells' number, wasn't significantly different between cells grown on different substrates except OVCAR.3 at day 2, were cells experienced a boost in proliferation on *R. Pulmo* collagen, growing 0.75 times more than rat tail substrate ($p>0.05$) (**Figure 5.4B-C** upper panels). Compared to plastic both SKOV.3 and OVCAR.3 didn't show any intraday difference in cells' number, with no significant differences in cells' number on different substrates (**Figure 5.4B-C** bottom panels).

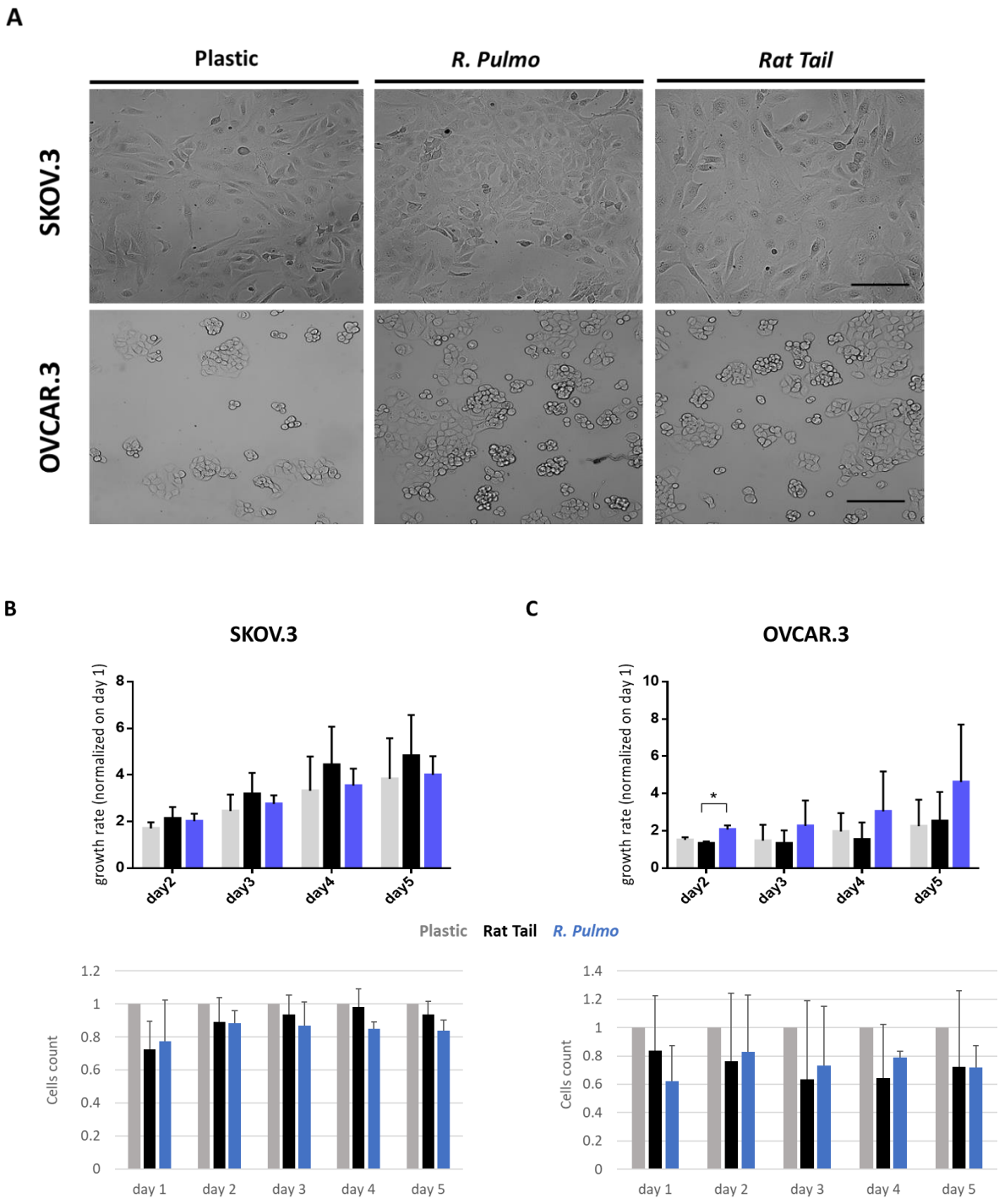

Figure 5.4. Ovarian cancer immortalized cell lines behaviour on *R. Pulmo* collagen substrate in 2D culture. (A) Brightfield acquisition after 3 days of culture, showing no cellular morphology changes after 2D OC cells culture on different substrates. (B) Cells number was obtained staining cells nuclei with Hoechst dye and analysed with in cell analyser 2000. Analysis of growth rate after 2-3-4-5 days normalized on day 1 cells number for SKOV.3. (upper

panel). Cell count comparison of cells grown on *R. Pulmo* or rat tail collagen normalized on cell number grown on plastic plates (bottom panel). (C) Cells number was obtained staining cells nuclei with Hoechst dye and analysed with in cell analyser 2000. Analysis of growth rate after 2-3-4-5 days normalized on day 1 cells number for OVCAR.3. (upper panel). Cell count comparison of cells grown on *R. Pulmo* or rat tail collagen normalized on cell number grown on plastic plates (bottom panel). *Data are shown as mean ± Standard Deviation (3 independent experiments). Statistical significance assessed by $p < 0.05$, Student's t-test.*

5.3.3 Jellyfish collagen doesn't interfere with OC cell gene expression.

EMT and mesenchymal to epithelial transition (MET) are cellular transformations that define metastatic cascade progression in OC development and differentiation [823]. To determine if *R. pulmo* collagen had any effect on EMT, the markers E-cadherin, N-cadherin and vimentin were measured at protein level and no significant difference was seen between cells grown on different substrates ($p>0.05$) (**Figure 5.5**). SKOV3 cells expressed high levels of N-cadherin and vimentin compared to OVCAR.3, which expressed the epithelial marker E-cadherin (**Figure 5.5A**).

The expression of pre-invasive metalloproteases is generally associated with a highly metastatic phenotype, and their expression appears fundamental for cancer cells to remodel surrounding extracellular matrix components including collagen [824]. *MT1-MMP* (MMP14), is a membrane type metalloprotease (MT-MMPs) present at high levels in OC cells, while others MMPs including MMP9, specific to collagens IV and V, are up-regulated in ovarian cancer stroma [825]. Furthermore, *COL11A1* expression, a component of type XI collagen, was recently associated with poor prognosis epithelial cancers including OC [826, 827]. When cultured in the presence of *R. pulmo* collagen *MT1-MMP* expression was 0.53 times higher in SKOV.3 than OVCAR.3, together with vimentin, 0.99, while OVCAR.3 showed 31 times higher expression of E-cadherin and 0.84 times higher *COL11A1* compared to SKOV.3 ($p>0.05$) (**Figure 5.5B**). Comparing EMT markers mRNA expression levels of cells cultured on *R. Pulmo* and rat tail collagen to plastic substrate we didn't find any significant difference ($p>0.05$) (**Figure 5.5C**). Unaltered mRNA expression of those markers further confirm that marine collagen can effectively substitute for mammalian collagen in 2D *in vitro* cell studies.

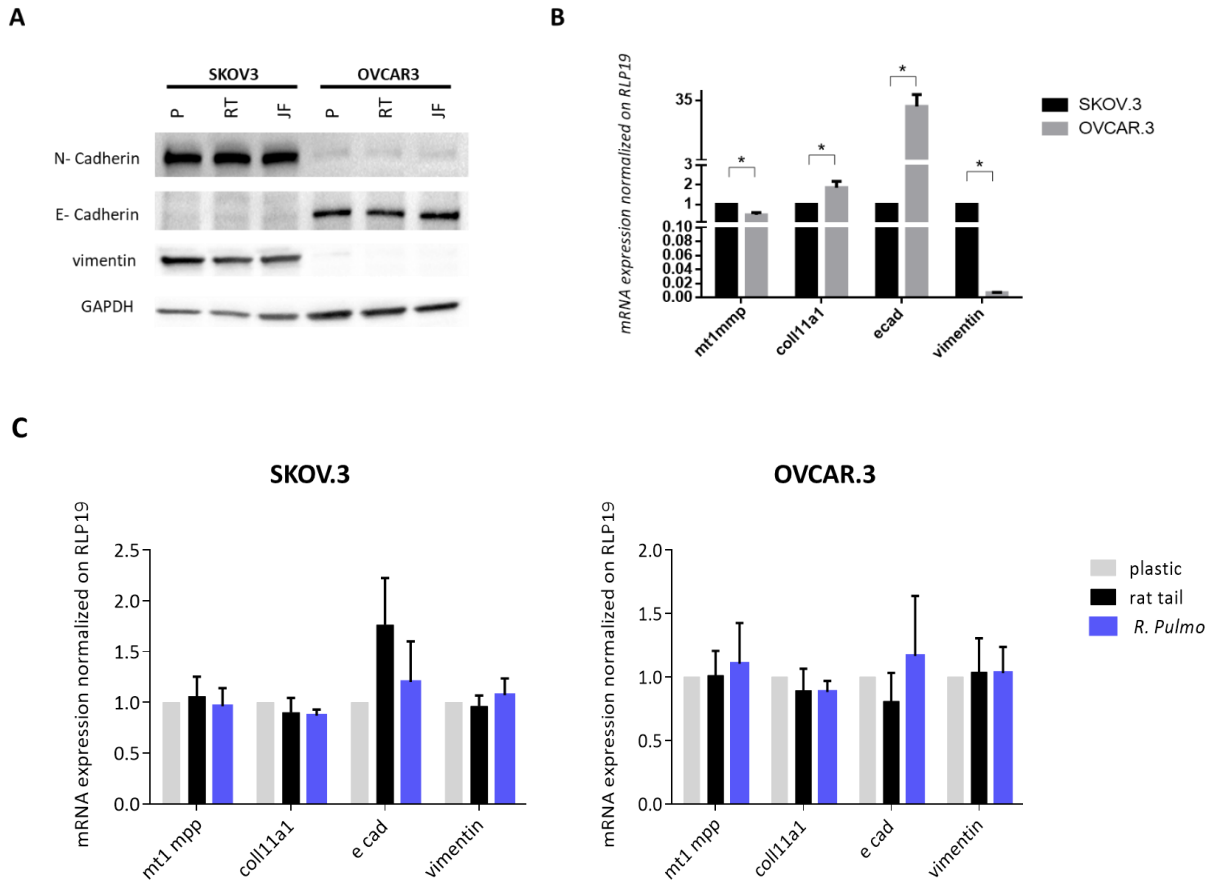

Figure 5.5 Ovarian cancer cell lines characterization. SKOV.3-highly metastatic OC cell line, is characterized by an overexpression of N-cadherin, vimentin at both (A) protein level and (B) mRNA and OVCAR.3-intermediate metastatic OC cell line, showing a typical E-cad overexpression at both (A) protein level and (B) mRNA. mRNA was extracted from cells grown on jellyfish substrate. (C) RT-qPCR analysis of a panel of genes related to EMT and OC progression in OC cells cultured on plastic, rat tail or *R. pulmo* collagen substrates. RLP19 was used as housekeeping gene and cells grown on plastic as control. AACt method was performed. *Data are shown as mean ± Standard Deviation (3 independent experiments). Statistical significance assessed by $p < 0.05$, Student's t-test.*

5.3.4 Jellyfish collagen substrate promotes focal adhesion formation in OC cells.

In a normal epithelium both cell-cell interaction and connections with the underlying basement membrane govern tissue structure [49]. Cell junctions contain a number of multiprotein complexes

that connect neighbouring cells [828] including Adherent Junctions (AJ), which contain cadherins that anchor intracellular actin filaments with intercellular of adjacent cell bridged by β-catenin [829]. In the presence of either rat tail or *R. pulmo* collagen β-catenin was distributed uniformly across the cell membrane in SKOV.3 cells (**Figure 5.6A**), whereas in OVCAR.3 β-catenin predominately localized at cell-cell junctions (**Figure 5.6C**). Similarly, vinculin [807], a component of focal adhesion complexes linking cells to basement membranes, was expressed in the membranes of cells grown on both collagen types (**Figure 5.6B-D**).

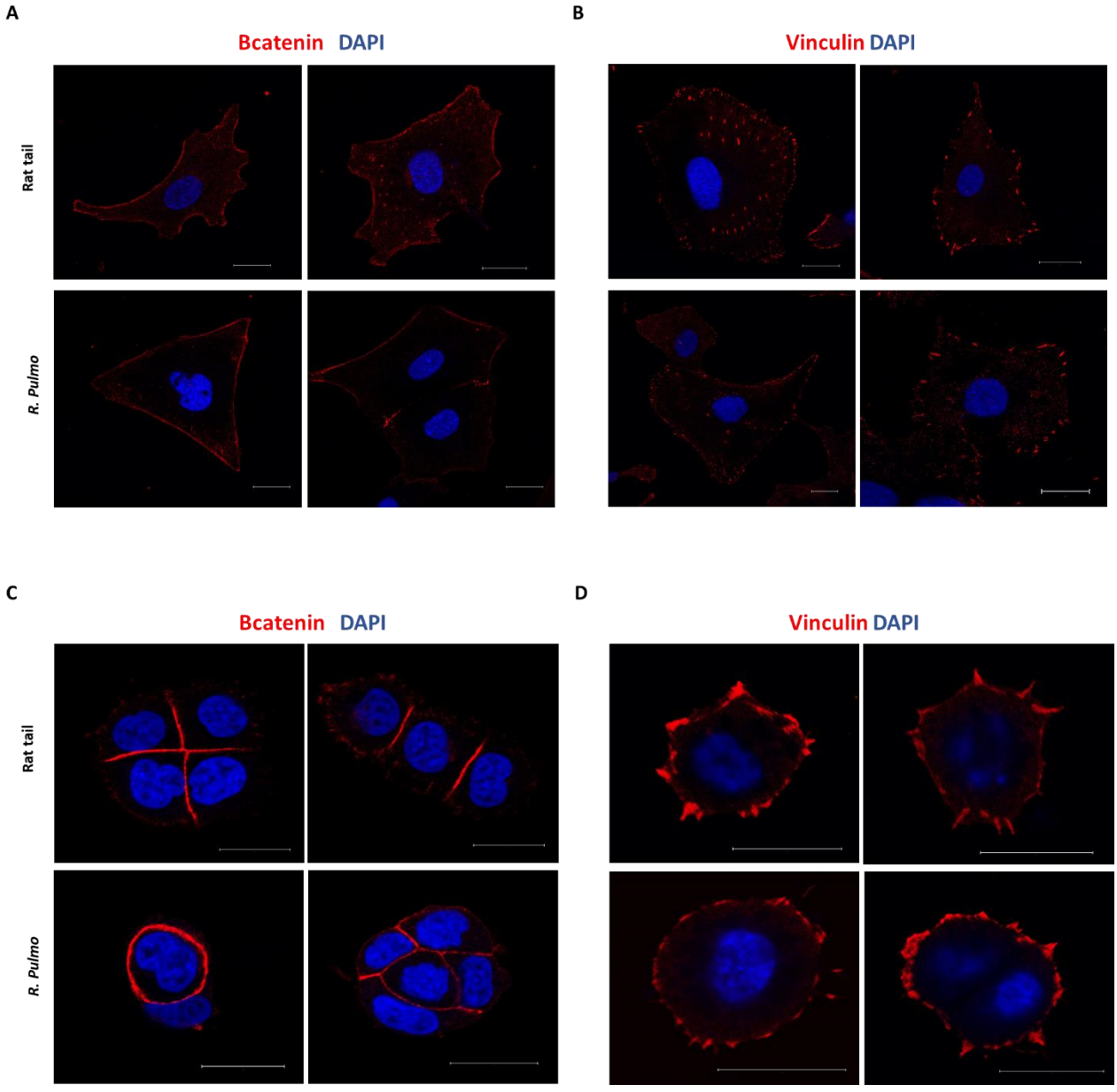

Figure 5.6. Adherents junctions and focal adhesion assembly in OC cells grown on *R. pulmo* and rat tail collagen substrate. SKOV.3 immunostaining of (A) B-catenin and (B) vinculin cells plated onto rat tail type I collagen, and R. Pulmo jellyfish collagen. OVCAR.3 immunostaining of (C) B-catenin and (D) vinculin cells plated onto rat tail type I collagen, and R. Pulmo jellyfish collagen. Scale bars represent 20um.

5.3.5 Jellyfish collagen coated plates sustain 2D OSE cell culture and proliferation.

Epithelial tumours, which are thought to arise from the ovarian surface epithelium (OSE), account for approximately 60% of all ovarian tumours and 90% of malignant ovarian cancers [830]. OSE is a single layer of flat/cuboidal epithelium that covers the surface of the ovary and has a mixed epithelial-mesenchymal phenotype, including keratin and mucin expression as well as the presence of desmosomes, apical microvilli and a basal lamina related to epithelial phenotype; and vimentin and N Cadherin expression and an absence of the epithelial differentiation markers CA125 and E-cadherin as mesenchymal markers expression [831]. Specifically the mesenchymal features are in common with ovarian carcinomas, suggesting that OSE may be the precursor tissue for ovarian epithelial malignancies [832]. Besides, overexpressing oncogenes in mouse OSE resulting in phenotypic changes that are characteristic of cellular transformation, providing a mouse model for ovarian cancer studies [833].

To further establish R. pulmo collagen biocompatibility we evaluated OSE cells proliferation and gene expression on R. pulmo coated culture plates over 5 days of culture. Growth rate over 5 days, normalized on day 1 cells' number, wasn't significantly different between cells grown on different substrates (**Figure 5.7A).** Then mRNA analysis of *OPN*, *EFEMP1*, *E CAD*, *COLL11A*, *VIMENTIN* and *MSLN* was performed on both OSE grown on 2D Rat Tail collagen coated plates (**Figure 5.7B)** and Jellyfish collagen coated plates (**Figure 5.7C).** Compared to previous analysis, new markers were tested to understand OSE oncogenic potential on different culturing substrates. Osteopontin (OPN) is a secreted non-collagenous, sialic acid rich, chemokine-like, matricellular phosphoglycoprotein that facilitates cell–matrix interactions and promotes tumour progression; it is expressed by several tissues in the human body, but also it is expressed at increased levels by

tumour cells from multiple cancer types like pancreatic, prostate and ovarian cancers [834, 835]. Epidermal growth factor–containing fibulin-like extracellular matrix protein 1 (EFEMP1) belongs to a multifunctional extracellular matrix protein fibulin family. It plays a role in maintain integrity of the basement membrane and the stability of the ECM structure and it was proved to positively contribute to ovarian cancer invasion and metastasis, indeed overexpression of EFEMP1 had significantly enhanced the abilities of ovarian cancer cells to invade and migrate [836, 837]. Mesothelin (MSLN) is a secreted protein anchored at the cell membrane by a glycosylphosphatidylinositol linkage that is overexpressed in ovarian cancer tissues, can influence chemotherapeutic sensitivity and enhance ovarian cancer invasion by inducing MMP-7 (matrix metalloproteinase) [838].

PCR experiments showed that while both Rat Tail and Jellyfish collagen promoted increase in *VIMENTIN* and *MSLN* with differences in time ($p<0.05$); Rat Tail collagen supported increase in *E-CAD* expression while Jellyfish collagen promoted its downregulation with similar effect on *OPN* expression, too ($p<0.05$). Those results suggest the need to further validation studies to understand how marine substrate nature can influence cellular gene expression.

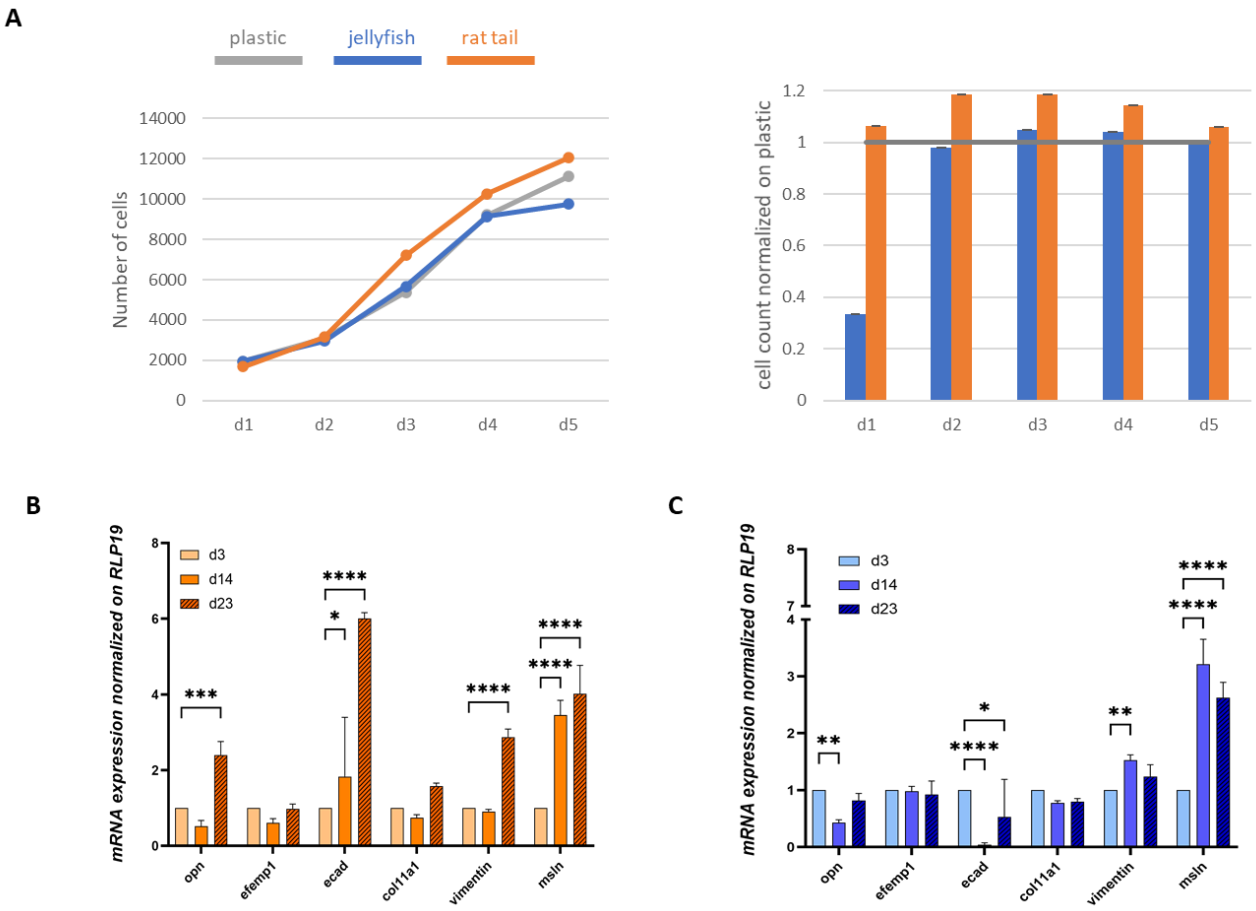

Figure 5.7. OSE cell lines proliferation and mRNA expression on *R. Pulmo* collagen substrate in 2D culture. (A) Cells number was obtained staining cells nuclei with Hoechst dye and analysed with in cell analyser 2000. Analysis of growth rate after 2-3-4-5 days normalized on day 1 cells number for OSE cells. Cell count comparison of cells grown on *R. Pulmo* or rat tail collagen normalized on cell number grown on plastic plates (right panel). (B) RT-qPCR analysis of a panel of genes related to EMT and OC progression in OSE cells grown on Rat Tail collagen coated plates. (C) RT-qPCR analysis of a panel of genes related to EMT and OC progression in OSE cells grown on Rat Tail collagen coated plates. RLP19 was used as housekeeping gene and cells at day3 as control. AACt method was performed. *Data are shown as mean ± Standard Deviation (3 independent experiments). Statistical significance assessed by $p < 0.05$, Student's t-test.*

*5.3.*6 *R. pulmo* collagen porous scaffolds sustain and support OC 3D cell culture adhesion and migration

Having confirmed the biocompatibility of *R. pulmo* collagen, we investigated its suitability as material for producing sponge scaffolds. Sponge scaffolds were produced using a freeze-dried protocol [806] and moulded into a cylindrical shape using a 96 well plate showing a diameter of 5 mm (**Figure 5.8A**). Freeze drying fabrication allow control of porosity and pore size dependent on the parameters such as ratio of water to polymer solution and viscosity of the emulsion [839] and a control of pore structure by varying the freezing temperature [840]. In general, different scaffolds pore sizes, from 20 to 1500 µm, have been used in tissue engineering for different applications and for example osteoblasts in PolyHIPE polymer (PHP), a type of highly porous polymeric foam, with a pore sizes of 100 µm showed cell migration facilitation [841]. SEM analysis of scaffold porosity showed that fabricated sponges had an average porosity of 98 nm +/- 11.33 (**Figure 5.8B**) with an ordinated pore structure (**Figure 5.8C**).

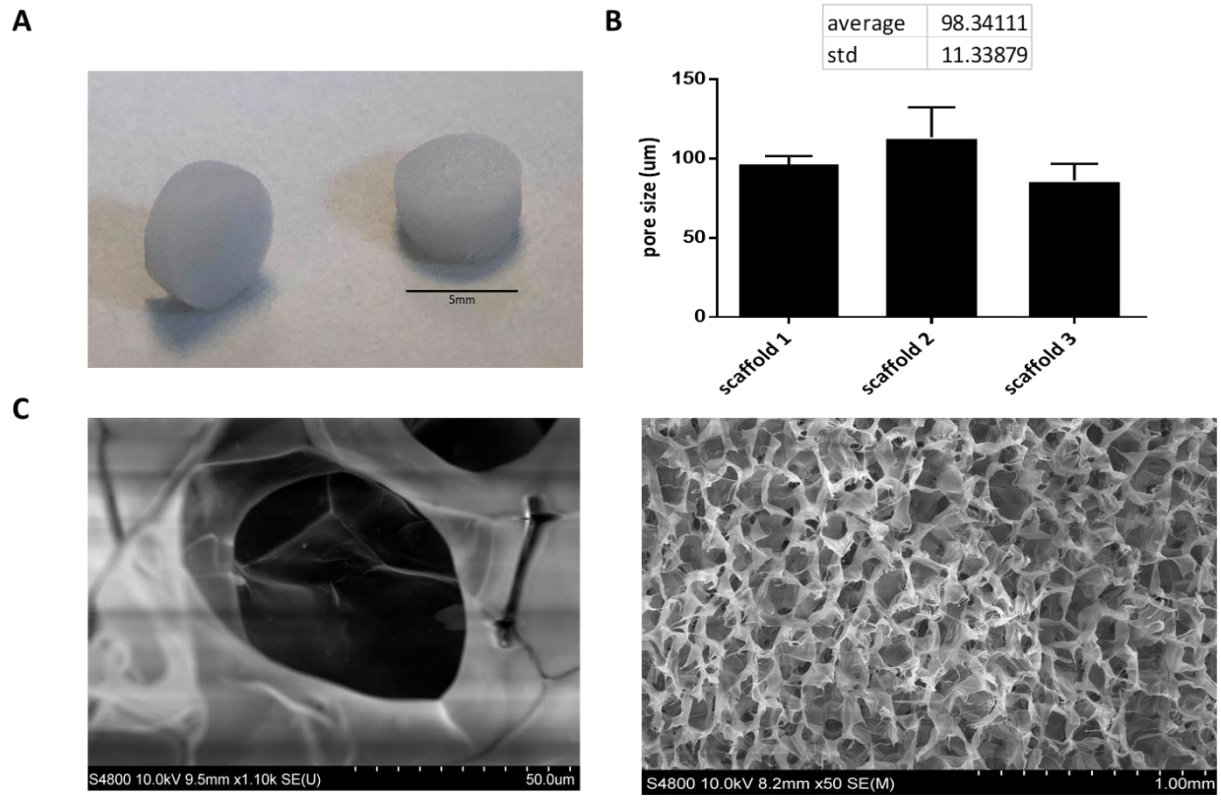

Figure 5.8. 3D R. Pulmo collagen scaffold pore characterization. (A) Picture of scaffold sponge moulded on 96 well plate (diameter of 5 mm) (B) SEM analysis of scaffold porosity. (C) SEM analysis of scaffold pore structure and pores arrangement. *Data shown as mean ± Standard Deviation (3 independent scaffold).*

Picro Sirius red staining, selectively highlights collagen networks. As previously reported in this chapter, *R. pulmo* exhibited very similar collagen chain composition compared to mammalian collagen but differences in amino acid content and this could affect formation and stability of collagen triple helix [814, 842]. It stained specifically *R. Pulmo* collagen unveiling its 3D collagen fibres' arrangement, which, together with the SEM data, closely resemble the pores organization and fibres distribution of mammalian scaffolds obtained in previous chapters (**Figure 5.9**).

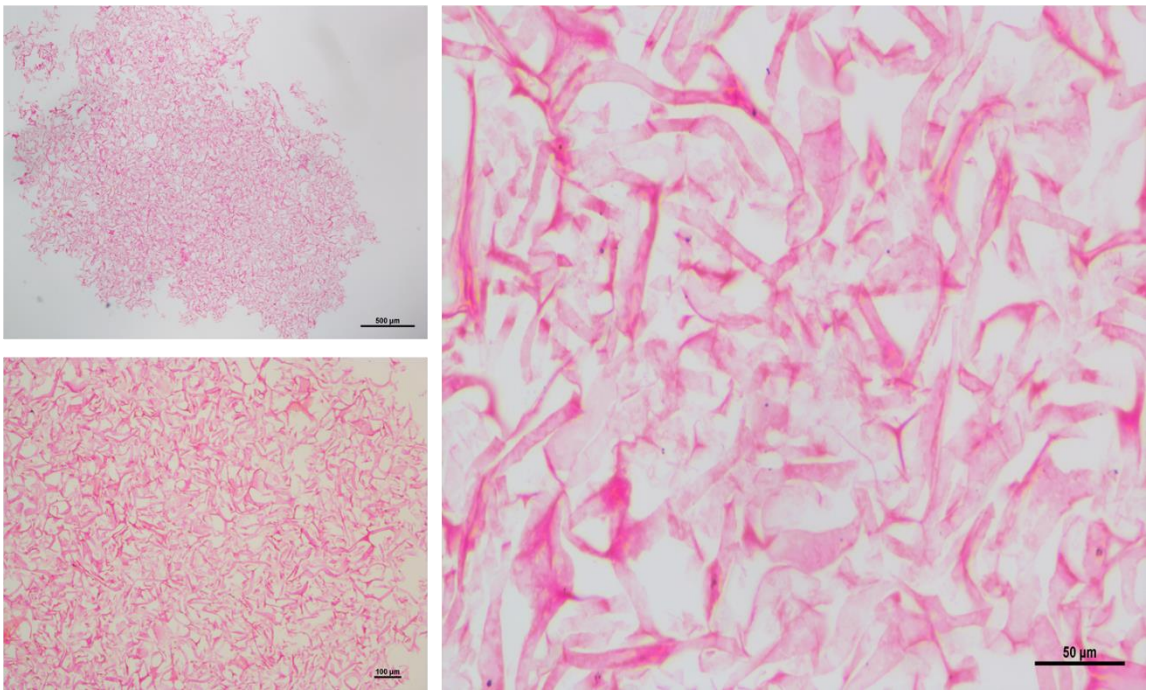

Figure 5.9. R. Pulmo collagen scaffold structure. Picro Sirius red staining of a jellyfish collagen scaffold showing collagen fibres arrangement at different magnifications.

Since large pore sizes greater than 300 µm have the ability to facilitate cell infiltration, but smaller pores usually provide greater initial cell attachment surface areas [843], we evaluated OC cell lines adhesion and migration across jellyfish collagen scaffolds. *R. pulmo* sponge scaffolds were seeded from the top surface with SKOV.3 and OVCAR.3 at a density of $2x10^5$ cells per scaffold, and cells' proliferation across collagen scaffold was examined at day 2-4-6. Both cell lines grew on *R. Pulmo* collagen showing double DNA quantification at day 6 compared to day 2, indicative of

cells proliferation (**Figure 5.10**). Cells distribution across *R. pulmo* collagen scaffold was analysed at day 2-4-6. Notably, at day 14 both SKOV.3 and OVCAR.3 cells were found to have successfully invaded and colonized the entire scaffold, from the top to the bottom section (**Fig. 5.10B-D**). During migration and proliferation SKOV.3 grew as single cells with mesenchymal morphology, an invasion phenotype typical of epithelial cancers following progressive dedifferentiation; while OVCAR.3 invaded in small clumps of cells, a cluster invasion phenotype is characteristic of epithelial tumours [760, 844] (**Fig. 5.10C-E**). We concluded that this collagen supports the development of a bioactive network enabling OC cell migration.

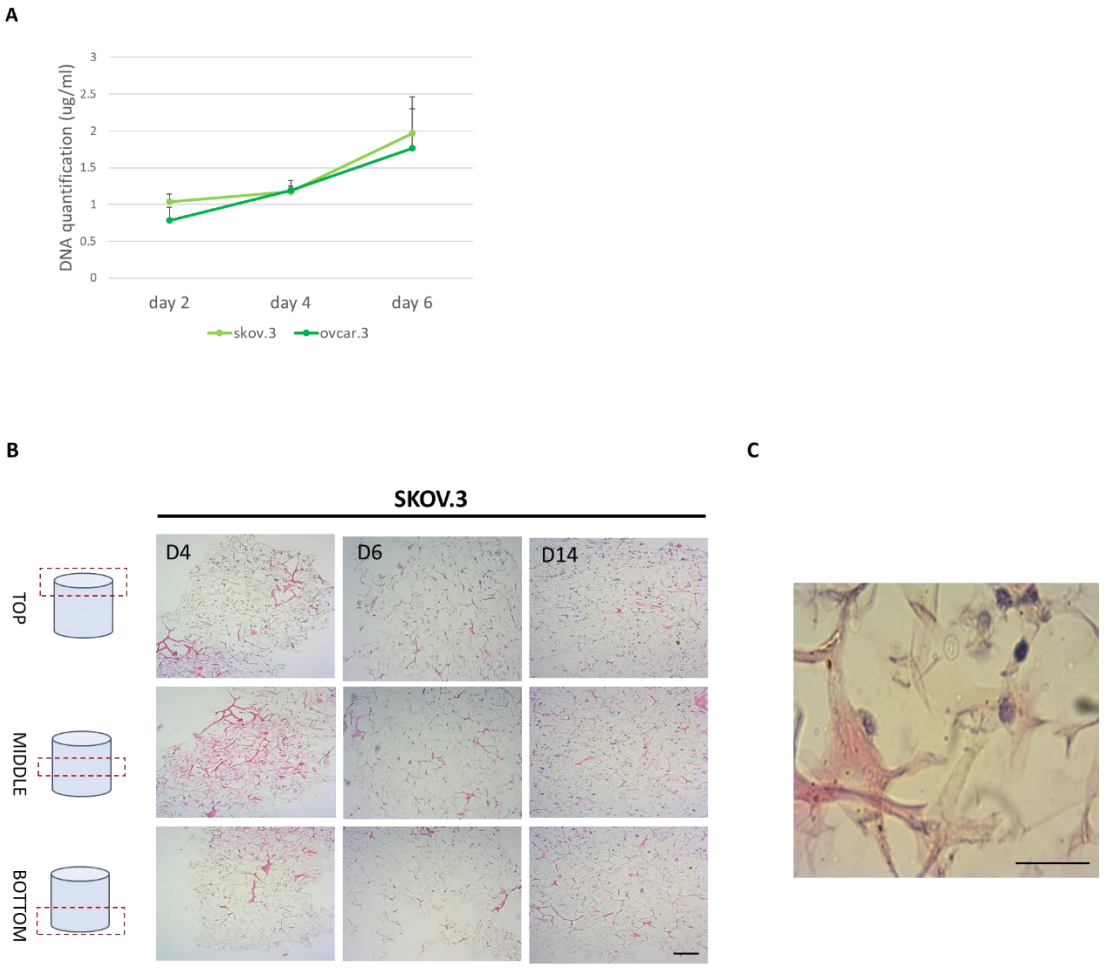

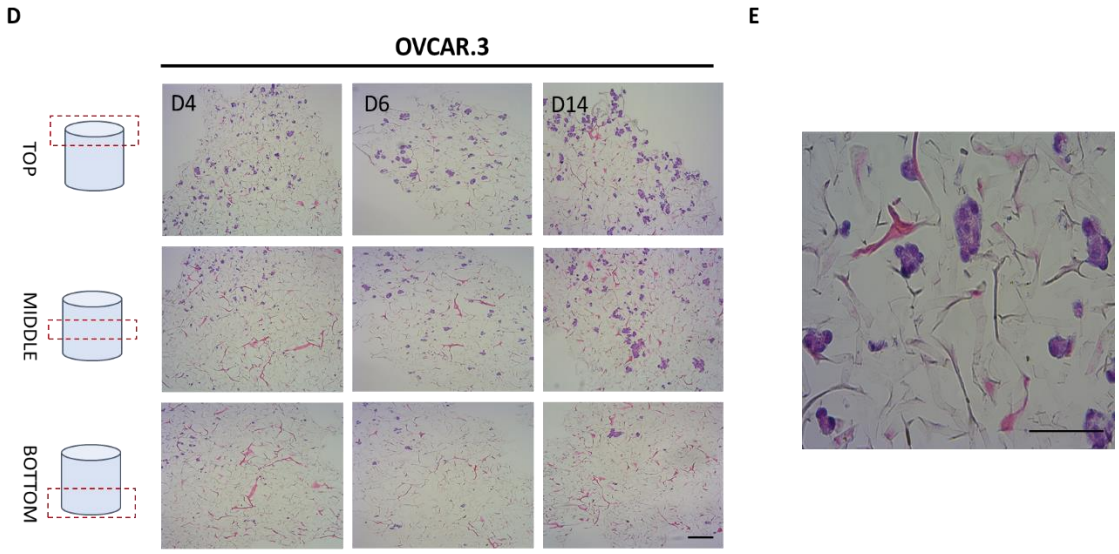

Figure 5.10. Cell proliferation and migration through a 3D-jellyfish collagen scaffold. (A) SKOV.3 and OVCAR.3 cells proliferation rate on 3D jellyfish scaffold from day 2 to day 6 assessed through DNA quantification using PicoGreen® dsDNA quantitation assay. (B) SKOV.3 cells were seeded on the top of the scaffold and they migrated and colonized the entire scaffold to the bottom from day 4 to day 14. (C) High magnification of SKOV.3 cells directly interacting with collagen as single cells. (D) OVCAR.3 cells were seeded on the top of the scaffold and they migrated and colonized the entire scaffold to the bottom from day 4 to day 14. (E) High magnification of OVCAR.3 cells directly interacting with collagen as cluster of cells. Scale bars indicate 100um.

5.3.7 3D cultures result in decreased expression of selected OC EMT related markers

A panel of metastasis/EMT-related markers were evaluated to understand if the scaffold promoted or repressed cancer cell metastatic properties. Gene expression of EMT-related markers was highly influenced by a 3D environment with a widespread lower expression of most genes compared to a simple 2D system. E-cadherin showed a difference of 0.70 lower expression in SKOV.3 cells grown on 3D scaffold compared to 2D scaffold, suggesting a possible strengthening of the metastatic phenotype. OVCAR.3 wide lower expression of *MT1MMP*, *COLL11A1*, vimentin ,0.40, 0.33, 0.45 respectively, seems to suggest the acquisition of an even less metastatic phenotype with the only exception of E-cad which was also downregulated of 0.45 times in 3D compared to 2D ($p>0.05$) (Fig. 6). Finally, *YAP1*, a transcriptional factor and mechano-transducer involved in

the initiation, progression, and metastasis of several cancers [588, 845], was downregulated of 0.49 times in SKOV.3 grown on 3D system compared to 3D, and 0.55 less expressed in OVCAR.3 cells cultured on 3D scaffolds, too, suggesting that multidimensional culturing methods strongly influence ovarian cancer gene expression compared to 2D systems ($p>0.05$) (**Figure 5.11**).

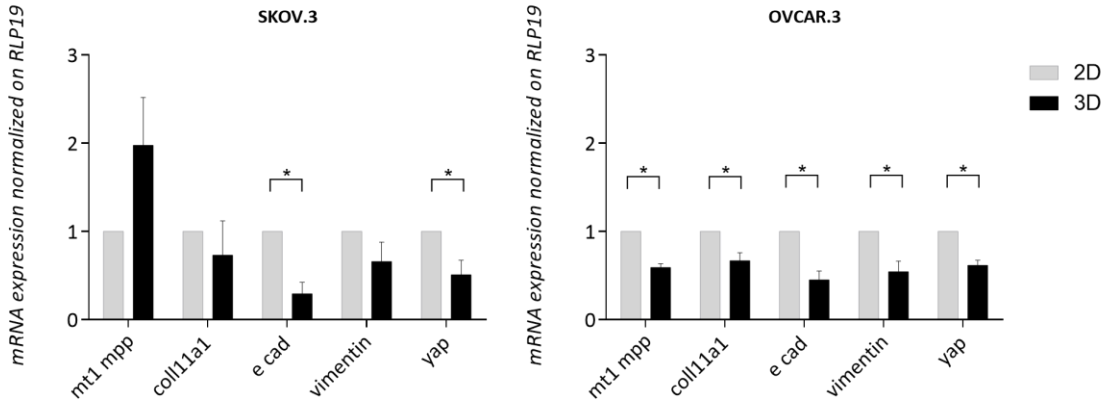

Figure 5.11. Transcript level expression of EMT and OC progression markers in 3D scaffolds compared to 2D systems. RT-qPCR analysis of a panel of genes related to EMT and OC progression. RLP19 was used as housekeeping gene and cells grown on 2D system as control. AACt method was performed. *Data are shown as mean ± Standard Deviation (3 independent experiments). Statistical significance assessed by (*) $p < 0.05$, Student's t-test.*

5.3.8 Jellyfish scaffold 3D culture resulted in decreased gene expression of OC cells markers

A growing recognition of the importance of spheroids in ovarian cancer dissemination has stimulated increased interest in this cell population [680]. To compare jellyfish 3D model with one of the gold standards in cancer modelling we evaluated their mRNA profile on both SKOV.3 and OVCAR.3 cells (**Figure 5.12A**). As described spheroids is a 3D scaffold-free system and made up of cell-cell self-assembly, like shown in **Figure 5.12B,** showing both SKOV.3 and OVCAR.3 spheroid culture aspect after 96hr. When compared to spheroids, SKOV.3 cells grown on jellyfish scaffolds reported a reduction in the expression of markers related to EMT and matrix remodelling ($p<0.0001$), except for vimentin which was comparable between the two 3D systems (**Figure 5.12C**). OVCAR.3 cultured on jellyfish 3D scaffolds resulted in no variation in the markers

expression except for *VIMENTIN* which was highly overexpressed compared to spheroids with a 12-time fold change ($p<0.001$) (**Figure 5.12D**).

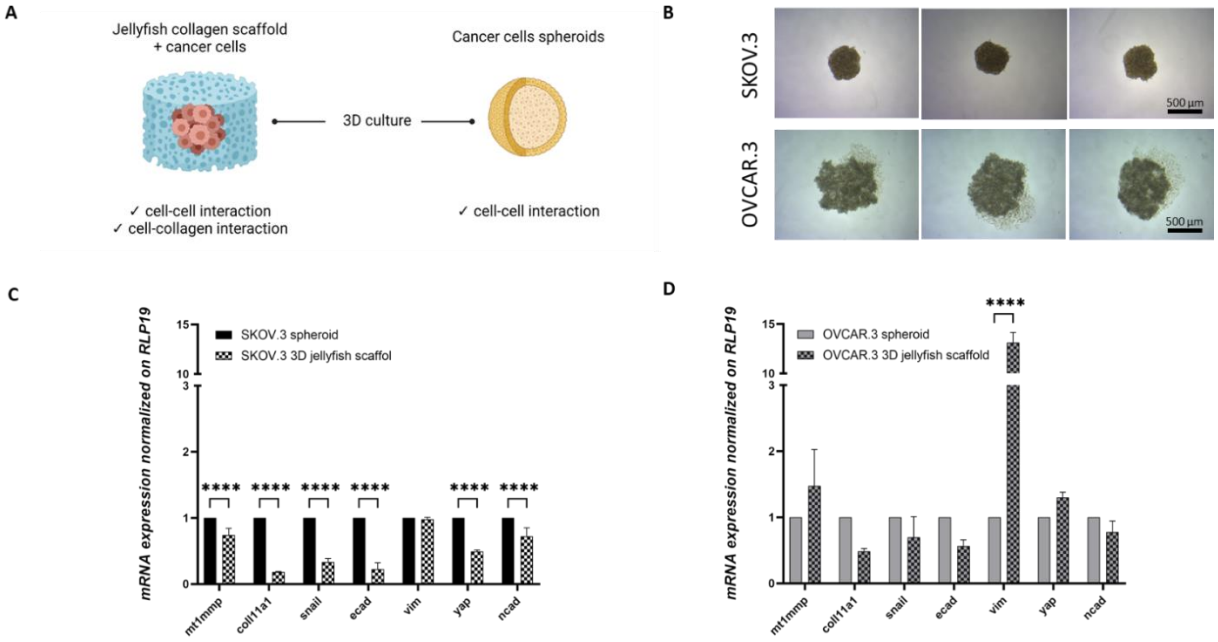

Figure 5.12. Transcript level expression of EMT and OC progression markers in 3D scaffolds compared to 2D systems. (A) Graphical representation of 3D scaffold and cancer cells spheroid characteristics made with Biorender. (B) SKOV.3 ad OVCAR.3 spheroids images collected after 96h of culture. (C) RT-qPCR analysis of a panel of genes related to EMT and matrix remodelling in SKOV.3 grown on spheroids and jellyfish collagen. (D) RT-qPCR analysis of a panel of genes related to EMT and matrix remodelling in SKOV.3 grown on spheroids and jellyfish collagen. RLP19 was used as housekeeping gene and cells grown on spheroids system as control. AACt method was performed. *Data are shown as mean ± Standard Deviation (3 independent experiments). Statistical significance assessed by (*) $p < 0.05$, Student's t-test.*

5.3.9 Jellyfish collagen substrates are suitable for ovarian and OC-derived primary cell culture.

Primary cancer cell cultures closely resemble the phenotype and behaviour of normal/cancer tissues to serve as a valid tool for clinical and preclinical analyses. Cell lines become relevant systems to study cancer given the conserved molecular and genetic features, ease of use and

management, storage, amplification, as well as the practicality and cost. As primary cultures are developed from fresh samples, single tumours can be established to allow comparative analyses between lesions in the same or different parts of the body.

To test Jellyfish collagen biocompatibility with primary cells culture we assessed normal ovary derived primary cells morphology on plastic and coated plates with both jellyfish collagen and rat tail collagen (**Figure 5.13**). Furthermore, we evaluated their survival, together with primary cells derived from OC stage I-II and III-IV, with and without the supplement of FBS, a fundamental supplement of basal media for most of the in vitro studies and especially to sustain primary cells proliferation, serving as a source of hormones, growth factors, amino acids, proteins, vitamins, inorganic salts, trace elements, carbohydrates, lipids, etc for cellular metabolisms and growth of cells [846].

Normal ovary derived cells seem to acquire a mesenchymal-like phenotype on all substrates, but higher confluency was reached by cells cultured on RT substrates with the supplement of FBS. Furthermore, only RT substrate was able to still support cells attachment and proliferation in FBS deprivation conditions (**Figure 5.13A**). Live cells percentage after 5 days of culturing on 2D substrates showed how FBS deprivation strongly promote OC I-II and OC II-III primary cells death when cultured on plastic and jellyfish coated plates, while normal ovary derived cells undergo cell death only when cultured on Jellyfish collagen. Overall, Rat Tail collagen where the only substrates able to sustain cells' survival without FBS supplement. Under FBS culturing conditions all primary cells live cells % was comparable among substrates (**Figure 5.13B**).

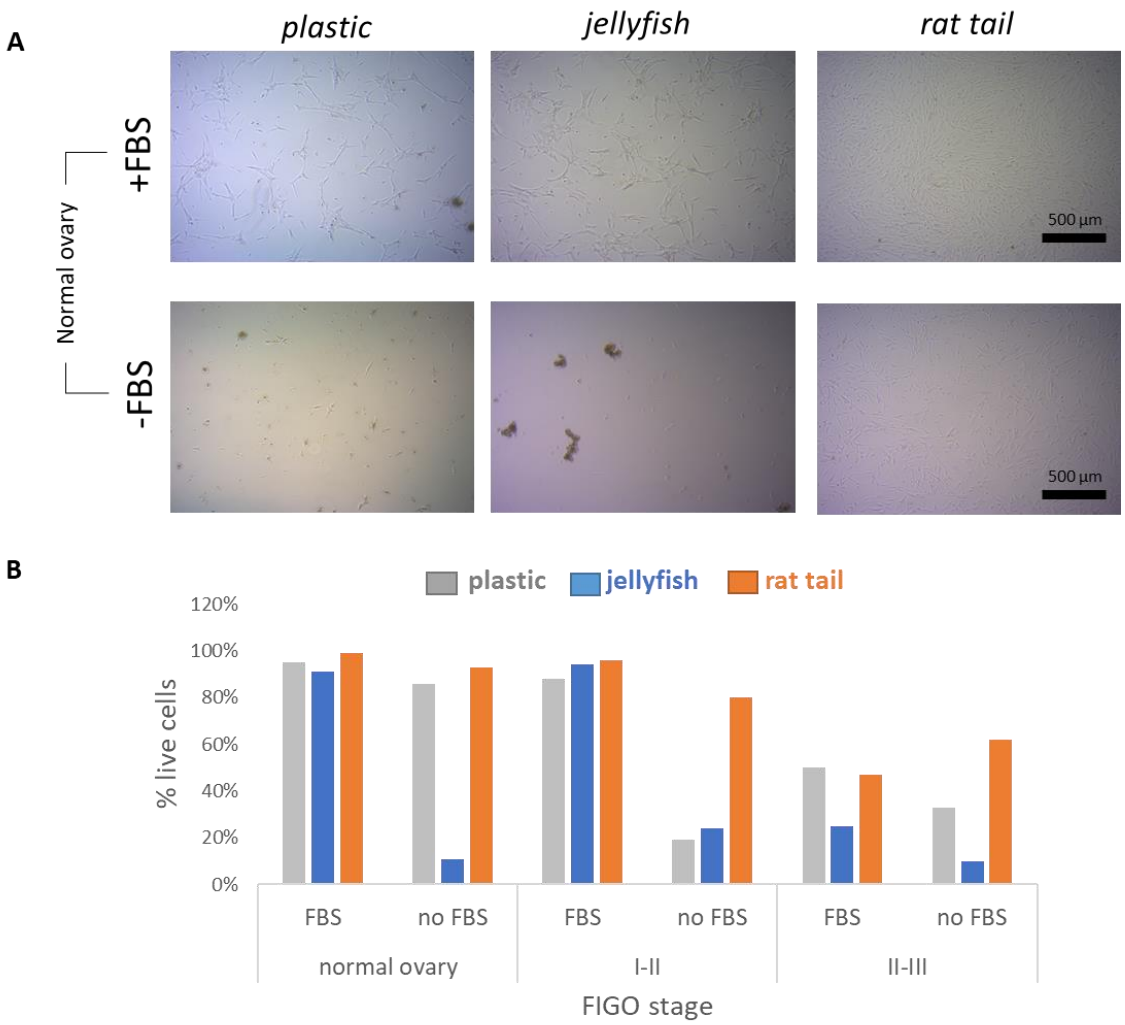

Figure 5.13. Patients' derived primary cells morphology and proliferation is influenced by FBS supplements and substrates coating in 2D culture. (A) Brightfield acquisition after 5 days of culture of normal ovary derived cells on plastic, jellyfish collagen and rat tail collagen coated plates with and without FBS supplement in the media. (B) Calcein staining/ live cells percentage of normal ovary/OC I-II/OC III-IV derived patients cells after 5 days culture. n=1

5.5 Discussion

Marine organisms represent an attractive new source of collagen not least because they could address the global imperative for developments that lead to the reduction in the use of mammals and their derived products in research [847]. Besides, collagen derived from marine organisms - fish, seaweeds, sponges, and jellyfish-, offers advantages over mammalian collagen due to its

biocompatibility, biodegradability, easy extractability, water solubility, safety, low immunogenicity, and low production costs [174]. Indeed, marine collagen has recently emerged as a promising biomaterial with great potential in regenerative medicine and drug delivery applications, i.e. bone [848], cartilage [849], wound dressing and skin repair [171], vascular [564], dental[850] tissue engineering and regeneration and many others [174]. Aside from biomedical applications, combination of cosmeceuticals with bioactive ingredients obtained from marine organisms has become the hallmark of cosmetic industries [851], indeed collagen obtained from fish, jellyfish and cuttlefish has been investigated for its moisturizing, regenerating and film-forming properties [852]. Among all those available alternative collagen sources, jellyfish have emerged as an attractive alternative to existing ones due to a plentiful supply [853], a safer source through lack of bovine spongiform encephalopathy (BSE) risk and potential viral vectors [177, 853].

Different biomedical applications have already been tested for jellyfish-derived collagen, i.e. fabrication of novel cartilage repair implant based on Rhizostoma Pulmo jellyfish collagen combined with active growth factor TGF-β3, a major driver of chondrogenesis and endochondral development, and adult human mesenchymal stem cells derived from bone marrow, to induce chondrogenic differentiation of mesenchymal stem cells [178]. Porous scaffolds were also engineered from jellyfish collagen by freeze-drying and subsequent chemical cross-linking, successfully supporting and maintaining chondrogenic differentiation of human mesenchymal stem cells [170]. Jellyfish collagen was also used in combination with other materials, i.e. to generate biphasic, but monolithic porous scaffolds for the regeneration of both cartilage and the subchondral bone layer, in which jellyfish collagen was used to simulate chondral part and biomimetically mineralized salmon collagen for the bony part, supporting chondroblast and osteogenic differentiation of human mesenchymal stem cells (hMSCs) in vitro [854]. Other porous scaffolds of jellyfish collagen fibres and sodium alginate hydrogels were also developed for chondrogenic differentiation of hMSC [855].

In this study we demonstrated that R. pulmo jellyfish collagen represents an excellent substrate for use in 2D and 3D in vitro cell culture for ovarian cancer studies, paving the road for future applications of this innovative marine biomaterial in the field of cancer research. Structural and

biological analysis demonstrated that it performed comparably with rat tail and bovine-derived collagen type I. Electrophoretic mobility in SDS-PAGE showed only minor differences in α-helixes band patterning with a high degree of conservation of triple helix organisation. Several previous studies have demonstrated that the amino acid composition of marine collagen is similar to that of mammalian origin [856, 857]. In our case, whilst hydroxyproline, proline, glycine and arginine content was lower that reported for rat tail and bovine collagens [177], the ability to support cell growth and interaction as well as basement substrate adherence suggests R. pulmo collagen is functionally analogous, and that it is likely to contain GPO and RGD signatures cannot be ruled out. Alternatively, whilst collagens are found in all metazoans and are considered to have contributed to the early evolution of multicellular animals [815], collagen receptors appeared much later, therefore R. pulmo collagen could provide different cell adhesion sites compared to mammalian sources.

Using metastatic OC cell lines established from ascites samples that are capable of collagen type I adherence, migration and remodelling, both SKOV3 and OVCAR3 cells were able to proliferate normally on R. pulmo (and rat tail) collagen coated plates. No cytotoxicity was noted and cell morphology and metastatic potential, evaluated through a panel of EMT-related markers, was not altered by the underlying substrate. Similarly, identical focal adhesions assembled on all substrates tested. 3D models offer the potential to mimic the dense matrix network associated with tumour microenvironments, providing a physiologically relevant tool for biomedical research and preclinical drug testing [858]. To address Rhizostoma pulmo jellyfish collagen suitability for biocompatible scaffold fabrication and cancer culture, collagen was first extracted from the jellyfish using an acid solubilisation procedure, with sodium acetate to remove non-collagenous materials, then freeze dried to obtain porous scaffolds and finally crosslinked with EDC. Moulded R. pulmo sponges provided excellent support for cancer cell growth in a type I-like collagen environment that is known to be a major ECM component in both normal and cancer tissues. OC cells exhibited different invasion/growing pattern through R. pulmo collagen, as single (highly metastatic SKOV3) or as clusters cells (low metastatic OVCAR3). Both cell types colonized the full extent of the collagen network and displayed altered expression of some EMT-related markers in a 3D environment compared to 2D culture. R. pulmo provides an alternative collagen source that can be produced at scale, and which replicates the functionality of mammalian collagen in

both 2D and 3D in vitro systems and could be further explored as affordable, tuneable and scalable scaffold system for cancer studies.

Chapter 6: Materials & Methods

Scaffolds Preparation

Chemicals were purchased from Sigma Aldrich. The scaffolds were synthesized from type I bovine collagen (Viscofan) and fabricated with the freeze-dry technique. Briefly, we prepared an acetic collagen slurry (200 mg/ml), which was precipitated to a pH of 5.5 with NaOH (2 N). For scaffolds crosslinked with BDDGE: The slurry was wet crosslinked in an aqueous solution of 0.01% w/v, 0.1% w/v and 1% w/v BDDGE at 4°C for 24 hours. Then, the slurry was washed with Milli-Q water (EMD Millipore) and casted onto a 48-well plate and freeze dried through an optimized freezing and heating ramp (from 25°C to -25°C and from -25°C to 25°C in 50 minutes under vacuum conditions, p=0.20 mbar) to obtain the desired pore size and porosity.

For scaffolds coll/HA LW 1:10-100-1000: The slurry was divided in 4 group, one part of collagen was not mixed with HA LW for control; the other three slurries were mixed with different dilutions of HA LW 1:10-1:100-1:1000 and then wet crosslinked in an aqueous solution of 0.01% w/v BDDGE at 4°C for 24 hours. Then, the slurry was washed with Milli-Q water (EMD Millipore) and casted onto a 48-well plate and freeze dried through an optimized freezing and heating ramp (from 25°C to -25°C and from -25°C to 25°C in 50 minutes under vacuum conditions, p=0.20 mbar) to obtain the desired pore size and porosity.

For scaffolds coll/HA LW and coll/HA HW: The slurry was divided in 3 group, one part of collagen was not mixed with HA LW for control; the other 3 slurry were mixed with different HA LW 1:10 and HA HW 1:10 and then wet crosslinked in 75mM EDC + 30Mm NHS in MES buffer at 4°C for 24 hours. Then, the slurry was washed with PBS 3 times and casted onto a 48-well plate and freeze dried through an optimized freezing and heating ramp (from 25°C to -25°C and from -25°C to 25°C in 50 minutes under vacuum conditions, p=0.20 mbar) to obtain the desired pore size and porosity.

For *R. Pulmo* collagen scaffolds: Fabrication R. pulmo collagen solution (4 mg/mL in 0.1 M acetic acid) was used for scaffold preparation. The collagen solution was frozen at −20 ◦C in a 96 well plate and then freeze-dried. The constructs were then chemically crosslinked with 1-ethyl-(3-3-dimethylaminopropyl) carbodiimide hydrochloride (EDC; 1% w/v in 80% ethanol) for 90 min, rinsed with deionised water and incubated with 1% glycine for 16 h. Cross-linked scaffolds were

rinsed in deionised water three times and left in 1% 217 glycine overnight, at room temperature, to quench the reaction. Finally, constructs were lyophilized again to get all the residual liquid out and preserve their cylindrical shape.

Collagen sources for R. Pulmo characterization

Type I collagen from Rhizostoma Pulmo jellyfish (© 2019 Jellagen), type I collagen from rat tail (Millipore) and type I collagen from bovine (Sigma-Aldrich) were used as references. R.pulmo jellyfish was fished from Camarthen Bay, immediately stored on ice and shipped back to Jellagen UK premises in Cardiff. Purified jellyfish collagen (JCol) solution (4 mg/mL in 0.1 M acetic acid) was derived from Rhizostoma pulmo jellyfish and provided by Jellagen Ltd. (Cardiff, UK). The collagen extraction protocol was optimized by Dr. Ahmed Zara, using a standardised acid solubilisation procedure, with sodium acetate to remove non-collagenous materials. The purity of the JCol was analysed using sodium dodecyl sulphate polyacrylamide gel electrophoresis (SDSPAGE) and Fourier transform infrared spectroscopy (ATR-FTIR, Perkin Elmer, Bucks, UK) [24].

Rheology

Wet and dry scaffolds of 1-mm thickness and 8-mm diameter were analysed using an Anton Paar/MCR 302 rheometer equipped with an aluminium, custom made 8-mm insert plate. For different experiments both empty scaffolds and cellularized scaffolds collected at days 1-7 were characterized. An amplitude sweep test (log ramp 0.001% to 10%, angular frequency of 10 Hz, 25 recorded points, T of 37°C) was used to verify the range of linear viscoelasticity. Frequency response was measured by frequency sweep tests in the range 1000 to 0.1 rad/s (shear strain of 0.1%, 40 data points, T of 37°C). Storage modulus was reported as 3-sample averages collected at 1 rad/sec angular frequency. Storage modulus and loss moduli measures were reported as 3-sample averages collected at 1 rad/sec angular frequency. Cellularized scaffold analyses were reported after normalization of both storage and loss moduli on D0 samples.

Atomic Force Microscopy

The AFM used in this experiment was the Bio-Catalyst AFM (Bruker). A spherical cantilever (Novascan) was used for the force measurement. For biopsy samples, the QNM in fluid mode was

used with a borosilicate tip (5 µm in diameter). For scaffolds, a silica bead (5 µm in diameter) was mounted onto the end of the cantilever. The spring constant of the cantilever was 0.06 N/m. Before the AFM experiment, both the spring constant and sensitivity of the cantilever were calibrated under thermal tune conditions with the controlling software (Catalyst Nanoscope 8.15 SR3R1, Bruker). For the AFM experiment, scaffolds were embedded in OCT and cryosectioned at 20-µm section thickness. The samples were pre-coated on a glass slide and kept at -80°C. Then, samples were carefully moved into a 60-mm dish on the AFM scanning stage. A volume of 3 ml phosphate-buffered saline (PBS) or media was pre-injected into the dish after sample incubation for 5 minutes at room temperature. For force measurement, we kept the ramping size at 10 µm. All experiments were conducted at room temperature (22°C). Young's modulus was calculated from the force curves with NanoScope Analysis 1.40 (Bruker), with three to five spots randomly tested per sample and recorded, and at least 50 force curves acquired from each spot. For Young's modulus calculations, extended ramp force curves and a linearized model (Hertzian, spherical) were used.

Chapter 4: The atomic force microscope used in this experiment was the Bio-Catalyst AFM (Bruker). A spherical cantilever (Novascan) was used for the force measurement. For biopsy samples, the QNM in fluid mode was used with a borosilicate tip (5 µm in diameter). For scaffolds, a silica bead (5 µm in diameter) was mounted onto the end of the cantilever. The spring constant of the cantilever was 0.06 N/m. Before the AFM experiment, both the spring constant and sensitivity of the cantilever were calibrated under thermal tune conditions with the controlling software (Catalyst Nanoscope 8.15 SR3R1, Bruker). For the AFM experiment, both biopsies and scaffolds were embedded in OCT and cryosectioned at 20-µm section thickness. The samples were pre-coated on a glass slide and kept at -80°C. Then, samples were carefully moved into a 60-mm dish on the AFM scanning stage. Fixed samples were incubated with 70% Ethanol for 10' before being washed withphosphate-buffered saline (PBS). For fresh samples, a volume of 3 ml of PBS or media was pre-injected into the dish after sample incubation for 5 minutes at room temperature. For force measurement, we kept the ramping size at 10 µm and we varied the trig threshold from 2nN to 6nn for initial tests, then we performed 6nN for all the analysis. All experiments were conducted at room temperature (22°C). Young's modulus was calculated from the force curves with NanoScope 169 Analysis 1.40 (Bruker), with three to five spots randomly tested per sample and recorded, and at least 50 force curves acquired from each spot. For Young's modulus calculations, extended ramp force curves and a linearized model (Hertzian, spherical) were used.

Compression test

NS and MS scaffolds of 0.5 cm thickness were soaked in PBS and loaded on UniVert Mechanical Test System. A load cell of 1 N was calibrated and used to perform a compression test with a stretch magnitude of 35%, stretch duration of 60 seconds, and relaxation time of 60 seconds. For each condition, 3 replicates were analyzed.

Amino acid sequencing

We analysed acid solubilized collagen derived from Rhizostoma pulmo tentacles (3.8 mg/ml in 0.1 M acetic acid), Type I collagen from rat tail (4.19 mg/ml, Millipore) and type I collagen from bovine (Sigma-Aldrich). 1 mg of each sample was placed in 1.5 ml microcentrifuge tubes, freeze dried overnight, resuspended in 200 µl of 6N constant boiling HCl (Thermo Scientific) and transferred to a vacuum hydrolysis tube (Thermo Scientific). The hydrolysis tube was purged with 214 nitrogen, evacuated and sealed. Samples were heated for 22 hours at 110°C in an oven to enable hydrolysis, the vacuum was released and the HCl was evaporated by placing the open tube in an oven at 60°C for 30-40 minutes. The hydrosylate was resuspended in 150 µl of lithium loading buffer (Biochrom) and transferred to a 1.5 ml microcentrifuge tube. Hydrolysed samples were transferred to glass vials and loaded in the autosampler tray after a dilution of 1:5. An injection volume of 20ul hydrolysed protein was analysed for each sample. In addition, 40 µl of amino acid standard (A9906, Sigma) and 40 µl of loading buffer (a blank solution) were analysed. Absorbance was read at 570nm and 440nm.

Scanning Electron Microscopy

The morphology of the scaffold was characterized by SEM. Scaffolds were coated with 7 nm of Pt/Pl (Nova NanoSEM 230) for SEM examination. Images were taken at different magnifications and angles (i.e. transversal). The pore diameter of scaffolds was measured from SEM images, and 3 images from each of 3 areas were used for each scaffold at the same magnitude. For each image, porosity analysis was performed using ‘analyse particles’ measurement in ImageJ software.

Chapter 5: Freeze-dried collagen scaffolds were examined using scanning electron microscopy (SEM) (JSM, Jeol, Japan). Scaffold pore size was detected using SEM software (Hitachi). A total

of 10 pores were analysed per images and a total of 3 images were analysed within 3 different scaffolds.

Fourier Transform Infrared Spectroscopy

The samples were analysed in attenuated total reflection (ATR) mode at 2 cm^{-1} resolution 64 times over the range of 500–4,000 cm^{-1} using a Nicolet 6700 spectrometer (ThermoFisher Scientific, Waltham, MA, http://www.thermofisher.com). The ATR/Fourier transform infrared spectroscopy (FTIR) spectra were reported after background subtraction, baseline correction, and normalization on Amide I. Graph reported a range of 800-1800 cm^{-1} wavelength.

Chapter 5: Fourier transform infrared spectra of freeze-dried R. pulmo collagen were obtained using a Perkin Elmer FTIR spectrometer. Infrared spectra were recorded in the range of 4000–400 cm-1 at an aperture of 1 and sensitivity of 1.5.

Thermal Gravimetric Analysis

The thermal stability and composition of scaffolds (1%-0.1%-0.01% BDDGE, coll/HA LW and HW) were analysed by TGA under nitrogen atmosphere using a Mettler Toledo TGA/DSC 1 instrument. A temperature ramp from 25 to 800°C with a heating rate of 10°C/minute was used to determine the onset decomposition temperatures. Approximately 10 mg samples were used.

Water Contact Angle (WCA)

Measurement The wettability of St and So scaffolds was assessed through WCA measurements using an Attension Theta optical tensiometer from Biolin Scientific. PBS droplets of 20 µL were deposited on the scaffold's surface and sessile drop measurements were performed. Side-view images of the deposited droplets were captured using the OneAttension software. The static contact angle formed 111 by the droplet on the dry scaffold's surface was described using Young-Laplace equation. Scaffold wettability was observed for 10 minutes, evaluating the WCA every 2.15 seconds, and the data were reported as a mean of the CA at 10 minutes.

Cell Culture

Chapter 2: MRC5 cells were purchased from ATCC. Cultures were established in standard media constituted by Dulbecco's Eagle medium (DMEM) supplemented with 10% fetal bovine serum

and 1% penicillin (100 UI/ml)-streptomycin (100 mg/ml). For maintenance of cultures, cells were plated at a cell density of $3x10^3$ cells per cm^2 and incubated at 37°C in a humidified atmosphere (90%) with 5% CO2. Medium was changed twice per week thereafter or according to the experiment requirements with the addition of TGFβ1. TGFβ1 was added to culture every 3 days, titration was performed using increasing dose of TGFβ1 (0-25-50 ng/ml) with analysis carried out at days 5 and 7. After establishment of 25 ng/ml as an elective dose for fibroblasts activation, all further experiments used 25 ng/ml concentration and analysis performed after 7 days of culture. To induce fibroblasts activation, 25 ng/ml of TGFβ1 was added to culture media at day 3 and day 6. Adherent cells were detached from plates using Trypsin before reaching confluence (80%) and subsequently re-plated for culture maintenance. When seeded onto scaffolds, MRC5 cells were harvested and re-suspended in cell culture medium. A 20-µl drop of medium containing 100k cells (or 25k and 300k for the scaffold shrinking experiment) was seeded on the centre of each scaffold (So and St) and kept in an incubator for 30 minutes. Culture medium was then added to each well, scaffolds were kept in agitation.

SKOV.3 (ATCC, Virginia, USA) cells were grown in McCoy's media supplemented with 10% FBS (10500-064, Gibco) and 1% Pen Strep (15140-122, Gibco); OVCAR.3 (ATCC, Virginia, USA) were grown in RPMI media supplemented with 20% FBS (10500-064, Gibco), 1% Pen Strep (15140-122, Gibco), insulin 0.01 mg/ml. Caov-3 (ATCC, Virginia, USA) cells were grown in Human Dulbecco's Modified Eagle's Medium with fetal bovine serum to a final concentration of 10%. All growth media were supplemented with 1% penicillin (100 UI/ml)-streptomycin (100 mg/ml). Adherent cells were detached from plates using trypsin before reaching confluence (80%) and subsequently re-plated for culture maintenance. For maintenance of cultures, cells were incubated at 37°C in a humidified atmosphere (90%) with 5% CO2. Medium was changed twice per week. Scaffolds were preconditioned with media for 1hr. When seeded onto scaffolds, ovarian cancer cells were harvested and re-suspended in cell culture medium. A 20-µl drop of medium containing 1x105 cells was seeded on the center of each scaffold and kept in an incubator for 30 minutes. Culture medium was then added to each well.

Ovarian Surface Epithelial Cells (HOSEpiC, Science Cell # 7310) were grown with Ovarian Epithelial Cell Medium (Science Cell #7311). For primary cells extraction from human tissue biopsies the protocol is the following. First, clean the biopsy in a tube with PBS, rinse it and place it in a petri dish to orientate it to identify the epithelial layer. Place the epithelial side towards 800µl

of 2mg/ml collagenase in a 6 multi-well plate. 2mg/ml of collagenase are prepared fresh in a biopsy media without FBS and filtered with 0.22 μm syringe filter. Biopsy media is a 1:1 mixture of MCDB 105 medium containing a final concentration of 1.5g/L sodium bicarbonate and Medium 199 containing a final concentration of 2.2g/L sodium bicarbonate. To make the complete media, add 20% FBS, 1% antibiotics (Pen/strep or AA). Digest the epithelial side 30' at 37ºC, swirling every 5'-10'. After digestion, with a scalpel help the epithelial layer of cells to detach from the ovary. Recover the collagenase containing the epithelial cells in 15ml tube. Rinse the well twice with 5ml of fresh complete media and keep it in the 15ml tube to dilute the collagenase. Add media up to 14ml to the tube and 2ml to the well. Centrifuge at 300g for 7'. Discard the supernatant and plate the pellet with the 2ml of fresh ovarian biopsy media.

2D coating plates preparation

Corning 6 well plates and Nunc™ Lab-Tek™ 8-well Chambered Coverglass (ThermoScientific) were coated with rat tail collagen and R. pulmo collagen. 90 ug of collagen was used to coat 6 well plates for In Cell analysis, WB, RT-PCR and 7.6 ug for 8-well Chambered Coverglass to perform immunofluorescence staining. Collagen specific amount was added on each plate and leaved overnight at 4 degree. Next day, supernatant was collected, and the plate left at 4 degree until use (they are stable for 1-2 days). Before seeding the cells, plate was washed with PBS and after dried under the hood for 20 mins. Finally, the plate was sterilized turning turn the UV on.

In cell analysis

InCell Analyser 2000 (GE Healthcare) was used to analyse number of cells on different coated plates. Following culture period media was removed from monolayer cultures and washed with PBS. Cells were seeded on pre-coated plates and grew up to 5 days before analysis. Cells grown for 1-2-3-4-5 days were stained with Hoechst 33342 (Life Technologies Corporation) (dilution of 215 1:2000 from a 10mg/ml solution in water) in normal media and incubated at room temperature for 10 minutes to stain the nuclei. For live % experiment calcein staining was performed at day5. Cells were immersed in PBS for analysis in the InCell Analyser 2000. Random distribution of fields across the surface of the well was used to capture 30 fields/well. Images were analysed using InCell Developer (GE Healthcare) to quantify number of cells using DAPI and Calcein staining depending on the experiment purpose.

Spheroid method

Dissolve 0.2g agarose in 20mL sterile distilled water in centrifuge tube, heat to 90 degree for few minutes until completely homogeneous. Transfer the 1% agarose solution to laminar bench. Keep it warm all the time. Cover a 96-well flat-bottom plate with 1% agarose, 100 uL each well. Plates are allowed to solidify at room temperature for at least 2 hours. Seed 600k cells for each spheroid and collect at 96h for analysis.

SDS page

SDS-PAGE was performed according to the method of Laemmli (1970) using a 4-20% gradient. Samples were mixed with Laemmli sample buffer (Bio-Rad) with b-mercaptoethanol and heated for 5 min at 95 °C. Different volumes of Rhizostoma pulmo collagen solution and 30 ug of rattail (rt) and bovine (bv) collagen were loaded to the gel and run at 100 V for 10 min followed by 120 V for 1.5 h. Following electrophoresis, protein bands were stained with Coomassie brilliant blue R- 250. Prestained-dual colour marker (Biorad) was used to estimate the approximate molecular weight of collagen samples. Type I collagen from rat tail (Millipore) and type I collagen from bovine (Sigma-Aldrich) were used as references.

PicoGreen assay

At day1,3 and 7 scaffolds were incubated in 500µl trypsin for 10' at 37ºC under shaking conditions (800rpm). After trypsin neutralization with complete media, scaffolds were removed, and remaining cells centrifuged at 2400 rpm for 5'. Cells pellet was washed twice with PBS and pellet resuspended in 50 µl of RLT lysis buffer (79216, QIAGEN). For the assay in a black opaque 96-well plate with transparent bottom, 10µl of sample or standard was added to 90µl of TE (1X). Then, 100µl of PicoGreen reagent from Quant-iT™ PicoGreen™ dsDNA Assay Kits and dsDNA Reagents (P11496, ThermoFiscer Scientific) was added to each well/sample and incubated for 5' in aluminium foil at RT. Tecan Spark plate reader was used to record fluorescence with excitation: 460nm and emission: 540nm.

Alamar Blue

At day3, day5 and da7 scaffolds were washed with PBS and incubated for 4 hours in media +10% alamarBlue™ Cell Viability Reagent (DAL1100, ThermoFiscer Scientific). The experiment was carried out in a 48 well plate with 300µl as final volume/scaffold/well. Absorbance was measured at 600nm and 570 nm.

Decellularization

After 7 days of culture collagen scaffolds seeded with fibroblasts were incubated for 2 hours under agitation at 650 rpm, 37ºC with 0.5% and 1% SDS (in PBS). DNA quantification before and after SDS incubation was detected using Pico Green assay.

Coculture seeding

Simultaneous seeding was used to establish coculture model. A total of 100k cells of different ratios between SKOV3/MRC-5 cells were seeded on 3D NS scaffolds, as representative of normal/stroma poor tissues (1:0.5); normal/pre-malignant tissues (1:1), pathological/malignant stroma rich tissues (1:3). MRC5 cells line membrane was stained in red (PKH26 Red Fluorescent 171 Cell Linker Kit) before seeding. Scaffolds were preconditioned with media for 1hr. A 20-µl drop of medium containing 1x105 cells (SKOV3 and MRC5) was seeded on the center of each scaffold and kept in an incubator for 30 minutes. Culture medium was then added to each well.

Biopsy samples

A total of 6 biopsy samples were collected and processed for AFM analysis. 3 were used as normal ovary controls because they derived from normal contralateral ovaries of patients with benign adenomas and fibromas. The other 3 represented HGSC stage IIIc patients' tissue. Patient eligibility criteria included the following: (a) primary or interval surgery; (b) pre-op diagnosis of high-risk pelvic mass with normal contralateral ovary or High-Grade Serous Cancer stage III; (c) ovarian pathology reference recorded.

H&E patients' biopsies staining

Paraffin sections were cut at 4 µm thickness. Hematoxylin and eosin staining was performed using the ST Infinity H&E Staining System (Leica Biosystems) in Leica Autostainer ST5010 XL. Paraffin was melted prior to staining by heating the slides at 60°C for 30 minutes, then slides were

deparaffinized by performing 3 x 2-minute washes in xylene, 3 x 1-minute washes in 100% ethanol, and 1 x 1-minute wash in 95% ethanol before rinsing in tap water. Slides were incubated for 30 seconds in Hemalast, for 5 minutes in hematoxylin, and were rinsed for 1 minute in tap water. Next, slides were incubated for 30 seconds in Differentiator and 1 minute in Bluing agent, with each step followed by a tap water rinse for 1 minute then 95% ethanol for 1 minute. Slides were stained with eosin for 30 seconds, dehydrated in 95% ethanol for 1 minute, 4 minutes in 100% Ethanol, and 2 x 1 minute in 100% ethanol, and cleared for 3 x 2 minutes in xylene. Every step after the initial heating of the slides was done at room temperature.

H&E Staining of mammalian (bovine)-derived scaffolds

Bovine derived collagen scaffolds seeded with cells were fixed in formalin 4% for 24h at 4 degree and then washed 2 times in PBS and embedded in paraffin. Microtome was used to cut 5um sections form each sample. Haematoxylin and Eosin (TSC biosciences, UK) staining was performed following these steps: 10’ in Histochoise (Sigma), 4’ EtOH 100%, 4’ EtOH 95%, 4’ EtOH 70%, 4’ dH20, Haematoxylin staining (tcs biosciences, 1:2 dilution in dH20) 1’ and wash with water. Eosin staining (tcs biosciences, 1:5 dilution in Dh20) 2’, wash with water, 2’ EtOH 70%, 2’ EtOH 95%, 2’ EtOH 100%, 5’ Histochoise (Sigma) and mounted with DPX.

H&E Staining of R.Pulmo-derived scaffolds

Haematoxylin and eosin staining were performed using the ST Infinity H&E Staining System (Leica Biosystems) in Leica Autostainer ST5010 XL. Paraffin was melted prior to staining by heating the slides at 60°C for 30 minutes, then slides were deparaffinized by performing 3 x 2-minute washes in xylene, 3 x 1-minute washes in 100% ethanol, and 1 x 1-minute wash in 95% ethanol before rinsing in tap water. Slides were incubated for 30 seconds in Hemalast, for 5 minutes in hematoxylin, and were rinsed for 1 minute in tap water. Next, slides were incubated for 30 seconds in Differentiator and 1 minute in Bluing agent, with each step followed by a tap water rinse for 1 minute then 95% ethanol for 1 minute. Slides were stained with eosin for 30 seconds, 112 dehydrated in 95% ethanol for 1 minute, 4 minutes in 100% Ethanol, and 2 x 1 minute in 100% ethanol, and cleared for 3 x 2 minutes in xylene. Every step after the initial heating of the slides was done at room temperature.

Picrosirious red staining

R. Pulmo-derived collagen scaffolds seeded with cells were fixed in formalin 4% for 24h at 4 degree and then washed 2 times in PBS and embedded in paraffin. Microtome was used to cut 5um sections form each sample. Collagen fibrils were indicated histologically with picrosirius red staining. Sections were hydrated through descending concentrations of ethanol and stained with 0.1% (w/v) picrosirius red solution for 1 hour at room temperature. After water wash, slides were dehydrated in ascendant concentrations of ethanol before being mounted in DPX and protect by a coverslip.

Microscopy

Brightfield images

After scaffold fabrication, Keyence BZX800 using a 4x objective and a final stich process was used to show the entire scaffold surface. The microscopy image stitching process consists of two main steps: acquiring the images and combining them. During image acquisition, the camera is moved across the area to be captured and a sequence of images are captured in a pre-defined pattern set to cover the entire scaffolds area. Combining these images is done in the Keyence BZX800 software (https://www.keyence.com/landing/microscope/lp_fluorescence.jsp).

Live-Death Imaging

After 7 days of culture, scaffolds with cells were incubated with 2 µl of 50 µM calcein AM working solution and 4 µl of ethidium homodimer-1 stock and incubated for 20 minutes at 37°C protected from the light. After several washes with warm media, cells were analysed by Keyence BZX800 using a 4x objective and a final stich process to show the entire scaffold surface.

F-Actin and nuclei Imaging

After 7 days of culture, scaffolds were collected and washed with 1% PBS. After fixation with 4% paraformaldehyde for 10 minutes at room temperature, cellularized scaffolds were washed twice with PBS + 0.1% Tween and permeabilized using Triton X-100 0.1% in PBS for 10 minutes at room temperature. Incubation with phalloidin-488 (A12379, Fisher Scientific, 1:100) was performed for 2 hours at room temperature protected from light. After washing with PBS + 0.1% tween twice, incubation with Hoechst 33342 (H1399, Thermo Fisher Scientific, 1:1000) was

performed for 10 minutes under shaking conditions and imaging was conducted with the Nikon A1 confocal imaging system, using a 20x objective. Volume recording was reported as maximum projection and performed collecting 3 z-stacks of 200 μm and step size of 10 μm for each scaffold. Chapter 4: . Incubation with phalloidin-555 (Aa34055, Fisher Scientific, 1:100) and Draq5 5 Mm (62251, Thermo Fisher Scientific, 1:20) was performed for 2 hours at room temperature protected from light. For coculture systems phalloidin-488 (A12379, Fisher Scientific, 1:100) and Hoechst (H3569, Fisher Scientific, 1:1000), were incubated 2 hours at room temperature protected from light. After washing with PBS + 0.1% tween twice, imaging was conducted with the Nikon A1 confocal imaging system, using a 20x objective. Volume recording was performed on z-stacks of 200 μm and step size of 10 μm.

Imaging of cells grown on Nunc™ Lab-Tek™8-well Chambered Coverglass (ThermoScientific) coated with rat tail collagen and R. pulmo collagen, was performed after 24h of growing. Then cells were washed twice with PBS and fixed with 4% paraformaldehyde for 15' at RT. Cells were washed 2xPBS and permeabilized with 0.1% Triton-X 100/1x PBS for 15' RT and then washed again 3xPBS. Blocking was performed using 3% BSA/1xPBS for 30' RT. All the antibodies were diluted in BSA 3%. Primary antibodies (β-catenin (ThermoScientific - PA5-19469) 1:100; Vinculin (Abcam - ab18058) 1:100) were incubated O.N. at 4 degree. The day after, cells were washed 3xPBS for 10' each. Incubation with secondary antibodies was performed in dark for 1 hour (antirabbit-Texas Red (life technologies - T6391) 1:400; antimouse-Texas Red (life technologies - T6390) 1:400). Cells were washed 3xPBS and finally incubated with Hoechst 33342 (Life Technologies Corporation, 1:4000/1xPBS). Image acquisition was performed on Zeiss LSM 710 confocal system.

PKH26 Staining protocol (Sigma-Aldrich)

Perform all further steps at ambient temperature (20–25 °C). Place a suspension containing 3x106 single cells in a conical bottom polypropylene tube and wash once using medium without serum. Centrifuge the cells (400 xg) for 5 minutes into a loose pellet. Note: The PKH67 ethanolic dye solution should not be added directly to the cell pellet. This will result in heterogeneous staining and reduced cell viability.After centrifuging cells, carefully aspirate the supernatant, being careful not to remove any cells but leaving no more than 25 μl of supernatant. Prepare a 2X Cell Suspension by adding 0.5 mL of Diluent C to the cell pellet and resuspend with gentle pipetting to

insure complete dispersion. Do not vortex and do not let cells stand in Diluent C for long periods of time. Immediately prior to staining, prepare a 2X Dye Solution (8 μM) in Diluent C by adding 4 μL of the PKH67/PKH26 ethanolic dye solution to 0.5 mL of Diluent C in a polypropylene centrifuge tube and mix well to disperse. Rapidly add the 0.5 mL of 2X Cell Suspension (step 4) to 0.5 mL of 2X Dye Solution (step 5) and immediately mix the sample by pipetting. The final concentration will be 4 μM. Note: Because staining is nearly instantaneous, rapid, and homogeneous dispersion of cells in dye solution is essential for bright, uniform, and reproducible labeling. Incubate the cell/dye suspension for 1–5 min with periodic mixing. Because staining is so rapid, longer times provide no advantage. Stop the staining by adding an equal volume (2 mL) of serum or other suitable protein solution (e.g., 1% BSA) and incubate for 1 min to allow binding of excess dye. Note: Serum (or an equivalent protein concentration) is preferred as the stop solution. Increase volume to 10 mL if complete medium is used instead of serum. Centrifuge the cells at 400 xg for 10 minutes at 20-25°C and carefully remove the supernatant, being sure not to remove cells. Seed cells to the desired amount.

Scaffold Shrinking

Cells were seeded on both 1%-0.1%-0.01% BDDGE scaffolds and imaged every day over a 7-day period using Keyence BZX800 with a 4x objective and performing a stich process to record the entire scaffold surface. Scaffold diameter analysis was performed using ImageJ. First, a Measurement Scale is set. Go to Analyze → Set Scale. In the Set Scale window, the length of the line, in pixels, will be displayed. Type the known distance and units of measure in the appropriate boxes and click OK. Measurements will now be shown using these settings. Then, to measure the distance between points (diameters of the scaffold), draw a line between two points (two extremities of the scaffolds). The status bar will show the angle (from horizontal) and the length. Analyze → Measure (or Ctrl+M or simply type M on the keyboard) transfers the values to a data window. Performed 4 measurements of diameters from different points of the scaffold and then make an average.

Chapter 3:Relative scaffold shrinking was measured as the ratio of the diameter of after 7 days of culture with MRC5 cells to the diameter at day 1.

Cells Orientation and elongation

Cells orientation and elongations on scaffolds was analysed using the built-in tools in NIS-Elements software from Nikon. For each sample, 6 images collected from the whole scaffold or from the edges and center were used as input for analysis. First, a thresholding (Binary Contrast Enhancement) was performed. A grayscale image is converted to binary by defining a grayscale cutoff point. Grayscale values below the cutoff become black and those above become white. The procedure: First convert the image to 8-bit grayscale as described above. Create a 'thresholded' binary image by using the automated procedure involves: Image → Adjust → Threshold, using the slider to adjust the threshold. The red areas will become the black portions in the binary image. Click 'Apply' to complete the conversion. Then proceed with orientation and elongations analysis following software commands. The analysis was performed for each z stack.

α-SMA Quantification

After 7 days of TGFβ1 treatment, cells were collected, centrifuged, and washed with 1% goat serum in PBS. After fixation with 4% paraformaldehyde (PFA) for 10 minutes at room temperature, cellularized scaffolds were permeabilized using Triton X-100 0.1% in PBS for 10 minutes at room temperature. After washes, blocking was performed using 1% BSA, 10% goat serum in PBS-Tween 0.1% for 30 minutes in a humified chamber at room temperature. Incubation with α-SMA-488 (ab197240, 1:250) was performed for 1 hour at room temperature protected from light. DAPI was added at 300 nM. Imaging was conducted with the Nikon A1 confocal imaging system, using a 40x objective and recording at least 3 z-stacks/scaffold.

Live Imaging

After 7 days of TGFβ1 treatment, scaffolds were incubated with 2 µl of 50 µM calcein AM working solution and incubated for 20 minutes at 37°C protected from the light. DAPI was added at 10 µg/mL. MatTek Glass bottom microwell dishes were used for imaging. Live imaging of 115 scaffold shrinking was performed using a Fluo ViewTM 3000 confocal microscope over 24 hours with a 10x objective for 13 cycles at intervals of 2 hours with a step size of 40 µm (slices: 20) for a total of 800 µm collected from the bottom of the scaffold. For cell migration tracking, analysis was performed over 24 hours with a 10x objective for 13 cycles at intervals of 2 hours, airy disk: 2, step size: 10 µm (slices: 43) and analysed using Olympus cellSens software.

Fibre Orientation

OrientationJ is a software package which consists of a series of plugins for ImageJ and Fiji that automates orientation analysis. The program computes the local orientation and the local coherency. For each sample, 6 images were used as input of the structure tensor computation.

Flow Cytometry

Cell survival and dead cell quantification

After 7 days of culturing, scaffolds were incubated for 10 minutes in trypsin under shaking conditions, then scaffolds were removed, and cell pellets were collected after centrifugation and washed with PBS. Cells were incubated with 2 µl of 50 µM calcein AM working solution and 4 µl of ethidium homodimer-1 stock and incubated for 20 minutes at 37°C protected from the light. After several washes with warm media, cells were analysed by flow cytometry using BD FACS Fortessa. For CM experiments cells were incubated for 48h with CM. After retrieval, cells were incubated with 2 µl of 50 µM calcein AM working solution and 4 µl of ethidium homodimer-1 stock and incubated for 20 minutes at 37°C protected from the light. After several washes with warm media, cells were analysed by flow cytometry using BD FACS Fortessa.

FAP Expression

For 2D analysis, after day5 and day7 of TGFβ1 treatment cells were detached from plate using trypsin, cells pellet was collected after centrifugation and washed with 1% goat serum in PBS. After 7 days of TGFβ1 treatment, scaffolds were incubated for 10 mins in Trypsin under shaking conditions, then scaffolds were removed, and cells pellet was collected after centrifugation and washed with 1% goat serum in PBS. Cells' pellets from 2D and 3D samples were incubated with FAP-PE (FAB37159) for 30 minutes at 37°C protected from the light. After several washes with 1% goat serum in PBS, cells were analysed by flow cytometry using BD FACS Fortessa. Physical parameters like forward-scatter and side-scatter were collected for each sample and monitored for experimental consistency across replicates. Fluorescent data were collected referred to the marker under investigation.

In conditioned media experiment, for 2D analysis, after 48h of CM 80-2/100 and TGFβ1 treatment cells were detached from plate using trypsin, cells pellet was collected after centrifugation and washed with 1% goat serum in PBS. For 3D analysis, after 48h of 100 and TGFβ1treatment,

scaffolds were incubated for 10’ in Trypsin under shaking conditions, then scaffolds were removed, and cells pellet was collected after centrifugation and washed with 1% goat serum in PBS. Cells were incubated with FAP-PE (FAB37159) for 30 minutes at 37°C protected from the light. After several washes with 1% goat serum in PBS, cells were analysed by flow cytometry using BD FACS Fortessa.

Propidium Iodide

After 7 days of TGFβ1 treatment, scaffolds were incubated for 10’ in Trypsin under shaking conditions, then scaffolds were removed and cells pellet was collected after centrifugation at 500 g for 5 minutes, and incubated overnight at 4°C with 1 ml cold 70% ethanol. After adding PBS, cells were centrifuged, and pellets resuspended in 1 ml of 0.1% Triton X-100/PBS containing 20 µl of 1 mg/ml propidium iodide and 10 µl 20 mg/mL RNase for 15 minutes at 37°C. After washing with PBS, cells were resuspended in 300 µl of PBS and cell cycle analysis was performed by flow cytometry using BD FACS Fortessa.

CellTracker™ Green CMFDA Dye

After 7 days of TGFβ1 treatment, scaffolds were incubated for 10’ in Trypsin under shaking conditions, then scaffolds were removed, and cells pellet was collected after centrifugation and 113 washed with PBS. Cells were incubated with CMFDA dye (1 µM) for 20 minutes at 37°C protected from the light. After several washes with warm media, cells were incubated for 10 minutes in fresh media before proliferation analyses were performed by flow cytometry using BD FACS Fortessa.

MTT Assay Protocol for Cell Viability and Proliferation

To perform this test, SKOV3 and Caov-3 cells were seeded at a concentration of 8K cells/well in 96-well plates while 20K OVCAR-3 cells were seeded/well in a final volume of 100 µl/well. MTT was added to achieve a final concentration of 0.5 mg/ml MTT in normal media. After incubating 2 hours at 37°C, MTT was removed and 100 µl DMSO added before mixing contents for 30 minutes on an orbital shaker protected from light. Absorbance was measured at 590 nm.

CellTiter-Glo® Luminescent Cell Viability Assay

For the proliferation assay, ovarian cancer cells were grown on scaffolds for 10 days and analysis performed at 4 time-points (day 1, day 4, day 7, day 10). For cytotoxic evaluation of doxorubicin, ovarian cancer cells were grown on scaffolds for 7 days and then treated with free doxorubicin (DOXO), doxorubicin-loaded liposomes (DOXO-LIPO), or empty liposomes for 72 hours. To perform the analysis, a volume of CellTiter-Glo® Reagent (Promega) equal to the volume of cell culture medium present in each well/scaffold was added. Contents were mixed for 10 minutes on an orbital shaker to induce cell lysis, protected from light. The plate was incubated at room temperature for 25 minutes to stabilize luminescent signal, before transferring 100 µl (or a dilution 1:10 in media for high signals) in white opaque-walled 96 well plates to measure luminescence.

Western Blot

Cells grown on 2D plates were collected after 7 days of TGFβ1 treatment using trypsin. After quenching with fresh media and washing with PBS, cells were suspended in RIPA buffer (89901, Thermo Fisher) and Protease Inhibitor Single-Use cocktail (100x) (78425, Thermo Fisher) and incubated for 15 minutes on ice. After BCA quantification, 10 µg protein was loaded in each gel lane (Mini PROTEAN TGX GELS Cat#4561096, 4-20%, Biorad). After protein transferring using Trans-Blot Turbo Transfer Pack (Cat#1704158), membranes were blocked in 5% fat milk (TBS-Tween 0.1%) for 1 hour and then incubated with primary antibodies: αSMA (ab5694, 1:1000) and GAPDH (ab9485, 1:1000) over night. Secondary α-rabbit-HRP was used (A16110, Invitrogen 1:1000) and membranes developed using ChemiDoc XRS+ (Biorad).

For cells grown on rat tail-coated, jellyfish-coated or plastic plates, when confluent, they were scraped into cold lysis buffer (RIPA buffer from Thermo Fisher Scientific) and a mixture of protease inhibitors (P8340, Sigma) while on ice. Cellular lysates were clarified, and protein was quantified by DC™ (detergent compatible) protein assay (Bio-Rad, Richmond, CA). Proteins (10 µg) were separated on a 10% SDS-polyacrylamide gel and blotted onto a PVDF membrane. PVDF membrane were blocked for 1 hr at room temperature with 5% BSA in Tris-saline buffer containing 0.02% Tween-20 and incubated in primary antibody (1:1000 of E-cadherin ab1416; N-cadherin ab12221; Vimentin sc-6260; GAPDH sc-47724) overnight at 4°C. After washing in TBST, blots were incubated for 1 hr at room temperature with mouse or rabbit IgG HRP (1:2000 of NA931V or NA934V, Ge Healthcare) and the immunoreactive complexes visualized by the ECL Western blotting system, using the ChemiDoc™ Imaging System.

Reverse-transcription Quantitative PCR

Reverse-transcription PCR was performed on cells grown in 2D culture and on 3D scaffolds after 7 days. Scaffolds with cells were washed in PBS and incubated with 1 ml TRIzol RT for 10 minutes under shaking. After removing the scaffolds, 200 µl of chloroform was added and samples were inverted for 15 minutes, incubated on ice for 2 minutes, and centrifuged at 12,000 g for 15 minutes at 4°C. The aqueous phase was transferred to a 1.5-ml tube and 500 µl of isopropyl alcohol added before incubating 10 minutes at 4°C and centrifuging 12,000 g for 10 minutes at 4°C. After washing the pellet twice with 1 ml 70% ethanol, it was aspirated and allowed to dry before resuspending in 20 µl of water. Total RNA (500 ng) was reverse transcribed into cDNA using Bio-Rad iScript™ cDNA Synthesis Kit. Quantitative PCR was performed using TaqMan™ Fast Advanced Master Mix on a StepOnePlus Real-time PCR System (Applied Biosystems). Expression of MMP1 (Hs00899658), MMP2 (Hs01548727), COL1A1 (Hs00164004), HMMR (Hs00234864), CD44 (Hs01075864), HYAL1 (Hs00201046), HAS2 (Hs00193435) was detected using TaqMan® Gene Expression Assays. 18S ribosomal RNA was used as an internal reference for normalization. Analysis was performed using relative ΔΔCt method.

Expression of *YAP*1 (Hs00902712), WWTR1 (reported as TAZ, Hs00210007_m1), MMP1 (Hs00899658), and MMP2 (Hs01548727) was detected using TaqMan® Gene Expression Assays. 18S ribosomal RNA was used as an internal reference for normalization. Analysis was performed using relative ΔΔCt method.

For Jellyfish collagen model, RNA was extracted from cells grown on 2D coated plates, 3D collagen scaffolds and spheroid using RNeasy Mini Kit (Qiagen) according to the manufacturer's instructions. 100 ng (cells grown on 3D collagen scaffolds/spheroids) or 1µg (cells grown on 2D coated plates) of total RNA were reverse transcribed into cDNA using the kit from Applied Biosystem. Primer sequences for each gene are summarized below. *GAPDH* and *RLP19* were used as internal references for normalisation. Quantitative polymerase chain reaction (qPCR) was undertaken using CFX96 Real Time PCR Detection system (Bio-Rad, UK) and analysed using relative AACt method.

MT1-MMP FW: 5'-GAGACACCCACTTTGACTC-3' REV: 5'-CAGCCACCAGGAAGATGTC-3'

COL11A1 FW: 5'-ACCTGACCTGCCGTCTAGAA-3' REV: 5'-TCCACCACCCTGTTGCTGTA-3'

SNAIL FW: 5′-ATCGGAAGCCTAACTACAGCGAGC-3′ REV: 5′-CAGAGTCCCAGATGAGCATTGG-3′
E-CADHERIN FW: 5'-TTATGATTCTCTGCTCGT-3' REV: 5'-TCTTTGTCTGACTCTGAG-3'
VIMENTIN FW: 5'-GAGAACTTTGCCGTTGAAGC-3' REV: 5'- TCCAGCAGCTTCCTGTAGGT-3'
YAP FW: 5'-TGAACAAACGTCCAGCAAGATAC-3' REV: 5'-CAGCCCCCAAAATGAACAGTAG-3'
Quantitative PCR for was performed using TaqMan™ Fast Advanced Master Mix on a StepOnePlus Real-time PCR System (Applied Biosystems). Expression of MSLN (Hs00245879_m1) and EFEMP1 (Hs00244575_m1) and OPN (SPP1, Hs00959010_m1) was detected using TaqMan® Gene Expression Assays. RPL19 ribosomal RNA was used as an internal reference for normalization. Analysis was performed using relative ΔΔCt method.

RNA sequencing

Library preparation and sequencing were carried out by Novogene (PE150). Raw fastq files were quality-checked using FastQC [561], a quality-control tool for high throughput sequencing data. Reads were aligned to the GRCh38/hg38 genome build using STAR [562]. Gene count tables were generated using the –quantMode GeneCounts argument in STAR. The DESeq2 median of means method [563] was used to normalize the gene count tables to account for sample depth. DESeq2 116 was used to correct for multiple hypothesis testing and determine significantly modified transcripts between control and experimental samples (FDR |1.5|).

RNA extraction from collagen scaffolds and spheroids

To collect cells from scaffold, wash in PBS, and freeze quickly (1min) in a hexane bath immersed on dry ice. Store them at -80 degree. To fully disrupt the scaffold, submerge it in lysis buffer (RLT, RNeasy Mini Kit, Qiagen) and use TissueRuptor II (Qiagen) for 20 sec maximum at full speed. Proceed to extract RNA following RNeasy Mini Kit (Qiagen) according to the manufacturer's instructions. To extract RNA from spheroids, wash in PBS and incubate in 350µl lysis buffer (RLT, RNeasy Mini Kit, Qiagen) for 5' in ice. Store at -20 ºC or extract RNA following RNeasy Mini Kit (Qiagen) according to the manufacturer's instructions.

DNA extraction from collagen scaffolds

We used Papain from papaya latex (P3125, Sigma) to digest R. pulmo scaffolds. A buffer made up of 300ug/ml of papain, 2mM DTT, 20mM NaAc ph 6.8, 1mM EDTA was used to incubate the sample at 60degree for up to 2 hours. Quant-iT picogreen dsDNA kit (Invitrogen) was used to assess double-stranded DNA in solution. Samples were read at the emission of 520nm.

Assembly and physical characterization of liposomes

To assemble liposomes, 20 mg of total lipids including DPPC, DSPC, DOPX, and cholesterol (molar ratio 5:1:3:1) were dissolved in methanol:chloroform solution (1:3 v/v) to a final volume of 1 ml. The solvent was evaporated through a rotary evaporator (Buchi Labortechnik AG, Switzerland) for 20 min at 45°C to form a thin lipid film. The film was hydrated with 1 ml sterile water to assemble empty liposomes or 250 mM ammonium sulfate for liposomes to be loaded with doxorubicin. The 1 ml solution was incubated for 3 minutes at 45°C followed by 3 minutes vortexing. Lipid suspension was forced through a polycarbonate filter (200 nm; GE Osmonics Labstore, Minnetonka, MN) ten times under nitrogen gas pressure at 45°C (filter was replaced after 5 extrusions). Size, zeta potential, and polydispersity index (PDI) was measured using dynamic light scattering. After the nanoparticles (NPs) were fabricated, they were loaded into dialysis floaters in order to exchange the outside buffer with 0.9% NaCl overnight. Lipid formulation was then incubated 1:1 v:v for 2 h at 45°C with 1 ml of 2 mg/ml doxorubicin hydrochloride (Sigma, D1515) (dissolved in DDW). Only DOXO-LIPO NPs were loaded again into dialysis floaters in order to exchange the outside buffer with 0.9 NaCl overnight. NanoSight for both empty and loaded NPs was performed at the end to measure lipid NPs concentration.

Evaluation of doxorubicin encapsulation efficiency & release

Doxorubicin encapsulation and drug release analysis was performed using a Tecan Microplate Reader. For the doxorubicin release experiment, DOXO-LIPO NPs were incubated with PBS +10% FBS (50:50) at 37°C under shaking and samples were collected and analyzed after 0.5/1/1.5/2/4/5/8/24/48 hours. For DOXO encapsulation, DOXO-LIPO NPs were diluted 1:200 in water and mixed (1:1 v:v) with 0.2% (v/v) triton x-100 (overall doxorubicin) or water (released doxorubicin) in a black 96-well plate for 5 minutes at room temperature under shaking conditions. Doxorubicin fluorescence was read at excitation 480 nm/emission 590 nm and Cy at 5.5 excitation 650 nm/emission 700 nm.

Statistical Analysis

All data were obtained from at least three independent experiments (**n = number of biological replicates**) and expressed as mean ± standard deviation. The two-tailed Student's t test with Welch's correction or one way/two-way ANOVA test was used to determine differences between groups. Results were considered to be statistically significant at P-value<0.05. The statistical analysis was processed with GraphPad Prism 6 Software (GraphPad; San Diego, CA, USA).

Chapter 7: Discussion & future directions

7.1 Reproducing mechanical features in a ovarian cancer 3D tumour model

Understanding the key underlying changes that happen during tumour initiation and progression is necessary to develop deeper knowledge of tumorigenesis and aggressive development to better design efficient diagnostic methods and/or treatment options. To achieve these goals, the complexity of the TME needs to be deconstructed, into smaller, simpler and more practicable systems-based approaches, as it is very difficult to construct 3D models comprising of, or mimicking, all aspects of a given solid tumour environment, i.e. ovarian cancer (**Figure 7.1**).

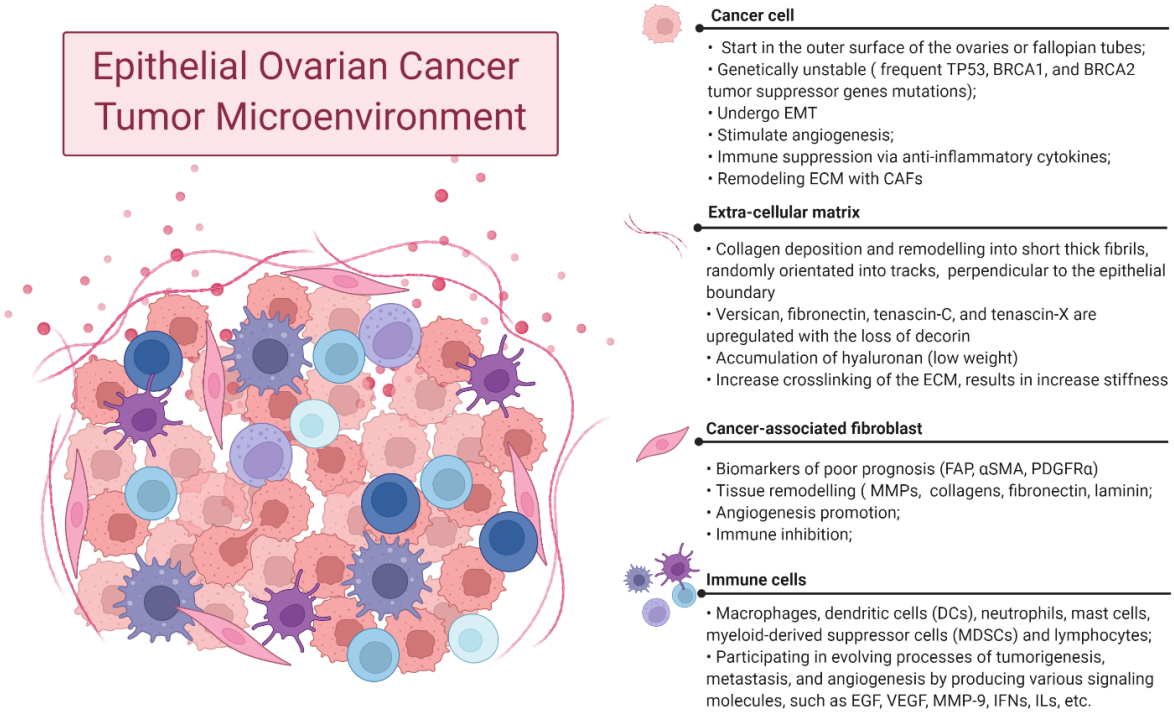

Figure 7.1. Schematic illustration of Epithelial Ovarian Cancer TME components. Made with Biorender.

Crucial to allow early diagnosis and preventive therapies in ovarian cancer is the recapitulation of pre-metastatic processes in 3D models, to mimic the progression staging happening in the ovary before the shredding of cancer cells in the peritoneal cavity. Indeed, located within the peritoneal cavity, the ovaries exist within the abdominal space where the peritoneal membrane (peritoneum), a serous membrane, separates the visceral organs from the bulk of the body and each other, providing lubrication for the movement of the visceral organs [859]. In healthy individuals, the peritoneal membrane modulates filtering 50–100 ml of fluid into the lymphatic vessels every hour [860] (post-menopausal women carrying an average of 2.3 ml [861]), instead, in a diseased state, this intraperitoneal fluid is not readily drained and a backup of liquid, termed ascites, start to accumulate (36.7% of all ovarian cancer patients [862, 863]) promoting metastasis [864], chemoresistance [865, 866], and mechanically stimulates the cancer with hydrostatic compression and shear forces to exfoliate from the ovaries to the peritoneal cavities [867]. One reason for this liquid formation is that ovarian cancer cells and cellular aggregates that are shed into the peritoneal

cavity can physically block the homeostatic lymphatic drainage system but the exact mechanisms have yet to be proven [868-870]. After this stage, free-floating cancer cells and cellular clusters self-assemble and aggregate to form spheroids, overcoming anoikis [282, 869], from the ascites have access to the most common metastatic sites of ovarian cancers: the peritoneum, the greater omentum, the right subphrenic region, the lung, and the liver [867, 871]. For this reason many research groups have developed bioreactors capable of systematic and controlled force stimulation that independently explore the effects of mechanical stimuli on ovarian cancer [682]. It is important to highlight that cancer induced or malignant ascites are not unique to ovarian cancer, indeed other cancers, including colon, pancreatic, gastrointestinal tract, lung, and breast, feature tumour cells in ascites and pleural effusion [860, 872].

The ovarian cancer risk factors of age and ovulation are curious because this cancer incidence increases in postmenopausal women, long after ovulations have ceased. In a recent article McCloskey et al. [873] provided the first evidence that human ovaries undergo additional structural changes with age, including a significant change in the collagen architecture, similar to fibrosis. Since in many tissues, fibrosis increases risks associated with tumorigenesis and metastasis and, ovarian aging is associated with significant changes in the structural organization of collagen, resulting in ovarian fibrosis, it is possible that ovarian fibrosis increases the risk of ovarian cancer by creating a microenvironment more permissive to tumour growth [14, 523].

Linked to fibrosis, in tumours like epithelial ovarian cancer, the role of ECM stiffness and cellular mechanotransduction is still much understudied. As previously discussed, a prominent feature of a cell's mechanical microenvironment is the rigidity of its ECM, but stiffness is not always systematically associated with tumorigenic phenotype [116, 874-878] as shown for NIH3T3 cells transformed with the H-Ras oncogene which are poorly sensitive to stiffness, or neuroblastoma cells increased proliferation on softer substrates, and colon and prostate cancerous cells undergoing to EMT at low stiffness [875, 879-881].

The outcomes derived from different studies trying to link substrate stiffness to enhanced metastatic phenotype in ovarian cancer resulted in contradictory conclusions. For example, in a model of peritoneum dissemination, ovarian cancer cells were found to be more adherent to softer adipocyte substrates with enhanced migratory capacity, as well as being more proliferative and

chemo resistant. [695]. In another system using PEG hydrogels, greater proliferation was found on arginylglycylaspartic acid (RGD) or MMP functionalized hydrogels compared to the PEG gels alone, and less instead on stiffer hydrogel constructs [327]. Contradictory finding of enhanced proliferation and cell aggregation within the stiffer constructs was observed in an investigation of SKOV3 cells grown on crosslinked egg white and poly[(methyl vinyl ether)-alt-(maleic acid)] [882]. Besides, it was reported that disaggregation of multicellular epithelial ovarian cancer spheroids, behaviour associated with dissemination and metastasis, is enhanced by matrix stiffness through a mechanotransduction pathway involving ROCK, actomyosin contractility, and FAK. This pattern of mechanosensitivity is maintained in highly metastatic SKOV3ip.1 cells [883]. As a result of microenvironment changes, epigenetic alterations can occur and play a key role in promoting transformation and tumour growth, although the underlying mechanisms are yet to be elucidated. Analysis of spheroid versus monolayer ovarian cancer cells showed an increase of two epigenetic processes, DNA methylation and histone acetylation, specifically during 3D growth. These findings support the hypothesis that ovarian cells in 3D culture are physiologically different from their monolayer counterparts. DNA methylation changes are seen in several cancer types and have been linked to changes in gene expression in highly metastatic tumours, while histone acetylation has important roles in diverse processes including gene regulation, DNA damage repair, and DNA replication, although it has been associated with both better and worse prognoses depending on the specific cancer type [884].

In summary, the mechanical microenvironments of ovarian cancer comprise the surrounding ECM stiffness within the primary tumour, shear stress on ovarian cancer cells/spheroid cell aggregates within the ascites, and eventually metastatic sites ECM rigidity [682] (**Figure 7.2**).

Given the minimal number of ovarian cancer ECM stiffness investigations on 3D substrates and contradictory evidences, further studies are needed to deepen our understanding of the role of substrate stiffness in ovarian cancer mechanotransduction. Preclinical informative models linking biophysical traits to cancer cells and stromal cells phenotype into a 3D model will help dissect the development and outcomes of fibrotic processes in cancer and will provide a tool to test tumour response under different mechanical constraints, and to test new strategies to target TME dysfunctions, i.e. fibrosis, in solid tumour like ovarian cancer. For example, the use of molecular probes for imaging fibrosis in preclinical models of liver and lung fibrosis is a new and promising

non-invasive assessment of organ fibrosis [885]. However, more work is needed to adapt and optimize those methods to small organs such as the ovaries. Functional imaging of ovarian fibrosis could revolutionize the field and improve the diagnosis, prevention and treatment of ovarian fibrosis linked to aging or cancer development.

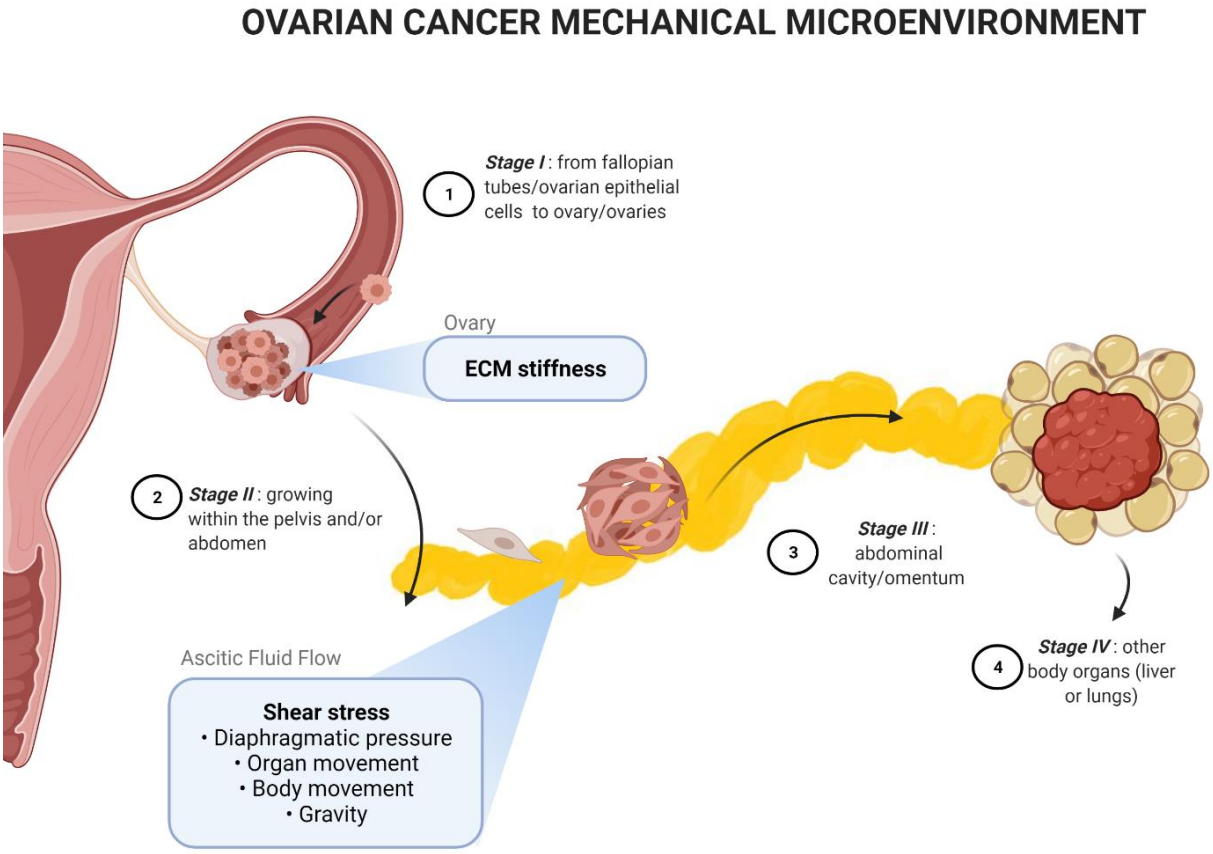

Figure 7.2. Epithelial ovarian cancer mechanical microenvironment. The ovarian cancer cells experience the surrounding ECM stiffness within the primary tumour, spheroid cell aggregates within the ascites, and potential metastatic sites. Rigidity of the ECM enhance the metastatic phenotypes of cancer cells promoting metastasis, invasion, proliferation, and chemoresistance. Shear stress stimulates the ovarian cancer cells via interstitial fluid flow within the primary tumour and ascitic fluid flow triggered by gravity, bodily movements, change in the diaphragmatic pressure from breathing, and organ movements from functions such as digestion. Made with Biorender.

Borrowing established scaffolding tools from TE, we extensively characterize sponge scaffolds to test them as platform for stromal cancer studies and ovarian cancer biophysical modelling. Based on a structure of collagen fibres, the most abundant ECM components in interstitial matrices, the material provided adequate structural support, bioactivity, and biocompatible features to test both stromal and cancer response to variations in microenvironment stiffness. On one side, collagens have been extensively used to model and study both primary and invasive tumours, as platforms to mimic either processes such as ECM degradation, migration, and epithelial-mesenchymal transition and the advanced process of intravasation, extravasation, and metastasis through mesenchymal-epithelial transition (MET) [179]. On the other hand, when fabricated into porous scaffolds, compared directly to the poor mechanical properties of hydrogels, this approach is well matched to research in tissues that have load-bearing functions or in any tissue where mechanical properties are thought to play a central role in the cellular differentiation processes under investigation, such as in cancer [254, 318]. Therefore, the strategy employed here supported the study null hypothesis, that porous collagen scaffolds are a meaningful model to include microenvironment mechanical cues to study stroma and cancer mechanosensing and its effects on activated phenotype or metastatic processes and drug sensitivity. Indeed, the major results and take-home messages compiled against the 5 primary aims of the thesis are summarised in **Figure 7.3**.

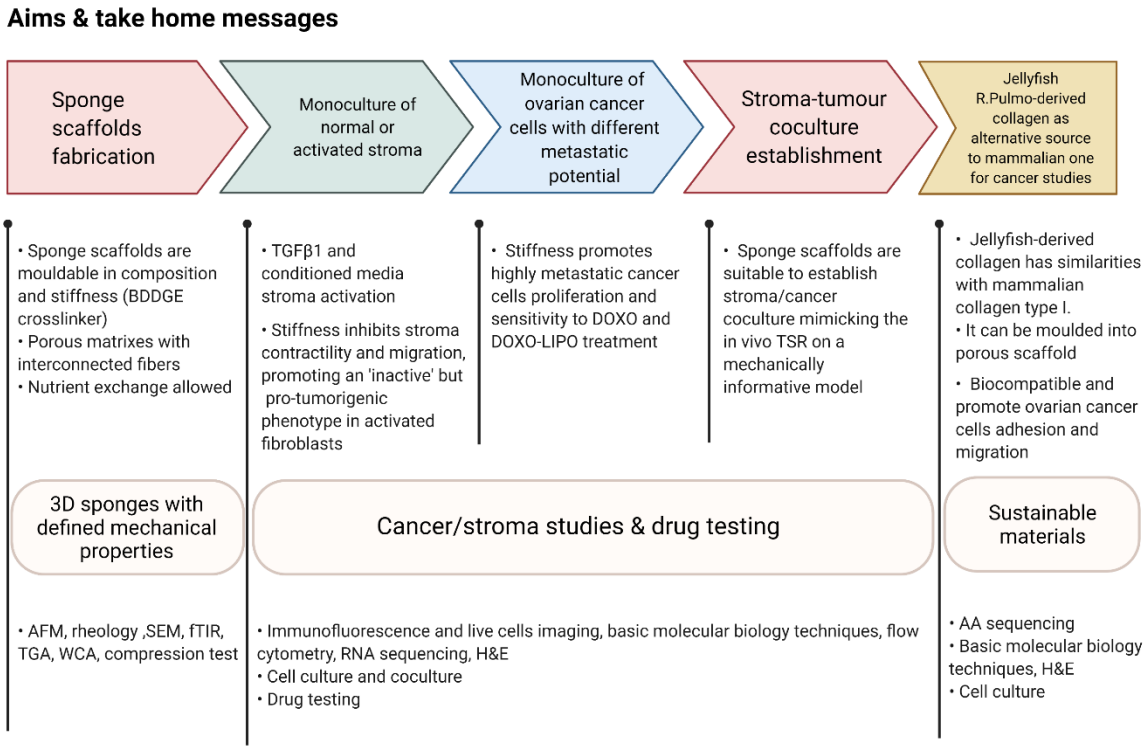

Figure 7.3. Aims and take-home messages summary. Our findings support the utility of porous scaffolds as meaningful mechanically informative platforms to tailor therapy for individual patients to improve clinical outcomes, while providing a preclinical model to test complex interaction in cancer TME, adding immune components and testing new therapies and diagnostic tools. Image made with Biorender.

We employed a crosslinking strategy to mimic the ECM physical dysfunctions occurring in normal and diseased states of the same tissue type. Matching the range of stiffness found in normal ovaries and patients with HGSC in the platform, we investigated both stromal and cancer cells response to the stiffness of the surrounding microenvironment, mimicking changes in ovaries' mechanical properties before pathology and at late stage cancer. To validate the model, we first studied the previously mentioned cells compartments as monoculture, envisioning to combine both for more complex studies on ovarian cancer early stages progression and biogenesis in the future. Indeed, the multicellularity nature of living tissues necessitates the incorporation of stromal cells and potentially also immune cells together with cancer cells and finally a vascular/lymphatic network simulating dynamic blood flow.

Interestingly stromal cells and cancer cells respond differently to the microenvironment stiffness. First, changes in matrix rigidity are not enough to prime fibroblasts conversion into activated fibroblasts, a feature which requires exposure to cytokines like TGFβ1 or a mix of signals derived from cancer cells like SKOV3 conditioned media in both 2D and 3D culturing conditions. Secondly, both NFs and AFs showed an increase in cells circularity, impairment in migration and contractility and a specific increase in YAP expression. Deeper analysis at RNA sequencing level reported a big impact on AFs transcriptomic when cultured on stiff (St) compared to soft (So) and a specific mechanosensing-derived effect on AFs compared to NFs when cultured on St scaffolds specifically. In the first case the main gene signatures impacted on St relate to decrease in locomotory behaviour, response to TGFβ1, tissue remodelling and a parallel upregulation of DNA replication, chromatin remodelling, p53 pathway which responds to stresses that can disrupt the fidelity of DNA replication and cell division, initiating a program of cell cycle arrest, cellular senescence or apoptosis [886].

Since both AFs and NFs were proven to be still viable on St materials, we hypothesized that increase mechanical stiffness could be a promoter, among others described in literature (replicative exhaustion, oncogenic RAS, p14(ARF), or hydrogen peroxide) [667], of fibroblasts senescence-like phenotype in a fibrotic tissue, leading their enter in a 'twilight zone', in which they still develop molecular, ultrastructural and contractile features typical of myofibroblasts and are dependent on canonical TGF-β signalling. Indeed it was shown that those cells still secrete soluble factors that promote tumour cell motility [666]. Whether fibroblast senescence functions to limit collagen deposition in tumours [887-889] or they acquire a senescence-associated secretory phenotype (SASP) that creates a permissive microenvironment favouring tumour development [890, 891], has yet to be determined. In this context the establishment of a coculture of cancer cells with stromal cells in a stiffer microenvironment could be beneficial to address those questions. Secondly, when activated, AFs on stiffer scaffolds upregulated pathways related to pathological diseases like prostate and colorectal cancer together with Hippo signalling pathways, focal adhesion and cell-substrate adherents' junctions, indicating a specific pathological-related phenotype acquisition. Under the same stiff conditions ovarian cancer cells tested responded differently, the most invasive (SKOV3 and Caov3) proliferate more on metastatic (MS) scaffolds

but they all similarly showed an enhanced drug sensitivity to doxorubicin (free and NP loaded) on stiffer substrate while viability and migratory phenotype were not impacted by the higher stiffness.

Overall, these results suggested that mechanical characteristics of the environment can impact cellular compartments in different ways. While the stroma loses its capacity to remodel the matrix, converging toward a 'senescent phenotype', possibly promoting tumour progression through the secretion of tumour-promoting signals; cancer cells respond to stiffness increasing proliferation but, at the same time, becoming more susceptible to treatment, which could be a promising observation for therapies development. As our model resemble physical characteristics of both normal ovaries and pathological ones, which represents the site where ovarian cancer originates, those observation lead to the conclusion that physical changes resulting in the ovaries during disease progression could be fundamental to increase cancer proliferation and further pushing metastasis processes. But at the same time, it opens an interesting window for cancer treatment since cancer cells are more sensitive to free doxo and lipo-doxo treatment on stiffer matrices. In the same scenario stiffness impairs fibroblasts contractility and promote their 'pro-tumoral dormancy'.

Not only this investigation leads the path to unveil complexes interactions of biophysical and biological signals in the TME but it represents a highly informative and effective model to optimize drug candidates, mimicking native tissue distribution, and reduce animal testing, improving cost effectiveness and avoiding ethical concerns. To this aim, 3D models like this one could gain high-throughput applicability, simple and standardized culture protocols, analysis techniques, and achieve high-resolution imaging as we demonstrated for our non-transparent model. In parallel, adoption of highly cost-effective and scalable alternative sources as scaffolding biomaterials like Jellyfish collagen reported in this thesis, could provide tuneable and bioactive materials with highly availability in the environment for cancer researcher studies. As discussed before in the thesis, even if marine resources harbour very promising chances, they suitability for cancer studies must require further optimizations and the addition of modifications with adhesion peptides to ensure that the signals provide to the cell under investigation will mimic the niche environment of interests as closely as possible. At this stage, we believe that the R. Pulmo collagen we

characterized in this thesis will be a more useful and interesting tool as biocompatible material in TE applications rather than cancer molecular studies.

Another important layer of investigation in our analysis is the assessment of mechanical properties of tissues at different levels, from nanometres to micrometres. Monitoring tissue bulk mechanics with rheology represents a fast and straightforward tool to assess these bulk 3D model mechanics in liquid state(s), and under physiological temperatures. Even if we were able to match our 3D model to patients' derived biopsies Young's modulus and replicate the bulk mechanic reported in literature, unfortunately, none of our investigations on the tissue mechanical properties changed in a predictable way, i.e. to replicate in vivo fibrosis/desmoplasia progression, fibroblasts activation on soft material should result in increased stiffness as consequence of remodelling. This effect was hypothesised to result from fibroblast activation and culturing, or in coculture settings, too. We concluded that coculture of cancer and stromal cells may be the only real representative way to reproduce fibrosis staging development *in vitro*, since many evidences showed that not only fibroblasts are crucial for ECM turnover, but also cancer cell influence.

More importantly, tissue rheology has been already tested as possible complementary procedure to advance histological diagnosis of colon cancer [385]. Researchers evaluated the potential of nanoscale AFM and macroscopic shear rheometry to assess the mechanical properties of healthy and cancerous human colon tissues, demonstrating that rheological parameters can be useful measures of colon cancer mechanopathology to be coupled with histopathological grading to allow more accurate colon cancer diagnosis and improve prognosis. Both AFM and shear rheometer can quantify the mechanical properties of soft tissues and are promising tools for cancer diagnosis and to assess potential anticancer effectiveness, in fact they are currently gaining a lot of interests in the clinical routine [315-317]. Even if there are non-invasive techniques, i.e. shear wave elastography (SWE) and magnetic resonance elastography (MRE) [310-312], these methods have drawbacks mainly related to the complex structure of the tissues and the location of the organs away from the source of excitation [310, 313]. AFM analysis is envisioned as a complementary procedure in the advanced diagnosis of cancer, ex vivo, providing surface imaging and nanomechanical characterization of cells and tissues under physiological conditions [892-894] coupled with ex vivo rheometric analysis.

7.2 Current 3D models in preclinical cancer for biophysical studies

Generation of multicellular spheroids that allow the formation of a core with hypoxic and quiescent cells. Growing as independent cellular aggregates, they mimic anticancer drug resistance compared to conventional cultures [895], but fail to reproduce cancer-environment interactions. In this framework, ECM components have been introduced to expose cells to appropriate physical, chemical, and mechanical cues. Those cultures reported significant phenotypical and behavioural differences between normal and metastatic epithelial cells. In scaffolds-based 3D model systems, different materials are exploited to model different tumour stages. Collagen, Matrigel and hyaluronic acid materials have been the most common natural materials used for modelling and studying both primary and invasive tumours, as platforms to mimic either processes like ECM degradation, migration, and epithelial-mesenchymal transition and the advanced processes of intravasation, extravasation, and metastasis through mesenchymal-epithelial transition (MET). Synthetic polymers like PEG or nanofibre scaffolds (RAD16-I) functionalized with adhesive/recognition sites for integrin binding or protease degradation are also useful to study the effect of tumours on ECM [179]. Among the most common cancer study models scaffold-base hydrogels (for simple cell culturing or as medium for spheroids or organoids creation), porous scaffolds and microfluidic devices all harbour advantages and disadvantages and their choice for cancer studies is highly context-dependent.

Assessment of the mechanical properties of a hydrogel system is usually performed at the macro scale (using tensional or shear rheometry) or using high-resolution tools such as AFM which are suited for sub-cellular nanoscale measurements, and are limited to measuring near-surface stiffness in 2D or cut tissue sections [896]. Other non-contact techniques such as ultrasound elastography or magnetic cytometry can give information at the macro scale but cannot capture local mechanical variations around cells or mimic a cell's ability to interrogate its surroundings [897]. Those technologies can support impactful research but also limit our technical ability to monitor and characterize tissue mechanics at the cellular length scale during tissue morphogenesis and disease.

The elective techniques used to detect the stiffness of single cells, including AFM or optical tweezers, can measure forces ranging from sub pN to a few hundred nN, which are not suitable for measurement of larger 3D cellular structures such as spheroids, whose mechanical characteristics have not been fully studied. One strategy is to use micro tweezers that measure forces from sub-hundred nN to mN. This wide force range was achieved by the use of a chopstick-like motion of two cantilevers, which facilitates easy handling of samples and microscopic observation for mechanical characterization on normal and cancerous spheroids [898].

Another interesting strategy to detect mechanical cues occurring during 3D cellular aggregate formation is the use of fabricated polyacrylamide microbeads as built-in pressure sensors to locally measure changes in mechanical stress to understand how a compressive stress (which occurs physiologically during tumour growth) is distributed within the 3D cellular aggregates. Dolega et al. reported that cells at the spheroid surface continuously proliferate and actively rearrange under compressive stress [377, 899]. Hypothetically, the high availability of oxygen and nutrients at the surface lead the outer layer to proliferate, generating tension and contraction. Compressive stresses dissipate towards the less dense core of multi-cellular spheroids, where contractility is reduced as nutrients and oxygen are depleted. Others used similar microscopy-compatible probes that report quantitative, directional, and real-time measurements of stress at cellular- and supra-cellular length scales within engineered tissues to achieve localized measurements at the length scale of individual cells (10s of μm) with a large dynamic range from 10–1000s of Pa. Those studies found that cells located at the spheroid's periphery exhibit greater contractility, as evidenced by increased expression of phosphorylated myosin, and that these differences in mechanical forces are associated with activation of mechanosensitive signalling pathways involving YAP/TAZ transcription factors, which hypothetically could give rise to distinct differentiation profiles and spatially regulated biological activity [900].

Embedding multicellular spheroids within gels of defined mechanical properties (e.g., agarose gels) was one of the first experimental approaches to mimic tumour growth in a constraining environment, reproducing the compressive stress accumulation at the tumour-stroma interface [901]. In particular, researchers reported that in homogeneities in the mechanical properties of the confining tissue can guide morphological changes in tumour growth, independent of cell

migration, by inducing apoptosis in regions of high compressive stress and allowing proliferation in regions of low stress [902]. Those models can provide useful insight into how compression directly influences tumour development, disclosing the role of mechanical stresses in the process.

Both hydrogels and porous scaffolds derived from regenerative medicine studies and, while the first found a wide application in cancer studies related to easy handling, transparency of the medium which allows easier imaging , porous scaffolds are still under investigation in the field but they offer a huge potential for tuneable and customizable biomechanical properties and structural stability. Another improvement strategy could be to couple them with bioreactors to provide close control and monitoring of the environment (e.g., temperature, pH, nutrient supply, waste removal), together with higher reproducibility and automation. Media flow systems will allow for circulation of nutrients, removal of wastes, and homogeneity of the environment within the reactor, ideal for high-volume cell production, drug testing (also employing nanoparticles) and ex vivo tissue engineering applications.

Alongside bioreactors, progresses in 3D bio-printing will improve the diversity, fidelity, and capacity of 3D culture models like hydrogels in cancer research. 3D bio-printing techniques can generate geometric constructs containing viable cells but can also simplify high-throughput applications with precise reproducibility [903]. Besides, to achieve a complexity closer to the *in vivo* and to mimic a living tissue and a more natural ECM secretion, it is the inclusion of cell types such as fibroblasts, endothelial cells, and mesenchymal stem cells in coculture with cancer cells to enable production of endogenous ECM by the stromal cells.

Sometimes the scaffold itself can be the innovative therapeutic strategy. The concept of creating an artificial niche can be integrated with the potential to capture tumour cells actively disseminating in the peritoneal cavity to create a therapeutic strategy modulating the interactions of metastatic cells with the ECM. This idea was tested with the aim of transforming a disseminated disease into a focal disease. Researchers developed a “biomimetic” ECM composed of a non-resorbable 3D scaffold with collagen coating on different murine preclinical models of advanced ovarian cancer, showing the possibility for control of peritoneal carcinomatosis upon primary

ovarian debulking surgery and to expand the percentage of patients who are candidates for second rescue surgeries at the time of relapse [904].

Perhaps the most exciting developments have been the recent organs on chip (OoC) methods, which allow for the construction of connected chambers that mimic different organ compartments, for example liver ducts and blood vasculature [696]. Tumour-on-chip platforms have been designed to recreate controllable culture environments, mainly to investigate blood circulation, drug delivery, intravasation, and extravasation processes occurring during tumour progression [905-907]. Unfortunately, the extensive user training required for multistep fabrication, specific set-up equipment, small-volume culture and staining protocols, the use of polydimethylsiloxane (PDMS) for fabrication which can absorb small hydrophobic molecules like biomolecules and drugs from the solution [908], and difficulties in recovering seeded cells for further characterization represent a few of the disadvantages in using such platforms. Finally, it is important to note that organ on chips can exhibit significant variation and inconsistency between different manufacturing batches, not only from different laboratories but even different fabricators in the same group [909].

Aside for drawbacks and limitations, all those models found applications in cancer mechanical studies, providing crucial information in the field of cancer biophysics.

7.3 Future directions: ECM complexity and coculture establishment

A good of the 3D platform is to enable molecular, cellular and tissue level resolution traits to be mimicked in the laboratory. In addition, any model needs to be compatible with small chemical, hormonal or peptide insult to enable mechanism of action to be studied and analysed using an array of tools, from gene therapies to small chemical tool compounds. Besides, downstream analysis tools such as the suites of cellular and molecular evaluation assays need to be compatible, to enable the efficacy of anticancer agents to be studied, discover potential target genes for therapy, and reveal signalling pathways relevant for tumour progression. With all the advantages of 3D monoculture and coculture systems, the insights they provide will increase our understanding of

the tumour micro-milieu while developing and testing new cancer therapies *in vitro*, attacking two possible targets: the tumour cell and its environment.

Many factors in the TME have multiple effects on different cellular compartments, as we confirmed in our investigation the TGF-β1 activation of stromal differentiation into ECM-remodelling CAFs, biochemical activation signals that can be specifically secreted by tumour cells. Additionally, TGF-β1 secreted by CAFs can induce STAT3 signalling in tumour cells [910]. However, in PDAC, TGF- β1 loss in tumour cells is associated with increased desmoplasia and enhanced matrix tension. The pronounced desmoplasia triggers β1-integrin mechanosignalling that promotes tumour progression through STAT3 activation. These observations show the complexity of TGF-β1 signalling in tumour and stromal cells, which can have pro- and anti-tumorigenic functions depending on the context. This further strengthens the need to tackle solid tumour cancers as multiple pathologies with a lot of commonalities but a lot of distinctive characteristics, too.

Most importantly pairing cancer cells with their specific milieu is the first step to achieve a meaningful *in vitro* preclinical model. To this aim, investigating ovarian cancer cell line SKOV3 ability to prime fibroblasts into CAFs through their secretome, compared to TGFβ1 effect was evaluated. The final goal would be to optimise a coculture system, where collagen type I based collagen scaffolds could accommodate both cancer cells and stroma, allowing both contact and chemical interactions to test new anticancer or anti-stroma drugs as mono or combine therapies. To achieve this, the tumour–stroma ratio (TSR) can be mimicked [742, 911]. The aim of this ongoing study would be to evaluate the reproducibility of the TSR phenotypes on a 3D model and elucidate the association between TSR and prognosis in ovarian cancer. Indeed, haematoxylin-and-eosin-stained tissue sections from the most invasive part of the primary tumour evaluated TSR in ovarian cancer patients reporting that stroma-rich tumours had worse prognosis and higher risk of relapse compared with those in stroma-poor tumours. Considered easy to determine for routine pathological examination, TSR may serve as a new prognostic histological parameter in OC [746] and 3D models could provide a platform to test drug sensitivity in this histological scenarios.

Indeed, anti-stromal therapies are already under evaluations in different cancers such as pancreatic (PC), in which despite the availability of potent chemotherapy regimens, such as 5-fluorouracil, folinic acid, irinotecan, and oxaliplatin (FOLFIRINOX) and nab-paclitaxel plus gemcitabine, treatment outcomes remain unsatisfactory. The presence of an abundant fibrous stroma in PC is considered a crucial factor for its unfavourable condition, acting as a physical barrier to restrict intertumoral cytotoxic drug penetration and creates a hypoxic environment that reduces the efficacy of radiotherapy [912]. Assessing the potential benefits of agents targeting several cellular (*e.g.*, trans retinoic acid, Vit A and D analogues, anti-fibrotic agents, angiotensin II antagonists, micro RNA and Hedgehog inhibitors to target the pancreatic CAFs called stellate cells) and acellular (*e.g.*, PEGPH20, PEGylated human recombinant hyaluronidase PH20, to target hyaluronan) elements of the stroma are under clinical studies evaluation [913]. Many strategies are currently under evaluation [748], i.e. employing neutralizing antibodies like Galunisertib and Fresolimumab to target TGFβ pathway prevents radiation-induced acceleration of breast cancer progression [914], or using Sibrotuzumab, a humanized monoclonal antibody binding FAP, which failed in 2003 a phase II clinical trial for metastatic colorectal cancer (NCT02198274) [915] but it was replaced by RO6874813 antibody against FAP in a clinical trial started in 2015 still ongoing (NCT02558140), to target solid tumours with FAP+ stroma [916] .

Beyond fibroblasts and the extracellular matrix, the tumour microenvironment of HGSOC has other important elements that may influence treatment response, such as immune cells. Interestingly, HGSOC was one of the first human cancers in which an association was found between an increased density of intraepithelial tumour-infiltrating lymphocytes (TILs) and longer patient survival [917], especially in BRCA1-mutant tumours for reasons that are unclear. An improved understanding of the determinants of TIL density in HGSOC may assist in the development of immune checkpoint therapies in this disease. Not only immune cells but also mesothelial cells which line the peritoneum and pleural cavity dynamically interact with HGSOC cells [918-920]. Studying the complexity of the HGSOC tumour microenvironment suggest that combination therapies targeting different elements are more likely to be successful than single agent approaches. For example, a current clinical trial combines a Toll-like receptor 8 (TLR8) agonist to activate antigen-presenting cells, liposomal doxorubicin to stimulate immunogenic

tumour cell death, and PDL1 blockade to activate T cells (ClinicalTrials.gov identifier NCT02431559).

As we continue to develop a better understanding of the complex interactions between a heterogeneous milieu of cellular and noncellular contributors in the TME, we will be able to improve stroma-targeting strategies and combinational therapies to promote immune responses and design more effective anticancer therapies starting from the preclinical evaluation.

Another important improvement that we are carrying on in our research is the fabrication of collagen-HA scaffolds to understand how HA with different length and molecular weight could promote chemoresistance in ovarian cancer cell lines. As reported here, the HA ratio tested mimicked differences in stiffness but not to the degree in pathogenicity, failing in inducing fibroblasts activation. Results showed that only 'physiological scaffold' col/HA HW was able to promote fibroblasts MMP1 and CD44 expression, suggesting an activation of remodelling functions and cell-matrix interaction. We believe that this scaffold will require further tuning to achieve a higher biological meaning and require an adjustment of the ratio between collagen/HA to achieve a significant biological readout and a detectable level to verify HA presence in the scaffold using analysis like TGA. We are currently carrying on further optimizations on the fabrication protocols to then investigate both SKOV3, OVCAR-3 and HA interactions role in mediating chemoresistance to carboplatin (CBP) as monotherapy or combination with paclitaxel in a 3D scaffold with LW (pathogenic) and HW (physiologic) HA. Carboplatin and paclitaxel association is, by now, the standard first-line chemotherapy regiment [921]. SKOV-3 cells represents the most resistant to CBP (LD_{50} = 184 μM), while OVCAR-3 showed lower resistance (LD_{50} = 113 μM) [922]; instead paclitaxel (taxol) sensitivity is similar among the 2 cell lines [923-926].

Specifically, previous studies showed that HA induces chemoresistance against CBP [927], and increases the expression of the ABC transporters, *ABCB3*, *ABCC1*, *ABCC2*, and *ABCC3* in ovarian cancer cell lines expressing the HA receptor, CD44 [928, 929]. Furthermore, HA production in ovarian cancer cells was increased in tissues from patients that received neoadjuvant chemotherapy and at recurrence compared to tissues collected at surgery prior to any treatment.

SKOV-3 cells, the most CBP-resistant cell line, produces the highest levels of HA but treatment with LD_{50} CBP dose significantly increased HA secretion in the CM of OVCAR-3 (4.1-fold) and SKOV-3 cells (1.6-fold). Indeed the addition of either neutralizing CD44 antibody or HA oligomers (6–10 sugar residues), which interact monovalently with CD44 and competitively block polyvalent interactions between CD44 and endogenous HA, blocked the HA induced chemoresistance in CD44 positive ovarian cancer cell lines (SKOV3) but not in the CD44 negative, OVCAR-3 cells [922]. Our model will help assess chemoresistance dependence from CD44-HA interaction and will provide new indications for ovarian cancer treatment therapy.

7.4 Improving the preclinical environment: mimicking tumour progression through the third dimension with patients derived models

From the experimental models presented so far, co-cultures and xenograft or syngeneic mice models are fundamental to preclinical cancer research, but substantial gaps still exist between the results of these experiments and those obtained in clinical settings. Not only communication between researchers and medical professionals will be crucial in determining the next steps to bring discoveries to patients but also inclusion of patient-specific genetic and epigenetic background in the preclinical evaluation will help design more effective anticancer therapies.

A summary evaluation of the 2015 American Cancer Society (ACS) challenge goal showed that overall US mortality from all cancers combined declined 26% over the period from 1990 to 2015. The projections for 2035, analysed using a statistical modelling approach, is a challenge goal for the American Cancer Society (ACS) of 40% reduction in cancer mortality from the 2015 level [930]. Accomplishing this reduction in cancer will clearly involve better application of today's tools for cancer prevention, detection, treatment, and assurance of quality of life for patients with cancer, survivors, and their families together with sustained research effort to develop the next generation of tools to understand, prevent, and better control all cancer types [931].

Although screening tests for the early detection of cancer include those for breast, cervical, colorectal, lung, and prostate cancers; enhancing diagnostic or prognostic accuracy of those

tests, decrease patients discomfort, a reduction of the costs related to testing are needed. With only 4 of the 20 most common cancer types in the United States having a proven screening method to reduce mortality by identifying early stage lesions, developing such tools for other high-incidence malignancies, with an annual cumulative incidence >300,000 and mortality >150,000, is equally and urgently pressing. Often those tumours are diagnosed at advanced stages, when complete surgical resection is difficult or impossible and chemotherapy or radiation are of limited benefit, i.e. pancreatic ductal adenocarcinoma and ovarian high-grade serous carcinoma, both with an unfortunate 5-year survival rates [932, 933].

In this framework, the future of medicine appears to be precision and personalized medicine. Precision medicine approaches patient care based on a genetic understanding of their disease (e.g., blood transfusion according to blood typing and autologous grafting), targeting specific disease variants and providing patient-tailored therapies. In this framework, patient-based models display unique features as a result of the cell donor's genetic and epigenetic backgrounds, lifestyle, and medical history, so the models can be used to evaluate drug efficacy and responses as a precision medicine approach. Technological advances, incorporation of multiple cell types, extracellular matrix proteins and soluble factors that constitute the tumour microenvironment are leading to a broader use of human-derived tissues in cancer research [934, 935]. In line with this, our investigation successfully reproduced physical features derived from patients tissue in a 3D model, providing new insight into the tumour matrix biophysical parameters effect on drug sensitivity, stromal responses and activation, creating a common ground to tackle solid cancers. When tumour tissue is cultured in vitro, the microenvironment can be tuned, and more features are easier to manipulate and analyse than in mouse models. Furthermore, we envision our scaffold as an easy to manufacture, handling, high throughput platform to create coculture systems which will mimic tissue biological and biophysical complexity, allowing drugs testing and helping building a tailored personalized treatment, while providing an informative platform to guide desmoplasia mechanisms characterization, chemoresistance and test new anti-stromal/fibrotic therapies (**Figure 6.4**).

Current patient-derived tumour models used in preclinical cancer research mainly include 3D culture systems (like organoids, spheroids, cancer-on-chip), organotypic tissue slices and patient-

derived xenograft models and each model system has its own intrinsic advantages and restrictions and no single model right now will be able to address all questions or accurately predict therapy response and drug resistance [936, 937]. Indeed, integration of data coming from multiple preclinical models coupled with computational systems biology analysis could help better predict clinical response. In fact, faithfully modelling the complex tissue architecture and cellular interactions as well as mimicking the genotypic and phenotypic evolution that can occur during treatment remain a huge challenge, with drug discovery representing the most striking disconnection point between promising preclinical results and unconclusive clinical outcomes (rate of success for oncologic drugs of <10% from Phase 1 to FDA approval) [938].

Inclusion of primary patient-derived cells will enable the development of more accurate 3D models, retaining the patient and tumour characteristics and more appropriately capturing tumour heterogeneity in the population [939]. More cancer type-specific models are also necessary for establishing aetiologies, studying cancer progression, testing interventions, assessing tumour dormancy/quiescence (like high-grade serous ovarian cancer [940]) to predict and monitor disease recurrence. Besides, biobanks of patient-derived 3D cancer models could refine our understanding of interpatient heterogeneity, paving the way for personalized cancer therapies.

Overall, these platforms represent a novel, reliable preclinical patient-specific platform to bridge the gap between *in vitro* and *in vivo* drug testing assays, providing preclinical evaluation of drug cytotoxicity, efficacy, and efficiency for effective cancer treatment [941-948]. Similarly, it could help identifying predictive biomarkers that, when advanced to clinical trials, will help to distinguish those patients who are likely to benefit from a drug.

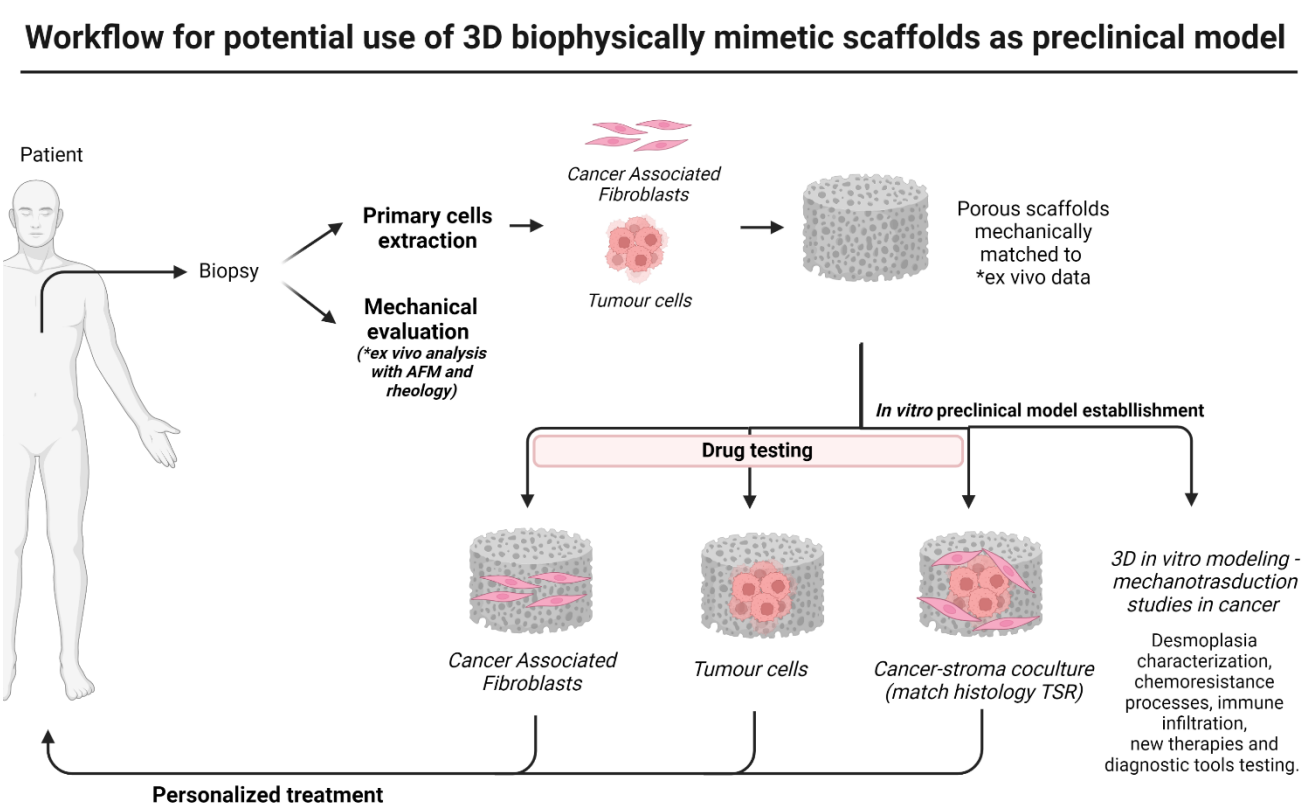

Figure 6.4. Porous scaffolds and mechanical evaluation implementation in clinical setting. Our findings support the utility of porous scaffolds as meaningful mechanically informative platforms to tailor therapy for individual patients to improve clinical outcomes, while providing a preclinical model to test complex interaction in cancer TME, adding immune components and testing new therapies and diagnostic tools. Image made with Biorender.

References

1. Kalluri, R. and M. Zeisberg, *Fibroblasts in cancer.* Nat Rev Cancer, 2006. **6**(5): p. 392-401.
2. Yue, B., *Biology of the extracellular matrix: an overview.* J Glaucoma, 2014. **23**(8 Suppl 1): p. S20-3.
3. Naba, A., et al., *The matrisome: in silico definition and in vivo characterization by proteomics of normal and tumor extracellular matrices.* Mol Cell Proteomics, 2012. **11**(4): p. M111.014647.
4. Naba, A., et al., *The extracellular matrix: Tools and insights for the "omics" era.* Matrix Biol, 2016. **49**: p. 10-24.
5. Mammoto, T. and D.E. Ingber, *Mechanical control of tissue and organ development.* Development, 2010. **137**(9): p. 1407-20.
6. Hynes, R.O., *The extracellular matrix: not just pretty fibrils.* Science, 2009. **326**(5957): p. 1216-9.
7. Oudin, M.J., et al., *Tumor Cell–Driven Extracellular Matrix Remodeling Drives Haptotaxis during Metastatic Progression.* Cancer Discovery, 2016. **6**(5): p. 516-531.
8. Ingber, D.E., *Extracellular matrix as a solid-state regulator in angiogenesis: identification of new targets for anti-cancer therapy.* Semin Cancer Biol, 1992. **3**(2): p. 57-63.
9. Painter, K.J., *Modelling cell migration strategies in the extracellular matrix.* Journal of Mathematical Biology, 2008. **58**(4): p. 511.
10. Bateman, J.F., R.P. Boot-Handford, and S.R. Lamandé, *Genetic diseases of connective tissues: cellular and extracellular effects of ECM mutations.* Nat Rev Genet, 2009. **10**(3): p. 173-83.
11. Winkler, J., et al., *Concepts of extracellular matrix remodelling in tumour progression and metastasis.* Nature Communications, 2020. **11**(1): p. 5120.
12. Sonbol, H.S., *Extracellular Matrix Remodeling in Human Disease.* J Microsc Ultrastruct, 2018. **6**(3): p. 123-128.
13. Bonnans, C., J. Chou, and Z. Werb, *Remodelling the extracellular matrix in development and disease.* Nat Rev Mol Cell Biol, 2014. **15**(12): p. 786-801.
14. Cox, T.R. and J.T. Erler, *Remodeling and homeostasis of the extracellular matrix: implications for fibrotic diseases and cancer.* Disease Models & Mechanisms, 2011. **4**(2): p. 165-178.
15. Naba, A., et al., *Extracellular matrix signatures of human mammary carcinoma identify novel metastasis promoters.* eLife, 2014. **3**: p. e01308.
16. Pickup, M.W., J.K. Mouw, and V.M. Weaver, *The extracellular matrix modulates the hallmarks of cancer.* EMBO reports, 2014. **15**(12): p. 1243-1253.
17. Senthebane, D.A., et al., *The Role of Tumor Microenvironment in Chemoresistance: To Survive, Keep Your Enemies Closer.* Int J Mol Sci, 2017. **18**(7).
18. Shaked, Y., *The pro-tumorigenic host response to cancer therapies.* Nat Rev Cancer, 2019. **19**(12): p. 667-685.
19. Hynes, R.O. and A. Naba, *Overview of the matrisome--an inventory of extracellular matrix constituents and functions.* Cold Spring Harb Perspect Biol, 2012. **4**(1): p. a004903.
20. Koliaraki, V., et al., *The mesenchymal context in inflammation, immunity and cancer.* Nat Immunol, 2020. **21**(9): p. 974-982.
21. Buechler, M.B., et al., *Cross-tissue organization of the fibroblast lineage.* Nature, 2021. **593**(7860): p. 575-579.

22. Chang, H.Y., et al., *Diversity, topographic differentiation, and positional memory in human fibroblasts.* Proc Natl Acad Sci U S A, 2002. **99**(20): p. 12877-82.
23. Buechler, M.B. and S.J. Turley, *A short field guide to fibroblast function in immunity.* Semin Immunol, 2018. **35**: p. 48-58.
24. Sonoki, A., Y. Okano, and Y. Yoshitake, *Dermal fibroblasts can activate matrix metalloproteinase-1 independent of keratinocytes via plasmin in a 3D collagen model.* Exp Dermatol, 2018. **27**(5): p. 520-525.
25. Lindner, D., et al., *Differential expression of matrix metalloproteases in human fibroblasts with different origins.* Biochemistry research international, 2012. **2012**: p. 875742-875742.
26. Boraas, L.C. and T. Ahsan, *Lack of vimentin impairs endothelial differentiation of embryonic stem cells.* Scientific Reports, 2016. **6**(1): p. 30814.
27. Yao, J.x., et al., *Prognostic Value of Vimentin Is Associated With Immunosuppression in Metastatic Renal Cell Carcinoma.* 2020. **10**.
28. Chen, M., et al., *Increased Neuronal Differentiation of Neural Progenitor Cells Derived from Phosphovimentin-Deficient Mice.* Molecular Neurobiology, 2018. **55**(7): p. 5478-5489.
29. Nakayama, H., et al., *The Role of Myofibroblasts at the Tumor Border of Invasive Colorectal Adenocarcinomas.* Japanese Journal of Clinical Oncology, 1998. **28**(10): p. 615-620.
30. Michalik, M., et al., *Fibroblast-to-myofibroblast transition in bronchial asthma.* Cell Mol Life Sci, 2018. **75**(21): p. 3943-3961.
31. Desideria, D., et al., *Importance of Fibroblasts-Myofibroblasts in Asthma-Induced Airway Remodeling.* Recent Patents on Inflammation & Allergy Drug Discovery, 2007. **1**(3): p. 237-241.
32. Takase, S., et al., *Desmin distinguishes cultured fat-storing cells from myofibroblasts, smooth muscle cells and fibroblasts in the rat.* J Hepatol, 1988. **6**(3): p. 267-76.
33. Paulin, D. and Z. Li, *Desmin: a major intermediate filament protein essential for the structural integrity and function of muscle.* Exp Cell Res, 2004. **301**(1): p. 1-7.
34. Kelly, T., et al., *Fibroblast activation protein-α: a key modulator of the microenvironment in multiple pathologies.* Int Rev Cell Mol Biol, 2012. **297**: p. 83-116.
35. Ramirez-Montagut, T., et al., *FAPalpha, a surface peptidase expressed during wound healing, is a tumor suppressor.* Oncogene, 2004. **23**(32): p. 5435-46.
36. Eckes, B., et al., *Mechanical tension and integrin alpha 2 beta 1 regulate fibroblast functions.* J Investig Dermatol Symp Proc, 2006. **11**(1): p. 66-72.
37. Turner, K.R., et al., *Crucial Role for Endothelial Cell α2β1 Integrin Receptor Clustering in Collagen-Induced Angiogenesis.* Anat Rec (Hoboken), 2020. **303**(6): p. 1604-1618.
38. Rubio, M.A., et al., *Monocyte activation: rapid induction of alpha 1/beta 1 (VLA-1) integrin expression by lipopolysaccharide and interferon-gamma.* Eur J Immunol, 1995. **25**(9): p. 2701-5.
39. Cowling, R.T., et al., *Discoidin domain receptor 2 germline gene deletion leads to altered heart structure and function in the mouse.* Am J Physiol Heart Circ Physiol, 2014. **307**(5): p. H773-81.
40. Zhao, H., et al., *Targeting of Discoidin Domain Receptor 2 (DDR2) Prevents Myofibroblast Activation and Neovessel Formation During Pulmonary Fibrosis.* Mol Ther, 2016. **24**(10): p. 1734-1744.

41. Öhlund, D., E. Elyada, and D. Tuveson, *Fibroblast heterogeneity in the cancer wound.* The Journal of experimental medicine, 2014. **211**(8): p. 1503-1523.
42. Yoshida, G.J., *Regulation of heterogeneous cancer-associated fibroblasts: the molecular pathology of activated signaling pathways.* Journal of Experimental & Clinical Cancer Research, 2020. **39**(1): p. 112.
43. Li, B. and J.H. Wang, *Fibroblasts and myofibroblasts in wound healing: force generation and measurement.* J Tissue Viability, 2011. **20**(4): p. 108-20.
44. Pankova, D., et al., *Cancer-Associated Fibroblasts Induce a Collagen Cross-link Switch in Tumor Stroma.* Mol Cancer Res, 2016. **14**(3): p. 287-95.
45. Chandler, C., et al., *The double edge sword of fibrosis in cancer.* Translational Research, 2019. **209**: p. 55-67.
46. Santos, A. and D. Lagares, *Matrix Stiffness: the Conductor of Organ Fibrosis.* Curr Rheumatol Rep, 2018. **20**(1): p. 2.
47. Netti, P.A., et al., *Role of extracellular matrix assembly in interstitial transport in solid tumors.* Cancer Res, 2000. **60**(9): p. 2497-503.
48. Nicolas-Boluda, A., et al., *Tumor stiffening reversion through collagen crosslinking inhibition improves T cell migration and anti-PD-1 treatment.* eLife, 2021. **10**: p. e58688.
49. Yurchenco, P.D., *Basement membranes: cell scaffoldings and signaling platforms.* Cold Spring Harb Perspect Biol, 2011. **3**(2).
50. Pozzi, A., P.D. Yurchenco, and R.V. Iozzo, *The nature and biology of basement membranes.* Matrix Biol, 2017. **57-58**: p. 1-11.
51. Jayadev, R. and D.R. Sherwood, *Basement membranes.* Curr Biol, 2017. **27**(6): p. R207-r211.
52. Kessenbrock, K., V. Plaks, and Z. Werb, *Matrix metalloproteinases: regulators of the tumor microenvironment.* Cell, 2010. **141**(1): p. 52-67.
53. Pompili, S., et al., *The Charming World of the Extracellular Matrix: A Dynamic and Protective Network of the Intestinal Wall.* 2021. **8**.
54. Mouw, J.K., G. Ou, and V.M. Weaver, *Extracellular matrix assembly: a multiscale deconstruction.* Nat Rev Mol Cell Biol, 2014. **15**(12): p. 771-85.
55. Theocharis, A.D., D. Manou, and N.K. Karamanos, *The extracellular matrix as a multitasking player in disease.* The FEBS Journal, 2019. **286**(15): p. 2830-2869.
56. Egeblad, M., M.G. Rasch, and V.M. Weaver, *Dynamic interplay between the collagen scaffold and tumor evolution.* Curr Opin Cell Biol, 2010. **22**(5): p. 697-706.
57. Fang, M., et al., *Collagen as a double-edged sword in tumor progression.* Tumour Biol, 2014. **35**(4): p. 2871-82.
58. Bosman, F.T. and I. Stamenkovic, *Functional structure and composition of the extracellular matrix.* 2003. **200**(4): p. 423-428.
59. Provenzano, P.P., et al., *Collagen density promotes mammary tumor initiation and progression.* BMC Medicine, 2008. **6**(1): p. 11.
60. Egeblad, M., E.S. Nakasone, and Z. Werb, *Tumors as Organs: Complex Tissues that Interface with the Entire Organism.* Developmental Cell, 2010. **18**(6): p. 884-901.
61. Helleman, J., et al., *Molecular profiling of platinum resistant ovarian cancer.* 2006. **118**(8): p. 1963-1971.
62. Jazaeri, A.A., et al., *Gene Expression Profiles Associated with Response to Chemotherapy in Epithelial Ovarian Cancers.* Clinical Cancer Research, 2005. **11**(17): p. 6300-6310.

63. Esposito, I., et al., *Tenascin C and annexin II expression in the process of pancreatic carcinogenesis.* J Pathol, 2006. **208**(5): p. 673-85.
64. Whatcott, C.J., et al., *Desmoplasia in Primary Tumors and Metastatic Lesions of Pancreatic Cancer.* Clin Cancer Res, 2015. **21**(15): p. 3561-8.
65. Iacobuzio-Donahue, C.A., et al., *The desmoplastic response to infiltrating breast carcinoma: gene expression at the site of primary invasion and implications for comparisons between tumor types.* Cancer Res, 2002. **62**(18): p. 5351-7.
66. Bohaumilitzky, L., et al., *A Trickster in Disguise: Hyaluronan's Ambivalent Roles in the Matrix.* Front Oncol, 2017. **7**: p. 242.
67. Takasugi, M., et al., *Naked mole-rat very-high-molecular-mass hyaluronan exhibits superior cytoprotective properties.* Nature Communications, 2020. **11**(1): p. 2376.
68. Anttila, M.A., et al., *High levels of stromal hyaluronan predict poor disease outcome in epithelial ovarian cancer.* Cancer Res, 2000. **60**(1): p. 150-5.
69. Auvinen, P., et al., *Hyaluronan in peritumoral stroma and malignant cells associates with breast cancer spreading and predicts survival.* Am J Pathol, 2000. **156**(2): p. 529-36.
70. Lipponen, P., et al., *High stromal hyaluronan level is associated with poor differentiation and metastasis in prostate cancer.* Eur J Cancer, 2001. **37**(7): p. 849-56.
71. Liu, M., C. Tolg, and E. Turley, *Dissecting the Dual Nature of Hyaluronan in the Tumor Microenvironment.* 2019. **10**.
72. Chanmee, T., P. Ontong, and N. Itano, *Hyaluronan: A modulator of the tumor microenvironment.* Cancer Lett, 2016. **375**(1): p. 20-30.
73. Sullivan, W.J., et al., *Extracellular Matrix Remodeling Regulates Glucose Metabolism through TXNIP Destabilization.* Cell, 2018. **175**(1): p. 117-132.e21.
74. Schinzel, R.T., et al., *The Hyaluronidase, TMEM2, Promotes ER Homeostasis and Longevity Independent of the UPR(ER).* Cell, 2019. **179**(6): p. 1306-1318.e18.
75. Socovich, A.M. and A. Naba, *The cancer matrisome: From comprehensive characterization to biomarker discovery.* Semin Cell Dev Biol, 2019. **89**: p. 157-166.
76. Yuzhalin, A.E., et al., *A core matrisome gene signature predicts cancer outcome.* Br J Cancer, 2018. **118**(3): p. 435-440.
77. Bergamaschi, A., et al., *Extracellular matrix signature identifies breast cancer subgroups with different clinical outcome.* J Pathol, 2008. **214**(3): p. 357-67.
78. Yuzhalin, A.E., et al., *Dynamic matrisome: ECM remodeling factors licensing cancer progression and metastasis.* Biochim Biophys Acta Rev Cancer, 2018. **1870**(2): p. 207-228.
79. Leeming, D.J., et al., *Post-translational modifications of the extracellular matrix are key events in cancer progression: opportunities for biochemical marker development.* Biomarkers, 2011. **16**(3): p. 193-205.
80. Kumari, S., T.K. Panda, and T. Pradhan, *Lysyl Oxidase: Its Diversity in Health and Diseases.* Indian J Clin Biochem, 2017. **32**(2): p. 134-141.
81. Wang, T.H., S.M. Hsia, and T.M. Shieh, *Lysyl Oxidase and the Tumor Microenvironment.* Int J Mol Sci, 2016. **18**(1).
82. Conklin, M.W., et al., *Aligned collagen is a prognostic signature for survival in human breast carcinoma.* Am J Pathol, 2011. **178**(3): p. 1221-32.
83. Riching, K.M., et al., *3D collagen alignment limits protrusions to enhance breast cancer cell persistence.* Biophys J, 2014. **107**(11): p. 2546-58.

84. Skrzydlewska, E., et al., *Proteolytic-antiproteolytic balance and its regulation in carcinogenesis.* World J Gastroenterol, 2005. **11**(9): p. 1251-66.
85. Koblinski, J.E., M. Ahram, and B.F. Sloane, *Unraveling the role of proteases in cancer.* Clin Chim Acta, 2000. **291**(2): p. 113-35.
86. Rakash, S., *Role of proteases in cancer: A review.* Biotechnology and Molecular Biology Reviews, 2012. **7**: p. 90-101.
87. Zhang, B., et al., *Tumor-derived matrix metalloproteinase-13 (MMP-13) correlates with poor prognoses of invasive breast cancer.* BMC Cancer, 2008. **8**: p. 83.
88. Upadhyay, J., et al., *Membrane Type 1-Matrix Metalloproteinase (MT1-MMP) and MMP-2 Immunolocalization in Human Prostate: Change in Cellular Localization Associated with High-Grade Prostatic Intraepithelial Neoplasia1*. Clinical Cancer Research, 1999. **5**(12): p. 4105-4110.
89. Gialeli, C., A.D. Theocharis, and N.K. Karamanos, *Roles of matrix metalloproteinases in cancer progression and their pharmacological targeting.* 2011. **278**(1): p. 16-27.
90. Sigrist, R.M.S., et al., *Ultrasound Elastography: Review of Techniques and Clinical Applications.* Theranostics, 2017. **7**(5): p. 1303-1329.
91. Butcher, D.T., T. Alliston, and V.M. Weaver, *A tense situation: forcing tumour progression.* Nat Rev Cancer, 2009. **9**(2): p. 108-22.
92. Stowers, R.S., et al., *Matrix stiffness induces a tumorigenic phenotype in mammary epithelium through changes in chromatin accessibility.* Nat Biomed Eng, 2019. **3**(12): p. 1009-1019.
93. Piersma, B., M.K. Hayward, and V.M. Weaver, *Fibrosis and cancer: A strained relationship.* Biochimica et biophysica acta. Reviews on cancer, 2020. **1873**(2): p. 188356-188356.
94. Levental, K.R., et al., *Matrix crosslinking forces tumor progression by enhancing integrin signaling.* Cell, 2009. **139**(5): p. 891-906.
95. Wang, N., *Instant integrin mechanosensing.* Nature Materials, 2017. **16**(12): p. 1173-1174.
96. Sun, Z., S.S. Guo, and R. Fässler, *Integrin-mediated mechanotransduction.* The Journal of cell biology, 2016. **215**(4): p. 445-456.
97. Revach, O.-Y., I. Grosheva, and B. Geiger, *Biomechanical regulation of focal adhesion and invadopodia formation.* Journal of Cell Science, 2020. **133**(20): p. jcs244848.
98. Hirata, H., M. Sokabe, and C.T. Lim, *Molecular Mechanisms Underlying the Force-Dependent Regulation of Actin-to-ECM Linkage at the Focal Adhesions.* Progress in molecular biology and translational science, 2014. **126**: p. 135-54.
99. Humphrey, J.D., E.R. Dufresne, and M.A. Schwartz, *Mechanotransduction and extracellular matrix homeostasis.* Nat Rev Mol Cell Biol, 2014. **15**(12): p. 802-12.
100. Kirby, T.J. and J. Lammerding, *Emerging views of the nucleus as a cellular mechanosensor*. Nature Cell Biology, 2018. **20**(4): p. 373-381.
101. Fedorchak, G.R., A. Kaminski, and J. Lammerding, *Cellular mechanosensing: getting to the nucleus of it all.* Prog Biophys Mol Biol, 2014. **115**(2-3): p. 76-92.
102. Enyedi, B. and P. Niethammer, *A Case for the Nuclear Membrane as a Mechanotransducer.* Cell Mol Bioeng, 2016. **9**(2): p. 247-251.
103. Alam, S., et al., *Nuclear forces and cell mechanosensing.* Prog Mol Biol Transl Sci, 2014. **126**: p. 205-15.

104. Wang, N., J.D. Tytell, and D.E. Ingber, *Mechanotransduction at a distance: mechanically coupling the extracellular matrix with the nucleus.* Nature Reviews Molecular Cell Biology, 2009. **10**(1): p. 75-82.
105. Hampoelz, B., et al., *Microtubule-induced nuclear envelope fluctuations control chromatin dynamics in Drosophila embryos.* Development, 2011. **138**(16): p. 3377-86.
106. Li, Y., et al., *Biophysical regulation of histone acetylation in mesenchymal stem cells.* Biophys J, 2011. **100**(8): p. 1902-9.
107. Cho, S., J. Irianto, and D.E. Discher, *Mechanosensing by the nucleus: From pathways to scaling relationships.* The Journal of cell biology, 2017. **216**(2): p. 305-315.
108. Chiquet, M., et al., *From mechanotransduction to extracellular matrix gene expression in fibroblasts.* Biochim Biophys Acta, 2009. **1793**(5): p. 911-20.
109. Peyton, S.R. and A.J. Putnam, *Extracellular matrix rigidity governs smooth muscle cell motility in a biphasic fashion.* J Cell Physiol, 2005. **204**(1): p. 198-209.
110. Kozyrina, A.N., T. Piskova, and J. Di Russo, *Mechanobiology of Epithelia From the Perspective of Extracellular Matrix Heterogeneity.* 2020. **8**.
111. Plotnikov, Sergey V., et al., *Force Fluctuations within Focal Adhesions Mediate ECM-Rigidity Sensing to Guide Directed Cell Migration.* Cell, 2012. **151**(7): p. 1513-1527.
112. Lo, C.M., et al., *Cell movement is guided by the rigidity of the substrate.* Biophysical journal, 2000. **79**(1): p. 144-152.
113. Klein, E.A., et al., *Cell-cycle control by physiological matrix elasticity and in vivo tissue stiffening.* Curr Biol, 2009. **19**(18): p. 1511-8.
114. Engler, A.J., et al., *Matrix elasticity directs stem cell lineage specification.* Cell, 2006. **126**(4): p. 677-89.
115. Samuel, Michael S., et al., *Actomyosin-Mediated Cellular Tension Drives Increased Tissue Stiffness and β-Catenin Activation to Induce Epidermal Hyperplasia and Tumor Growth.* Cancer Cell, 2011. **19**(6): p. 776-791.
116. Northey, J.J., L. Przybyla, and V.M. Weaver, *Tissue Force Programs Cell Fate and Tumor Aggression.* Cancer Discovery, 2017. **7**(11): p. 1224-1237.
117. Mouw, J.K., et al., *Tissue mechanics modulate microRNA-dependent PTEN expression to regulate malignant progression.* Nat Med, 2014. **20**(4): p. 360-7.
118. Li, Y., et al., *Matrix Stiffness Regulates Chemosensitivity, Stemness Characteristics, and Autophagy in Breast Cancer Cells.* ACS Applied Bio Materials, 2020. **3**(7): p. 4474-4485.
119. Tilghman, R.W., et al., *Matrix rigidity regulates cancer cell growth and cellular phenotype.* PLoS One, 2010. **5**(9): p. e12905.
120. Calvo, F., et al., *Mechanotransduction and YAP-dependent matrix remodelling is required for the generation and maintenance of cancer-associated fibroblasts.* Nat Cell Biol, 2013. **15**(6): p. 637-46.
121. Georges, P.C., et al., *Increased stiffness of the rat liver precedes matrix deposition: implications for fibrosis.* Am J Physiol Gastrointest Liver Physiol, 2007. **293**(6): p. G1147-54.
122. Vandenbroucke, R.E. and C. Libert, *Is there new hope for therapeutic matrix metalloproteinase inhibition?* Nat Rev Drug Discov, 2014. **13**(12): p. 904-27.
123. Järveläinen, H., et al., *Extracellular matrix molecules: potential targets in pharmacotherapy.* Pharmacol Rev, 2009. **61**(2): p. 198-223.

124. Yao, L., et al., *Identification of EFEMP2 as a serum biomarker for the early detection of colorectal cancer with lectin affinity capture assisted secretome analysis of cultured fresh tissues.* J Proteome Res, 2012. **11**(6): p. 3281-94.
125. Schierwagen, R., et al., *Serum markers of the extracellular matrix remodeling reflect antifibrotic therapy in bile-duct ligated rats.* Frontiers in physiology, 2013. **4**: p. 195-195.
126. BUNATOVA, K., et al., *Plasma TIMP1 Level Is a Prognostic Factor in Patients with Liver Metastases.* 2012. **32**(10): p. 4601-4606.
127. Mushtaq, M.U., et al., *Tumor matrix remodeling and novel immunotherapies: the promise of matrix-derived immune biomarkers.* J Immunother Cancer, 2018. **6**(1): p. 65.
128. Hope, C., et al., *Immunoregulatory roles of versican proteolysis in the myeloma microenvironment.* Blood, 2016. **128**(5): p. 680-5.
129. Papadas, A., et al., *Versican and Versican-matrikines in Cancer Progression, Inflammation, and Immunity.* The journal of histochemistry and cytochemistry : official journal of the Histochemistry Society, 2020. **68**(12): p. 871-885.
130. Jailkhani, N., et al., *Noninvasive imaging of tumor progression, metastasis, and fibrosis using a nanobody targeting the extracellular matrix.* 2019. **116**(28): p. 14181-14190.
131. Ishihara, J., et al., *Improving Efficacy and Safety of Agonistic Anti-CD40 Antibody Through Extracellular Matrix Affinity.* Molecular Cancer Therapeutics, 2018. **17**(11): p. 2399-2411.
132. Ishihara, J., et al., *Matrix-binding checkpoint immunotherapies enhance antitumor efficacy and reduce adverse events.* 2017. **9**(415): p. eaan0401.
133. Ishihara, J., et al., *Targeted antibody and cytokine cancer immunotherapies through collagen affinity.* Sci Transl Med, 2019. **11**(487).
134. Momin, N., et al., *Anchoring of intratumorally administered cytokines to collagen safely potentiates systemic cancer immunotherapy.* Sci Transl Med, 2019. **11**(498).
135. Seif-Naraghi, S.B., et al., *Safety and efficacy of an injectable extracellular matrix hydrogel for treating myocardial infarction.* Science translational medicine, 2013. **5**(173): p. 173ra25-173ra25.
136. Sachs, N., et al., *A Living Biobank of Breast Cancer Organoids Captures Disease Heterogeneity.* Cell, 2018. **172**(1-2): p. 373-386.e10.
137. Smalley, K.S., M. Lioni, and M. Herlyn, *Life isn't flat: taking cancer biology to the next dimension.* In Vitro Cell Dev Biol Anim, 2006. **42**(8-9): p. 242-7.
138. Ihalainen, T.O., et al., *Differential basal-to-apical accessibility of lamin A/C epitopes in the nuclear lamina regulated by changes in cytoskeletal tension.* Nat Mater, 2015. **14**(12): p. 1252-1261.
139. Kilian, K.A., et al., *Geometric cues for directing the differentiation of mesenchymal stem cells.* Proc Natl Acad Sci U S A, 2010. **107**(11): p. 4872-7.
140. Zhang, D. and K.A. Kilian, *The effect of mesenchymal stem cell shape on the maintenance of multipotency.* Biomaterials, 2013. **34**(16): p. 3962-3969.
141. Théry, M., et al., *Cell distribution of stress fibres in response to the geometry of the adhesive environment.* Cell Motil Cytoskeleton, 2006. **63**(6): p. 341-55.
142. Covello, K.L., et al., *HIF-2alpha regulates Oct-4: effects of hypoxia on stem cell function, embryonic development, and tumor growth.* Genes Dev, 2006. **20**(5): p. 557-70.
143. Ito, K. and T. Suda, *Metabolic requirements for the maintenance of self-renewing stem cells.* Nature reviews. Molecular cell biology, 2014. **15**(4): p. 243-256.
144. Hutchinson, L. and R. Kirk, *High drug attrition rates—where are we going wrong?* Nature Reviews Clinical Oncology, 2011. **8**(4): p. 189-190.

145. Kola, I. and J. Landis, *Can the pharmaceutical industry reduce attrition rates?* Nat Rev Drug Discov, 2004. **3**(8): p. 711-5.
146. Seruga, B., et al., *Failures in Phase III: Causes and Consequences.* 2015. **21**(20): p. 4552-4560.
147. Stanford, S.C., *Some Reasons Why Preclinical Studies of Psychiatric Disorders Fail to Translate: What Can Be Rescued from the Misunderstanding and Misuse of Animal 'Models'?* Altern Lab Anim, 2020. **48**(3): p. 106-115.
148. Pound, P. and M. Ritskes-Hoitinga, *Is it possible to overcome issues of external validity in preclinical animal research? Why most animal models are bound to fail.* Journal of Translational Medicine, 2018. **16**(1): p. 304.
149. Prinz, F., T. Schlange, and K. Asadullah, *Believe it or not: how much can we rely on published data on potential drug targets?* Nat Rev Drug Discov, 2011. **10**(9): p. 712.
150. Begley, C.G. and L.M. Ellis, *Drug development: Raise standards for preclinical cancer research.* Nature, 2012. **483**(7391): p. 531-3.
151. Ireson, C.R., et al., *The role of mouse tumour models in the discovery and development of anticancer drugs.* British Journal of Cancer, 2019. **121**(2): p. 101-108.
152. Tentler, J.J., et al., *Patient-derived tumour xenografts as models for oncology drug development.* Nature Reviews Clinical Oncology, 2012. **9**(6): p. 338-350.
153. Combest, A.J., et al., *Genetically Engineered Cancer Models, But Not Xenografts, Faithfully Predict Anticancer Drug Exposure in Melanoma Tumors.* 2012. **17**(10): p. 1303-1316.
154. Kim, W.Y. and N.E. Sharpless, *Drug efficacy testing in mice.* Current topics in microbiology and immunology, 2012. **355**: p. 19-38.
155. Roskelley, C.D., P.Y. Desprez, and M.J. Bissell, *Extracellular matrix-dependent tissue-specific gene expression in mammary epithelial cells requires both physical and biochemical signal transduction.* Proceedings of the National Academy of Sciences of the United States of America, 1994. **91**(26): p. 12378-12382.
156. Bissell, M.J., A. Rizki, and I.S. Mian, *Tissue architecture: the ultimate regulator of breast epithelial function.* Curr Opin Cell Biol, 2003. **15**(6): p. 753-62.
157. Paszek, M.J. and V.M. Weaver, *The tension mounts: mechanics meets morphogenesis and malignancy.* J Mammary Gland Biol Neoplasia, 2004. **9**(4): p. 325-42.
158. Lowe, J.S. and P.G. Anderson, *Chapter 4 - Support Cells and the Extracellular Matrix*, in *Stevens & Lowe's Human Histology (Fourth Edition) (Fourth Edition)*, J.S. Lowe and P.G. Anderson, Editors. 2015, Mosby: Philadelphia. p. 55-70.
159. Schmeichel, K.L. and M.J. Bissell, *Modeling tissue-specific signaling and organ function in three dimensions.* J Cell Sci, 2003. **116**(Pt 12): p. 2377-88.
160. Huebsch, N. and D.J. Mooney, *Inspiration and application in the evolution of biomaterials.* Nature, 2009. **462**(7272): p. 426-432.
161. Lee, K.Y. and D.J. Mooney, *Hydrogels for tissue engineering.* Chem Rev, 2001. **101**(7): p. 1869-79.
162. Whitesides, G.M. and B. Grzybowski, *Self-assembly at all scales.* Science, 2002. **295**(5564): p. 2418-21.
163. Gu, L. and D.J. Mooney, *Biomaterials and emerging anticancer therapeutics: engineering the microenvironment.* Nature reviews. Cancer, 2016. **16**(1): p. 56-66.
164. Elsdale, T. and J. Bard, *Collagen substrata for studies on cell behavior.* J Cell Biol, 1972. **54**(3): p. 626-37.

165. Lee, C.H., A. Singla, and Y. Lee, *Biomedical applications of collagen.* Int J Pharm, 2001. **221**(1-2): p. 1-22.
166. Pacak, C.A., A.A. MacKay, and D.B. Cowan, *An improved method for the preparation of type I collagen from skin.* J Vis Exp, 2014(83): p. e51011.
167. Rajan, N., et al., *Preparation of ready-to-use, storable and reconstituted type I collagen from rat tail tendon for tissue engineering applications.* Nat Protoc, 2006. **1**(6): p. 2753-8.
168. Terzi, A., et al., *Sub- and Supramolecular X-Ray Characterization of Engineered Tissues from Equine Tendon, Bovine Dermis, and Fish Skin Type-I Collagen.* Macromol Biosci, 2020. **20**(5): p. e2000017.
169. Brown, J.C., et al., *Structure and binding properties of collagen type XIV isolated from human placenta.* J Cell Biol, 1993. **120**(2): p. 557-67.
170. Hoyer, B., et al., *Jellyfish collagen scaffolds for cartilage tissue engineering.* Acta Biomaterialia, 2014. **10**(2): p. 883-892.
171. Liu, S., et al., *Marine collagen scaffolds in tissue engineering.* Current Opinion in Biotechnology, 2022. **74**: p. 92-103.
172. Felician, F.F., et al., *Collagen from Marine Biological Sources and Medical Applications.* 2018. **15**(5): p. e1700557.
173. Langasco, R., et al., *Natural collagenic skeleton of marine sponges in pharmaceutics: Innovative biomaterial for topical drug delivery.* Materials Science and Engineering: C, 2017. **70**: p. 710-720.
174. Lim, Y.-S., et al., *Marine Collagen as A Promising Biomaterial for Biomedical Applications.* Marine drugs, 2019. **17**(8): p. 467.
175. Rahman, M.A., *Collagen of Extracellular Matrix from Marine Invertebrates and Its Medical Applications.* Mar Drugs, 2019. **17**(2).
176. Avila Rodríguez, M.I., L.G. Rodríguez Barroso, and M.L. Sánchez, *Collagen: A review on its sources and potential cosmetic applications.* 2018. **17**(1): p. 20-26.
177. Song, E., et al., *Collagen scaffolds derived from a marine source and their biocompatibility.* Biomaterials, 2006. **27**(15): p. 2951-61.
178. Keller, L. and M. Pugliano, *Combined Jellyfish Collagen Type II, Human Stem Cells and Tgf-β3 as a Therapeutic Implant for Cartilage Repair.* Journal of Stem Cell Research & Therapy, 2017. **07**.
179. Alemany-Ribes, M. and C.E. Semino, *Bioengineering 3D environments for cancer models.* Adv Drug Deliv Rev, 2014. **79-80**: p. 40-9.
180. He, L., et al., *Alginate-Based Platforms for Cancer-Targeted Drug Delivery.* BioMed research international, 2020. **2020**: p. 1487259-1487259.
181. Li, J., et al., *A Novel 3D in Vitro Tumor Model Based on Silk Fibroin/Chitosan Scaffolds To Mimic the Tumor Microenvironment.* ACS Applied Materials & Interfaces, 2018. **10**(43): p. 36641-36651.
182. Chang, P.-H., et al., *Chitosan promotes cancer progression and stem cell properties in association with Wnt signaling in colon and hepatocellular carcinoma cells.* Scientific Reports, 2017. **7**(1): p. 45751.
183. Riehl, B.D., et al., *The Role of Microenvironmental Cues and Mechanical Loading Milieus in Breast Cancer Cell Progression and Metastasis.* Front Bioeng Biotechnol, 2020. **8**: p. 608526.
184. Alcoser, T.A., et al., *Probing the biophysical properties of primary breast tumor-derived fibroblasts.* Cell Mol Bioeng, 2015. **8**(1): p. 76-85.

185. Azadi, S., M. Tafazzoli Shadpour, and M.E. Warkiani, *Characterizing the effect of substrate stiffness on the extravasation potential of breast cancer cells using a 3D microfluidic model.* Biotechnol Bioeng, 2021. **118**(2): p. 823-835.
186. Vitale, C., et al., *3D Perfusable Hydrogel Recapitulating the Cancer Dynamic Environment to in Vitro Investigate Metastatic Colonization.* Polymers (Basel), 2020. **12**(11).
187. Pasini, A., et al., *Perfusion Flow Enhances Viability and Migratory Phenotype in 3D-Cultured Breast Cancer Cells.* Ann Biomed Eng, 2021.
188. Bascetin, R., et al., *A biomimetic model of 3D fluid extracellular macromolecular crowding microenvironment fine-tunes ovarian cancer cells dissemination phenotype.* Biomaterials, 2021. **269**: p. 120610.
189. Deszcz, I., et al., *Utility of direct 3D co-culture model for chondrogenic differentiation of mesenchymal stem cells on hyaluronan scaffold (Hyaff-11).* Regen Biomater, 2020. **7**(6): p. 543-552.
190. Sahai, N., M. Gogoi, and R.P. Tewari, *3D printed Chitosan Composite Scaffold for Chondrocytes differentiation.* Curr Med Imaging, 2020.
191. Norouzi, M., B. Nazari, and D.W. Miller, *Injectable hydrogel-based drug delivery systems for local cancer therapy.* Drug Discov Today, 2016. **21**(11): p. 1835-1849.
192. Nii, T., K. Makino, and Y. Tabata, *A Cancer Invasion Model Combined with Cancer-Associated Fibroblasts Aggregates Incorporating Gelatin Hydrogel Microspheres Containing a p53 Inhibitor.* Tissue Eng Part C Methods, 2019. **25**(12): p. 711-720.
193. Cao, H., et al., *Mechanoregulation of Cancer-Associated Fibroblast Phenotype in Three-Dimensional Interpenetrating Hydrogel Networks.* Langmuir, 2019. **35**(23): p. 7487-7495.
194. Jensen, C. and Y. Teng, *Is It Time to Start Transitioning From 2D to 3D Cell Culture?* Frontiers in molecular biosciences, 2020. **7**: p. 33-33.
195. Brock, E.J., et al., *In Vitro Models for Studying Invasive Transitions of Ductal Carcinoma In Situ.* J Mammary Gland Biol Neoplasia, 2019. **24**(1): p. 1-15.
196. Lintz, M., A. Muñoz, and C.A. Reinhart-King, *The Mechanics of Single Cell and Collective Migration of Tumor Cells.* J Biomech Eng, 2017. **139**(2): p. 0210051-9.
197. Friedl, P. and E.B. Bröcker, *The biology of cell locomotion within three-dimensional extracellular matrix.* Cell Mol Life Sci, 2000. **57**(1): p. 41-64.
198. Liu, C., et al., *Hybrid collagen alginate hydrogel as a platform for 3D tumor spheroid invasion.* Acta Biomater, 2018. **75**: p. 213-225.
199. Kar, S., et al., *Tissue-engineered nanoclay-based 3D in vitro breast cancer model for studying breast cancer metastasis to bone.* J Tissue Eng Regen Med, 2019. **13**(2): p. 119-130.
200. Holen, I., et al., *Human breast cancer bone metastasis in vitro and in vivo: a novel 3D model system for studies of tumour cell-bone cell interactions.* Clin Exp Metastasis, 2015. **32**(7): p. 689-702.
201. Devarasetty, M., et al., *Simulating the human colorectal cancer microenvironment in 3D tumor-stroma co-cultures in vitro and in vivo.* Sci Rep, 2020. **10**(1): p. 9832.
202. Shimojo, A.A.M., et al., *Scaffolds for Tissue Engineering: A State-of-the-Art Review Concerning Types, Properties, Materials, Processing, and Characterization*, in *Racing for the Surface: Antimicrobial and Interface Tissue Engineering*, B. Li, et al., Editors. 2020, Springer International Publishing: Cham. p. 647-676.

203. Qiao, H. and T. Tang, *Engineering 3D approaches to model the dynamic microenvironments of cancer bone metastasis.* Bone Research, 2018. **6**(1): p. 3.
204. González Díaz, E.C., et al., *Tissue-engineered 3D models for elucidating primary and metastatic bone cancer progression.* Acta Biomater, 2019. **99**: p. 18-32.
205. Liaw, C.Y., S. Ji, and M. Guvendiren, *Engineering 3D Hydrogels for Personalized In Vitro Human Tissue Models.* Adv Healthc Mater, 2018. **7**(4).
206. García-Gareta, E., et al., *Decellularised scaffolds: just a framework? Current knowledge and future directions.* J Tissue Eng, 2020. **11**: p. 2041731420942903.
207. Hoshiba, T., *Decellularized Extracellular Matrix for Cancer Research.* 2019. **12**(8): p. 1311.
208. Jin, Q., et al., *Decellularized breast matrix as bioactive microenvironment for in vitro three-dimensional cancer culture.* J Cell Physiol, 2019. **234**(4): p. 3425-3435.
209. Weiswald, L.B., D. Bellet, and V. Dangles-Marie, *Spherical cancer models in tumor biology.* Neoplasia, 2015. **17**(1): p. 1-15.
210. Kim, S.-j., et al., *Engineering Multi-Cellular Spheroids for Tissue Engineering and Regenerative Medicine.* Advanced Healthcare Materials, 2020. **n/a**(n/a): p. 2000608.
211. Rodrigues, T., et al., *Emerging tumor spheroids technologies for 3D in vitro cancer modeling.* Pharmacol Ther, 2018. **184**: p. 201-211.
212. Lin, R.Z. and H.Y. Chang, *Recent advances in three-dimensional multicellular spheroid culture for biomedical research.* Biotechnol J, 2008. **3**(9-10): p. 1172-84.
213. Singh, S.K., et al., *Critical role of three-dimensional tumorsphere size on experimental outcome.* 2020. **69**(5): p. 333-338.
214. Lee, J.M., et al., *Generation of uniform-sized multicellular tumor spheroids using hydrogel microwells for advanced drug screening.* Scientific reports, 2018. **8**(1): p. 17145-17145.
215. Rouwkema, J., et al., *Supply of nutrients to cells in engineered tissues.* Biotechnol Genet Eng Rev, 2010. **26**: p. 163-78.
216. Rademakers, T., et al., *Oxygen and nutrient delivery in tissue engineering: Approaches to graft vascularization.* Journal of tissue engineering and regenerative medicine, 2019. **13**(10): p. 1815-1829.
217. Malda, J., T.J. Klein, and Z. Upton, *The roles of hypoxia in the in vitro engineering of tissues.* Tissue Eng, 2007. **13**(9): p. 2153-62.
218. Volkmer, E., et al., *Hypoxia in static and dynamic 3D culture systems for tissue engineering of bone.* Tissue Eng Part A, 2008. **14**(8): p. 1331-40.
219. Leek, R., et al., *Methods: Using Three-Dimensional Culture (Spheroids) as an In Vitro Model of Tumour Hypoxia.* Adv Exp Med Biol, 2016. **899**: p. 167-96.
220. Däster, S., et al., *Induction of hypoxia and necrosis in multicellular tumor spheroids is associated with resistance to chemotherapy treatment.* Oncotarget, 2017. **8**(1): p. 1725-1736.
221. Riffle, S. and R.S. Hegde, *Modeling tumor cell adaptations to hypoxia in multicellular tumor spheroids.* Journal of experimental & clinical cancer research : CR, 2017. **36**(1): p. 102-102.
222. L'Espérance, S., et al., *Global gene expression analysis of early response to chemotherapy treatment in ovarian cancer spheroids.* BMC Genomics, 2008. **9**: p. 99.
223. Tofani, L.B., et al., *Establishment and characterization of an in vitro 3D ovarian cancer model for drug screening assays.* Biotechnology Progress, 2020. **n/a**(n/a): p. e3034.

224. Linxweiler, J., et al., *Patient-derived, three-dimensional spheroid cultures provide a versatile translational model for the study of organ-confined prostate cancer.* J Cancer Res Clin Oncol, 2019. **145**(3): p. 551-559.
225. Kunz-Schughart, L.A., et al., *The use of 3-D cultures for high-throughput screening: the multicellular spheroid model.* J Biomol Screen, 2004. **9**(4): p. 273-85.
226. Fang, Y. and R.M. Eglen, *Three-Dimensional Cell Cultures in Drug Discovery and Development.* SLAS discovery : advancing life sciences R & D, 2017. **22**(5): p. 456-472.
227. Cui, X., Y. Hartanto, and H. Zhang, *Advances in multicellular spheroids formation.* 2017. **14**(127): p. 20160877.
228. Tan, B., et al., *Advances and trends of hydrogel therapy platform in localized tumor treatment: A review.* J Biomed Mater Res A, 2021. **109**(4): p. 404-425.
229. Park, K.M., D. Lewis, and S. Gerecht, *Bioinspired Hydrogels to Engineer Cancer Microenvironments.* Annu Rev Biomed Eng, 2017. **19**: p. 109-133.
230. Kumar, S. and A. Bajaj, *Advances in self-assembled injectable hydrogels for cancer therapy.* Biomater Sci, 2020. **8**(8): p. 2055-2073.
231. Zhu, Y., et al., *Hierarchical Hydrogel Composite Interfaces with Robust Mechanical Properties for Biomedical Applications.* Adv Mater, 2019. **31**(45): p. e1804950.
232. Tse, J.R. and A.J. Engler, *Preparation of hydrogel substrates with tunable mechanical properties.* Curr Protoc Cell Biol, 2010. **Chapter 10**: p. Unit 10.16.
233. Caliari, S.R. and J.A. Burdick, *A practical guide to hydrogels for cell culture.* Nat Methods, 2016. **13**(5): p. 405-14.
234. Catoira, M.C., et al., *Overview of natural hydrogels for regenerative medicine applications.* J Mater Sci Mater Med, 2019. **30**(10): p. 115.
235. Wichterle, O. and D. LÍM, *Hydrophilic Gels for Biological Use.* Nature, 1960. **185**(4706): p. 117-118.
236. Zhu, J. and R.E. Marchant, *Design properties of hydrogel tissue-engineering scaffolds.* Expert review of medical devices, 2011. **8**(5): p. 607-626.
237. Zhu, J., *Bioactive modification of poly(ethylene glycol) hydrogels for tissue engineering.* Biomaterials, 2010. **31**(17): p. 4639-56.
238. Tibbitt, M.W. and K.S. Anseth, *Hydrogels as extracellular matrix mimics for 3D cell culture.* Biotechnol Bioeng, 2009. **103**(4): p. 655-63.
239. Sokol, E.S., et al., *Growth of human breast tissues from patient cells in 3D hydrogel scaffolds.* Breast Cancer Research, 2016. **18**(1): p. 19.
240. Xu, X., M.C. Farach-Carson, and X. Jia, *Three-dimensional in vitro tumor models for cancer research and drug evaluation.* Biotechnol Adv, 2014. **32**(7): p. 1256-1268.
241. Lancaster, M.A. and M. Huch, *Disease modelling in human organoids.* Dis Model Mech, 2019. **12**(7).
242. Drost, J. and H. Clevers, *Organoids in cancer research.* Nat Rev Cancer, 2018. **18**(7): p. 407-418.
243. Rossi, G., A. Manfrin, and M.P. Lutolf, *Progress and potential in organoid research.* Nat Rev Genet, 2018. **19**(11): p. 671-687.
244. Devarasetty, M., et al., *In Vitro Modeling of the Tumor Microenvironment in Tumor Organoids.* Tissue Eng Regen Med, 2020.
245. Tuveson, D. and H. Clevers, *Cancer modeling meets human organoid technology.* Science, 2019. **364**(6444): p. 952-955.

246. Simian, M. and M.J. Bissell, *Organoids: A historical perspective of thinking in three dimensions.* The Journal of cell biology, 2017. **216**(1): p. 31-40.
247. Abdel Fattah, A.R. and A. Ranga, *Nanoparticles as Versatile Tools for Mechanotransduction in Tissues and Organoids.* Frontiers in bioengineering and biotechnology, 2020. **8**: p. 240-240.
248. Abdeen, A.A., et al., *Temporal Modulation of Stem Cell Activity Using Magnetoactive Hydrogels.* Advanced healthcare materials, 2016. **5**(19): p. 2536-2544.
249. Gjorevski, N., et al., *Designer matrices for intestinal stem cell and organoid culture.* Nature, 2016. **539**(7630): p. 560-564.
250. Hushka, E.A., et al., *Relaxation of Extracellular Matrix Forces Directs Crypt Formation and Architecture in Intestinal Organoids.* Adv Healthc Mater, 2020. **9**(8): p. e1901214.
251. Kim, J., B.-K. Koo, and J.A. Knoblich, *Human organoids: model systems for human biology and medicine.* Nature reviews. Molecular cell biology, 2020. **21**(10): p. 571-584.
252. Lu, T., Y. Li, and T. Chen, *Techniques for fabrication and construction of three-dimensional scaffolds for tissue engineering.* International journal of nanomedicine, 2013. **8**: p. 337-350.
253. Paradiso, F., et al., *Marine Collagen Substrates for 2D and 3D Ovarian Cancer Cell Systems.* Frontiers in bioengineering and biotechnology, 2019. **7**: p. 343-343.
254. Chan, B.P. and K.W. Leong, *Scaffolding in tissue engineering: general approaches and tissue-specific considerations.* European spine journal : official publication of the European Spine Society, the European Spinal Deformity Society, and the European Section of the Cervical Spine Research Society, 2008. **17 Suppl 4**(Suppl 4): p. 467-479.
255. Karami, D., N. Richbourg, and V. Sikavitsas, *Dynamic in vitro models for tumor tissue engineering.* Cancer Lett, 2019. **449**: p. 178-185.
256. Sergio, S., et al., *3D-microenvironments initiate TCF4 expression rescuing nuclear β-catenin activity in MCF-7 breast cancer cells.* Acta Biomater, 2020. **103**: p. 153-164.
257. Balachander, G.M., et al., *Enhanced Metastatic Potential in a 3D Tissue Scaffold toward a Comprehensive in Vitro Model for Breast Cancer Metastasis.* ACS Applied Materials & Interfaces, 2015. **7**(50): p. 27810-27822.
258. Hayn, A., T. Fischer, and C.T. Mierke, *Inhomogeneities in 3D Collagen Matrices Impact Matrix Mechanics and Cancer Cell Migration.* Frontiers in cell and developmental biology, 2020. **8**: p. 593879-593879.
259. Liverani, C., et al., *Investigating the Mechanobiology of Cancer Cell-ECM Interaction Through Collagen-Based 3D Scaffolds.* Cell Mol Bioeng, 2017. **10**(3): p. 223-234.
260. Sapudom, J., et al., *Fibril bending stiffness of 3D collagen matrices instructs spreading and clustering of invasive and non-invasive breast cancer cells.* Biomaterials, 2019. **193**: p. 47-57.
261. Ferlay, J., et al., *Cancer incidence and mortality patterns in Europe: Estimates for 40 countries and 25 major cancers in 2018.* Eur J Cancer, 2018. **103**: p. 356-387.
262. Dyba, T., et al., *The European cancer burden in 2020: Incidence and mortality estimates for 40 countries and 25 major cancers.* Eur J Cancer, 2021. **157**: p. 308-347.
263. Webb, P.M. and S.J. Jordan, *Epidemiology of epithelial ovarian cancer.* Best Pract Res Clin Obstet Gynaecol, 2017. **41**: p. 3-14.
264. International, W.C.R.F., *Diet, nutrition, physical activity and ovarian cancer.* 2018.
265. Roett, M.A. and P. Evans, *Ovarian cancer: an overview.* Am Fam Physician, 2009. **80**(6): p. 609-16.

266. Cress, R.D., et al., *Characteristics of Long-Term Survivors of Epithelial Ovarian Cancer.* Obstet Gynecol, 2015. **126**(3): p. 491-497.
267. Menon, U., M. Griffin, and A. Gentry-Maharaj, *Ovarian cancer screening--current status, future directions.* Gynecol Oncol, 2014. **132**(2): p. 490-5.
268. Jacobs, I.J., et al., *Ovarian cancer screening and mortality in the UK Collaborative Trial of Ovarian Cancer Screening (UKCTOCS): a randomised controlled trial.* The Lancet, 2016. **387**(10022): p. 945-956.
269. Kroeger, P.T., Jr. and R. Drapkin, *Pathogenesis and heterogeneity of ovarian cancer.* Curr Opin Obstet Gynecol, 2017. **29**(1): p. 26-34.
270. Kurman, R.J. and M. Shih Ie, *The Dualistic Model of Ovarian Carcinogenesis: Revisited, Revised, and Expanded.* Am J Pathol, 2016. **186**(4): p. 733-47.
271. Hu, Y., et al., *Are Epithelial Ovarian Cancers of the Mesenchymal Subtype Actually Intraperitoneal Metastases to the Ovary?* 2020. **8**.
272. Perets, R., et al., *Transformation of the fallopian tube secretory epithelium leads to high-grade serous ovarian cancer in Brca;Tp53;Pten models.* Cancer Cell, 2013. **24**(6): p. 751-65.
273. Kim, J., et al., *The ovary is an alternative site of origin for high-grade serous ovarian cancer in mice.* Endocrinology, 2015. **156**(6): p. 1975-81.
274. Zhang, S., et al., *Both fallopian tube and ovarian surface epithelium are cells-of-origin for high-grade serous ovarian carcinoma.* Nature Communications, 2019. **10**(1): p. 5367.
275. Bowtell, D.D., et al., *Rethinking ovarian cancer II: reducing mortality from high-grade serous ovarian cancer.* Nature Reviews Cancer, 2015. **15**(11): p. 668-679.
276. Nieman, K.M., et al., *Adipocytes promote ovarian cancer metastasis and provide energy for rapid tumor growth.* Nat Med, 2011. **17**(11): p. 1498-503.
277. Kurman, R.J. and I.-M. Shih, *The origin and pathogenesis of epithelial ovarian cancer: a proposed unifying theory.* The American journal of surgical pathology, 2010. **34**(3): p. 433-443.
278. Karst, A.M. and R. Drapkin, *Ovarian Cancer Pathogenesis: A Model in Evolution.* Journal of Oncology, 2010. **2010**: p. 932371.
279. Levanon, K., C. Crum, and R. Drapkin, *New insights into the pathogenesis of serous ovarian cancer and its clinical impact.* Journal of clinical oncology : official journal of the American Society of Clinical Oncology, 2008. **26**(32): p. 5284-5293.
280. Berek, J.S., et al., *Cancer of the ovary, fallopian tube, and peritoneum.* Int J Gynaecol Obstet, 2018. **143 Suppl 2**: p. 59-78.
281. Gadducci, A., et al., *Current strategies for the targeted treatment of high-grade serous epithelial ovarian cancer and relevance of BRCA mutational status.* Journal of Ovarian Research, 2019. **12**(1): p. 9.
282. Lengyel, E., *Ovarian cancer development and metastasis.* Am J Pathol, 2010. **177**(3): p. 1053-64.
283. Lengyel, E., et al., *Epithelial ovarian cancer experimental models.* Oncogene, 2014. **33**(28): p. 3619-3633.
284. Mieulet, V., et al., *Stiffness increases with myofibroblast content and collagen density in mesenchymal high grade serous ovarian cancer.* Scientific Reports, 2021. **11**(1): p. 4219.
285. Givel, A.-M., et al., *miR200-regulated CXCL12β promotes fibroblast heterogeneity and immunosuppression in ovarian cancers.* Nature Communications, 2018. **9**(1): p. 1056.

286. Zhang, Q., C. Wang, and W.A. Cliby, *Cancer-associated stroma significantly contributes to the mesenchymal subtype signature of serous ovarian cancer.* Gynecol Oncol, 2019. **152**(2): p. 368-374.
287. Davidson, B., C.G. Trope, and R. Reich, *The role of the tumor stroma in ovarian cancer.* Frontiers in oncology, 2014. **4**: p. 104-104.
288. Winterhoff, B.J., et al., *Single cell sequencing reveals heterogeneity within ovarian cancer epithelium and cancer associated stromal cells.* Gynecol Oncol, 2017. **144**(3): p. 598-606.
289. Yang, Z., et al., *Reprogramming of stromal fibroblasts by SNAI2 contributes to tumor desmoplasia and ovarian cancer progression.* Molecular Cancer, 2017. **16**(1): p. 163.
290. Cheon, D.J., et al., *A collagen-remodeling gene signature regulated by TGF-β signaling is associated with metastasis and poor survival in serous ovarian cancer.* Clin Cancer Res, 2014. **20**(3): p. 711-23.
291. Zhang, H., et al., *Integrated Proteogenomic Characterization of Human High-Grade Serous Ovarian Cancer.* Cell, 2016. **166**(3): p. 755-765.
292. Pearce, O.M.T., et al., *Deconstruction of a Metastatic Tumor Microenvironment Reveals a Common Matrix Response in Human Cancers.* Cancer Discov, 2018. **8**(3): p. 304-319.
293. Morin, P.J. and A.T. Weeraratna, *Genetically-defined ovarian cancer mouse models.* J Pathol, 2016. **238**(2): p. 180-4.
294. Karnezis, A.N. and K.R. Cho, *Of mice and women - Non-ovarian origins of "ovarian" cancer.* Gynecol Oncol, 2017. **144**(1): p. 5-7.
295. Perets, R. and R. Drapkin, *It's Totally Tubular....Riding The New Wave of Ovarian Cancer Research.* Cancer Res, 2016. **76**(1): p. 10-7.
296. Karnezis, A.N. and K.R. Cho, *Preclinical Models of Ovarian Cancer: Pathogenesis, Problems, and Implications for Prevention.* Clinical obstetrics and gynecology, 2017. **60**(4): p. 789-800.
297. Hasan, N., A.W. Ohman, and D.M.J.T.C.R. Dinulescu, *The promise and challenge of ovarian cancer models.* 2015, 2015. **4**(1): p. 14-28.
298. Johnson, P.A. and J.R. Giles, *The hen as a model of ovarian cancer.* Nat Rev Cancer, 2013. **13**(6): p. 432-6.
299. Barbolina, M.V., et al., *Microenvironmental regulation of membrane type 1 matrix metalloproteinase activity in ovarian carcinoma cells via collagen-induced EGR1 expression.* J Biol Chem, 2007. **282**(7): p. 4924-4931.
300. Allen, H.J., et al., *Isolation and morphologic characterization of human ovarian carcinoma cell clusters present in effusions.* Exp Cell Biol, 1987. **55**(4): p. 194-208.
301. Kenny, H.A., et al., *The first line of intra-abdominal metastatic attack: breaching the mesothelial cell layer.* Cancer Discov, 2011. **1**(2): p. 100-2.
302. Kenny, H.A., et al., *Use of a novel 3D culture model to elucidate the role of mesothelial cells, fibroblasts and extra-cellular matrices on adhesion and invasion of ovarian cancer cells to the omentum.* Int J Cancer, 2007. **121**(7): p. 1463-72.
303. Khan, S.M., et al., *In vitro metastatic colonization of human ovarian cancer cells to the omentum.* Clin Exp Metastasis, 2010. **27**(3): p. 185-96.
304. Nanki, Y., et al., *Patient-derived ovarian cancer organoids capture the genomic profiles of primary tumours applicable for drug sensitivity and resistance testing.* Scientific Reports, 2020. **10**(1): p. 12581.
305. Sisman, Y., et al., *Organoids and epithelial ovarian cancer - a future tool for personalized treatment decisions? (Review).* Mol Clin Oncol, 2022. **16**(2): p. 29.

306. Weeber, F., et al., *Tumor Organoids as a Pre-clinical Cancer Model for Drug Discovery.* Cell Chemical Biology, 2017. **24**(9): p. 1092-1100.
307. Driehuis, E. and H. Clevers, *CRISPR/Cas 9 genome editing and its applications in organoids.* Am J Physiol Gastrointest Liver Physiol, 2017. **312**(3): p. G257-g265.
308. Nie, J. and E. Hashino, *Organoid technologies meet genome engineering.* EMBO Rep, 2017. **18**(3): p. 367-376.
309. Aboulkheyr Es, H., et al., *Personalized Cancer Medicine: An Organoid Approach.* Trends Biotechnol, 2018. **36**(4): p. 358-371.
310. Costa, J. and A. Ahluwalia, *Advances and Current Challenges in Intestinal in vitro Model Engineering: A Digest.* Front Bioeng Biotechnol, 2019. **7**: p. 144.
311. Mariappan, Y.K., K.J. Glaser, and R.L. Ehman, *Magnetic resonance elastography: a review.* Clin Anat, 2010. **23**(5): p. 497-511.
312. Johnson, C.L. and E.H. Telzer, *Magnetic resonance elastography for examining developmental changes in the mechanical properties of the brain.* Developmental Cognitive Neuroscience, 2018. **33**: p. 176-181.
313. Ozturk, A., et al., *Principles of ultrasound elastography.* Abdom Radiol (NY), 2018. **43**(4): p. 773-785.
314. Cieśluk, M., et al., *Nanomechanics and Histopathology as Diagnostic Tools to Characterize Freshly Removed Human Brain Tumors.* Int J Nanomedicine, 2020. **15**: p. 7509-7521.
315. Engstrom, T.A., et al., *Compression stiffening in biological tissues: On the possibility of classic elasticity origins.* Physical Review E, 2019. **99**(5): p. 052413.
316. Perepelyuk, M., et al., *Normal and Fibrotic Rat Livers Demonstrate Shear Strain Softening and Compression Stiffening: A Model for Soft Tissue Mechanics.* PLoS One, 2016. **11**(1): p. e0146588.
317. Pogoda, K. and P.A. Janmey, *Glial Tissue Mechanics and Mechanosensing by Glial Cells.* Front Cell Neurosci, 2018. **12**: p. 25.
318. Chen, H., et al., *Porous Scaffold Design for Additive Manufacturing in Orthopedics: A Review.* 2020. **8**.
319. Imamura, Y., et al., *Comparison of 2D- and 3D-culture models as drug-testing platforms in breast cancer.* Oncol Rep, 2015. **33**(4): p. 1837-43.
320. Pampaloni, F., E.G. Reynaud, and E.H. Stelzer, *The third dimension bridges the gap between cell culture and live tissue.* Nat Rev Mol Cell Biol, 2007. **8**(10): p. 839-45.
321. Thoma, C.R., et al., *3D cell culture systems modeling tumor growth determinants in cancer target discovery.* Adv Drug Deliv Rev, 2014. **69-70**: p. 29-41.
322. Zimmermann, M., C. Box, and S.A. Eccles, *Two-dimensional vs. three-dimensional in vitro tumor migration and invasion assays.* Methods Mol Biol, 2013. **986**: p. 227-52.
323. Fischbach, C., et al., *Engineering tumors with 3D scaffolds.* Nat Methods, 2007. **4**(10): p. 855-60.
324. Fischbach, C., et al., *Cancer cell angiogenic capability is regulated by 3D culture and integrin engagement.* Proceedings of the National Academy of Sciences of the United States of America, 2009. **106**(2): p. 399-404.
325. Kenny, P.A. and M.J. Bissell, *Tumor reversion: correction of malignant behavior by microenvironmental cues.* International journal of cancer, 2003. **107**(5): p. 688-695.
326. Liang, Y., et al., *A cell-instructive hydrogel to regulate malignancy of 3D tumor spheroids with matrix rigidity.* Biomaterials, 2011. **32**(35): p. 9308-15.

327. Loessner, D., et al., *Bioengineered 3D platform to explore cell-ECM interactions and drug resistance of epithelial ovarian cancer cells.* Biomaterials, 2010. **31**(32): p. 8494-506.
328. Kenny, P.A., et al., *The morphologies of breast cancer cell lines in three-dimensional assays correlate with their profiles of gene expression.* Mol Oncol, 2007. **1**(1): p. 84-96.
329. Akter, F., *Chapter 2 - Principles of Tissue Engineering*, in *Tissue Engineering Made Easy*, F. Akter, Editor. 2016, Academic Press. p. 3-16.
330. Horch, R.E., et al., *Cancer research by means of tissue engineering--is there a rationale?* Journal of cellular and molecular medicine, 2013. **17**(10): p. 1197-1206.
331. Almouemen, N., H.M. Kelly, and C. O'Leary, *Tissue Engineering: Understanding the Role of Biomaterials and Biophysical Forces on Cell Functionality Through Computational and Structural Biotechnology Analytical Methods.* Computational and structural biotechnology journal, 2019. **17**: p. 591-598.
332. Mhanna, R. and A.J.T.E.f.A.O. Hasan, *Introduction to tissue engineering.* 2017: p. 1-34.
333. Gu, L. and D.J. Mooney, *Biomaterials and emerging anticancer therapeutics: engineering the microenvironment.* Nature Reviews Cancer, 2016. **16**(1): p. 56-66.
334. Hollister, S.J., *Porous scaffold design for tissue engineering.* Nat Mater, 2005. **4**(7): p. 518-24.
335. Taraballi, F., et al., *Biomimetic collagenous scaffold to tune inflammation by targeting macrophages.* 2016. **7**: p. 2041731415624667.
336. Corradetti, B., et al., *Immune tuning scaffold for the local induction of a pro-regenerative environment.* Scientific Reports, 2017. **7**(1): p. 17030.
337. Corradetti, B., et al., *Chondroitin Sulfate Immobilized on a Biomimetic Scaffold Modulates Inflammation While Driving Chondrogenesis.* Stem cells translational medicine, 2016. **5**(5): p. 670-682.
338. Minardi, S., et al., *Multiscale patterning of a biomimetic scaffold integrated with composite microspheres.* Small (Weinheim an der Bergstrasse, Germany), 2014. **10**(19): p. 3943-3953.
339. Ma, Y.J., et al. *Growth of DLD-1 Colon Cancer Cells on Variotis™ Scaffolds of Controlled Porosity: A Preliminary Study*. in *Journal of Biomimetics, Biomaterials and Tissue Engineering*. 2010. Trans Tech Publ.
340. Le, M.N., et al., *Evaluation of the effect of 3D porous Chitosan-alginate scaffold stiffness on breast cancer proliferation and migration.* J Biomed Mater Res A, 2021. **109**(10): p. 1990-2000.
341. Xu, K., et al., *3D porous chitosan-alginate scaffold stiffness promotes differential responses in prostate cancer cell lines.* Biomaterials, 2019. **217**: p. 119311.
342. Florczyk, S.J., et al., *3D Porous Chitosan-Alginate Scaffolds Promote Proliferation and Enrichment of Cancer Stem-Like Cells.* J Mater Chem B, 2016. **4**(38): p. 6326-6334.
343. Florczyk, S.J., et al., *3D porous chitosan-alginate scaffolds: a new matrix for studying prostate cancer cell-lymphocyte interactions in vitro.* Adv Healthc Mater, 2012. **1**(5): p. 590-9.
344. Florczyk, S.J., et al., *Porous chitosan-hyaluronic acid scaffolds as a mimic of glioblastoma microenvironment ECM.* Biomaterials, 2013. **34**(38): p. 10143-50.
345. Miller, E.J. and S. Gay, *Collagen: an overview.* Methods Enzymol, 1982. **82 Pt A**: p. 3-32.
346. Dong, C. and Y. Lv, *Application of Collagen Scaffold in Tissue Engineering: Recent Advances and New Perspectives.* Polymers (Basel), 2016. **8**(2).

347. King, M.W., *Extracellular Matrix: Glycosaminoglycans and Proteoglycans*, in *Integrative Medical Biochemistry Examination and Board Review*. 2014, McGraw-Hill Education: New York, NY.
348. Fraser, J.R.E., T.C. Laurent, and U.B.G. Laurent, *Hyaluronan: its nature, distribution, functions and turnover.* 1997. **242**(1): p. 27-33.
349. Jiang, D., J. Liang, and P.W. Noble, *Hyaluronan as an immune regulator in human diseases.* Physiological reviews, 2011. **91**(1): p. 221-264.
350. Simpson, M.A. and P. Heldin, *Hyaluronan signaling and turnover. Preface.* Adv Cancer Res, 2014. **123**: p. xv-xvi.
351. Mohammadi, H. and E. Sahai, *Mechanisms and impact of altered tumour mechanics.* Nature Cell Biology, 2018. **20**(7): p. 766-774.
352. Paszek, M.J., et al., *Tensional homeostasis and the malignant phenotype.* Cancer Cell, 2005. **8**(3): p. 241-254.
353. Barnes, J.M., L. Przybyla, and V.M. Weaver, *Tissue mechanics regulate brain development, homeostasis and disease.* Journal of Cell Science, 2017. **130**(1): p. 71-82.
354. Boehm, K., et al., *Shear wave elastography for localization of prostate cancer lesions and assessment of elasticity thresholds: implications for targeted biopsies and active surveillance protocols.* J Urol, 2015. **193**(3): p. 794-800.
355. Walker, C., E. Mojares, and A. Del Río Hernández, *Role of Extracellular Matrix in Development and Cancer Progression.* International journal of molecular sciences, 2018. **19**(10): p. 3028.
356. Toole, B.P., T.N. Wight, and M.I. Tammi, *Hyaluronan-cell interactions in cancer and vascular disease.* J Biol Chem, 2002. **277**(7): p. 4593-6.
357. Misra, S., et al., *Hyaluronan-CD44 interactions as potential targets for cancer therapy.* Febs j, 2011. **278**(9): p. 1429-43.
358. Toole, B.P., *Hyaluronan promotes the malignant phenotype.* Glycobiology, 2002. **12**(3): p. 37R-42R.
359. Aya, K.L. and R. Stern, *Hyaluronan in wound healing: rediscovering a major player.* Wound Repair Regen, 2014. **22**(5): p. 579-93.
360. Laurent, T.C., U.B. Laurent, and J.R. Fraser, *The structure and function of hyaluronan: An overview.* Immunol Cell Biol, 1996. **74**(2): p. A1-7.
361. Jiang, H. and F. Grinnell, *Cell–Matrix Entanglement and Mechanical Anchorage of Fibroblasts in Three-dimensional Collagen Matrices.* 2005. **16**(11): p. 5070-5076.
362. Delmage, J.M., et al., *The selective suppression of immunogenicity by hyaluronic acid.* Ann Clin Lab Sci, 1986. **16**(4): p. 303-10.
363. Ponta, H., L. Sherman, and P.A. Herrlich, *CD44: from adhesion molecules to signalling regulators.* Nat Rev Mol Cell Biol, 2003. **4**(1): p. 33-45.
364. Tian, X., et al., *High-molecular-mass hyaluronan mediates the cancer resistance of the naked mole rat.* Nature, 2013. **499**(7458): p. 346-9.
365. Litwiniuk, M., et al., *Hyaluronic Acid in Inflammation and Tissue Regeneration.* Wounds, 2016. **28**(3): p. 78-88.
366. Ruppert, S.M., et al., *Tissue integrity signals communicated by high-molecular weight hyaluronan and the resolution of inflammation.* Immunologic research, 2014. **58**(2-3): p. 186-192.

367. Mohammadkarim, A., et al., *The Mechanical Characteristics of Human Endothelial Cells in Response to Single Ionizing Radiation Doses By Using Micropipette Aspiration Technique.* 2019. **16**(4): p. 275--287.
368. González-Bermúdez, B., G.V. Guinea, and G.R. Plaza, *Advances in Micropipette Aspiration: Applications in Cell Biomechanics, Models, and Extended Studies.* Biophysical Journal, 2019. **116**(4): p. 587-594.
369. Hogan, B., et al., *Characterizing Cell Adhesion by Using Micropipette Aspiration.* Biophysical Journal, 2015. **109**(2): p. 209-219.
370. Yousafzai, M.S., et al., *Investigating the effect of cell substrate on cancer cell stiffness by optical tweezers.* J Biomech, 2017. **60**: p. 266-269.
371. Huang, H., et al., *Recent Advances on the Model, Measurement Technique, and Application of Single Cell Mechanics.* Int J Mol Sci, 2020. **21**(17).
372. Kim, H., et al., *Quantitative measurements of intercellular adhesion between a macrophage and cancer cells using a cup-attached AFM chip.* Colloids and Surfaces B: Biointerfaces, 2017. **155**: p. 366-372.
373. Hayashi, K. and M. Iwata, *Stiffness of cancer cells measured with an AFM indentation method.* Journal of the Mechanical Behavior of Biomedical Materials, 2015. **49**: p. 105-111.
374. Luo, Q., et al., *Cell stiffness determined by atomic force microscopy and its correlation with cell motility.* Biochimica et Biophysica Acta (BBA) - General Subjects, 2016. **1860**(9): p. 1953-1960.
375. Xu, W., et al., *Cell Stiffness Is a Biomarker of the Metastatic Potential of Ovarian Cancer Cells.* PLOS ONE, 2012. **7**(10): p. e46609.
376. Li, M., et al., *Atomic force microscopy for revealing micro/nanoscale mechanics in tumor metastasis: from single cells to microenvironmental cues.* Acta Pharmacologica Sinica, 2021. **42**(3): p. 323-339.
377. Taubenberger, A.V., et al., *3D Microenvironment Stiffness Regulates Tumor Spheroid Growth and Mechanics via p21 and ROCK.* Advanced Biosystems, 2019. **3**(9): p. 1900128.
378. Glentis, A., et al., *Cancer-associated fibroblasts induce metalloprotease-independent cancer cell invasion of the basement membrane.* Nature Communications, 2017. **8**(1): p. 924.
379. Picout, D.R. and S.B. Ross-Murphy, *Rheology of biopolymer solutions and gels.* ScientificWorldJournal, 2003. **3**: p. 105-21.
380. Janmey, P.A. and M. Schliwa, *Rheology.* Current biology : CB, 2008. **18**(15): p. R639-R641.
381. Mathieu, S. and J.-B. Manneville, *Intracellular mechanics: connecting rheology and mechanotransduction.* Current Opinion in Cell Biology, 2019. **56**: p. 34-44.
382. Andrikakou, P., K. Vickraman, and H. Arora, *On the behaviour of lung tissue under tension and compression.* Sci Rep, 2016. **6**: p. 36642.
383. Park, S. and G.A. Ateshian, *Dynamic response of immature bovine articular cartilage in tension and compression, and nonlinear viscoelastic modeling of the tensile response.* J Biomech Eng, 2006. **128**(4): p. 623-30.
384. Frank, E., et al., *A versatile shear and compression apparatus for mechanical stimulation of tissue culture explants.* Journal of biomechanics, 2000. **33**: p. 1523-7.

385. Deptuła, P., et al., *Tissue Rheology as a Possible Complementary Procedure to Advance Histological Diagnosis of Colon Cancer.* ACS Biomaterials Science & Engineering, 2020. **6**(10): p. 5620-5631.
386. Eltom, A., G. Zhong, and A. Muhammad, *Scaffold Techniques and Designs in Tissue Engineering Functions and Purposes: A Review.* Advances in Materials Science and Engineering, 2019. **2019**: p. 3429527.
387. Han, F., et al., *Tissue Engineering and Regenerative Medicine: Achievements, Future, and Sustainability in Asia.* 2020. **8**.
388. Bussard, K.M., et al., *Tumor-associated stromal cells as key contributors to the tumor microenvironment.* Breast Cancer Research, 2016. **18**(1): p. 84.
389. Ogawa, Y., et al., *Three Distinct Stroma Types in Human Pancreatic Cancer Identified by Image Analysis of Fibroblast Subpopulations and Collagen.* Clinical Cancer Research, 2021. **27**(1): p. 107.
390. Li, L., S. Tang, and X. Tang, *Thymic Stromal Lymphopoietin Promotes Fibrosis and Activates Mitogen-Activated Protein Kinases in MRC-5 Cells.* Med Sci Monit, 2016. **22**: p. 2357-62.
391. Heylen, N., et al., *Effect of MRC-5 fibroblast conditioned medium on breast cancer cell motility and invasion in vitro.* Clin Exp Metastasis, 1998. **16**(2): p. 193-203.
392. Wang, W., et al., *Met kinase inhibitor E7050 reverses three different mechanisms of hepatocyte growth factor-induced tyrosine kinase inhibitor resistance in EGFR mutant lung cancer.* Clin Cancer Res, 2012. **18**(6): p. 1663-71.
393. Ding, S.-M., et al., *The role of cancer-associated fibroblast MRC-5 in pancreatic cancer.* Journal of Cancer, 2018. **9**(3): p. 614-628.
394. Ding, S., et al., *MRC-5 fibroblast-conditioned medium influences multiple pathways regulating invasion, migration, proliferation, and apoptosis in hepatocellular carcinoma.* Journal of Translational Medicine, 2015. **13**(1): p. 237.
395. Bissell, M.J. and D. Radisky, *Putting tumours in context.* Nat Rev Cancer, 2001. **1**(1): p. 46-54.
396. Xu, J., et al., *Advances in 3D peptide hydrogel models in cancer research.* npj Science of Food, 2021. **5**(1): p. 14.
397. Ishiguro, T., et al., *Tumor-derived spheroids: Relevance to cancer stem cells and clinical applications.* Cancer Sci, 2017. **108**(3): p. 283-289.
398. Acerbi, I., et al., *Human breast cancer invasion and aggression correlates with ECM stiffening and immune cell infiltration.* Integr Biol (Camb), 2015. **7**(10): p. 1120-34.
399. Apoorva, F.N.U., et al., *Award Winner in the Young Investigator Category, 2017 Society for Biomaterials Annual Meeting and Exposition, Minneapolis, MN, April 05-08, 2017: Lymph node stiffness-mimicking hydrogels regulate human B-cell lymphoma growth and cell surface receptor expression in a molecular subtype-specific manner.* J Biomed Mater Res A, 2017. **105**(7): p. 1833-1844.
400. Zeeman, R., et al., *Crosslinking and modification of dermal sheep collagen using 1, 4-butanediol diglycidyl ether.* J Biomed Mater Res, 1999. **46**(3): p. 424-33.
401. Guimarães, C.F., et al., *The stiffness of living tissues and its implications for tissue engineering.* Nature Reviews Materials, 2020. **5**(5): p. 351-370.
402. Park, J.S., et al., *The effect of matrix stiffness on the differentiation of mesenchymal stem cells in response to TGF-β.* Biomaterials, 2011. **32**(16): p. 3921-30.

403. Asano, S., et al., *Matrix stiffness regulates migration of human lung fibroblasts.* Physiol Rep, 2017. **5**(9).
404. Dittmar, R., et al., *Assessment of cell viability in three-dimensional scaffolds using cellular auto-fluorescence.* Tissue Eng Part C Methods, 2012. **18**(3): p. 198-204.
405. Tam, T.T., et al., *Evaluation of cell viability of porous scaffold fabricated via freeze-drying technique for vascular tissue engineering.* 2020. **2267**(1): p. 020007.
406. Monteran, L. and N. Erez, *The Dark Side of Fibroblasts: Cancer-Associated Fibroblasts as Mediators of Immunosuppression in the Tumor Microenvironment.* 2019. **10**.
407. Khalil, H., et al., *Fibroblast-specific TGF-β-Smad2/3 signaling underlies cardiac fibrosis.* J Clin Invest, 2017. **127**(10): p. 3770-3783.
408. Yue, X., B. Shan, and J.A. Lasky, *TGF-β: Titan of Lung Fibrogenesis.* Current enzyme inhibition, 2010. **6**(2): p. 10.2174/10067.
409. Chen, H., et al., *TGF-beta induces fibroblast activation protein expression; fibroblast activation protein expression increases the proliferation, adhesion, and migration of HO-8910PM [corrected].* Exp Mol Pathol, 2009. **87**(3): p. 189-94.
410. Holm Nielsen, S., et al., *Serological Assessment of Activated Fibroblasts by alpha-Smooth Muscle Actin (α-SMA): A Noninvasive Biomarker of Activated Fibroblasts in Lung Disorders.* Transl Oncol, 2019. **12**(2): p. 368-374.
411. Yoon, H., et al., *TGF-β1-mediated transition of resident fibroblasts to cancer-associated fibroblasts promotes cancer metastasis in gastrointestinal stromal tumor.* Oncogenesis, 2021. **10**(2): p. 13.
412. Papageorgis, P. and T. Stylianopoulos, *Role of TGFβ in regulation of the tumor microenvironment and drug delivery (Review).* Int J Oncol, 2015. **46**(3): p. 933-943.
413. Farhat, Y., *PicoGreen Cell Proliferation Assay Protocol.* The Protocol Place, July 2012.
414. DeLeon-Pennell, K.Y., T.H. Barker, and M.L. Lindsey, *Fibroblasts: The arbiters of extracellular matrix remodeling.* Matrix Biology, 2020. **91-92**: p. 1-7.
415. Kim, J.B., *Three-dimensional tissue culture models in cancer biology.* Seminars in Cancer Biology, 2005. **15**(5): p. 365-377.
416. Carlson, M.W., et al., *Three-dimensional tissue models of normal and diseased skin.* Curr Protoc Cell Biol, 2008. **Chapter 19**: p. Unit 19.9.
417. Tolg, C., et al., *Hyaluronan and RHAMM in wound repair and the "cancerization" of stromal tissues.* Biomed Res Int, 2014. **2014**: p. 103923.
418. Tavianatou, A.G., et al., *Hyaluronan: molecular size-dependent signaling and biological functions in inflammation and cancer.* 2019. **286**(15): p. 2883-2908.
419. Tavianatou, A.-G., et al., *Molecular size-dependent specificity of hyaluronan on functional properties, morphology and matrix composition of mammary cancer cells.* Matrix Biology Plus, 2019. **3**: p. 100008.
420. Yang, C., et al., *The high and low molecular weight forms of hyaluronan have distinct effects on CD44 clustering.* J Biol Chem, 2012. **287**(51): p. 43094-107.
421. Scott, J.E., *Supramolecular organization of extracellular matrix glycosaminoglycans, in vitro and in the tissues.* Faseb j, 1992. **6**(9): p. 2639-45.
422. Huang, J., et al., *Extracellular matrix and its therapeutic potential for cancer treatment.* Signal Transduction and Targeted Therapy, 2021. **6**(1): p. 153.
423. Nikolova, M.P. and M.S. Chavali, *Recent advances in biomaterials for 3D scaffolds: A review.* Bioactive materials, 2019. **4**: p. 271-292.

424. Al-Nasiry, S., et al., *The use of Alamar Blue assay for quantitative analysis of viability, migration and invasion of choriocarcinoma cells.* Human Reproduction, 2007. **22**(5): p. 1304-1309.
425. Gaggioli, C., et al., *Fibroblast-led collective invasion of carcinoma cells with differing roles for RhoGTPases in leading and following cells.* Nature Cell Biology, 2007. **9**(12): p. 1392-1400.
426. Erdogan, B., et al., *Cancer-associated fibroblasts promote directional cancer cell migration by aligning fibronectin.* The Journal of cell biology, 2017. **216**(11): p. 3799-3816.
427. Ao, M., et al., *Stretching Fibroblasts Remodels Fibronectin and Alters Cancer Cell Migration.* Scientific Reports, 2015. **5**(1): p. 8334.
428. Jia, W., et al., *Fabrication and Comprehensive Characterization of Biomimetic Extracellular Matrix Electrospun Scaffold for Vascular Tissue Engineering Applications.* Journal of Materials Science, 2019. **54**.
429. Chang, C. and Z. Werb, *The many faces of metalloproteases: cell growth, invasion, angiogenesis and metastasis.* Trends in cell biology, 2001. **11**(11): p. S37-S43.
430. Ma, Y., et al., *Chapter 4 - Cross Talk Between Inflammation and Extracellular Matrix Following Myocardial Infarction*, in *Inflammation in Heart Failure*, W.M. Blankesteijn and R. Altara, Editors. 2015, Academic Press: Boston. p. 67-79.
431. Kawana, H., et al., *CD44 suppresses TLR-mediated inflammation.* J Immunol, 2008. **180**(6): p. 4235-45.
432. Hautmann Stefan, H., et al., *ELEVATED TISSUE EXPRESSION OF HYALURONIC ACID AND HYALURONIDASE VALIDATES THE HA-HAase URINE TEST FOR BLADDER CANCER.* Journal of Urology, 2001. **165**(6 Part 1): p. 2068-2074.
433. Witzel, I., et al., *Role of HYAL1 expression in primary breast cancer in the formation of brain metastases.* Breast Cancer Research and Treatment, 2017. **162**(3): p. 427-438.
434. Tan, J.-X., et al., *HYAL1 overexpression is correlated with the malignant behavior of human breast cancer.* 2011. **128**(6): p. 1303-1315.
435. O'Brien, F.J., *Biomaterials & scaffolds for tissue engineering.* Materials Today, 2011. **14**(3): p. 88-95.
436. Ambrosio, A.M., et al., *A novel amorphous calcium phosphate polymer ceramic for bone repair: I. Synthesis and characterization.* J Biomed Mater Res, 2001. **58**(3): p. 295-301.
437. Wang, M., *Developing bioactive composite materials for tissue replacement.* Biomaterials, 2003. **24**(13): p. 2133-51.
438. Kuriakose, A.E., et al., *Scaffold-based lung tumor culture on porous PLGA microparticle substrates.* PLoS One, 2019. **14**(5): p. e0217640.
439. Sahoo, S.K., A.K. Panda, and V. Labhasetwar, *Characterization of porous PLGA/PLA microparticles as a scaffold for three dimensional growth of breast cancer cells.* Biomacromolecules, 2005. **6**(2): p. 1132-9.
440. Rijal, G., C. Bathula, and W. Li, *Application of Synthetic Polymeric Scaffolds in Breast Cancer 3D Tissue Cultures and Animal Tumor Models.* International Journal of Biomaterials, 2017. **2017**: p. 8074890.
441. Liu, H., E.B. Slamovich, and T.J. Webster, *Less harmful acidic degradation of poly(lacticco-glycolic acid) bone tissue engineering scaffolds through titania nanoparticle addition.* International journal of nanomedicine, 2006. **1**(4): p. 541-545.

442. Ricard-Blum, S., *The collagen family.* Cold Spring Harbor perspectives in biology, 2011. **3**(1): p. a004978-a004978.
443. Sawadkar, P., et al., *Three dimensional porous scaffolds derived from collagen, elastin and fibrin proteins orchestrate adipose tissue regeneration.* J Tissue Eng, 2021. **12**: p. 20417314211019238.
444. Baccetti, B., *Collagen and Animal Phylogeny*, in *Biology of Invertebrate and Lower Vertebrate Collagens*, A. Bairati and R. Garrone, Editors. 1985, Springer US: Boston, MA. p. 29-47.
445. Offeddu, G.S., et al., *Multi-scale mechanical response of freeze-dried collagen scaffolds for tissue engineering applications.* Journal of the Mechanical Behavior of Biomedical Materials, 2015. **42**: p. 19-25.
446. O'Brien, F.J., et al., *The effect of pore size on cell adhesion in collagen-GAG scaffolds.* Biomaterials, 2005. **26**(4): p. 433-441.
447. Ueda, H., et al., *Use of collagen sponge incorporating transforming growth factor-β1 to promote bone repair in skull defects in rabbits.* Biomaterials, 2002. **23**(4): p. 1003-1010.
448. Pawelec, K.M., et al., *Understanding anisotropy and architecture in ice-templated biopolymer scaffolds.* Materials Science and Engineering: C, 2014. **37**: p. 141-147.
449. Habanjar, O., et al., *3D Cell Culture Systems: Tumor Application, Advantages, and Disadvantages.* Int J Mol Sci, 2021. **22**(22).
450. Pratt, S.J.P., R.M. Lee, and S.S. Martin, *The Mechanical Microenvironment in Breast Cancer.* 2020. **12**(6): p. 1452.
451. Riehl, B.D., et al., *The Role of Microenvironmental Cues and Mechanical Loading Milieus in Breast Cancer Cell Progression and Metastasis.* Frontiers in bioengineering and biotechnology, 2021. **8**: p. 608526-608526.
452. Brauchle, E., et al., *Biomechanical and biomolecular characterization of extracellular matrix structures in human colon carcinomas.* Matrix Biology, 2018. **68-69**: p. 180-193.
453. Mierke, C.T., *The fundamental role of mechanical properties in the progression of cancer disease and inflammation.* Rep Prog Phys, 2014. **77**(7): p. 076602.
454. Skardal, A., et al., *Substrate elasticity controls cell proliferation, surface marker expression and motile phenotype in amniotic fluid-derived stem cells.* J Mech Behav Biomed Mater, 2013. **17**: p. 307-16.
455. Wu, W., et al., *Hyaluronic acid predicts poor prognosis in breast cancer patients: A protocol for systematic review and meta analysis.* Medicine, 2020. **99**(22).
456. Kim, P.K., et al., *Hyaluronic acid fuels pancreatic cancer cell growth.* eLife, 2021. **10**: p. e62645.
457. Price, Z.K., N.A. Lokman, and C. Ricciardelli, *Differing Roles of Hyaluronan Molecular Weight on Cancer Cell Behavior and Chemotherapy Resistance.* Cancers, 2018. **10**(12): p. 482.
458. Multhaupt, H.A., et al., *Extracellular matrix component signaling in cancer.* Adv Drug Deliv Rev, 2016. **97**: p. 28-40.
459. Tzeranis, D.S., et al., *In Situ Quantification of Surface Chemistry in Porous Collagen Biomaterials.* Annals of Biomedical Engineering, 2016. **44**(3): p. 803-815.
460. Davidenko, N., et al., *Optimisation of UV irradiation as a binding site conserving method for crosslinking collagen-based scaffolds.* Journal of Materials Science: Materials in Medicine, 2015. **27**(1): p. 14.

461. Taubenberger, A.V., et al., *The effect of unlocking RGD-motifs in collagen I on pre-osteoblast adhesion and differentiation.* Biomaterials, 2010. **31**(10): p. 2827-35.
462. Knight, C.G., et al., *The collagen-binding A-domains of integrins alpha(1)beta(1) and alpha(2)beta(1) recognize the same specific amino acid sequence, GFOGER, in native (triple-helical) collagens.* J Biol Chem, 2000. **275**(1): p. 35-40.
463. Ye, K., et al., *Matrix Stiffness and Nanoscale Spatial Organization of Cell-Adhesive Ligands Direct Stem Cell Fate.* Nano Letters, 2015. **15**(7): p. 4720-4729.
464. Farndale, Richard W., et al., *Cell–collagen interactions: the use of peptide Toolkits to investigate collagen–receptor interactions.* Biochemical Society Transactions, 2008. **36**(2): p. 241-250.
465. Davidenko, N., et al., *Control of crosslinking for tailoring collagen-based scaffolds stability and mechanics.* Acta Biomaterialia, 2015. **25**: p. 131-142.
466. Grover, C.N., et al., *Crosslinking and composition influence the surface properties, mechanical stiffness and cell reactivity of collagen-based films.* Acta Biomaterialia, 2012. **8**(8): p. 3080-3090.
467. van Luyn, M.J.A., et al., *Relations between in vitro cytotoxicity and crosslinked dermal sheep collagens.* 1992. **26**(8): p. 1091-1110.
468. Tampieri, A., et al., *Design of graded biomimetic osteochondral composite scaffolds.* Biomaterials, 2008. **29**(26): p. 3539-46.
469. Nam, K., et al., *Study on the physical properties of tissue-engineered blood vessels made by chemical cross-linking and polymer-tissue cross-linking.* J Artif Organs, 2009. **12**(1): p. 47-54.
470. Koh, L.B., et al., *Epoxy cross-linked collagen and collagen-laminin Peptide hydrogels as corneal substitutes.* J Funct Biomater, 2013. **4**(3): p. 162-77.
471. Zeeman, R., *Cross-linking of collagen-based materials.* University of Twente, Enschede., 1998: p. 199
472. Olde Damink, L.H.H., et al., *Cross-linking of dermal sheep collagen using a water-soluble carbodiimide.* Biomaterials, 1996. **17**(8): p. 765-773.
473. Ghosh, D. and M.R. Dawson, *Microenvironment Influences Cancer Cell Mechanics from Tumor Growth to Metastasis.* Adv Exp Med Biol, 2018. **1092**: p. 69-90.
474. Weigelt, B., C.M. Ghajar, and M.J. Bissell, *The need for complex 3D culture models to unravel novel pathways and identify accurate biomarkers in breast cancer.* Adv Drug Deliv Rev, 2014. **69-70**: p. 42-51.
475. Correia, A.L. and M.J. Bissell, *The tumor microenvironment is a dominant force in multidrug resistance.* Drug Resist Updat, 2012. **15**(1-2): p. 39-49.
476. Giannetti, A., J. Revilloud, and C. Verdier, *Mechanical properties of 3D tumor spheroids measured by AFM.* Computer Methods in Biomechanics and Biomedical Engineering, 2020. **23**(sup1): p. S125-S127.
477. Gillies, A.R. and R.L. Lieber, *Structure and function of the skeletal muscle extracellular matrix.* Muscle Nerve, 2011. **44**(3): p. 318-31.
478. Malandrino, A., et al., *Complex mechanics of the heterogeneous extracellular matrix in cancer.* Extreme Mechanics Letters, 2018. **21**: p. 25-34.
479. Chang, C.-Y. and C.-C. Lin, *Hydrogel Models with Stiffness Gradients for Interrogating Pancreatic Cancer Cell Fate.* Bioengineering (Basel, Switzerland), 2021. **8**(3): p. 37.
480. Denisin, A.K. and B.L. Pruitt, *Tuning the Range of Polyacrylamide Gel Stiffness for Mechanobiology Applications.* ACS Appl Mater Interfaces, 2016. **8**(34): p. 21893-902.

481. Qin, X., et al., *Matrix stiffness modulates ILK-mediated YAP activation to control the drug resistance of breast cancer cells.* Biochimica et Biophysica Acta (BBA) - Molecular Basis of Disease, 2020. **1866**(3): p. 165625.
482. Baker, B.M. and C.S. Chen, *Deconstructing the third dimension – how 3D culture microenvironments alter cellular cues.* 2012. **125**(13): p. 3015-3024.
483. Kim, C., et al., *Stem Cell Mechanosensation on Gelatin Methacryloyl (GelMA) Stiffness Gradient Hydrogels.* Ann Biomed Eng, 2020. **48**(2): p. 893-902.
484. Lavrentieva, A., et al., *Fabrication of Stiffness Gradients of GelMA Hydrogels Using a 3D Printed Micromixer.* Macromol Biosci, 2020. **20**(7): p. e2000107.
485. Liu, H.Y., M. Korc, and C.C. Lin, *Biomimetic and enzyme-responsive dynamic hydrogels for studying cell-matrix interactions in pancreatic ductal adenocarcinoma.* Biomaterials, 2018. **160**: p. 24-36.
486. Koshy, S.T., et al., *Click-Crosslinked Injectable Gelatin Hydrogels.* Adv Healthc Mater, 2016. **5**(5): p. 541-7.
487. Rape, A.D., et al., *A synthetic hydrogel for the high-throughput study of cell–ECM interactions.* Nature Communications, 2015. **6**(1): p. 8129.
488. Khetan, S., J.S. Katz, and J.A. Burdick, *Sequential crosslinking to control cellular spreading in 3-dimensional hydrogels.* Soft Matter, 2009. **5**(8): p. 1601-1606.
489. Hadjipanayi, E., V. Mudera, and R.A. Brown, *Close dependence of fibroblast proliferation on collagen scaffold matrix stiffness.* J Tissue Eng Regen Med, 2009. **3**(2): p. 77-84.
490. Peyton, S.R., et al., *Marrow-derived stem cell motility in 3D synthetic scaffold is governed by geometry along with adhesivity and stiffness.* Biotechnol Bioeng, 2011. **108**(5): p. 1181-93.
491. Lang, N.R., et al., *Biphasic response of cell invasion to matrix stiffness in three-dimensional biopolymer networks.* Acta Biomater, 2015. **13**: p. 61-7.
492. Joaquin, D., et al., *Cell migration and organization in three-dimensional in vitro culture driven by stiffness gradient.* Biotechnol Bioeng, 2016. **113**(11): p. 2496-506.
493. Gallagher, C., et al., *Three-dimensional In Vitro Biomimetic Model of Neuroblastoma using Collagen-based Scaffolds.* J Vis Exp, 2021(173).
494. Peyton, S.R., et al., *The use of poly(ethylene glycol) hydrogels to investigate the impact of ECM chemistry and mechanics on smooth muscle cells.* Biomaterials, 2006. **27**(28): p. 4881-93.
495. Dokukina, I.V. and M.E. Gracheva, *A Model of Fibroblast Motility on Substrates with Different Rigidities.* Biophysical Journal, 2010. **98**(12): p. 2794-2803.
496. Sun, M., et al., *Effects of Matrix Stiffness on the Morphology, Adhesion, Proliferation and Osteogenic Differentiation of Mesenchymal Stem Cells.* International journal of medical sciences, 2018. **15**(3): p. 257-268.
497. Mason, B.N., J.P. Califano, and C.A. Reinhart-King. *Matrix Stiffness: A Regulator of Cellular Behavior and Tissue Formation*. 2012.
498. Wells, R.G., *The role of matrix stiffness in regulating cell behavior.* Hepatology, 2008. **47**(4): p. 1394-400.
499. Louis, S.F. and P. Zahradka, *Vascular smooth muscle cell motility: From migration to invasion.* Exp Clin Cardiol, 2010. **15**(4): p. e75-85.
500. Rilla, K., et al., *Hyaluronan-coated extracellular vesicles--a novel link between hyaluronan and cancer.* Adv Cancer Res, 2014. **123**: p. 121-48.

501. Theocharis, A.D. and N.K. Karamanos, *Proteoglycans remodeling in cancer: Underlying molecular mechanisms.* Matrix Biol, 2019. **75-76**: p. 220-259.
502. Montgomery, N., et al., *CD44 enhances invasion of basal-like breast cancer cells by upregulating serine protease and collagen-degrading enzymatic expression and activity.* Breast Cancer Res, 2012. **14**(3): p. R84.
503. Bourguignon, L.Y., et al., *Hyaluronan-CD44 interaction promotes c-Src-mediated twist signaling, microRNA-10b expression, and RhoA/RhoC up-regulation, leading to Rho-kinase-associated cytoskeleton activation and breast tumor cell invasion.* J Biol Chem, 2010. **285**(47): p. 36721-35.
504. Li, L., et al., *Transforming growth factor-β1 induces EMT by the transactivation of epidermal growth factor signaling through HA/CD44 in lung and breast cancer cells.* Int J Mol Med, 2015. **36**(1): p. 113-22.
505. Termeer, C.C., et al., *Oligosaccharides of hyaluronan are potent activators of dendritic cells.* J Immunol, 2000. **165**(4): p. 1863-70.
506. Fieber, C., et al., *Hyaluronan-oligosaccharide-induced transcription of metalloproteases.* J Cell Sci, 2004. **117**(Pt 2): p. 359-67.
507. Sapudom, J., et al., *Matrix Remodeling and Hyaluronan Production by Myofibroblasts and Cancer-Associated Fibroblasts in 3D Collagen Matrices.* Gels, 2020. **6**(4).
508. Kajita, M., et al., *Membrane-type 1 matrix metalloproteinase cleaves CD44 and promotes cell migration.* The Journal of cell biology, 2001. **153**(5): p. 893-904.
509. Kung, C.I., et al., *Enhanced membrane-type 1 matrix metalloproteinase expression by hyaluronan oligosaccharides in breast cancer cells facilitates CD44 cleavage and tumor cell migration.* Oncol Rep, 2012. **28**(5): p. 1808-14.
510. Cox, T.R., *The matrix in cancer.* Nat Rev Cancer, 2021.
511. Bissell, M.J. and J. Aggeler, *Dynamic reciprocity: how do extracellular matrix and hormones direct gene expression?* Prog Clin Biol Res, 1987. **249**: p. 251-62.
512. Karsdal, M.A., et al., *The good and the bad collagens of fibrosis – Their role in signaling and organ function.* Advanced Drug Delivery Reviews, 2017. **121**: p. 43-56.
513. Eming, S.A., P. Martin, and M. Tomic-Canic, *Wound repair and regeneration: mechanisms, signaling, and translation.* Sci Transl Med, 2014. **6**(265): p. 265sr6.
514. Henderson, N.C., F. Rieder, and T.A. Wynn, *Fibrosis: from mechanisms to medicines.* Nature, 2020. **587**(7835): p. 555-566.
515. Wynn, T.A. and T.R. Ramalingam, *Mechanisms of fibrosis: therapeutic translation for fibrotic disease.* Nat Med, 2012. **18**(7): p. 1028-40.
516. Santos, A. and D. Lagares, *Matrix Stiffness: the Conductor of Organ Fibrosis.* Current Rheumatology Reports, 2018. **20**(1): p. 2.
517. Paradiso, F., et al., *Mechanical Studies of the Third Dimension in Cancer: From 2D to 3D Model.* International Journal of Molecular Sciences, 2021. **22**: p. 10098.
518. van Putten, S., Y. Shafieyan, and B. Hinz, *Mechanical control of cardiac myofibroblasts.* J Mol Cell Cardiol, 2016. **93**: p. 133-42.
519. Angelini, A., et al., *Mechanosensing dysregulation in the fibroblast: A hallmark of the aging heart.* Ageing Res Rev, 2020. **63**: p. 101150.
520. Paolillo, M. and S. Schinelli, *Extracellular Matrix Alterations in Metastatic Processes.* International journal of molecular sciences, 2019. **20**(19): p. 4947.
521. DeClerck, Y.A., *Desmoplasia: A Response or a Niche?* Cancer Discovery, 2012. **2**(9): p. 772-774.

522. Damjanov, I., *Chapter 5 - Neoplasia*, in *Pathology Secrets (Third Edition)*, I. Damjanov, Editor. 2009, Mosby: Philadelphia. p. 76-97.
523. Cox, T.R. and J.T. Erler, *Molecular pathways: connecting fibrosis and solid tumor metastasis.* Clin Cancer Res, 2014. **20**(14): p. 3637-43.
524. Breuninger, H., et al., *Desmoplastic squamous cell carcinoma of skin and vermilion surface.* 1997. **79**(5): p. 915-919.
525. Ebelt, N.D., V. Zamloot, and E.R. Manuel, *Targeting desmoplasia in pancreatic cancer as an essential first step to effective therapy.* 2020. **11**(38).
526. Walker, R.A., *The complexities of breast cancer desmoplasia.* Breast cancer research : BCR, 2001. **3**(3): p. 143-145.
527. Lu, P., V.M. Weaver, and Z. Werb, *The extracellular matrix: a dynamic niche in cancer progression.* The Journal of cell biology, 2012. **196**(4): p. 395-406.
528. Provenzano, P.P., et al., *Collagen reorganization at the tumor-stromal interface facilitates local invasion.* BMC Med, 2006. **4**(1): p. 38.
529. Neesse, A., et al., *Stromal biology and therapy in pancreatic cancer: a changing paradigm.* Gut, 2015. **64**(9): p. 1476-84.
530. Seewaldt, V., *ECM stiffness paves the way for tumor cells.* Nature Medicine, 2014. **20**(4): p. 332-333.
531. Koay, E.J., et al., *A Visually Apparent and Quantifiable CT Imaging Feature Identifies Biophysical Subtypes of Pancreatic Ductal Adenocarcinoma.* Clin Cancer Res, 2018. **24**(23): p. 5883-5894.
532. Liu, T., et al., *Noninvasive In-Vivo Quantification of Mechanical Heterogeneity of Invasive Breast Carcinomas.* PLoS One, 2015. **10**(7): p. e0130258.
533. Wynn, T.A., *Cellular and molecular mechanisms of fibrosis.* J Pathol, 2008. **214**(2): p. 199-210.
534. de Oliveira, R.C. and S.E. Wilson, *Fibrocytes, Wound Healing, and Corneal Fibrosis.* Invest Ophthalmol Vis Sci, 2020. **61**(2): p. 28.
535. Pakshir, P., et al., *The myofibroblast at a glance.* Journal of Cell Science, 2020. **133**(13).
536. Hinz, B., et al., *Recent developments in myofibroblast biology: paradigms for connective tissue remodeling.* Am J Pathol, 2012. **180**(4): p. 1340-55.
537. Tomasek, J.J., et al., *Myofibroblasts and mechano-regulation of connective tissue remodelling.* Nature Reviews Molecular Cell Biology, 2002. **3**(5): p. 349-363.
538. Ciobanasu, C., B. Faivre, and C. Le Clainche, *Integrating actin dynamics, mechanotransduction and integrin activation: the multiple functions of actin binding proteins in focal adhesions.* European journal of cell biology, 2013. **92**(10-11): p. 339-348.
539. Li, S., et al., *Targeting Mechanics-Induced Fibroblast Activation through CD44-RhoA-YAP Pathway Ameliorates Crystalline Silica-Induced Silicosis.* Theranostics, 2019. **9**(17): p. 4993-5008.
540. Bhowmick, N.A., et al., *TGF-beta signaling in fibroblasts modulates the oncogenic potential of adjacent epithelia.* Science, 2004. **303**(5659): p. 848-51.
541. Drabsch, Y. and P. ten Dijke, *TGF-β signalling and its role in cancer progression and metastasis.* Cancer Metastasis Rev, 2012. **31**(3-4): p. 553-68.
542. Evans, R.A., et al., *TGF-beta1-mediated fibroblast-myofibroblast terminal differentiation-the role of Smad proteins.* Exp Cell Res, 2003. **282**(2): p. 90-100.
543. Liu, S., J. Ren, and P. Ten Dijke, *Targeting TGFβ signal transduction for cancer therapy.* Signal Transduct Target Ther, 2021. **6**(1): p. 8.

544. Pietras, K. and A. Ostman, *Hallmarks of cancer: interactions with the tumor stroma*. Exp Cell Res, 2010. **316**(8): p. 1324-31.
545. Bhowmick, N.A., E.G. Neilson, and H.L. Moses, *Stromal fibroblasts in cancer initiation and progression.* Nature, 2004. **432**(7015): p. 332-7.
546. Bonollo, F., et al., *The Role of Cancer-Associated Fibroblasts in Prostate Cancer Tumorigenesis.* Cancers, 2020. **12**(7): p. 1887.
547. Gao, Y., et al., *TNFα-YAP/p65-HK2 axis mediates breast cancer cell migration.* Oncogenesis, 2017. **6**(9): p. e383-e383.
548. Bassi, G., et al., *Scaffold-based 3D cellular models mimicking the heterogeneity of osteosarcoma stem cell niche.* Scientific Reports, 2020. **10**(1): p. 22294.
549. Zhang, M., et al., *The use of porous scaffold as a tumor model.* International journal of biomaterials, 2013. **2013**: p. 396056-396056.
550. Rijal, G. and W. Li, *Native-mimicking in vitro microenvironment: an elusive and seductive future for tumor modeling and tissue engineering.* Journal of Biological Engineering, 2018. **12**(1): p. 20.
551. Bauza, G., et al., *Improving the immunosuppressive potential of articular chondroprogenitors in a three-dimensional culture setting.* Scientific Reports, 2020. **10**(1): p. 16610.
552. Paradiso, F., et al., *Marine Collagen Substrates for 2D and 3D Ovarian Cancer Cell Systems.* 2019. **7**(343).
553. Taraballi, F., et al., *Biomimetic Tissue Engineering: Tuning the Immune and Inflammatory Response to Implantable Biomaterials.* 2018. **7**(17): p. 1800490.
554. Taraballi, F., et al., *Biomimetic collagenous scaffold to tune inflammation by targeting macrophages.* J Tissue Eng, 2016. **7**: p. 2041731415624667.
555. Wei, R., et al., *Cellular and Extracellular Components in Tumor Microenvironment and Their Application in Early Diagnosis of Cancers.* Analytical Cellular Pathology, 2020. **2020**: p. 6283796.
556. Dowling, P. and M. Clynes, *Conditioned media from cell lines: a complementary model to clinical specimens for the discovery of disease-specific biomarkers.* Proteomics, 2011. **11**(4): p. 794-804.
557. Cai, J., et al., *Fibroblasts in omentum activated by tumor cells promote ovarian cancer growth, adhesion and invasiveness.* Carcinogenesis, 2012. **33**(1): p. 20-9.
558. Hanahan, D. and Lisa M. Coussens, *Accessories to the Crime: Functions of Cells Recruited to the Tumor Microenvironment.* Cancer Cell, 2012. **21**(3): p. 309-322.
559. Kubiczkova, L., et al., *TGF-β – an excellent servant but a bad master.* Journal of Translational Medicine, 2012. **10**(1): p. 183.
560. Huang, J.J. and G.C. Blobe, *Dichotomous roles of TGF-β in human cancer.* Biochem Soc Trans, 2016. **44**(5): p. 1441-1454.
561. Bioinformatics., B., *FastQC A Quality Control tool for High Throughput Sequence Data n.d.* .
562. Dobin, A., et al., *STAR: ultrafast universal RNA-seq aligner.* Bioinformatics, 2013. **29**(1): p. 15-21.
563. Love, M.I., W. Huber, and S. Anders, *Moderated estimation of fold change and dispersion for RNA-seq data with DESeq2.* Genome Biology, 2014. **15**(12): p. 550.

564. Wang, J., et al., *WebGestalt 2017: a more comprehensive, powerful, flexible and interactive gene set enrichment analysis toolkit.* Nucleic Acids Res, 2017. **45**(W1): p. W130-w137.
565. Venny., O.J., *An interactive tool for comparing lists with Venn's diagrams. n.d.*
566. H., W., *ggplot2: Elegant Graphics for Data Analysis. .* 2016. **Springer-Verlag New York**.
567. Team., R.C., *R: A Language and Environment for Statistical Computing.* 2018.
568. Wickham, H., *ggplot2: Elegant Graphics for Data Analysis*. 2009: Springer Publishing Company, Incorporated.
569. Nissen, N.I., M. Karsdal, and N. Willumsen, *Collagens and Cancer associated fibroblasts in the reactive stroma and its relation to Cancer biology.* Journal of experimental & clinical cancer research : CR, 2019. **38**(1): p. 115-115.
570. Wells, R.G., *Tissue mechanics and fibrosis.* Biochimica et biophysica acta, 2013. **1832**(7): p. 884-890.
571. DuChez, B.J., et al., *Durotaxis by Human Cancer Cells.* Biophys J, 2019. **116**(4): p. 670-683.
572. Kadry, H., D. Lagares, and T.A. Al-Hilal, *Method for Investigating Fibroblast Durotaxis.* Methods Mol Biol, 2021. **2299**: p. 227-236.
573. Wong, S., W.-H. Guo, and Y.-L. Wang, *Fibroblasts probe substrate rigidity with filopodia extensions before occupying an area.* 2014. **111**(48): p. 17176-17181.
574. Conklin, M.W., et al., *Collagen Alignment as a Predictor of Recurrence after Ductal Carcinoma In Situ.* Cancer Epidemiology, Biomarkers & Prevention, 2018. **27**(2): p. 138-145.
575. Gurrala, R., et al., *Quantifying Breast Cancer-Driven Fiber Alignment and Collagen Deposition in Primary Human Breast Tissue.* 2021. **9**.
576. Cao, L., R. Lafyatis, and L.C. Burkly, *Increased dermal collagen bundle alignment in systemic sclerosis is associated with a cell migration signature and role of Arhgdib in directed fibroblast migration on aligned ECMs.* PLoS One, 2017. **12**(6): p. e0180751.
577. Brett, E.A., et al., *Tumor-associated collagen signatures: pushing tumor boundaries.* Cancer Metab, 2020. **8**: p. 14.
578. Provenzano, P.P., et al., *Contact guidance mediated three-dimensional cell migration is regulated by Rho/ROCK-dependent matrix reorganization.* Biophys J, 2008. **95**(11): p. 5374-84.
579. Brownfield, D.G., et al., *Patterned collagen fibers orient branching mammary epithelium through distinct signaling modules.* Curr Biol, 2013. **23**(8): p. 703-9.
580. Kim, A., N. Lakshman, and W.M. Petroll, *Quantitative assessment of local collagen matrix remodeling in 3-D culture: the role of Rho kinase.* Exp Cell Res, 2006. **312**(18): p. 3683-92.
581. Wang, J.H., et al., *Cell orientation determines the alignment of cell-produced collagenous matrix.* J Biomech, 2003. **36**(1): p. 97-102.
582. Taufalele, P.V., et al., *Fiber alignment drives changes in architectural and mechanical features in collagen matrices.* PLoS One, 2019. **14**(5): p. e0216537.
583. Sánchez-Iranzo, H., et al., *Transient fibrosis resolves via fibroblast inactivation in the regenerating zebrafish heart.* 2018. **115**(16): p. 4188-4193.
584. Ormerod, M.G., B. Tribukait, and W. Giaretti, *Consensus report of the task force on standardisation of DNA flow cytometry in clinical pathology. DNA Flow Cytometry Task*

Force of the European Society for Analytical Cellular Pathology. Anal Cell Pathol, 1998. **17**(2): p. 103-10.
585. Davies, D., *FACS Laboratory*. London Research Institute, Cancer Research UK
586. Malumbres, M. and M. Barbacid, *Cell cycle, CDKs and cancer: a changing paradigm.* Nat Rev Cancer, 2009. **9**(3): p. 153-66.
587. Paradiso, F., et al., *Mechanical Studies of the Third Dimension in Cancer: From 2D to 3D Model.* Int J Mol Sci, 2021. **22**(18).
588. Zanconato, F., M. Cordenonsi, and S. Piccolo, *YAP/TAZ at the Roots of Cancer*. Cancer Cell, 2016. **29**(6): p. 783-803.
589. Nguyen, C.D.K. and C. Yi, *YAP/TAZ Signaling and Resistance to Cancer Therapy*. Trends in cancer, 2019. **5**(5): p. 283-296.
590. Francisco, J., et al., *AAV-mediated YAP expression in cardiac fibroblasts promotes inflammation and increases fibrosis.* Scientific Reports, 2021. **11**(1): p. 10553.
591. Heasman, S.J. and A.J. Ridley, *Mammalian Rho GTPases: new insights into their functions from in vivo studies.* Nat Rev Mol Cell Biol, 2008. **9**(9): p. 690-701.
592. Hall, A., *Rho family GTPases.* Biochem Soc Trans, 2012. **40**(6): p. 1378-82.
593. Parimon, T., et al., *Syndecan-1 promotes lung fibrosis by regulating epithelial reprogramming through extracellular vesicles.* JCI Insight, 2019. **4**(17).
594. Didem, T., et al., *Clinical significance of serum tenascin-c levels in epithelial ovarian cancer*. Tumour Biol, 2014. **35**(7): p. 6777-82.
595. De Wever, O., et al., *Tenascin-C and SF/HGF produced by myofibroblasts in vitro provide convergent pro-invasive signals to human colon cancer cells through RhoA and Rac.* Faseb j, 2004. **18**(9): p. 1016-8.
596. Carey, W.A., et al., *Tenascin-C deficiency attenuates TGF-ß-mediated fibrosis following murine lung injury*. Am J Physiol Lung Cell Mol Physiol, 2010. **299**(6): p. L785-93.
597. Oberhauser, A.F., et al., *The molecular elasticity of the extracellular matrix protein tenascin.* Nature, 1998. **393**(6681): p. 181-5.
598. van Niel, G., G. D'Angelo, and G. Raposo, *Shedding light on the cell biology of extracellular vesicles.* Nat Rev Mol Cell Biol, 2018. **19**(4): p. 213-228.
599. Vis, M.A.M., K. Ito, and S. Hofmann, *Impact of Culture Medium on Cellular Interactions in in vitro Co-culture Systems.* 2020. **8**.
600. Amirfakhri, S., A. Salimi, and N. Fernandez, *Effects of Conditioned Medium from Breast Cancer Cells on Tlr2 Expression in Nb4 Cells.* Asian Pac J Cancer Prev, 2015. **16**(18): p. 8445-50.
601. Henriksson, M.L., et al., *Colorectal cancer cells activate adjacent fibroblasts resulting in FGF1/FGFR3 signaling and increased invasion.* The American journal of pathology, 2011. **178**(3): p. 1387-1394.
602. Giusti, I., et al., *Ovarian cancer-derived extracellular vesicles affect normal human fibroblast behavior.* Cancer biology & therapy, 2018. **19**(8): p. 722-734.
603. Yang, C., et al., *Conditioned media from human adipose tissue-derived mesenchymal stem cells and umbilical cord-derived mesenchymal stem cells efficiently induced the apoptosis and differentiation in human glioma cell lines in vitro.* BioMed research international, 2014. **2014**: p. 109389-109389.

604. Kolomeyer, A.M., I.K. Sugino, and M.A. Zarbin, *Characterization of Conditioned Media Collected from Cultured Adult versus Fetal Retinal Pigment Epithelial Cells.* Investigative Ophthalmology & Visual Science, 2011. **52**(8): p. 5973-5986.
605. Jeong, D., et al., *Effect of Concentrated Fibroblast-Conditioned Media on In Vitro Maintenance of Rat Primary Hepatocyte.* PloS one, 2016. **11**(2): p. e0148846-e0148846.
606. Teichgräber, V., et al., *Specific inhibition of fibroblast activation protein (FAP)-alpha prevents tumor progression in vitro.* Adv Med Sci, 2015. **60**(2): p. 264-72.
607. Kobayashi, T., S. Hattori, and H. Shinkai, *Matrix metalloproteinases-2 and -9 are secreted from human fibroblasts.* Acta Derm Venereol, 2003. **83**(2): p. 105-7.
608. Brücher, B.L.D.M. and I.S. Jamall, *Epistemology of the origin of cancer: a new paradigm.* BMC Cancer, 2014. **14**(1): p. 331.
609. Barcellos-Hoff, M.H., D. Lyden, and T.C. Wang, *The evolution of the cancer niche during multistage carcinogenesis.* Nat Rev Cancer, 2013. **13**(7): p. 511-8.
610. Schäfer, M. and S. Werner, *Cancer as an overhealing wound: an old hypothesis revisited.* Nat Rev Mol Cell Biol, 2008. **9**(8): p. 628-38.
611. Rybinski, B., J. Franco-Barraza, and E. Cukierman, *The wound healing, chronic fibrosis, and cancer progression triad.* Physiol Genomics, 2014. **46**(7): p. 223-44.
612. Cirri, P. and P. Chiarugi, *Cancer associated fibroblasts: the dark side of the coin.* Am J Cancer Res, 2011. **1**(4): p. 482-97.
613. Serini, G. and G. Gabbiani, *Mechanisms of myofibroblast activity and phenotypic modulation.* Exp Cell Res, 1999. **250**(2): p. 273-83.
614. Colpaert, C.G., et al., *The presence of a fibrotic focus in invasive breast carcinoma correlates with the expression of carbonic anhydrase IX and is a marker of hypoxia and poor prognosis.* Breast Cancer Res Treat, 2003. **81**(2): p. 137-47.
615. Affo, S., L.X. Yu, and R.F. Schwabe, *The Role of Cancer-Associated Fibroblasts and Fibrosis in Liver Cancer.* Annu Rev Pathol, 2017. **12**: p. 153-186.
616. Thomas, D. and P. Radhakrishnan, *Tumor-stromal crosstalk in pancreatic cancer and tissue fibrosis.* Mol Cancer, 2019. **18**(1): p. 14.
617. Roeder, B.A., et al., *Tensile mechanical properties of three-dimensional type I collagen extracellular matrices with varied microstructure.* J Biomech Eng, 2002. **124**(2): p. 214-22.
618. Mondragón, E., et al., *Mimicking the Organic and Inorganic Composition of Anabolic Bone Enhances Human Mesenchymal Stem Cell Osteoinduction and Scaffold Mechanical Properties.* 2020. **8**(753).
619. Minardi, S., et al., *Evaluation of the osteoinductive potential of a bio-inspired scaffold mimicking the osteogenic niche for bone augmentation.* Biomaterials, 2015. **62**: p. 128-37.
620. Ayad, N.M.E., S. Kaushik, and V.M. Weaver, *Tissue mechanics, an important regulator of development and disease.* 2019. **374**(1779): p. 20180215.
621. Yeung, T., et al., *Effects of substrate stiffness on cell morphology, cytoskeletal structure, and adhesion.* 2005. **60**(1): p. 24-34.
622. Discher, D.E., P. Janmey, and Y.-l. Wang, *Tissue Cells Feel and Respond to the Stiffness of Their Substrate.* Science, 2005. **310**(5751): p. 1139.
623. Kawano, S., et al., *Assessment of elasticity of colorectal cancer tissue, clinical utility, pathological and phenotypical relevance.* 2015. **106**(9): p. 1232-1239.
624. Goffin , J.r.m.M., et al., *Focal adhesion size controls tension-dependent recruitment of α-smooth muscle actin to stress fibers.* Journal of Cell Biology, 2006. **172**(2): p. 259-268.

625. Bružauskaitė, I., et al., *Scaffolds and cells for tissue regeneration: different scaffold pore sizes-different cell effects.* Cytotechnology, 2016. **68**(3): p. 355-369.
626. O'Brien, F.J., et al., *The effect of pore size on cell adhesion in collagen-GAG scaffolds.* Biomaterials, 2005. **26**(4): p. 433-41.
627. Yannas, I.V., *Tissue regeneration by use of collagen-glycosaminoglycan copolymers.* Clin Mater, 1992. **9**(3-4): p. 179-87.
628. Wolf, K., et al., *Physical limits of cell migration: Control by ECM space and nuclear deformation and tuning by proteolysis and traction force.* The Journal of cell biology, 2013. **201**: p. 1069-1084.
629. Park, J.E., et al., *Fibroblast Activation Protein, a Dual Specificity Serine Protease Expressed in Reactive Human Tumor Stromal Fibroblasts *.* Journal of Biological Chemistry, 1999. **274**(51): p. 36505-36512.
630. Chen, X. and E. Song, *Turning foes to friends: targeting cancer-associated fibroblasts.* Nat Rev Drug Discov, 2019. **18**(2): p. 99-115.
631. Kayalar, O., F. Oztay, and H.G. Ongen, *Gastrin-releasing peptide induces fibrotic response in MRC5s and proliferation in A549s.* Cell Communication and Signaling, 2020. **18**(1): p. 96.
632. Huang, M., et al., *Inhibition of connective tissue growth factor attenuates paraquat-induced lung fibrosis in a human MRC-5 cell line.* Environ Toxicol, 2016. **31**(11): p. 1620-1626.
633. Yang, Z., et al., *MARCKS contributes to stromal cancer-associated fibroblast activation and facilitates ovarian cancer metastasis.* Oncotarget, 2016. **7**(25): p. 37649-37663.
634. Ding, S.-M., et al., *MRC-5 Cancer-associated Fibroblasts Influence Production of Cancer Stem Cell Markers and Inflammation-associated Cell Surface Molecules, in Liver Cancer Cell Lines.* International journal of medical sciences, 2019. **16**(8): p. 1157-1170.
635. Ding, S., et al., *MRC-5 fibroblast-conditioned medium influences multiple pathways regulating invasion, migration, proliferation, and apoptosis in hepatocellular carcinoma.* Journal of translational medicine, 2015. **13**: p. 237-237.
636. Biernacka, A., M. Dobaczewski, and N.G. Frangogiannis, *TGF-β signaling in fibrosis.* Growth factors (Chur, Switzerland), 2011. **29**(5): p. 196-202.
637. Meng, X.M., D.J. Nikolic-Paterson, and H.Y. Lan, *TGF-β: the master regulator of fibrosis.* Nat Rev Nephrol, 2016. **12**(6): p. 325-38.
638. Yeung, T.-L., et al., *TGF-β modulates ovarian cancer invasion by upregulating CAF-derived versican in the tumor microenvironment.* Cancer research, 2013. **73**(16): p. 5016-5028.
639. Fitzgerald, A.A. and L.M. Weiner, *The role of fibroblast activation protein in health and malignancy.* Cancer metastasis reviews, 2020. **39**(3): p. 783-803.
640. Chadli, L., et al., *Identification of regulators of the myofibroblast phenotype of primary dermal fibroblasts from early diffuse systemic sclerosis patients.* Scientific reports, 2019. **9**(1): p. 4521-4521.
641. Amornsupak, K., et al., *High ASMA(+) Fibroblasts and Low Cytoplasmic HMGB1(+) Breast Cancer Cells Predict Poor Prognosis.* Clin Breast Cancer, 2017. **17**(6): p. 441-452.e2.
642. Lu, Y.-Y., et al., *Interaction of Src and Alpha-V Integrin Regulates Fibroblast Migration and Modulates Lung Fibrosis in A Preclinical Model of Lung Fibrosis.* Scientific Reports, 2017. **7**(1): p. 46357.

643. Kunz-Schughart, L.A. and R. Knuechel, *Tumor-associated fibroblasts (Part I): Active stromal participants in tumor development and progression?* Histology and Histopathology, 2002. **17**(2): p. 599-621.
644. Waldeland, J.O., W.J. Polacheck, and S. Evje, *Collective tumor cell migration in the presence of fibroblasts.* Journal of Biomechanics, 2020. **100**: p. 109568.
645. Miyazaki, K., et al., *Cancer cell migration on elongate protrusions of fibroblasts in collagen matrix.* Scientific Reports, 2019. **9**(1): p. 292.
646. Schwager, S.C., P.V. Taufalele, and C.A. Reinhart-King, *Cell-Cell Mechanical Communication in Cancer.* Cellular and molecular bioengineering, 2019. **12**(1): p. 1-14.
647. Öhlund, D., et al., *Distinct populations of inflammatory fibroblasts and myofibroblasts in pancreatic cancer.* J Exp Med, 2017. **214**(3): p. 579-596.
648. Heldin, C.-H., et al., *High interstitial fluid pressure — an obstacle in cancer therapy.* Nature Reviews Cancer, 2004. **4**(10): p. 806-813.
649. Sahai, E., et al., *A framework for advancing our understanding of cancer-associated fibroblasts.* Nature Reviews Cancer, 2020. **20**(3): p. 174-186.
650. Menzel, T. and C.D. Fletcher, *The emerging role of myofibroblasts in soft tissue neoplasia.* Am J Clin Pathol, 1997. **107**(1): p. 2-5.
651. Desmoulière, A., I.A. Darby, and G. Gabbiani, *Normal and Pathologic Soft Tissue Remodeling: Role of the Myofibroblast, with Special Emphasis on Liver and Kidney Fibrosis.* Laboratory Investigation, 2003. **83**(12): p. 1689-1707.
652. Guo, X., et al., *Stromal Fibroblasts Activated by Tumor Cells Promote Angiogenesis in Mouse Gastric Cancer*.* Journal of Biological Chemistry, 2008. **283**(28): p. 19864-19871.
653. Assoian, R.K., et al., *Expression and secretion of type beta transforming growth factor by activated human macrophages.* Proc Natl Acad Sci U S A, 1987. **84**(17): p. 6020-4.
654. Wakefield, L.M., et al., *Latent transforming growth factor-beta from human platelets. A high molecular weight complex containing precursor sequences.* J Biol Chem, 1988. **263**(16): p. 7646-54.
655. Yao, Q., et al., *CLIC4 mediates TGF-beta1-induced fibroblast-to-myofibroblast transdifferentiation in ovarian cancer.* Oncol Rep, 2009. **22**(3): p. 541-8.
656. Fintha, A., et al., *Therapeutic Targeting of Fibrotic Epithelial-Mesenchymal Transition-An Outstanding Challenge.* Frontiers in pharmacology, 2019. **10**: p. 388-388.
657. Franco-Barraza, J., et al., *Preparation of Extracellular Matrices Produced by Cultured and Primary Fibroblasts.* Curr Protoc Cell Biol, 2016. **71**: p. 10.9.1-10.9.34.
658. Yazdani, S., R. Bansal, and J. Prakash, *Drug targeting to myofibroblasts: Implications for fibrosis and cancer.* Adv Drug Deliv Rev, 2017. **121**: p. 101-116.
659. Tai, Y., et al., *Myofibroblasts: Function, Formation, and Scope of Molecular Therapies for Skin Fibrosis.* Biomolecules, 2021. **11**(8): p. 1095.
660. Kuehl, T. and D. Lagares, *BH3 mimetics as anti-fibrotic therapy: Unleashing the mitochondrial pathway of apoptosis in myofibroblasts.* Matrix Biol, 2018. **68-69**: p. 94-105.
661. Haak Andrew, J., et al., *Selective YAP/TAZ inhibition in fibroblasts via dopamine receptor D1 agonism reverses fibrosis.* Science Translational Medicine, 2019. **11**(516): p. eaau6296.
662. Afratis, N.A., et al., *Emerging insights into the role of matrix metalloproteases as therapeutic targets in fibrosis.* Matrix Biology, 2018. **68-69**: p. 167-179.

663. Walraven, M. and B. Hinz, *Therapeutic approaches to control tissue repair and fibrosis: Extracellular matrix as a game changer.* Matrix Biol, 2018. **71-72**: p. 205-224.
664. De Vita, A., et al., *Lysyl oxidase engineered lipid nanovesicles for the treatment of triple negative breast cancer.* Scientific Reports, 2021. **11**(1): p. 5107.
665. Schosserer, M., J. Grillari, and M. Breitenbach, *The Dual Role of Cellular Senescence in Developing Tumors and Their Response to Cancer Therapy.* Frontiers in oncology, 2017. **7**: p. 278-278.
666. Mellone, M., et al., *Induction of fibroblast senescence generates a non-fibrogenic myofibroblast phenotype that differentially impacts on cancer prognosis.* Aging (Albany NY), 2016. **9**(1): p. 114-132.
667. Krtolica, A., et al., *Senescent fibroblasts promote epithelial cell growth and tumorigenesis: A link between cancer and aging.* 2001. **98**(21): p. 12072-12077.
668. Butcher, D.T., T. Alliston, and V.M. Weaver, *A tense situation: forcing tumour progression.* Nature reviews. Cancer, 2009. **9**(2): p. 108-122.
669. Nia, H.T., L.L. Munn, and R.K. Jain, *Physical traits of cancer.* Science, 2020. **370**(6516).
670. Schedin, P. and P.J. Keely, *Mammary gland ECM remodeling, stiffness, and mechanosignaling in normal development and tumor progression.* Cold Spring Harbor perspectives in biology, 2011. **3**(1): p. a003228-a003228.
671. Shieh, A.C., *Biomechanical forces shape the tumor microenvironment.* Ann Biomed Eng, 2011. **39**(5): p. 1379-89.
672. Han, W., et al., *Oriented collagen fibers direct tumor cell intravasation.* Proceedings of the National Academy of Sciences of the United States of America, 2016. **113**(40): p. 11208-11213.
673. Nadiarnykh, O., et al., *Alterations of the extracellular matrix in ovarian cancer studied by Second Harmonic Generation imaging microscopy.* BMC Cancer, 2010. **10**(1): p. 94.
674. Kirkpatrick, N.D., M.A. Brewer, and U. Utzinger, *Endogenous Optical Biomarkers of Ovarian Cancer Evaluated with Multiphoton Microscopy.* Cancer Epidemiology Biomarkers & Prevention, 2007. **16**(10): p. 2048.
675. Williams, R.M., et al., *Strategies for high-resolution imaging of epithelial ovarian cancer by laparoscopic nonlinear microscopy.* Translational oncology, 2010. **3**(3): p. 181-194.
676. Freedman, R.S., et al., *Peritoneal inflammation – A microenvironment for Epithelial Ovarian Cancer (EOC).* Journal of Translational Medicine, 2004. **2**(1): p. 23.
677. Nezhat, F., et al., *The relationship of endometriosis and ovarian malignancy: a review.* Fertil Steril, 2008. **90**(5): p. 1559-70.
678. Erickson, B.K., M.G. Conner, and C.N. Landen, Jr., *The role of the fallopian tube in the origin of ovarian cancer.* American journal of obstetrics and gynecology, 2013. **209**(5): p. 409-414.
679. Klotz, D.M. and P. Wimberger, *Cells of origin of ovarian cancer: ovarian surface epithelium or fallopian tube?* Arch Gynecol Obstet, 2017. **296**(6): p. 1055-1062.
680. Shield, K., et al., *Multicellular spheroids in ovarian cancer metastases: Biology and pathology.* Gynecol Oncol, 2009. **113**(1): p. 143-8.
681. Naora, H. and D.J. Montell, *Ovarian Cancer Metastasis: Integrating insights from disparate model organisms.* Nature Reviews Cancer, 2005. **5**(5): p. 355-366.
682. Novak, C., E. Horst, and G. Mehta, *Review: Mechanotransduction in ovarian cancer: Shearing into the unknown.* APL bioengineering, 2018. **2**(3): p. 031701-031701.

683. Kim, S., B. Kim, and Y.S. Song, *Ascites modulates cancer cell behavior, contributing to tumor heterogeneity in ovarian cancer.* Cancer Sci, 2016. **107**(9): p. 1173-8.
684. Qu, Y., et al., *Constructing an ovarian cancer metastasis index by dissecting medical records.* Oncotarget, 2017. **8**(60): p. 102212-102222.
685. Agarwal, R. and S.B. Kaye, *Ovarian cancer: strategies for overcoming resistance to chemotherapy.* Nature Reviews Cancer, 2003. **3**(7): p. 502-516.
686. Kim, A., et al., *Therapeutic strategies in epithelial ovarian cancer.* J Exp Clin Cancer Res, 2012. **31**(1): p. 14.
687. Pignata, S., et al., *Residual neurotoxicity in ovarian cancer patients in clinical remission after first-line chemotherapy with carboplatin and paclitaxel: the Multicenter Italian Trial in Ovarian cancer (MITO-4) retrospective study.* BMC Cancer, 2006. **6**: p. 5.
688. Abraham, S.A., et al., *The liposomal formulation of doxorubicin.* Methods Enzymol, 2005. **391**: p. 71-97.
689. Staropoli, N., et al., *Pegylated liposomal doxorubicin in the management of ovarian cancer: a systematic review and metaanalysis of randomized trials.* Cancer biology & therapy, 2014. **15**(6): p. 707-720.
690. Gordon, A.N., et al., *Recurrent epithelial ovarian carcinoma: a randomized phase III study of pegylated liposomal doxorubicin versus topotecan.* J Clin Oncol, 2001. **19**(14): p. 3312-22.
691. Weng, C.-S., et al., *Retrospective Analysis Of Comparative Outcomes In Recurrent Platinum-Sensitive Ovarian Cancer Treated With Pegylated Liposomal Doxorubicin (Lipo-Dox) And Carboplatin Versus Paclitaxel And Carboplatin.* Cancer management and research, 2019. **11**: p. 9899-9905.
692. Acerbi, I., et al., *Human breast cancer invasion and aggression correlates with ECM stiffening and immune cell infiltration.* Integrative Biology, 2015. **7**(10): p. 1120-1134.
693. Caja, L., et al., *TGF-β and the Tissue Microenvironment: Relevance in Fibrosis and Cancer.* 2018. **19**(5): p. 1294.
694. McKenzie, A.J., et al., *The mechanical microenvironment regulates ovarian cancer cell morphology, migration, and spheroid disaggregation.* Scientific Reports, 2018. **8**(1): p. 7228.
695. McGrail, D.J., Q.M.N. Kieu, and M.R. Dawson, *The malignancy of metastatic ovarian cancer cells is increased on soft matrices through a mechanosensitive Rho–ROCK pathway.* Journal of Cell Science, 2014. **127**(12): p. 2621-2626.
696. Huh, D., G.A. Hamilton, and D.E. Ingber, *From 3D cell culture to organs-on-chips.* Trends in Cell Biology, 2011. **21**(12): p. 745-754.
697. Svenson, S., *Clinical translation of nanomedicines.* Current Opinion in Solid State and Materials Science, 2012. **16**: p. 287–294.
698. Yakavets, I., et al., *Advanced co-culture 3D breast cancer model for investigation of fibrosis induced by external stimuli: optimization study.* Scientific Reports, 2020. **10**(1): p. 21273.
699. Colombo, E. and M.G. Cattaneo, *Multicellular 3D Models to Study Tumour-Stroma Interactions.* Int J Mol Sci, 2021. **22**(4).
700. Millard, M., et al., *Drug delivery to solid tumors: the predictive value of the multicellular tumor spheroid model for nanomedicine screening.* Int J Nanomedicine, 2017. **12**: p. 7993-8007.

701. Wang, Z., et al., *Cancer-associated fibroblasts in radiotherapy: challenges and new opportunities.* Cell Communication and Signaling, 2019. **17**(1): p. 47.
702. Saraiva, D.P., et al., *Establishment of a 3D Co-culture With MDA-MB-231 Breast Cancer Cell Line and Patient-Derived Immune Cells for Application in the Development of Immunotherapies.* 2020. **10**.
703. Rodriguez, M., P. McGarry, and N. Sniadecki, *Review on Cell Mechanics: Experimental and Modeling Approaches.* Applied Mechanics Reviews, 2013. **65**: p. 60801.
704. Moeendarbary, E. and A.R. Harris, *Cell mechanics: principles, practices, and prospects.* Wiley Interdiscip Rev Syst Biol Med, 2014. **6**(5): p. 371-88.
705. Zemła, J., et al., *Atomic force microscopy as a tool for assessing the cellular elasticity and adhesiveness to identify cancer cells and tissues.* Semin Cell Dev Biol, 2018. **73**: p. 115-124.
706. Alcaraz, J., et al., *Bidirectional mechanobiology between cells and their local extracellular matrix probed by atomic force microscopy.* Semin Cell Dev Biol, 2018. **73**: p. 71-81.
707. Rianna, C. and M. Radmacher, *Cell mechanics as a marker for diseases: Biomedical applications of AFM.* 2016. **1760**(1): p. 020057.
708. Ciasca, G., et al., *Nano-mechanical signature of brain tumours.* Nanoscale, 2016. **8**(47): p. 19629-19643.
709. Plodinec, M., et al., *The nanomechanical signature of breast cancer.* Nature Nanotechnology, 2012. **7**(11): p. 757-765.
710. Azzalini, E., et al., *Cell-stiffness and morphological architectural patterns in clinical samples of high grade serous ovarian cancers.* Nanomedicine: Nanotechnology, Biology and Medicine, 2021. **37**: p. 102452.
711. Cui, Y., et al., *Nanomechanical Characteristics of Cervical Cancer and Cervical Intraepithelial Neoplasia Revealed by Atomic Force Microscopy.* Medical science monitor : international medical journal of experimental and clinical research, 2017. **23**: p. 4205-4213.
712. Lekka, M., et al., *Cancer cell detection in tissue sections using AFM.* Archives of Biochemistry and Biophysics, 2012. **518**(2): p. 151-156.
713. Tian, M., et al., *The nanomechanical signature of liver cancer tissues and its molecular origin.* Nanoscale, 2015. **7**(30): p. 12998-13010.
714. Zhao, X., et al., *Discrimination Between Cervical Cancer Cells and Normal Cervical Cells Based on Longitudinal Elasticity Using Atomic Force Microscopy.* Nanoscale Res Lett, 2015. **10**(1): p. 482.
715. Zemła, J., et al., *AFM-based nanomechanical characterization of bronchoscopic samples in asthma patients.* J Mol Recognit, 2018. **31**(12): p. e2752.
716. Keaton, J.R., *Young's Modulus*, in *Encyclopedia of Engineering Geology*, P.T. Bobrowsky and B. Marker, Editors. 2018, Springer International Publishing: Cham. p. 955-956.
717. Martinez, A.W., et al., *Effects of crosslinking on the mechanical properties, drug release and cytocompatibility of protein polymers.* Acta biomaterialia, 2014. **10**(1): p. 26-33.
718. Britannica, T.E., Editors of Encyclopaedia (2020, March 5) *elastic limit.* Encyclopedia Britannica.
719. Limaiem, F., M.R. Lekkala, and M. Mlika, *Ovarian Cystadenoma*, in *StatPearls*. 2022, StatPearls Publishing

720. Seidman, J.D. and A. Mehrotra, *Benign ovarian serous tumors: a re-evaluation and proposed reclassification of serous "cystadenomas" and "cystadenofibromas".* Gynecol Oncol, 2005. **96**(2): p. 395-401.
721. Freedman, B.R., et al., *The (dys)functional extracellular matrix.* Biochim Biophys Acta, 2015. **1853**(11 Pt B): p. 3153-64.
722. Plodinec, M. and R.Y. Lim, *Nanomechanical characterization of living mammary tissues by atomic force microscopy.* Methods Mol Biol, 2015. **1293**: p. 231-46.
723. Yang, S. and S.V. Plotnikov, *Mechanosensitive Regulation of Fibrosis.* Cells, 2021. **10**(5).
724. Sciences, F.o.B., *Histology Guide* University of Leeds
725. Fogh, J., J.M. Fogh, and T. Orfeo, *One Hundred and Twenty-Seven Cultured Human Tumor Cell Lines Producing Tumors in Nude Mice23.* JNCI: Journal of the National Cancer Institute, 1977. **59**(1): p. 221-226.
726. Weaver, V.M., *Cell and tissue mechanics: the new cell biology frontier.* Molecular biology of the cell, 2017. **28**(14): p. 1815-1818.
727. Alibert, C., B. Goud, and J.B. Manneville, *Are cancer cells really softer than normal cells?* Biol Cell, 2017. **109**(5): p. 167-189.
728. Xu, M.Z., et al., *Yes-associated protein is an independent prognostic marker in hepatocellular carcinoma.* 2009. **115**(19): p. 4576-4585.
729. Kapoor, A., et al., *Yap1 Activation Enables Bypass of Oncogenic Kras Addiction in Pancreatic Cancer.* Cell, 2014. **158**(1): p. 185-197.
730. Steinhardt, A.A., et al., *Expression of Yes-associated protein in common solid tumors.* Human Pathology, 2008. **39**(11): p. 1582-1589.
731. Hall, C.A., et al., *Hippo pathway effector Yap is an ovarian cancer oncogene.* Cancer research, 2010. **70**(21): p. 8517-8525.
732. Sudol, M., *YAP1 oncogene and its eight isoforms.* Oncogene, 2013. **32**(33): p. 3922.
733. Lee, K.-W., et al., *Significant association of oncogene YAP1 with poor prognosis and cetuximab resistance in colorectal cancer patients.* Clinical cancer research : an official journal of the American Association for Cancer Research, 2015. **21**(2): p. 357-364.
734. Gibson, J.-M., et al., *The role of pegylated liposomal doxorubicin in ovarian cancer: a meta-analysis of randomized clinical trials.* The oncologist, 2013. **18**(9): p. 1022-1031.
735. Nisini, R., et al., *The Multirole of Liposomes in Therapy and Prevention of Infectious Diseases.* 2018. **9**.
736. Green, A.E. and P.G. Rose, *Pegylated liposomal doxorubicin in ovarian cancer.* International journal of nanomedicine, 2006. **1**(3): p. 229-239.
737. Olson, F., et al., *Preparation of liposomes of defined size distribution by extrusion through polycarbonate membranes.* Biochim Biophys Acta, 1979. **557**(1): p. 9-23.
738. Zinger, A., et al., *Reproducible and Characterized Method for Ponatinib Encapsulation into Biomimetic Lipid Nanoparticles as a Platform for Multi-Tyrosine Kinase-Targeted Therapy.* ACS Applied Bio Materials, 2020. **3**(10): p. 6737-6745.
739. Molinaro, R., et al., *Leukocyte-mimicking nanovesicles for effective doxorubicin delivery to treat breast cancer and melanoma.* Biomaterials Science, 2020. **8**(1): p. 333-341.
740. Refai, H., D. Hassan, and R. Abdelmonem, *Development and characterization of polymer-coated liposomes for vaginal delivery of sildenafil citrate.* Drug delivery, 2017. **24**(1): p. 278-288.
741. Collaboration, G.B.o.D.C., *Global, Regional, and National Cancer Incidence, Mortality, Years of Life Lost, Years Lived With Disability, and Disability-Adjusted Life-years for 32*

Cancer Groups, 1990 to 2015: A Systematic Analysis for the Global Burden of Disease Study. JAMA Oncology, 2017. **3**(4): p. 524-548.
742. Kemi, N., et al., *Tumour-stroma ratio and prognosis in gastric adenocarcinoma.* British Journal of Cancer, 2018. **119**(4): p. 435-439.
743. Lee, D., et al., *Intratumor stromal proportion predicts aggressive phenotype of gastric signet ring cell carcinomas.* Gastric Cancer, 2017. **20**(4): p. 591-601.
744. van Pelt, G.W., et al., *The tumour-stroma ratio in colon cancer: the biological role and its prognostic impact.* Histopathology, 2018. **73**(2): p. 197-206.
745. van Pelt, G.W., et al., *The value of tumor-stroma ratio as predictor of pathologic response after neoadjuvant chemoradiotherapy in esophageal cancer.* Clinical and Translational Radiation Oncology, 2020. **20**: p. 39-44.
746. Chen, Y., et al., *Prognostic Significance of the Tumor-Stroma Ratio in Epithelial Ovarian Cancer.* Biomed Res Int, 2015. **2015**: p. 589301.
747. Lan, C., et al., *Quantitative histology analysis of the ovarian tumour microenvironment.* Scientific Reports, 2015. **5**(1): p. 16317.
748. Valkenburg, K.C., A.E. de Groot, and K.J. Pienta, *Targeting the tumour stroma to improve cancer therapy.* Nature reviews. Clinical oncology, 2018. **15**(6): p. 366-381.
749. Northey, J.J., L. Przybyla, and V.M. Weaver, *Tissue Force Programs Cell Fate and Tumor Aggression.* Cancer Discov, 2017. **7**(11): p. 1224-1237.
750. Jaalouk, D.E. and J. Lammerding, *Mechanotransduction gone awry.* Nat Rev Mol Cell Biol, 2009. **10**(1): p. 63-73.
751. Wirtz, D., K. Konstantopoulos, and P.C. Searson, *The physics of cancer: the role of physical interactions and mechanical forces in metastasis.* Nature Reviews Cancer, 2011. **11**(7): p. 512-522.
752. Nagelkerke, A., et al., *The mechanical microenvironment in cancer: How physics affects tumours.* Seminars in Cancer Biology, 2015. **35**: p. 62-70.
753. Jonietz, E., *Mechanics: The forces of cancer.* Nature, 2012. **491**(7425): p. S56-S57.
754. Zhang, J. and C.A. Reinhart-King, *Targeting Tissue Stiffness in Metastasis: Mechanomedicine Improves Cancer Therapy.* Cancer Cell, 2020. **37**(6): p. 754-755.
755. Stewart, D.C., et al., *Mechanical characterization of human brain tumors from patients and comparison to potential surgical phantoms.* PloS one, 2017. **12**(6): p. e0177561-e0177561.
756. Rice, A.J., et al., *Matrix stiffness induces epithelial–mesenchymal transition and promotes chemoresistance in pancreatic cancer cells.* Oncogenesis, 2017. **6**(7): p. e352-e352.
757. Martino, F., et al., *Cellular Mechanotransduction: From Tension to Function.* 2018. **9**(824).
758. Domcke, S., et al., *Evaluating cell lines as tumour models by comparison of genomic profiles.* Nature Communications, 2013. **4**(1): p. 2126.
759. Beaufort, C.M., et al., *Ovarian cancer cell line panel (OCCP): clinical importance of in vitro morphological subtypes.* PLoS One, 2014. **9**(9): p. e103988.
760. Hallas-Potts, A., J.C. Dawson, and C.S. Herrington, *Ovarian cancer cell lines derived from non-serous carcinomas migrate and invade more aggressively than those derived from high-grade serous carcinomas.* Scientific Reports, 2019. **9**(1): p. 5515.
761. Hernandez, L., et al., *Characterization of ovarian cancer cell lines as in vivo models for preclinical studies.* Gynecologic Oncology, 2016. **142**(2): p. 332-340.

762. Dupont, S., et al., *Role of YAP/TAZ in mechanotransduction.* Nature, 2011. **474**(7350): p. 179-83.
763. Zanconato, F., M. Cordenonsi, and S. Piccolo, *YAP and TAZ: a signalling hub of the tumour microenvironment.* Nature Reviews Cancer, 2019. **19**(8): p. 454-464.
764. Díaz-Martín, J., et al., *Nuclear TAZ expression associates with the triple-negative phenotype in breast cancer.* Endocr Relat Cancer, 2015. **22**(3): p. 443-54.
765. Kim, H.M., W.H. Jung, and J.S. Koo, *Expression of Yes-associated protein (YAP) in metastatic breast cancer.* Int J Clin Exp Pathol, 2015. **8**(9): p. 11248-57.
766. Li, Y.W., et al., *Characterization of TAZ domains important for the induction of breast cancer stem cell properties and tumorigenesis.* Cell Cycle, 2015. **14**(1): p. 146-56.
767. Skibinski, A., et al., *The Hippo transducer TAZ interacts with the SWI/SNF complex to regulate breast epithelial lineage commitment.* Cell Rep, 2014. **6**(6): p. 1059-1072.
768. Zhang, X., et al., *The Hippo pathway transcriptional co-activator, YAP, is an ovarian cancer oncogene.* Oncogene, 2011. **30**(25): p. 2810-2822.
769. Galluzzi, L., et al., *Molecular mechanisms of cisplatin resistance.* Oncogene, 2012. **31**(15): p. 1869-83.
770. Wu, Q., et al., *YAP drives fate conversion and chemoresistance of small cell lung cancer.* Sci Adv, 2021. **7**(40): p. eabg1850.
771. Kharaishvili, G., et al., *The role of cancer-associated fibroblasts, solid stress and other microenvironmental factors in tumor progression and therapy resistance.* Cancer Cell International, 2014. **14**(1): p. 41.
772. Östman, A., *The tumor microenvironment controls drug sensitivity.* Nature Medicine, 2012. **18**(9): p. 1332-1334.
773. Fan, Y., et al., *Substrate Stiffness Modulates the Growth, Phenotype, and Chemoresistance of Ovarian Cancer Cells.* Frontiers in cell and developmental biology, 2021. **9**: p. 718834-718834.
774. Network., N.C.C., *Ovarian Cancer, Including Fallopian Tube Cancer and Primary Peritoneal Cancer.* . NCCN Clinical Practice Guidelines (NCCN Guidelines), June 3, 2016. . **Version 1**.
775. Ozols, R.F., et al., *Phase III trial of carboplatin and paclitaxel compared with cisplatin and paclitaxel in patients with optimally resected stage III ovarian cancer: a Gynecologic Oncology Group study.* J Clin Oncol, 2003. **21**(17): p. 3194-200.
776. Luvero, D., A. Milani, and J.A. Ledermann, *Treatment options in recurrent ovarian cancer: latest evidence and clinical potential.* Ther Adv Med Oncol, 2014. **6**(5): p. 229-39.
777. Bookman, M.A., *Extending the platinum-free interval in recurrent ovarian cancer: the role of topotecan in second-line chemotherapy.* Oncologist, 1999. **4**(2): p. 87-94.
778. Pignata, S., et al., *Randomized Controlled Trial Testing the Efficacy of Platinum-Free Interval Prolongation in Advanced Ovarian Cancer: The MITO-8, MaNGO, BGOG-Ov1, AGO-Ovar2.16, ENGOT-Ov1, GCIG Study.* J Clin Oncol, 2017. **35**(29): p. 3347-3353.
779. Tomao, F., et al., *Restoring platinum sensitivity in recurrent ovarian cancer by extending the platinum-free interval: Myth or reality?* Cancer, 2017. **123**(18): p. 3450-3459.
780. Zang, R. and J. Zhu, *Which patients benefit from secondary cytoreductive surgery in recurrent ovarian cancer?* J Gynecol Oncol, 2019. **30**(6): p. e116.
781. Barenholz, Y., *Doxil®--the first FDA-approved nano-drug: lessons learned.* J Control Release, 2012. **160**(2): p. 117-34.

782. Yuan, Z., et al., *Pegylated liposomal doxorubicin in patients with epithelial ovarian cancer.* Journal of Ovarian Research, 2021. **14**(1): p. 12.
783. Pisano, C., et al., *Clinical trials with pegylated liposomal Doxorubicin in the treatment of ovarian cancer.* Journal of drug delivery, 2013. **2013**: p. 898146-898146.
784. Sun, X., et al., *SIRT5 Promotes Cisplatin Resistance in Ovarian Cancer by Suppressing DNA Damage in a ROS-Dependent Manner via Regulation of the Nrf2/HO-1 Pathway.* 2019. **9**(754).
785. Kim, M.G., et al., *The relationship between cisplatin resistance and histone deacetylase isoform overexpression in epithelial ovarian cancer cell lines.* J Gynecol Oncol, 2012. **23**(3): p. 182-9.
786. Tsunetoh, S., et al., *Topotecan as a molecular targeting agent which blocks the Akt and VEGF cascade in platinum-resistant ovarian cancers.* Cancer biology & therapy, 2010. **10**(11): p. 1137-1146.
787. Ebata, T., et al., *Substrate Stiffness Influences Doxorubicin-Induced p53 Activation via ROCK2 Expression.* Biomed Res Int, 2017. **2017**: p. 5158961.
788. Thorn, C.F., et al., *Doxorubicin pathways: pharmacodynamics and adverse effects.* Pharmacogenetics and genomics, 2011. **21**(7): p. 440-446.
789. de Kruijf, E.M., et al., *Tumor-stroma ratio in the primary tumor is a prognostic factor in early breast cancer patients, especially in triple-negative carcinoma patients.* Breast Cancer Res Treat, 2011. **125**(3): p. 687-96.
790. Sandberg, T.P., et al., *Increased expression of cancer-associated fibroblast markers at the invasive front and its association with tumor-stroma ratio in colorectal cancer.* BMC Cancer, 2019. **19**(1): p. 284.
791. Xi, K.-X., et al., *Tumor-stroma ratio (TSR) in non-small cell lung cancer (NSCLC) patients after lung resection is a prognostic factor for survival.* 2017, 2017. **9**(10): p. 4017-4026.
792. Gelse, K., E. Pöschl, and T. Aigner, *Collagens--structure, function, and biosynthesis.* Adv Drug Deliv Rev, 2003. **55**(12): p. 1531-46.
793. Miller, E.J. and V.J. Matukas, *Chick cartilage collagen: a new type of alpha 1 chain not present in bone or skin of the species.* Proceedings of the National Academy of Sciences of the United States of America, 1969. **64**(4): p. 1264-1268.
794. Gordon, M.K. and R.A. Hahn, *Collagens.* Cell Tissue Res, 2010. **339**(1): p. 247-57.
795. Ricard-Blum, S., *The collagen family.* Cold Spring Harb Perspect Biol, 2011. **3**(1): p. a004978.
796. Shoulders, M.D. and R.T. Raines, *Collagen structure and stability.* Annual review of biochemistry, 2009. **78**: p. 929-958.
797. Redmond, J., et al., *Advances in biofabrication techniques for collagen-based 3D in vitro culture models for breast cancer research.* Materials Science and Engineering: C, 2021. **122**: p. 111944.
798. Sorushanova, A., et al., *The Collagen Suprafamily: From Biosynthesis to Advanced Biomaterial Development.* 2019. **31**(1): p. 1801651.
799. Sorushanova, A., et al., *The Collagen Suprafamily: From Biosynthesis to Advanced Biomaterial Development.* Adv Mater, 2019. **31**(1): p. e1801651.
800. Felician, F.F., et al., *Collagen from Marine Biological Sources and Medical Applications.* Chem Biodivers, 2018. **15**(5): p. e1700557.
801. Silva, T.H., et al., *Marine origin collagens and its potential applications.* Marine drugs, 2014. **12**(12): p. 5881-5901.

802. Rahman, M.A., *Collagen of Extracellular Matrix from Marine Invertebrates and Its Medical Applications.* Marine drugs, 2019. **17**(2): p. 118.
803. Parenteau-Bareil, R., R. Gauvin, and F. Berthod, *Collagen-Based Biomaterials for Tissue Engineering Applications.* Materials, 2010. **3**(3): p. 1863-1887.
804. Nagai, T., et al., *Collagen of edible jellyfish exumbrella.* 1999. **79**(6): p. 855-858.
805. Barzideh, Z., et al., *Isolation and characterisation of collagen from the ribbon jellyfish (Chrysaora sp.).* International Journal of Food Science & Technology, 2014. **49**(6): p. 1490-1499.
806. Hoyer, B., et al., *Jellyfish collagen scaffolds for cartilage tissue engineering.* Acta Biomater, 2014. **10**(2): p. 883-92.
807. Addad, S., et al., *Isolation, characterization and biological evaluation of jellyfish collagen for use in biomedical applications.* Marine drugs, 2011. **9**(6): p. 967-983.
808. Provenzano, P.P., et al., *Collagen reorganization at the tumor-stromal interface facilitates local invasion.* BMC Medicine, 2006. **4**(1): p. 38.
809. Cho, A., V.M. Howell, and E.K. Colvin, *The Extracellular Matrix in Epithelial Ovarian Cancer – A Piece of a Puzzle.* 2015. **5**.
810. Adur, J., et al., *Second harmonic generation microscopy as a powerful diagnostic imaging modality for human ovarian cancer.* 2014. **7**(1-2): p. 37-48.
811. Gurler, H., et al., *Three-dimensional collagen type I matrix up-regulates nuclear isoforms of the microtubule associated protein tau implicated in resistance to paclitaxel therapy in ovarian carcinoma.* Int J Mol Sci, 2015. **16**(2): p. 3419-33.
812. Mitra, A.K., et al., *Ligand-independent activation of c-Met by fibronectin and α(5)β(1)-integrin regulates ovarian cancer invasion and metastasis.* Oncogene, 2011. **30**(13): p. 1566-76.
813. Owczarzy, A., et al., *Collagen - structure, properties and application.* 2020(156): p. 17-23.
814. Shoulders, M.D. and R.T. Raines, *Collagen structure and stability.* Annu Rev Biochem, 2009. **78**: p. 929-58.
815. Exposito, J.Y., et al., *The fibrillar collagen family.* Int J Mol Sci, 2010. **11**(2): p. 407-26.
816. Heino, J., *The collagen family members as cell adhesion proteins.* Bioessays, 2007. **29**(10): p. 1001-10.
817. Leitinger, B., *Transmembrane Collagen Receptors.* 2011. **27**(1): p. 265-290.
818. Riaz, T., et al., *FTIR analysis of natural and synthetic collagen.* Applied Spectroscopy Reviews, 2018. **53**(9): p. 703-746.
819. Duan, R., et al., *Properties of collagen from skin, scale and bone of carp (Cyprinus carpio).* 2009. **112**: p. 702-706.
820. Lengyel, E., *Ovarian Cancer Development and Metastasis.* The American Journal of Pathology, 2010. **177**(3): p. 1053-1064.
821. Ahmed, N. and K. Stenvers, *Getting to Know Ovarian Cancer Ascites: Opportunities for Targeted Therapy-Based Translational Research.* 2013. **3**.
822. Geisinger, K.R., et al., *Characterization of a human ovarian carcinoma cell line with estrogen and progesterone receptors.* Cancer, 1989. **63**(2): p. 280-8.
823. Davidson, B., C.G. Tropé, and R. Reich, *Epithelial-mesenchymal transition in ovarian carcinoma.* Front Oncol, 2012. **2**: p. 33.

824. Krempski, J., et al., *Tumor-infiltrating programmed death receptor-1+ dendritic cells mediate immune suppression in ovarian cancer.* Journal of immunology (Baltimore, Md. : 1950), 2011. **186**(12): p. 6905-6913.
825. Kamat, A.A., et al., *The clinical relevance of stromal matrix metalloproteinase expression in ovarian cancer.* Clin Cancer Res, 2006. **12**(6): p. 1707-14.
826. Jia, D., et al., *A COL11A1-correlated pan-cancer gene signature of activated fibroblasts for the prioritization of therapeutic targets.* Cancer letters, 2016. **382**(2): p. 203-214.
827. Wu, Y.H., et al., *COL11A1 promotes tumor progression and predicts poor clinical outcome in ovarian cancer.* Oncogene, 2014. **33**(26): p. 3432-3440.
828. Cooper, G.M., *The cell : a molecular approach.* 2000, Washington, D.C.; Sunderland, Mass.: ASM Press ; Sinauer Associates.
829. Takeichi, M., *Cadherin cell adhesion receptors as a morphogenetic regulator.* Science, 1991. **251**(5000): p. 1451-5.
830. Chen, V.W., et al., *Pathology and classification of ovarian tumors.* Cancer, 2003. **97**(10 Suppl): p. 2631-42.
831. Li, N.F., et al., *A modified medium that significantly improves the growth of human normal ovarian surface epithelial (OSE) cells in vitro.* Lab Invest, 2004. **84**(7): p. 923-31.
832. Wong, A.S. and N. Auersperg, *Normal ovarian surface epithelium.* Cancer Treat Res, 2002. **107**: p. 161-83.
833. Orsulic, S., et al., *Induction of ovarian cancer by defined multiple genetic changes in a mouse model system.* Cancer Cell, 2002. **1**(1): p. 53-62.
834. Shevde, L.A. and R.S. Samant, *Role of osteopontin in the pathophysiology of cancer.* Matrix Biol, 2014. **37**: p. 131-41.
835. Zhao, H., et al., *The role of osteopontin in the progression of solid organ tumour.* Cell Death & Disease, 2018. **9**(3): p. 356.
836. Yin, X., et al., *EFEMP1 promotes ovarian cancer cell growth, invasion and metastasis via activated the AKT pathway.* Oncotarget, 2016. **7**(30): p. 47938-47953.
837. Chen, J., et al., *Overexpression of EFEMP1 Correlates with Tumor Progression and Poor Prognosis in Human Ovarian Carcinoma.* PLOS ONE, 2013. **8**(11): p. e78783.
838. Chang, M.C., et al., *Mesothelin enhances invasion of ovarian cancer by inducing MMP-7 through MAPK/ERK and JNK pathways.* Biochem J, 2012. **442**(2): p. 293-302.
839. Mikos, A.G. and J.S. Temenoff, *Formation of highly porous biodegradable scaffolds for tissue engineering %J Electronic Journal of Biotechnology.* 2000. **3**: p. 23-24.
840. O'Brien, F.J., et al., *Influence of freezing rate on pore structure in freeze-dried collagen-GAG scaffolds.* Biomaterials, 2004. **25**(6): p. 1077-86.
841. Akay, G., M.A. Birch, and M.A. Bokhari, *Microcellular polyHIPE polymer supports osteoblast growth and bone formation in vitro.* Biomaterials, 2004. **25**(18): p. 3991-4000.
842. Fallas, J.A., et al., *Structural insights into charge pair interactions in triple helical collagen-like proteins.* The Journal of biological chemistry, 2012. **287**(11): p. 8039-8047.
843. Kuboki, Y., Q. Jin, and H. Takita, *Geometry of carriers controlling phenotypic expression in BMP-induced osteogenesis and chondrogenesis.* J Bone Joint Surg Am, 2001. **83-A Suppl 1**(Pt 2): p. S105-15.
844. Friedl, P. and K. Wolf, *Tumour-cell invasion and migration: diversity and escape mechanisms.* Nature Reviews Cancer, 2003. **3**(5): p. 362-374.

845. Quintela, M., et al., *HBO1 directs histone H4 specific acetylation, potentiating mechano-transduction pathways and membrane elasticity in ovarian cancer cells.* Nanomedicine, 2019. **17**: p. 254-265.
846. Subbiahanadar Chelladurai, K., et al., *Alternative to FBS in animal cell culture - An overview and future perspective.* Heliyon, 2021. **7**(8): p. e07686.
847. Stephens, M.L., *Book Review: The Three Rs and the Humanity Criterion.* Alternatives to Laboratory Animals, 2009. **37**(3): p. 333-334.
848. Alkildani, S., O. Jung, and M. Barbeck, *In Vitro Investigation of Jellyfish Collagen as a Tool in Cell Culture and (Bone) Tissue Engineering.* Anticancer Res, 2021. **41**(2): p. 707-717.
849. Ahmed, Z., et al., *Jellyfish Collagen: A Biocompatible Collagen Source for 3D Scaffold Fabrication and Enhanced Chondrogenicity.* Marine drugs, 2021. **19**(8): p. 405.
850. Tang, J. and T. Saito, *Biocompatibility of Novel Type I Collagen Purified from Tilapia Fish Scale: An In Vitro Comparative Study.* BioMed research international, 2015. **2015**: p. 139476.
851. Venkatesan, J., et al., *Marine Fish Proteins and Peptides for Cosmeceuticals: A Review.* 2017. **15**(5): p. 143.
852. Mitura, S., A. Sionkowska, and A. Jaiswal, *Biopolymers for hydrogels in cosmetics: review.* J Mater Sci Mater Med, 2020. **31**(6): p. 50.
853. Widdowson, J.P., et al., *In vivo comparison of jellyfish and bovine collagen sponges as prototype medical devices.* Journal of biomedical materials research. Part B, Applied biomaterials, 2018. **106**(4): p. 1524-1533.
854. Bernhardt, A., B. Paul, and M. Gelinsky, *Biphasic Scaffolds from Marine Collagens for Regeneration of Osteochondral Defects.* Mar Drugs, 2018. **16**(3).
855. Pustlauk, W., et al., *Jellyfish collagen and alginate: Combined marine materials for superior chondrogenesis of hMSC.* Mater Sci Eng C Mater Biol Appl, 2016. **64**: p. 190-198.
856. Nagai, T., et al., *Isolation and characterisation of collagen from the outer skin waste material of cuttlefish (Sepia lycidas).* Food Chemistry, 2001. **72**(4): p. 425-429.
857. Nagai, N., et al., *Application of cross-linked salmon atelocollagen to the scaffold of human periodontal ligament cells.* J Biosci Bioeng, 2004. **97**(6): p. 389-94.
858. Kapałczyńska, M., et al., *2D and 3D cell cultures - a comparison of different types of cancer cell cultures.* Arch Med Sci, 2018. **14**(4): p. 910-919.
859. Gray, H., *Gray's Anatomy.* unning Press: Philadelphia, 1901.
860. Kipps, E., D.S.P. Tan, and S.B. Kaye, *Meeting the challenge of ascites in ovarian cancer: new avenues for therapy and research.* Nature Reviews Cancer, 2013. **13**(4): p. 273-282.
861. Yoshikawa, T., et al., *Peritoneal Fluid Accumulation in Healthy Men and Postmenopausal Women: Evaluation on Pelvic MRI.* American Journal of Roentgenology, 2013. **200**(6): p. 1181-1185.
862. Ayantunde, A.A. and S.L. Parsons, *Pattern and prognostic factors in patients with malignant ascites: a retrospective study.* Annals of Oncology, 2007. **18**(5): p. 945-949.
863. Cvetkovic, D., *Early events in ovarian oncogenesis.* Reproductive Biology and Endocrinology, 2003. **1**(1): p. 68.
864. Tan, D.S.P., R. Agarwal, and S.B. Kaye, *Mechanisms of transcoelomic metastasis in ovarian cancer.* The Lancet Oncology, 2006. **7**(11): p. 925-934.

865. Ip, C.K.M., et al., *Stemness and chemoresistance in epithelial ovarian carcinoma cells under shear stress.* Scientific Reports, 2016. **6**(1): p. 26788.
866. Mo, L., et al., *Ascites Increases Expression/Function of Multidrug Resistance Proteins in Ovarian Cancer Cells.* PLOS ONE, 2015. **10**(7): p. e0131579.
867. Rizvi, I., et al., *Flow induces epithelial-mesenchymal transition, cellular heterogeneity and biomarker modulation in 3D ovarian cancer nodules.* 2013. **110**(22): p. E1974-E1983.
868. Cohen, M. and P. Petignat, *The bright side of ascites in ovarian cancer.* Cell Cycle, 2014. **13**(15): p. 2319-2319.
869. Puiffe, M.-L., et al., *Characterization of Ovarian Cancer Ascites on Cell Invasion, Proliferation, Spheroid Formation, Gene Expression in an In Vitro Model of Epithelial Ovarian Cancer.* Neoplasia, 2007. **9**(10): p. 820-IN8.
870. Holm-Nielsen, P., *PATHOGENESIS OF ASCITES IN PERITONEAL CARCINOMATOSIS1.* 1953. **33**(1): p. 10-21.
871. Healy, J.C. and R.H. Reznek, *The peritoneum, mesenteries and omenta: normal anatomy and pathological processes.* European Radiology, 1998. **8**(6): p. 886-900.
872. Cavazzoni, E., et al., *Malignant ascites: pathophysiology and treatment.* International Journal of Clinical Oncology, 2013. **18**(1): p. 1-9.
873. McCloskey, C.W., et al., *Metformin Abrogates Age-Associated Ovarian Fibrosis.* Clin Cancer Res, 2020. **26**(3): p. 632-642.
874. Krndija, D., et al., *Substrate stiffness and the receptor-type tyrosine-protein phosphatase alpha regulate spreading of colon cancer cells through cytoskeletal contractility.* Oncogene, 2010. **29**(18): p. 2724-38.
875. Tang, X., et al., *A mechanically-induced colon cancer cell population shows increased metastatic potential.* Mol Cancer, 2014. **13**: p. 131.
876. Broders-Bondon, F., et al., *Mechanotransduction in tumor progression: The dark side of the force.* J Cell Biol, 2018. **217**(5): p. 1571-1587.
877. Kumar, S. and V.M. Weaver, *Mechanics, malignancy, and metastasis: the force journey of a tumor cell.* Cancer Metastasis Rev, 2009. **28**(1-2): p. 113-27.
878. Erdemci-Tandogan, G. and M.L. Manning, *Effect of cellular rearrangement time delays on the rheology of vertex models for confluent tissues.* PLOS Computational Biology, 2021. **17**(6): p. e1009049.
879. Wang, H.B., M. Dembo, and Y.L. Wang, *Substrate flexibility regulates growth and apoptosis of normal but not transformed cells.* Am J Physiol Cell Physiol, 2000. **279**(5): p. C1345-50.
880. Wong, S.Y., et al., *Constitutive activation of myosin-dependent contractility sensitizes glioma tumor-initiating cells to mechanical inputs and reduces tissue invasion.* Cancer Res, 2015. **75**(6): p. 1113-22.
881. Runge, J., et al., *Evaluation of single-cell biomechanics as potential marker for oral squamous cell carcinomas: a pilot study.* Oral Dis, 2014. **20**(3): p. e120-7.
882. Guo, Z., et al., *The effects of macroporosity and stiffness of poly[(methyl vinyl ether)-alt-(maleic acid)] cross-linked egg white simulations of an aged extracellular matrix on the proliferation of ovarian cancer cells.* RSC Advances, 2016. **6**(50): p. 43892-43900.
883. McKenzie, A.J., et al., *The mechanical microenvironment regulates ovarian cancer cell morphology, migration, and spheroid disaggregation.* Sci Rep, 2018. **8**(1): p. 7228.
884. Paullin, T., et al., *Spheroid growth in ovarian cancer alters transcriptome responses for stress pathways and epigenetic responses.* PLoS One, 2017. **12**(8): p. e0182930.

885. Montesi, S.B., et al., *Molecular imaging of fibrosis: recent advances and future directions.* J Clin Invest, 2019. **129**(1): p. 24-33.
886. Harris, S.L. and A.J. Levine, *The p53 pathway: positive and negative feedback loops.* Oncogene, 2005. **24**(17): p. 2899-2908.
887. Hanley, C.J., et al., *A subset of myofibroblastic cancer-associated fibroblasts regulate collagen fiber elongation, which is prognostic in multiple cancers.* Oncotarget, 2016. **7**(5): p. 6159-74.
888. Demaria, M., et al., *An essential role for senescent cells in optimal wound healing through secretion of PDGF-AA.* Developmental cell, 2014. **31**(6): p. 722-733.
889. Krizhanovsky, V., et al., *Senescence of activated stellate cells limits liver fibrosis.* Cell, 2008. **134**(4): p. 657-667.
890. Coppé, J.P., et al., *The senescence-associated secretory phenotype: the dark side of tumor suppression.* Annu Rev Pathol, 2010. **5**: p. 99-118.
891. Bavik, C., et al., *The gene expression program of prostate fibroblast senescence modulates neoplastic epithelial cell proliferation through paracrine mechanisms.* Cancer Res, 2006. **66**(2): p. 794-802.
892. Stylianou, A., M. Lekka, and T. Stylianopoulos, *AFM assessing of nanomechanical fingerprints for cancer early diagnosis and classification: from single cell to tissue level.* Nanoscale, 2018. **10**(45): p. 20930-20945.
893. Minelli, E., et al., *A fully-automated neural network analysis of AFM force-distance curves for cancer tissue diagnosis.* 2017. **111**(14): p. 143701.
894. Ding, Y., G.K. Xu, and G.F. Wang, *On the determination of elastic moduli of cells by AFM based indentation.* Sci Rep, 2017. **7**: p. 45575.
895. Sutherland, R.M., J.A. McCredie, and W.R. Inch, *Growth of Multicell Spheroids in Tissue Culture as a Model of Nodular Carcinomas2.* JNCI: Journal of the National Cancer Institute, 1971. **46**(1): p. 113-120.
896. Li, X., et al., *Functional Hydrogels With Tunable Structures and Properties for Tissue Engineering Applications.* 2018. **6**(499).
897. Oyen, M.L., *Mechanical characterisation of hydrogel materials.* International Materials Reviews, 2014. **59**(1): p. 44-59.
898. Jaiswal, D., et al., *Stiffness analysis of 3D spheroids using microtweezers.* PLoS One, 2017. **12**(11): p. e0188346.
899. Dolega, M.E., et al., *Cell-like pressure sensors reveal increase of mechanical stress towards the core of multicellular spheroids under compression.* Nat Commun, 2017. **8**: p. 14056.
900. Lee, W., et al., *Dispersible hydrogel force sensors reveal patterns of solid mechanical stress in multicellular spheroid cultures.* Nature Communications, 2019. **10**(1): p. 144.
901. Helmlinger, G., et al., *Solid stress inhibits the growth of multicellular tumor spheroids.* Nature Biotechnology, 1997. **15**(8): p. 778-783.
902. Cheng, G., et al., *Micro-Environmental Mechanical Stress Controls Tumor Spheroid Size and Morphology by Suppressing Proliferation and Inducing Apoptosis in Cancer Cells.* PLOS ONE, 2009. **4**(2): p. e4632.
903. Pati, F., J. Gantelius, and H.A. Svahn, *3D Bioprinting of Tissue/Organ Models.* Angew Chem Int Ed Engl, 2016. **55**(15): p. 4650-65.

904. Alonso-Alconada, L., et al., *Biomimetic device and foreign body reaction cooperate for efficient tumour cell capture in murine advanced ovarian cancer.* Disease Models & Mechanisms, 2020. **13**(6): p. dmm043653.
905. Kim, H.J., et al., *Human gut-on-a-chip inhabited by microbial flora that experiences intestinal peristalsis-like motions and flow.* Lab on a Chip, 2012. **12**(12): p. 2165-2174.
906. Huh, D., et al., *Reconstituting Organ-Level Lung Functions on a Chip.* 2010. **328**(5986): p. 1662-1668.
907. Benam, K.H., et al., *Small airway-on-a-chip enables analysis of human lung inflammation and drug responses in vitro.* Nature Methods, 2016. **13**(2): p. 151-157.
908. Wu, Q., et al., *Organ-on-a-chip: recent breakthroughs and future prospects.* BioMedical Engineering OnLine, 2020. **19**(1): p. 9.
909. Ingber, D.E., *Developmentally inspired human 'organs on chips'.* Development (Cambridge, England), 2018. **145**(16): p. dev156125.
910. Liu, R.Y., et al., *JAK/STAT3 signaling is required for TGF-β-induced epithelial-mesenchymal transition in lung cancer cells.* Int J Oncol, 2014. **44**(5): p. 1643-51.
911. Wu, J., et al., *Association between tumor-stroma ratio and prognosis in solid tumor patients: a systematic review and meta-analysis.* Oncotarget, 2016. **7**(42): p. 68954-68965.
912. Vonlaufen, A., et al., *Pancreatic stellate cells: partners in crime with pancreatic cancer cells.* Cancer Res, 2008. **68**(7): p. 2085-93.
913. Kanat, O. and H. Ertas, *Shattering the castle walls: Anti-stromal therapy for pancreatic cancer.* World journal of gastrointestinal oncology, 2018. **10**(8): p. 202-210.
914. Biswas, S., et al., *Inhibition of TGF-beta with neutralizing antibodies prevents radiation-induced acceleration of metastatic cancer progression.* J Clin Invest, 2007. **117**(5): p. 1305-13.
915. Hofheinz, R.D., et al., *Stromal Antigen Targeting by a Humanised Monoclonal Antibody: An Early Phase II Trial of Sibrotuzumab in Patients with Metastatic Colorectal Cancer.* Oncology Research and Treatment, 2003. **26**(1): p. 44-48.
916. Brünker, P., et al., *RG7386, a Novel Tetravalent FAP-DR5 Antibody, Effectively Triggers FAP-Dependent, Avidity-Driven DR5 Hyperclustering and Tumor Cell Apoptosis.* Mol Cancer Ther, 2016. **15**(5): p. 946-57.
917. Zhang, L., et al., *Intratumoral T cells, recurrence, and survival in epithelial ovarian cancer.* N Engl J Med, 2003. **348**(3): p. 203-13.
918. Kenny, H.A., et al., *Mesothelial cells promote early ovarian cancer metastasis through fibronectin secretion.* J Clin Invest, 2014. **124**(10): p. 4614-28.
919. Davidowitz, R.A., et al., *Mesenchymal gene program-expressing ovarian cancer spheroids exhibit enhanced mesothelial clearance.* J Clin Invest, 2014. **124**(6): p. 2611-25.
920. Iwanicki, M.P., et al., *Ovarian cancer spheroids use myosin-generated force to clear the mesothelium.* Cancer Discov, 2011. **1**(2): p. 144-57.
921. Ozols, R.F., *Treatment goals in ovarian cancer.* Int J Gynecol Cancer, 2005. **15 Suppl 1**: p. 3-11.
922. Ricciardelli, C., et al., *Chemotherapy-induced hyaluronan production: a novel chemoresistance mechanism in ovarian cancer.* BMC cancer, 2013. **13**: p. 476-476.
923. McGrail, D.J., et al., *Alterations in ovarian cancer cell adhesion drive taxol resistance by increasing microtubule dynamics in a FAK-dependent manner.* Sci Rep, 2015. **5**: p. 9529.

924. Smith, J.A., et al., *An evaluation of cytotoxicity of the taxane and platinum agents combination treatment in a panel of human ovarian carcinoma cell lines.* Gynecologic Oncology, 2005. **98**(1): p. 141-145.
925. Ofir, R., et al., *Taxol-induced apoptosis in human SKOV3 ovarian and MCF7 breast carcinoma cells is caspase-3 and caspase-9 independent.* Cell Death & Differentiation, 2002. **9**(6): p. 636-642.
926. Brozovic, A., et al., *The miR-200 family differentially regulates sensitivity to paclitaxel and carboplatin in human ovarian carcinoma OVCAR-3 and MES-OV cells.* Molecular oncology, 2015. **9**(8): p. 1678-1693.
927. Bourguignon, L.Y., et al., *Hyaluronan-CD44 interaction activates stem cell marker Nanog, Stat-3-mediated MDR1 gene expression, and ankyrin-regulated multidrug efflux in breast and ovarian tumor cells.* J Biol Chem, 2008. **283**(25): p. 17635-51.
928. Cordo Russo, R.I., et al., *Hyaluronan oligosaccharides sensitize lymphoma resistant cell lines to vincristine by modulating P-glycoprotein activity and PI3K/Akt pathway.* Int J Cancer, 2008. **122**(5): p. 1012-8.
929. Misra, S., S. Ghatak, and B.P. Toole, *Regulation of MDR1 expression and drug resistance by a positive feedback loop involving hyaluronan, phosphoinositide 3-kinase, and ErbB2.* J Biol Chem, 2005. **280**(21): p. 20310-5.
930. Ma, J., et al., *The American Cancer Society 2035 challenge goal on cancer mortality reduction.* 2019. **69**(5): p. 351-362.
931. Elmore, L.W., et al., *Blueprint for cancer research: Critical gaps and opportunities.* 2021. **71**(2): p. 107-139.
932. Rahib, L., et al., *Projecting Cancer Incidence and Deaths to 2030: The Unexpected Burden of Thyroid, Liver, and Pancreas Cancers in the United States.* Cancer Research, 2014. **74**(11): p. 2913-2921.
933. Torre, L.A., et al., *Ovarian cancer statistics, 2018.* 2018. **68**(4): p. 284-296.
934. Jackson, S.J. and G.J. Thomas, *Human tissue models in cancer research: looking beyond the mouse.* Disease Models & Mechanisms, 2017. **10**(8): p. 939-942.
935. Albritton, J.L. and J.S. Miller, *3D bioprinting: improving in vitro models of metastasis with heterogeneous tumor microenvironments.* Disease Models & Mechanisms, 2017. **10**(1): p. 3-14.
936. Vlachogiannis, G., et al., *Patient-derived organoids model treatment response of metastatic gastrointestinal cancers.* Science (New York, N.Y.), 2018. **359**(6378): p. 920-926.
937. Fong, E.L.S., et al., *3D Culture as a Clinically Relevant Model for Personalized Medicine.* SLAS Technol, 2017. **22**(3): p. 245-253.
938. Lazo, J.S., *The hubris and humility of cancer pharmacology in the post immuno-oncology era.* 2019. **7**(6): p. e00527.
939. Roy, V., et al., *Human Organ-Specific 3D Cancer Models Produced by the Stromal Self-Assembly Method of Tissue Engineering for the Study of Solid Tumors.* BioMed Research International, 2020. **2020**: p. 6051210.
940. Lisio, M.-A., et al., *High-Grade Serous Ovarian Cancer: Basic Sciences, Clinical and Therapeutic Standpoints.* 2019. **20**(4): p. 952.
941. Sensi, F., et al., *Recellularized Colorectal Cancer Patient-derived Scaffolds as in vitro Pre-clinical 3D Model for Drug Screening.* Cancers (Basel), 2020. **12**(3).

942. D'Angelo, E., et al., *Patient-Derived Scaffolds of Colorectal Cancer Metastases as an Organotypic 3D Model of the Liver Metastatic Microenvironment.* Cancers (Basel), 2020. **12**(2).
943. Piccoli, M., et al., *Decellularized colorectal cancer matrix as bioactive microenvironment for in vitro 3D cancer research.* J Cell Physiol, 2018. **233**(8): p. 5937-5948.
944. Agarwal, T., et al., *PAMAM dendrimer grafted cellulose paper scaffolds as a novel in vitro 3D liver model for drug screening applications.* Colloids Surf B Biointerfaces, 2018. **172**: p. 346-354.
945. Candini, O., et al., *A Novel 3D In Vitro Platform for Pre-Clinical Investigations in Drug Testing, Gene Therapy, and Immuno-oncology.* Scientific Reports, 2019. **9**(1): p. 7154.
946. Brancato, V., et al., *Could 3D models of cancer enhance drug screening?* Biomaterials, 2020. **232**: p. 119744.
947. Booij, T.H., L.S. Price, and E.H.J. Danen, *3D Cell-Based Assays for Drug Screens: Challenges in Imaging, Image Analysis, and High-Content Analysis.* SLAS Discov, 2019. **24**(6): p. 615-627.
948. Augustine, R., et al., *3D Bioprinted cancer models: Revolutionizing personalized cancer therapy.* Transl Oncol, 2021. **14**(4): p. 101015.